UNIVERSITÉ DU QUÉBEC

THÈSE PRÉSENTÉE À L'UNIVERSITÉ DU QUÉBEC À CHICOUTIMI

COMME EXIGENCE PARTIELLE

DU DOCTORAT EN RESSOURCES MINÉRALES

PAR

SOUAD GUERNINA

M.Sc.A.

FORMATION AND EVOLUTION OF GRANITE MAGMAS FROM MIGMATITES: AN EXAMPLE FROM THE ASHUANIPI SUBPROVINCE IN THE SUPERIOR PROVINCE, QUÉBEC

Mars, 2007

Bibliothèque Paul-Émile-Boulet

UQAC Université du Québec à Chicoutimi

Mise en garde/Advice

Afin de rendre accessible au plus grand nombre le résultat des travaux de recherche menés par ses étudiants gradués et dans l'esprit des règles qui régissent le dépôt et la diffusion des mémoires et thèses produits dans cette Institution, **l'Université du Québec à Chicoutimi (UQAC)** est fière de rendre accessible une version complète et gratuite de cette œuvre.

Motivated by a desire to make the results of its graduate students' research accessible to all, and in accordance with the rules governing the acceptation and diffusion of dissertations and theses in this Institution, the **Université du Québec à Chicoutimi (UQAC)** is proud to make a complete version of this work available at no cost to the reader.

L'auteur conserve néanmoins la propriété du droit d'auteur qui protège ce mémoire ou cette thèse. Ni le mémoire ou la thèse ni des extraits substantiels de ceux-ci ne peuvent être imprimés ou autrement reproduits sans son autorisation.

The author retains ownership of the copyright of this dissertation or thesis. Neither the dissertation or thesis, nor substantial extracts from it, may be printed or otherwise reproduced without the author's permission.

RÉSUMÉ

Plusieurs magmas dans la croûte continentale sont considérés comme le produit de fusion partielle dans la croûte inférieure à moyenne et le transfert de ce magma vers la croûte supérieure. Cependant, l'évolution exacte de ces magmas granitiques est très peu connue. En général, les processus impliqués sont la redistribution et la contamination de la fraction de fondu par la roche encaissante qu'elle traverse. Le magma commence à cristalliser une fois à l'extérieur de la zone anatectique. La nature de la transition protolithe-migmatite-granite et le processus qui génère un magma granitique durant la fusion partielle, ainsi que le processus qui contrôle la composition du magma à l'extérieur de la région source sont d'un intérêt particulier car ils expliquent les variations morphologiques, minéralogiques et géochimiques des produits de fusion à partir de roches métasédimentaires de type greywacke.

La sous-province d'Ashuanipi et les sous-provinces métasédimentaires avoisinantes de la Province du Supérieur contiennent une croûte Archéenne composée de roches anatectiques de la croûte moyenne et de plutons granitiques à des niveaux superficiels. En d'autres mots, la Province du Supérieur représente une section continue de la croûte allant d'une source profonde partiellement fondue à des niveaux supérieurs d'écoulement magmatique. La sous province d'Ashuanipi est l'exemple d'une source potentielle pour les magmas granulitiques. La transition à partir du paléosome jusqu'au granite s'est faite dans un système ouvert en passant par des étapes intermédiaires de métatexite et de diatexite.

Les méthodes de terrain, de pétrographie et de géochimie ont été utilisées pour estimer la quantité de fondu granitique produite et extraite à partir d'un terrain au facies granulitique, et pour déterminer à l'échelle de la lame mince et de l'affleurement le chemin emprunté par l'écoulement du fondu durant le processus de ségrégation. Plus de 85% des métasédiments dans la sous-province d'Ashuanipi ont la composition de métagreywacke, métamorphisé dans des conditions de la croûte moyenne (820-900 °C et 6-7 kbar). La diminution modale de la biotite et du quartz aux dépens de l'orthopyroxène et du plagioclase ainsi que la préservation de microstructures de fondu préexistant indiquent que la fusion partielle était selon la réaction de déshydratation de la biotite: biotite + quartz + plagioclase = fondu + orthopyroxène + oxides. En appliquant à cette réaction le rapport fondu/orthopyroxène dérivé à partir des études expérimentales, la composition modale d'orthopyroxène contenue dans les roches d'Ashuanipi indique que les métagreywackes ont subi en moyenne 31 % de fusion partielle.

Les métagreywackes sont enrichis en MgO, CaO et FeO et appauvris en SiO_2, K_2O, Rb, Cs and U, ont des anomalies positives en Eu et des rapports Rb/SR plus bas que le protolithe, par contre les rapports Rb/Cs et Th/U sont nettement plus élevés. Ces compositions sont modelées après l'extraction entre 20 et 40 wt % d'un fondu granitique à partir de métagreywackes archéen de bas-grade métamorphique.

La distribution du fondu résiduel à l'échelle du microscope et à l'échelle de l'affleurement indique un écoulement pénétrant du fondu sur les bordures des grains le long des couches métasédimentaires, suivi par un écoulement du fondu canalisé dans un réseau de conduits interconnectés. Les leucosomes ont gardé très peu (<5% biotite + orthopyroxène) de matériel résiduel. Ceci indique que la fraction de fondu a été bien séparée du résiduum demeuré lui *in situ* en tant qu'une granulite appauvrie en fondu. Par contre, la quantité de fondu qui a demeuré dans les granulites appauvris en fondu est entre 1 à 3 vol %, donc, l'extraction du fondu généré après une fusion par déshydratation de la biotite dans ces granulites, était complète sous des conditions de P, T et de déformation qui prédominaient durant la fusion partielle.

Chapitre IV et Chapitre V se concentrent sur la continuité morphologique, pétrologique et géochimique d'une diatexite vers une roche granitique dans la Sous-province d'Ashuanipi. Le fondu extrait après la fusion partielle était redistribué à l'intérieur de larges sites à basse pression, où il sera par la suite contaminé par les roches résiduelles qu'il traverse. La fraction solide et la fraction fondu dans le magma de diatexite se séparent progressivement durant l'écoulement magmatique afin de générer des diatexites enrichies en cristaux et des diatexites enrichies en fondu. La diatexite enrichie en plagioclase est une roche contaminée riche en cumulât et contient principalement des plagioclses résiduels et des plagioclases précoces ayant cristallisé à partir du fondu anatectique, alors que la diatexite enrichie en K-feldspath est considérée comme le liquide putatif extrait de la diatexite-enrichi en plagioclase. La diatexite enrichie en plagioclases et en K-feldspath a une composition proche du fondu anatectique contaminé. La plupart des magmas de la diatexite dans la Sous province d'Ashuanipi sont modifiés par les effets de la cristallisation fractionnée et très peu de magmas préservent la composition originelle.

Il existe une continuité morphologique, minéralogique et géochimique à partir des migmatites type métatexite jusqu'aux migmatites de type diatexite et aux granites anatectiques dans la Sous province d'Ashuanipi. Ceci indique que la fusion partielle et le remaniement de la croûte dans l'Ashuanipi étaient un processus intervenant dans un système ouvert à petite échelle (e.g. pluton) et probablement fermé à plus grande échelle (e.g. épaisseur de la croûte continentale).

ABSTRACT

Many magmas in the continental crust are believed to have formed by partial melting in the lower to middle crust, and the transfer of that melt to the upper crust. However, it is poorly known how the compositions of these magmas evolve. In general, the principal processes involved are redistribution and contamination of the melt fraction with some of the host-rock it passes through and once magma ascends out of the anatectic zone and traverses cooler crust and begins to crystallize. The nature of the protolith-migmatite-granite transition and the process that creates a granitic magma during anatexis, as well as the processes that control the magma composition outside the source region are of a particular interest as they enable us to constrain the morphological, mineralogical and geochemical variations of anatectic melts produced during anatexis of greywacke metasedimentary rocks.

The Ashuanipi subprovince and contiguous metasedimentary subprovinces in the Superior province contains reworked Archaean crust that displays a continuous section from mid-crustal anatectic rocks to shallow level granite plutons. In other words, the superior province represents a crustal section which is continuous from partially melted source to upper crustal magma sink and the Ashaunipi portion of it is an example of a source region for granulitic magma. There, the transition from palaesome to granite was an open system process through intermediate stages of metatexite and diatexite.

Field, petrographic and geochemical methods have been used to estimate how much granitic melt was formed and extracted from granulite facies terrane, and to determine what the grain and outcrop-scale melt-flow paths were during the melt segregation process.
More than 85 % of the metasediments in the Ashuanipi subprovince are of metagreywacke composition that was metamorphosed at mid-crustal conditions (820-900 °C and 6-7 kbar). Decrease in modal biotite and quartz as orthopyroxene and plagioclase contents increase, together with preserved former melt microstructures indicate that anatexis was by the biotite dehydration reaction: biotite + quartz + plagioclase = melt + orthopyroxene + oxides. Using melt/orthopyroxene ratios for this reaction derived from experimental studies, the modal orthopyroxene contents present in the Ashuanipi rocks indicate that the metagreywacke rocks underwent an average of 31 vol% partial melting.

The metagreywackes are enriched in MgO, CaO and FeO and depleted in SiO_2, K_2O, Rb, Cs and U, have lower Rb/SR, higher Rb/Cs and Th/U ratios and positive Eu anomalies compared to their likely protolith. These compositions are modelled by the extraction of between 20 and 40 wt % granitic melt from typical Achaean low-grade metagreywackes.

The distribution of relict melt at thin section and outcrop scales indicates that in layers without leucosomes melt extraction occurred by a pervasive grain boundary (porous) flow from the site of melting, across the layers and into bedding planes between adjacent layers. In other rocks, pervasive grain boundary flow of melt occurred along the layers for few to tens centimetres followed by channelled flow of melt in a network of short interconnected conduits. Very little (<5% biotite + orthopyroxene) residual material remained in the leucosomes, indicating that the melt fraction was well separated from the residuum left *in situ* as melt-depleted granulite. Only 1-3 vol percentage melt remained in the melt-depleted granulites, hence, the extraction of melt generated by biotite dehydration melting in these granulites, was virtually complete under the conditions of P, T and deformation that prevailed during partial melting.

Chapter IV and Chapter V focus on the morphological, petrological and geochemical continuity from diatexite migmatites to granitic rocks in the Ashuanipi subprovince. The extracted anatectic melt was pooled and redistributed into large low pressure sites and become contaminated with some of the residuum it passed through. These bodies of contaminated anatectic melt form diatexite migmatites. The solid and melt fractions in the diatexite magma became progressively separated during flow of the diatexite magma, and thus generated both crystal-enriched and melt-enriched diatexite migmatites. Plagioclase-rich diatexite is a contaminated cumulate rock composed principally of plagioclase that crystallised from the anatectic melt, whereas the K-feldspar rich diatexite is consistent with the putative liquid lost from the plagioclase-rich diatexite rocks. Plagioclase + K-feldspar-rich diatexites approximate to the contaminated anatectic melt composition. Most of the diatexite magmas in the Ashuanipi subprovince are modified by the effects of fractional crystallization and very few actually preserve primary melt compositions.

The diatexite magma is parental to the monzogranites at the same level and probably higher crustal levels. The range of monzogranite compositions from low silica low potassium (LSLP) to high silica high potassium (HSHP) is consistent with a derivation from a common parent that resembled the evolved diatexites. The LSLP group, represent magma enriched in orthopyroxene and early crystallized plagioclase, in which major and trace elements distribution probably reflects both crystallization and/or fractionation, and contamination by host rock material. Geochemical modelling of the diatexite migmatites and monzogranites showed for both major and trace elements that, most diatexites and few granites (LSLP) have the geochemistry of contaminated cumulates (accumulations of plagioclase + quartz plus a trapped liquid), whereas, others represent fractionated or evolved granitic melts.

There is a morphological, mineralogical and geochemical continuity from metatexite migmatites to diatexite migmatites and anatectic granites in the Ashuanipi subprovince, and this indicates that anatexis and crustal reworking in the Ashuanipi were an open system process at the smaller (e.g. pluton scale) but was probably closed at the larger scale (e.g thickness of the continental crust).

REMERCIEMENTS

Tout d'abord, ma reconnaissance et ma gratitude s'adresse à mon directeur de thèse, Ed Sawyer pour l'écoute, l'encouragement, la patience et le support moral qu'il m'a témoigné.

Je remercie aussi les membres de mon comité de recherche, Sarah-Jane Barnes et Alain Leclair pour les nombreuses critiques constructives lors de nos rencontres.

Un grand merci à Daniel Lamothe, qui m'a fait confiance en acceptant que je participe aux deux périodes de cartographie (Été 97, Été 98) dans le cadre du projet d'Ashuanipi et de travailler sur ce projet.

Je voudrais également remercier le Ministère des Ressources naturelles du Québec (MRNQ-Direction de la Géologie), pour le soutien financier accordé lors des travaux de terrain et de laboratoire.

Merci à mes ami(es) : Dr. Marie-Annick Forget pour avoir jeté un coup d'œil à la grammaire, Dr. David Dolejs pour avoir utilisé son "Least square" programme et Dr. Pierre Hudon pour ses conseils constructifs.

Enfin, je voudrais exprimer une sincère gratitude envers mon conjoint Ilyes Kouklas pour sa patience et son aide avec les figures ainsi que toute ma famille pour le soutien moral et les encouragements des dernières années.

Merci à Mira et Adam d'être à mes côtés.

TABLE DES MATIÈRES

LISTE DES TABLEAUX

LISTE DES FIGURES

CHAPITRE II. REGIONAL GEOLOGY (Figures 1 à 2)

CHAPITRE III. LARGE-SCALE MELT-DEPLETION IN GRANULITE TERRANES: AN EXAMPLE FROM THE ARCHAEAN ASHAUNIPI SUBPROVINCE OF QUÉBEC (Figures 3 à 13)

Figure 13. A model for the extraction of melt from granulites, based on the Ashuanipi subprovince. a) Distribution of melt (black), biotite (stripped), orthopyroxene (dotted), plagioclase and quartz (both unpatterned) in a typical metagreywacke rock. The melt occupies some of the space created by the destruction of reactant biotite, quartz and plagioclase. The location of melt is controlled by the distribution of biotite and is, therefore, primarily along the foliation planes. Melt pools in foliation plane 1 are better connected laterally than melt in foliation plane 2. Melt pools in foliation planes 3 and 4 are also connected along grain boundaries (X) orthogonal to the layering. Further cross-foliation interconnectivity of melt pools will occur at Y and Z when melt spreads along grain boundaries there, either because more melt is generated, or because driving forces cause melt movement. b) When melt movement (arrows) in the matrix (box) is primarily orthogonal to the layering the resulting migmatite consists of layers (beds) with residual compositions separated by layer-parallel leucosomes; note there are few leucosomes in the melt-depleted layers. c) If melt movement (arrows) in the matrix is primarily within the plane of the layer and towards dilatant sites forming as the layers deform, then the resulting

CHAPTER I

INTRODUCTION

1.1 PROBLEM

1.1.1 Migmatites and the generation of granites

The word "melt" describes a crystal-free silicate liquid, whereas magma refers to a silicate liquid which contains suspended crystals. Magmas with few crystals are dilute suspensions, whereas those with many crystals are concentrated suspensions. Felsic magma is a general term used to describe magma that is broadly granitic or tonalitic in composition and contains greater than 10 % of quartz. Magmas which have an initial bulk composition of granite (subequal amounts of K-feldspar, quartz and plagioclase) can give rise to more diverse bulk compositions through the effects of fractional crystallization. Felsic magma bodies may take the form of batholiths, sills, sheets, swarms of plutonic intrusions or migmatite complexes. They form a significant part of the surface exposure of the continental crust. In general, two types of magmatic theories explain the generation of granites: 1) the magmatic theory which states that granite is derived by the crystal fractionation of mafic magma through the steps outlined by Bowen (1928). Thus, if crystal fractionation of a magma of tholeiitic basalt composition were to occur, one of its end products would be granite. 2) The anatectic theory explains the origin of granite by the process of ultrametamorphism and partial melting of crustal rocks. Anatexis is defined as the melting, or remelting, of pre-existing rock. When such melting makes magmas of granitic composition, migmatites are commonly formed and are regarded as crucial, intermediate state, in the anatectic theory for the origin of granitic rocks. Migmatites are rocks consisting of a light coloured felsic component, called leucosome, a dark, or melanocratic, component called

a melanosome that collectively comprise the neosome, and an intermediate coloured component which represents non-melted rock and is called paleosome. There are a wide variety of ways in which these main components can be arranged; hence migmatites have diverse and complex morphologies. The neosome is the product of anatexis; in which case it may have formed by partial melting of the rock in place (*in situ*), or by the migration of the melt from its point of origin and into its present host rock.

1.1.2 Historical perspective

Two centuries ago, James Hutton visited the Caledonides in Scotland and described granite as having been forced to flow, in a state of fusion, among strata broken by a subterraneous force and distorted in every manner and degree (Hutton 1794). Since this statement, the study of migmatites and granites has evolved into two distinct subjects of research. Granites are within the scope of igneous petrologists, whereas migmatites are the preserve of metamorphic petrologists. This artificial division isolates most studies of granitic plutons from consideration of their source rocks, and so does not aid our understanding of the behavior of granitic magmas within the Earth's crust.

Migmatites and granites generated by crustal anatexis form the core of eroded orogenic belts of various age (e.g. Brown 1993; Menhert 1968; Powell 1983). The link between high grade metamorphism, migmatites and partial melting has led many workers to propose a model for high grade metamorphism in which the extraction of a

granitic melt has left refractory, anhydrous mineral assemblages (e.g. Fyfe 1973; White & Chappel 1977). The early reference given for the melting and melt extraction model is commonly Fyfe (1973), who for the Lewisian Complex suggested that granulites could be regarded as restites after the removal of relatively large amounts of partial melt. A substantial boost for the anatectic model came from the realization, based on experimental studies, that dehydration melting, i.e. vapour-absent incongruent melting of assemblages containing hydrous phases (e.g. muscovite, biotite and hornblende) is likely to be an important source of granitic melt in high grade metamorphic terranes (Brown & Fyfe 1970). Some authors (White & Chapell 1990; Clemens & Mawer 1992) argued that the progression from high grade metamorphic rocks to granites is not through migmatites, which they view as a separate sequence of processes. Furthermore, Le Breton and Thompson (1988) have argued that migmatites represent "failed granites", but their study does not solve the problem of how granite is generated because it does not consider all the aspects in generating a granitic magma. A genetic relationship between migmatite and granite was supported by Read (1956), Sawyer (1998), Vanderhaeghe (2000, 2001), Solar & Brown (2001), Ledru *et al.* (2001) and Milord *et al.* (2001) who demonstrated that some migmatites are transitional to granites. However, the mechanisms by which anatectic magmas formed in the deeper crust have evolved to the granitic magmas emplaced in the upper crust, is still poorly known.

1.1.3 Melt-residuum separation and its implication to crustal differentiation

Numerous field studies of regional metamorphic terranes show that partial melting of metapelitic rocks begins in the upper amphibolite facies and involves

muscovite, either with excess water or, more generally, without water present (Thompson & Algor 1977; Thompson & Tracy 1979; Patiño Douce & Harris 1998; Pickering & Johnston 1998; Clemens & Watkins 2001). Higher temperature anatexis involving the incongruent melting of biotite, or hornblende, without excess water, is generally considered to be the principal means of generating large volumes of water-undersaturated felsic melts and granulite facies mineral assemblages (Brown & Fyfe 1970; Fyfe 1973; Powell 1983; Ellis & Thompson 1986; Clemens & Vielzeuf 1987; Waters 1988; Clemens 1990; Vielzeuf & Montel 1994; Le Breton & Thompson 1988; Stevens & Clemens 1993; Patiño Douce & Beard 1995, 1996; Stevens *et al.* 1997). Many of the diagnostic mineral parageneses formed in the granulite facies are the more-or-less *in situ* solid products of melt-producing reactions. The fate of the melt fraction is complex, it could; 1) remain distributed throughout the source rock at its place of formation on the grain boundaries (e.g. Waters & Whales 1984) if the degree of melting is small, or there is no deformation to drive movement of the melt (Sawyer 1999), 2) remain in the vicinity of its source, but have migrated locally and collected into leucosomes and form a typical migmatite, and 3) have migrated out of its source region altogether leaving the middle and lower crust with a melt-depleted, or residual, composition. This last possibility corresponds to the large-scale process of crustal differentiation proposed by Lambert & Heier (1968) and Fyfe (1973) to explain the geochemical observation that the upper crust is enriched in SiO_2, K_2O, Cs, Pb, Rb, Cs and U relative to the lower crust which is enriched in TiO_2, Al_2O_3, FeO, MgO and CaO.

Not all rocks from granulite facies terrains have residual compositions (Barbey & Cuney 1982; Rudnick & Taylor 1987; Stevens *et al.* 1997). This may be because, at

the conditions of metamorphism, these rocks were infertile and did not partially melt, or that a melt fraction formed, but did not segregate. Alternatively, mafic magmas underplating, or intraplating, the lower crust may crystallize with granulite facies mineral assemblages and have non-residual compositions (Clemens 1990). In any case, melt undepleted, granulite facies rocks are not part of the large-scale mass transfer involved in crustal differentiation and granite magma-generating process envisaged by Lambert & Heier (1968), or Fyfe (1973), although non-restitic, granulite facies metagabbros in the lower crust may have contributed heat for crustal anatexis (Clemens 1990).

1.1.4 The metatexite-diatexite division in migmatites

The migmatites can be subdivided into metatexites and diatexites on the basis of their field appearances (Sawyer 1987, 1996). Thus, metatexite migmatites still retain the gross primary fabric (e.g. bedding, compositional and lithological layering) of the country rock (i.e. the paleosome). In contrast the diatexite migmatites show widespread textural modification and have lost their pre-anatexis structures, such as continuous bedding or foliation, but have the widespread development of flow structures (Brown 1973, Sawyer 1996). Metatexites include rocks that have been affected by limited amount of partial melting as well as rocks affected by much larger degrees of partial melting, but with segregation efficient enough to keep the partially molten rock below the threshold for transition to melt-dominated rocks (Sawyer 1994). These various types of metatexites can be distinguished on the basis of the morphology of their pre-anatexis structures. However, the morphology of diatexites was acquired in the

magmatic state (Brown 1973; Burg & Vanderhaeghe 1993; Menhert 1968; Sawyer 1994), and they contain a variety of enclaves that represent highly disrupted layers which correspond to refractory layers, or to melanosomes (Menhert 1968). The transition from rock-dominated metatexite to melt-dominated diatexite migmatites is correlated with the disruption of the solid crystal framework (Sawyer 1994; Vanderhaeghe 2001b) in the melt-bearing rock. Therefore, the most important factor in the transition from metatexite to diatexite in migmatites is the development of a pervasive melt fraction throughout a substantial rock volume (Brown 1973) and this may not be simply due to a higher degree of partial melting (Sawyer 1996). Two principal processes occur in the presence of a pervasive melt. 1) The coarsening of grain size and the development of igneous-like textures (Platten 1982, 1983), and 2) the bulk flow of melt and residuum, which consequently destroys the crystal framework. Thus, the transition from metatexite to diatexite also marks a change in crustal rheology, metatexite migmatites represent the rheology of a solid, albeit a weaker one, whereas diatexite migmatites have the rheology of a magma (Sawyer 1996, 1998). However, we should always question ourselves where does the melt fraction in a diatexite migmatite come from? It could be the result of a high degree of *in situ* partial melting of the protolith (e.g. Brown 1973), or it could be the result of the movement of melt within the anatectic region. Movement could involve only local redistribution, or it could involve injections of a magma from an external source, to increase the proportion of the melt in the anatectic region and so form a diatexite migmatite as suggested by Greenfield *et al.* (1996) who called these hybrid diatexites. Alternatlively, anatectic melt may move within its source, accumulating in some places and being depleted in others (Stevenson 1989; Sawyer 1996, 1998; Sawyer *et al.* 1999).

An interesting question that arises at this point is; which migmatites might represent the source regions of granites?

1.1.5 Conditions for melt segregation and magma mobility

Only melt segregation is required to form metatexite migmatites, whereas magma mobility alone with, or without, melt segregation is necessary for diatexite migmatites. For either melt segregation or magma mobility to occur there must be a differential movement between the melt and residuum, or between melt and its entrained crystals (in magma) relative to a pre-melting reference frame (Sawyer 1996). The velocity of the melt-rich part V_m and that of the residuum V_s were used by Sawyer (1996) in order to consider this differential movement. Indeed, when $V_m > V_s > 0$ both the melt and the residuum move (magma mobility), but because the melt fraction has the greater velocity, melt segregation also occurs and diatexites form. Such diatexite migmatites are more likely to represent the source regions of granitic magmas than metatexite migmatites because melt segregation and movement of melt at this stage are conducive to large scale processes.

Finally, the questions that remain are: how did the melt segregate from its residue and how much melt is needed to make segregation possible?

The volume of neosome (melt + residuum, or leucosome + melanosome) increases relative to the paleosome as temperature rises. In addition, the morphology of migmatites depends critically on the interplay between the rate of melting and the rate of melt segregation, i.e. whether melt segregation or melt accumulation occurred

(Sawyer 1994). Consequently, the morphology of a migmatite changes as anatexis progresses. If the melt fraction accumulates in the matrix, then once the melt fraction reaches a threshold of about 20 to 30 % (Wickham 1987; Vigneresse *et al.* 1996) magma (crystals suspended in melt) flow occurs, and a diatexite migmatite forms. This type of flow results in the destruction of pre-anatectic structures. If, on the other hand, the melt fraction is continually drained from the matrix and does not accumulate, then a different type of migmatite, one dominated by residual rocks but containing leucosomes with little entrained residual material, is formed. In this type of process, anatectic structures are preserved, but the protolith bulk composition is not. Some melanosomes in metatexite migmatites formed in this way (Tait & Harley 1988; Barbey *et al.* 1989; Nédélec *et al.* 1993; Shimura *et al.* 1998). Petrographic evidence from a number of melt-depleted rocks has shown that melt formed first on grain boundaries in the matrix of the protolith, but was then drained from these grain boundaries through a branch-like network of channels and into an array of mesoscopic channels, preserved as leucosomes (Brown *et al.* 1999; Sawyer 2001; Holness & Watt 2002; Marchildon & Brown 2002). Broad-scale concepts of how granulite terranes may be related to granites have been developed (e.g. Clemens 1990). However, it remains to be determined if the hand sample- and outcrop-scale processes of melt segregation and migration combine at much larger scales to generate voluminous granite magma and large, melt-depleted granulite terrains; understanding the latter is fundamental to understanding crustal differentiation (Vielzeuf *et al.* 1990).

1.1.6 The choice of a study area

The Ashuanipi subprovince is particularly appropriate to this kind of study as it represents a very large (90 000 km^2), high grade, granulite facies terrane of metasedimentary migmatites in which a large degree of partial melting occurred (Eade 1966; Chevé & Brouillette 1995; Lapointe 1996; James 1997; Percival 1993, Leclair *et al.* 1998a, 1998b). Furthermore, the distribution of the metasedimentary rocks, the migmatites derived from them, and the associated monzogranites is now reasonably well known following regional mapping done by the Ministère des Ressources naturelles du Québec (Leclair *et al.* 1998a, 1998b; Lamothe *et al.* 1998, 2000; Thériault & Chevé 2001) which makes the Ashuanipi an ideal area to understand how melt-depleted granulites formed.

1.1.7 Objectives

This study will be principally focused on the origin of the migmatites in the Ashuanipi subprovince of Quebec and how the generated magma evolved to produce granitic rocks. In other words, we would like to understand the generation of magma and residual material during an anatectic event. Partial melting of the lower crust and the transfer of the melt towards the upper crust is probably the main cause of the compositional differentiation of the continental crust (Fyfe 1973). However, the most important step in the transition from a partially molten source to a differentiated magma is the physical separation of a large volume of magma from its residue (Sawyer 1996). Unfortunately, the exact nature of this separation is not clear yet, and its understanding

could be an asset to explain crustal differentiation. In general, this study tackles the fundamental problem of how partial melting at low- to mid-crustal depths generates migmatites, granulites and granite.

1.2 METHODOLOGY AND THESIS ORGANIZATION

The genetic history of magma starts when its protolith undergoes partial melting, and ends when all its products are fully crystallized. Migmatites are good examples of rocks that were partially molten, whereas granitic intrusions display structures formed when magma crystallized (Vigneresse *et al.* 1996).

The starting point in understanding the relationship between migmatites and granites in the Ashuanipi subprovince, is the field relationships amongst the main rock types. Deciphering the processes involved in creating these relationships are best addressed from petrographic and geochemical observations.

Detailed field observations will allow us to determine; 1) morphological continuity or discontinuity from protolith though migmatite to granite and; 2) the nature of the protolith that generated migmatites. Mapping at 1/250 000 scale in the study area was done during two summers of field work, and established the spatial distribution of diatexite migmatites with respect to the granite bodies, and the nature of their contacts.

Precise sampling has been done in order for petrographic and geochemical analysis. The fresh samples included in this study are of three different rock types,

metasedimentary granulite, diatexite migmatite and monzogranite. A key part of the petrographic study was the identification of both, macroscopic and microscopic structures that can be used in to identify which rocks are residual, which were derived largely from anatectic melt and, within these, which rocks may represent accumulations of crystals.

Whole rock geochemistry will be used to model the partial melting process, and to test the evidence for continuity from metasediment through diatexite migmatite to granite. However, it is important to mention that in such terranes, where melting has been extensive, it is difficult to identify the paleosome, and unmodified melt compositions.

Chapter II of this thesis describes the regional setting of the Ashuanipi subprovince, the local geology, the lithologic units and their respective ages, as well as the structure and metamorphism in the region.

Chapter III documents the melt-depleted, granulite facies migmatites which occur over a very large area (90 000 km^2) in the Ashuanipi subprovince of northern Québec. Petrographic and geochemical data are used to estimate the degree of partial melting and melt depletion from individual samples and, when combined with the results of regional mapping, to estimate the volume of melt lost from this granulite terrane. The geometry of the melt-loss process is examined using thin section and outcrop-scale observations of the distribution of former anatectic melt. Finally, a general model is proposed for the extraction of melt from partially melted middle and lower crust. This

contribution focuses on the residual rocks and is part of a paper published in Journal of Metamorphic Geology (Guernina & Sawyer 2003).

Chapter IV concentrates on the evolution of the extracted melt, its fractional crystallization and its contamination by the surrounding melt-depleted rocks to form diatexite migmatites. We focus mainly on the changes in microstructure, mineralogy and bulk geochemistry caused by successive segregation of melt during crystallization within diatexite migmatite. Geochemical modelling is used to explain the compositional trends in the whole rock geochemical data set and the mixing trends in the suite of diatexite migmatite samples.

Chapter V demonstrates the fractionation of diatexite migmatite to parautochthonous monzogranite, using morphological, petrographical and geochemical data. Major and trace element modelling is used to show the relationship between diatexite migmatites and their associated monzogranites.

Chapter VI presents a model for the formation of migmatites and granite in the Ashuanipi subprovince and discusses some of the recent findings by others working on the migmatite to granite transition.

Chapter VII includes the general conclusions of the whole thesis.

CHAPTER II

THE REGIONAL GEOLOGY

2.1 THE REGIONAL SETTING

The Ashuanipi subprovince (Fig. 1) of Québec is located at the northeastern end of a 2000 km long metasedimentary belt that crosses the entire Archaean Superior province (Card & Ciesielski 1986; Percival *et al.* 1992). It is bounded to the east by early Proterozoic rocks of the Labrador Trough, and to the southeast by Archaean and Proterozoic rocks reworked during the Grenville Orogeny. Other boundaries are with Archaean rocks little affected by Proterozoic deformation; the La Grande subprovince to the northwest and the Opatica subprovince to the south. Both of these consist predominantly of plutonic rocks, and are believed to be eroded, late-Archaean volcanic arcs (Leclair *et al.* 1998a, 1998b).

Based on the similarity of rock types and sedimentary features, Percival (1989) suggested that the Quetico, Nemiscau, Opinaca and Ashuanipi subprovinces (Fig. 1) are remnants of a single, late Archaean accretionary prism. The deposition of sediments in the Quetico subprovince has been tightly constrained between the youngest detrital zircon ages *ca.* 2698 Ma, and the oldest plutons *ca.* 2687 Ma that intrude the metasediments (Percival & Sullivan 1988; Davis *et al.* 1990; Fralick & Davies 1999; Zaleski *et al.* 1999). Percival *et al.* (1992) argued for a similar age of sediment deposition in the Ashuanipi subprovince, bracketed by the youngest detrital zircons, 2700 Ma, and the 2690 Ma zircon crystallization age (Percival 1991a; Chevé & Brouillette 1991) of the Desliens igneous suite that intrudes them. In contrast, the age of sediment deposition in the Opinaca and Nemiscau subprovinces is poorly constrained.

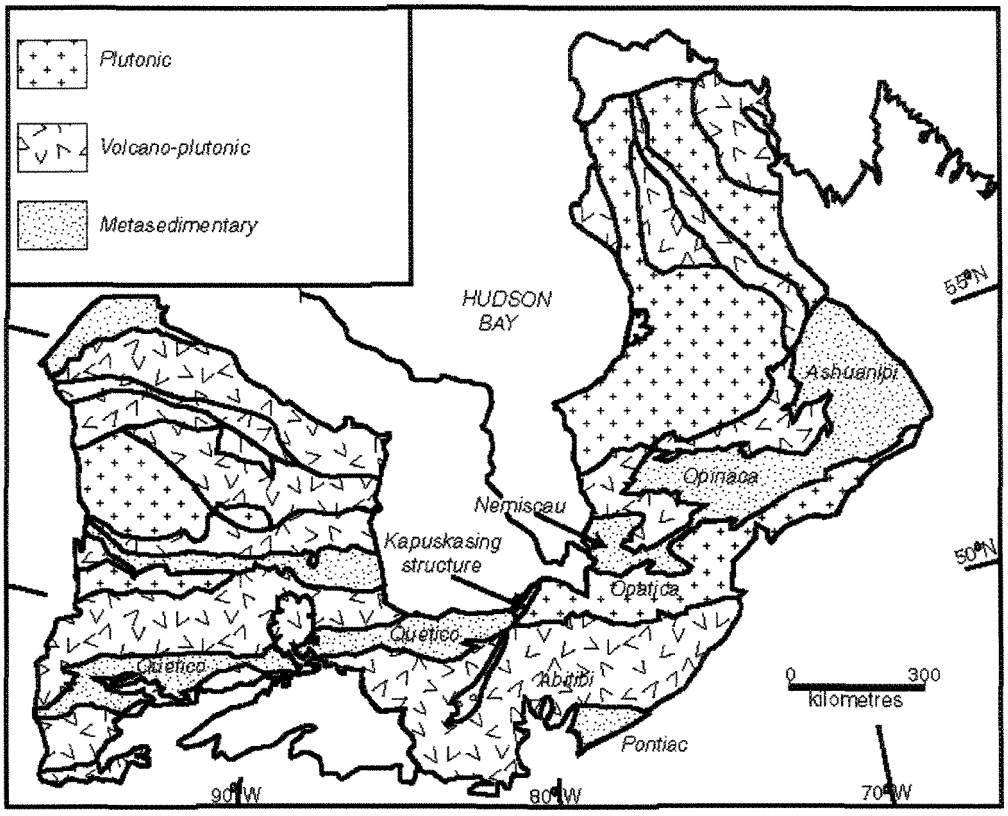

Figure 1. Simplified geological map of the Superior province modified from Percival (1989) showing the location of the Ashuanipi subprovince at the eastern end of the Opinaca, Nemiscau and Quetico line of metasedimentary belts.

Detrital zircons from a conglomerate in the Opinaca subprovince yield a very imprecise U-Pb age of 2648+/-50 Ma (Gouthier *et al.* 2001a), and the minimum deposition age is better constrained by the 2674+/-12 Ma, U-Pb zircon crystallization age (Goutier *et al.* 2001b) of the Bezier pluton, which intrudes the Opinaca metasediments. The upper age limit of sediment deposition, *ca.* 2700 Ma, is constrained by several U-Pb ages obtained from deformed plutons and volcanic rocks at the edge of the Opinaca subprovince (Moukhsil *et al.* 2003). Metasedimentary rocks in the Nemiscau subprovince are continuous with the Opinaca subprovince (Moukhsil *et al.* 2001) and have a minimum deposition age of 2672+/-2 Ma, the age of granite intruded into the Nemiscau metasediments (Davies *et al.* 1995). Thus, deposition of sediments in the Quetico, Nemiscau, Opinaca and Ashuanipi subprovinces was believed to have occurred in a short time interval between 2698 Ma and 2688 Ma (e.g. Percival *et al.* 1992). However, Percival *et al.* (2003) present SHRIMP U-Pb zircon data from a tonalite belonging to the Desliens igneous suite, and interpret oscillatory zoned zircons as recording the 2723 to 2725 Ma crystallization age of the pluton, and a group of featureless zircons with ages between 2700 and 2691 Ma as being metamorphic. Interpretation of the oscillatory zoned zircons may not be so simple as they do not show a systematic progression of ages from core to rim, some zircons (e.g. A-15, Percival *et al.* 2003) appear to have cores younger (2698+/-7 Ma) than the crystallization age. If the Desliens igneous suite is *ca.* 2725 Ma old, then the sediments in the Ashuanipi subprovince are older than those in the Quetico subprovince. However, this does not preclude them from having similar metamorphic ages and compositions to the metasediments in the Quetico subprovince.

Lapointe (1996) noted that the major and trace element composition of metasediments in the northeastern Ashuanipi subprovince were very similar to metasediments from the Quetico subprovince. A statistical comparison of the major and trace elements composition of non-anatectic metasediments in the southeastern Superior province (Doyon 2004) indicates that the Quetico, Nemiscau and Opinaca metasediments are indistinguishable, but metasediments from the Pontiac subprovince, the Beardmore-Geraldton belt and from sedimentary basins within the Abitibi subprovince are significantly different. Thus, notwithstanding that the Ashuanipi subprovince may possibly be older, its sediment composition and age of metamorphism are very similar to those of the Quetico subprovince.

2.2 THE PRINCIPAL ROCK TYPES

The distributions of the principal rock types in the Ashuanipi subprovince is shown on Fig. 2 compiled from new (Lamothe 1998, Leclair *et al.* 1998a; 1998b; Thériault & Chevé 2001) and older detailed mapping (Percival 1991a & b, 1993). There are seven principal map units.

1) *Metasediment;* the oldest unit recognised consists of widespread, migmatitic, siliclastic metasediments (paragneiss of other workers); deposition ages are 2700 to 2690 Ma, but possibly as old as 2725 Ma (see above). Typically, the metasediments consist of thick (5 to 50 cm), pale-coloured, metagreywacke layers containing orthopyroxene + biotite + quartz + plagioclase and thin, (1 to 5 cm) darker, metapelite

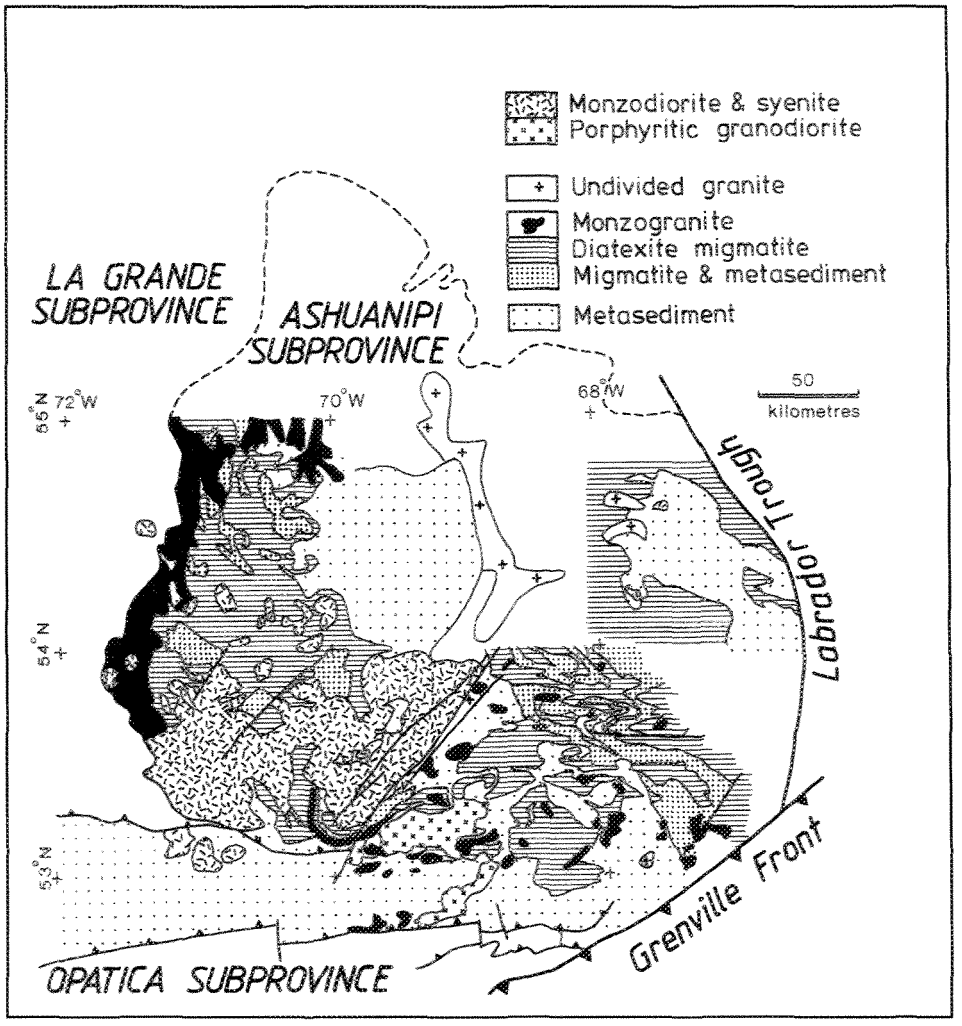

Figure 2: Simplified geological map of the southern and central parts of the Ashuanipi subprovince showing the distribution of metasedimentary rocks (dominated by metagreywacke), migmatites derived from them, monzogranite and undivided granitic rocks formed during the same anatectic event, and younger intrusive rocks of granodiorite, monzodiorite and syenite compositions. Compiled from new mapping carried out by the Ministere des Ressourses naturelles du Québec (Lamothe et al. 1998; 2000; Leclair *et al.* 1998b; Thériault & Chevé 2001).

layers containing quartz + plagioclase + biotite + garnet + corderite + K-feldspar +/- orthopyroxene; metagreywacke layers dominate (>85%). In places graded bedding is still preserved as a gradational passage from metagreywacke bottoms to metapelite layer tops. Very rarely, in the least deformed areas, wispy laminae are preserved in the upper parts of some metagreywacke layers; these may represent relic ripple laminations. Thin metasedimentary layers that contain quartz + biotite + clinopyroxene + plagioclase +/- hornblende +/- orthopyroxene occur locally, and are interpreted to be the granulite facies equivalent of rare, but widespread, high CaO/K_2O calc-silicate, or tuff, layers described in other Archaean turbidite sequences; e.g. the Quetico subprovince (Pirie & Mackasey 1978), and the Slave province (Ramsey & Kamineni 1977). There are some minor differences in the northeastern Ashuanipi subprovince, garnet is common in the metagreywacke layers there, and sequences of alternating, thinly bedded quartz-rich and iron-rich layers are more common (Lapointe 1996). Metamorphosed mafic and ultramafic layers are widespread, but not abundant (<1%) in the metasediments. Most metabasites are coarse-grained orthopyroxene + clinopyroxene + hornblende + plagioclase rocks of undetermined origin, but locally, pillow structures are preserved indicating that some were lava flows. Rare, thin bands of coarse-grained, massive, ultramafic rocks may be metakomatiites, but Cadéron *et al.* (1999) have suggested that they are fragments of oceanic crust.

2) *Migmatites and metasediments;* these are the same as (1) above, except that the proportion of leucosome is greater, mostly due to the injection of granitic melt, and consequently bedding is less evident.

3) *Diatexite migmatites;* these are abundant in the Ashuanipi subprovince (Fig. 2) and have the mineral paragenesis orthopyroxene + biotite + quartz + plagioclase +/- K-feldspar +/- garnet. The diatexites are coarse-grained rocks and occur as sheets ranging from several to hundreds of metres thick oriented subparallel to the layering in the metasediments or, as kilometre-scale intrusive bodies. Contacts with the metasediments range from gradational to intrusive. All the diatexites contain between 2 and 50 vol % metasedimentary enclaves.

4) *Monzogranite;* bodies (the Gamart suite of Leclair *et al.* 1998a) of monzogranite occur at all scales, from leucosomes to plutons, throughout the Ashuanipi subprovince. They are spatially associated with the diatexite migmatites from which they may have been derived. The monzogranite bodies are leucocratic with a distinctive porphyritic texture, and in places contain biotite schlieren. At the scale of Fig. 2, the largest monzogranite bodies are equant intrusions a few kilometres long, but along the western edge of the Ashuanipi subprovince monzogranite forms an extensive sheet along the contact with the La Grande subprovince (Thériault & Chevé 2001).

5) *Undivided granite;* this map unit comprises many small intrusions and a few larger bodies of granite and granodiorite of uncertain origin, possibly derived by anatexis of the metasediments, but they fall outside of the diatexite-monzogranite textural suite.

6) *Porphyritic granodiorite;* the Dusterlo and Delmothe plutons (*ca.* 2638 Ma Lamothe *et al.* 1998) consist of coarse-grained, porphyritic granite/granodiorite that are locally melanocratic, and contain rare microgranular inclusions.

7) *Monzonite and syenite;* this division consists of three plutonic suites believed to be unrelated to anatexis of the metasediments; a) plutons of coarse grained tonalite 2636 Ma, b) Niaux suite (2625+/-3 Ma, Chevé & Brouillette 1992) of nepheline syenites, monzonites and monzodiorites, and c) Viau suite (2571+/-2 Ma, Parent 1998) of small alkali granite and syenogranite intrusions.

The oldest intrusive rocks in the Ashuanipi subprovince belong to the Desliens igneous suite (Percival 1991a), not shown because the intrusions are too small to show at the scale of Fig. 2. However, the Desliens igneous suite is widely distributed along the eastern and southern edge of the Ashuanipi subprovince (Thériault & Chevé 2001). The common rock type of the Desliens igneous suite in the central part of the Ashuanipi subprovince is a grey, fine-grained, strongly foliated, biotite + orthopyroxene + quartz + plagioclase tonalite that occurs as sheets intruded parallel to the compositional layering in the metasediments. Rocks of the Desliens igneous suite have undergone local partial melting, but generally have fewer leucosomes than their host metasediments (Percival 1991a). The Desliens tonalites have a similar mineralogy to the host metasediments, but are distinguished by their lighter colour, greater uniformity and the lack of a compositional alternation corresponding to the metagreywacke-metapelite interlayering.

2.3 THE STRUCTURE

Structural style in the metasedimentary belts changes across the Superior province. In the western part of the Quetico subprovince the principal foliation (S_2) and bedding (S_0) are predominantly subvertical, but downwards- and sideways-facing fold

closures indicate an early (D_1) set of recumbent fold nappes (Poulsen *et al,* 1980; Sawyer 1983). In the deeper crustal levels exposed in the Nemiscau and Opinaca subprovinces, the bedding and a penetrative foliation generally dip moderately, or gently, to the northwest, and asymmetric shear sense indicators give a dominant north-over-south movement sense (Sawyer & Benn 1994). Late- to post-anatexis structures include low-angle normal faulting and subvertical strike-slip and oblique-slip shear zones of various trends.

The southern Ashuanipi subprovince is dominated by gently to moderately north-dipping bedding (S_0) and subparallel (S_1) foliation in the metasedimentary rocks. Many diatexite migmatites occur as sheets subparallel to the compositional layering (bedding S_0) in their hosts. Systematic changes in the orientation of S_0 and S_1 between adjacent metasedimentary enclaves in the diatexite sheets reveals asymmetric, south-vergent F_2 folds. The magmatic foliation in the diatexite migmatites is S_2, and the shear sense derived from asymmetric enclaves, schlieren, and the tiling of feldspar crystals is consistently south-vergent in the diatexites, the same as in small-scale asymmetric F2 folds in the adjacent metagreywackes. This suggests that anatectic melt was segregated into south-vergent thrust planes formed during F_2. Moderately to steeply dipping shear zones with northeast, north and northwest trends developed during, and after, the south-vergent thrusting; anatectic melt was also segregated into these shear zones. Large F_3 folds in the Ashuanipi subprovince have approximately east-trending axial planes and represent a late-stage of regional contraction which locally reoriented S_0, S_1, and S_2. Structural style changes across the Ashuanipi subprovince; Percival (1991b) and Lapointe (1996) mapped subcircular domains of steeply dipping foliation some 150 to

200 km farther north. Prominent discontinuities in the foliation trajectories in that region (Lapointe 1996) indicate the presence of major east-trending shear zones. The structural pattern from the Quetico to the Ashuanipi subprovinces indicates that anatexis occurred in a dextral, oblique contractional tectonic setting. Similar timing relations between thrusting and strike-slip shearing and the segregation of anatectic melt have been described from the late-Precambrian St. Malo migmatite terrane where crustal anatexis occurred during oblique, sinistral, contractional deformation (Brown 1979; 1995).

2.4 THE METAMORPHISM

Peak metamorphic temperatures increase from west to east along the Quetico, Nemiscau, Opinaca and Ashuanipi subprovinces, which Percival (1989) linked to a systematic tilting of the Superior province that exposes deeper crustal levels in the east. Northwest of Lake Superior the highest grade rocks in the Quetico subprovince record 2.5 to 3 kbar and 670°C upper-amphibolite facies metamorphism (Sawyer 1986). Farther east, metamorphic conditions in the centre of the Nemiscau subprovince reached the "orthopyroxene in" isograd and some metagreywackes contain small amounts of orthopyroxene (Sawyer unpublished data). The Opinaca subprovince recorded slightly higher metamorphic temperatures and many metagreywacke rocks contain small amounts of relict orthopyroxene, however, retrogression to amphibolite and greenschist facies assemblages is extensive. New (Lamothe et al. 1998, 2000; Leclair *et al.* 1998a, 1998b; Thériault & Chevé 2001) and older mapping (Eade 1996; Stevenson 1964; Fahrig 1967; Lapointe 1996; Percival 1993; Chevé & Brouillette 1995; James 1997)

shows that the Ashuanipi subprovince is a large, high-grade, granulite facies terrane; migmatitic metagreywackes are widespread and contain the paragenesis orthopyroxene + biotite + plagioclase + quartz + former melt +/- garnet. Percival (1991b) estimated metamorphic temperatures in the northeast to be 700 to 825°C and pressures 6 to 6.5 kbars. Biotite is not present in some metagreywackes in the central part of the Ashuanipi subprovince, indicating that locally metamorphic temperatures were higher there and exceeded the "biotite-out" isograd.

Regional amphibolite facies metamorphism in the Quetico subprovince occurred between 2671 and 2665 Ma in the Thunder Bay area (Percival & Sullivan 1988). Pan *et al.* (1998) obtained U-Pb zircon ages of 2666+/-1 Ma from a pegmatite and 2650+/-1 Ma from a metabasite from a granulite facies region within the Quetico subprovince near Manitouwadge; they interpreted these as dating high-grade, progressive metamorphism and the peak of granulite facies metamorphism respectively. Zaleski *et al.* (1999) found crystallization ages as young as 2640 Ma for late granites and pegmatites in the same area, and suggested that regional metamorphism in the Quetico subprovince was a single, protracted event lasting 40 million years. Percival *et al.* (1992) interpreted U-Pb zircon dates from diatexite migmatites in the northeastern Ashuanipi subprovince as indicating high grade metamorphism there between 2682 Ma and 2668 Ma. Leclair *et al.* (1998a) found a similar zircon age range (2675 to 2664 Ma), and also a younger 2633 +6/-4 Ma age from diatexites migmatites in the central and southern Ashuanipi subprovince. Furthermore, Parent (1998) obtained a 2647+/-2 Ma zircon U-Pb crystallization age for the Gamart suite of monzogranite plutons, which textural and geochemical evidence suggests, may have been derived from the diatexite

migmatites by fractional crystallization (Thériault & Chevé 2001). These results suggest that metamorphism in the Ashuanipi was also a protracted event, lasting 40 or 50 million years, coeval with metamorphism in the Quetico subprovince. Other long-lived granulite facies metamorphic events have been identified in the Reynolds Range (Rubatto *et al.* 2001) and the Nagssugtoqidian orogen (Willigers *et al.* 2001).

Cadéron (Université du Québec à Montréal, UQAM) has completed a PhD thesis on some tectonic and metamorphic aspects of rocks from part of the Ashuanipi subprovince. Although, the study carried out by Cadéron covers, at least in part, the same area as this study, we are not permitted either to read or to quote her thesis because of a two year period of confidentiality on the work.

CHAPTER III

LARGE-SCALE MELT-DEPLETION IN GRANULITE TERRANES: AN EXAMPLE FROM THE ARCHAEAN ASHUANIPI SUBPROVINCE OF QUÉBEC

PART OF PUBLISHED PAPER: Guernina & Sawyer 2003. *Journal of Metamorphic Geology 21, 181-201*

In this chapter we use field, petrographic and geochemical methods to estimate how much granitic melt was formed and extracted from a granulite facies terrain, and to determine what the grain- and outcrop-scale melt-flow paths were during the melt segregation process.

3.1 POSSIBLE PROTOLITH COMPOSITION

The interpretation of modal and compositional trends in partially melted rocks requires knowledge of their starting composition. Unlike the other metasedimentary subprovinces the Ashuanipi does not have low metamorphic grade margins, therefore, it is unlikely that metasediments that could be used to define the pre-anatexis protolith composition, are preserved there. The composition of an average Archaean greywacke could serve as a model protolith. However, we prefer to use sediments derived from the same source region, i.e. the *ca.* 2700 Ma southern edge of the Superior craton. The similarity in sediment type between the Quetico, Nemiscau, Opinaca and Ashuanipi subprovinces, and in composition between the Ashuanipi and Quetico have been noted by Percival (1989), Lapointe (1996) and Doyon (2004). Therefore, since only the Quetico metasediments are presently well characterized (Sawyer 1986 and unpublished data) they will be used as the protolith composition for the Ashuanipi.

Typically, bedding is preserved in the Quetico metasediments and indicated by changes in colour (Fig. 3a) and, in places, graded bedding, gradational contacts, Bouma sequences and locally, rip-up clasts and sedimentary slump structures are also

preserved. Mineral assemblages in the metagreywackes are simple; those from the greenschist facies contain biotite + quartz + plagioclase ± chlorite ± muscovite (minor), whereas, those from the lower and middle amphibolite facies contain biotite + quartz + plagioclase ± garnet (minor). There are two variations; 1) rare metagreywackes contain trace amounts (<1 %) of muscovite and, 2) some metagreywackes contain biotite + quartz + hornblende + plagioclase +/- clinopyroxene +/-garnet, in the amphibolite facies. The average modal composition of 30 metagreywackes is 28 % quartz, 30 % biotite and 42 % plagioclase (Sawyer 1986). Greenschist facies metapelitic rocks contain the mineral assemblage biotite + chlorite + muscovite + quartz + plagioclase. Chlorite is generally in excess over muscovite, thus, although they may contain aluminosilicate, staurolite and/or cordierite in the amphibolite facies, most lack muscovite.

3.2 ANATECTIC METASEDIMENTS IN THE ASHUANIPI SUBPROVINCE

The metasedimentary rocks in the Ashuanipi subprovince are migmatites and the principal variation from outcrop to outcrop is in the proportion of leucosomes.

3.2.1 Metasediments with many leucosomes

Typical outcrops of metasediment with many leucosomes contain about 20 % leucosomes (Fig. 3b). In these outcrops some metagreywacke layers contain lens-shaped leucosomes, oriented normal to the layering and surrounded by wide orthopyroxene + quartz + plagioclase selvedges that suggest *in situ* melting with only

Figure 3a: Greenschist facies metagreywacke and interbedded metapelite, Quetico subprovince.

short-distance melt migration. More commonly, thin (< 2 cm) leucosomes, without melanocratic selvedges, are parallel to the foliation and bedding (Fig. 3b).

Other leucosomes, typically 2 to 5 cm, but up to 15 cm wide, are subparallel to the foliation, and either have thin melanocratic selvedges (generally biotite-rich), or none at all, suggesting that the melt was injected. Some outcrops have abundant (30 to 50 %) leucosomes, dominated by slightly discordant leucosomes without melanocratic selvedges, which suggests that these outcrops are sites of net melt accumulation. In general, all the leucosome types contain few mafic minerals.

3.2.2 Metasediments with few leucosomes

The outcrops containing leucosomes related to only the melt extraction process are critical to understanding melt segregation processes. Therefore, this section summarises observation on outcrops without significant melt addition, i.e. leucosomes resulting from melt injection are absent.

Such outcrops occur throughout the Ashuanipi subprovince and are common in its central and southern parts. These outcrops have a compositional banding interpreted to be bedding, but very few (< 5 %) leucosomes (Fig. 3c). Typically the leucosomes occur either as; 1) thin (1 to 5 mm) discontinuous layers parallel to the compositional layering, 2) as short (1 to 5 cm), thin lenses in small, layer-scale shear bands, 3) small (1 to 3 cm), narrow irregular shaped bodies in the space between boudinaged

Figure 3b: Granulite facies metagreywacke rocks with many leucosomes, most are parallel to the bedding and foliation; southern Ashuanipi subprovince. Width of the photograph corresponds to 2 metres.

metasedimentary layers or, 4) small (< 1 cm) patches in the pressure shadows around competent minerals, such as garnet or orthopyroxene. In some outcrops leucosomes occupying different structural sites are linked together for several tens of centimetres along the direction of the layering. None of these leucosomes have melanocratic selvedges, they occur in metagreywackes with modal compositions typically around 13 % quartz, 10 % orthopyroxene, 17 % biotite and 60 % plagioclase. A few outcrops, still with compositional layering, have metasediments with more extreme modal mineralogies. In these, some metagreywacke layers are nearly devoid of quartz or biotite, but all have abundant (15 to 18 modal %) orthopyroxene. The absence of leucosomes in these outcrops suggests that they have lost almost all the melt fraction that was generated in them.

3.3 PARTIAL MELTING IN THE ASHUANIPI SUBPROVINCE

Clemens & Vielzeuf (1987) and Thompson (1996) have shown that metapelites can produce more melt than metagreywackes, but the paucity of metapelites in the Ashuanipi subprovince means that melting, melt segregation and melt volume there was determined by the Al-poor metagreywackes. Therefore, this study now concentrates on the metagreywacke rocks.

3.3.1 Microstructural and modal variations

Figure 3c: Granulite facies metagreywacke with few leucosomes; central Ashuanipi subprovince.

The metagreywackes are generally medium to fine grained (0.7 to 1 mm) rocks with granoblastic-polygonal microstructures and simple biotite + plagioclase + quartz + orthopyroxene + accessory minerals (opaque oxides, sulphides, zircon, apatite) parageneses; 8 to 10 modal % orthopyroxene is typical. The schistosity is defined principally by the preferred orientation of biotite, but in most rocks orthopyroxene has a shape-preferred orientation parallel to that of biotite. Compared to the low-grade metagreywackes from the Quetico subprovince (Fig. 4a), there is a systematic textural change to coarser grain size and polygonal (foam) microstructure as orthopyroxene and plagioclase contents increase, and quartz + biotite contents decrease (Figs. 4b & c). Quartz is generally equant and polygonal, but in some rocks has conspicuous undulose extinction and irregular grain boundaries indicating grain boundary migration. Plagioclase grains commonly exhibit minor zoning, and are not antiperthitic.

Small (3 to 5 mm), subidioblastic porphyroblasts (poikiloblasts in some rocks) of strongly pleochroic orthopyroxene surrounded by biotite and quartz-depleted, plagioclase-enriched halos are developed in some metagreywacke layers (Fig. 4d); some halos contain minor amounts of K-feldspar. Biotite-poor, K-feldspar-rich halos are developed in some pelitic rocks around aggregates of orthopyroxene + cordierite. Percival (1991a) noted biotite-depletion halos around orthopyroxene in the northern Ashuanipi subprovince, and regarded them as indicating metamorphic growth of the orthopyroxene.

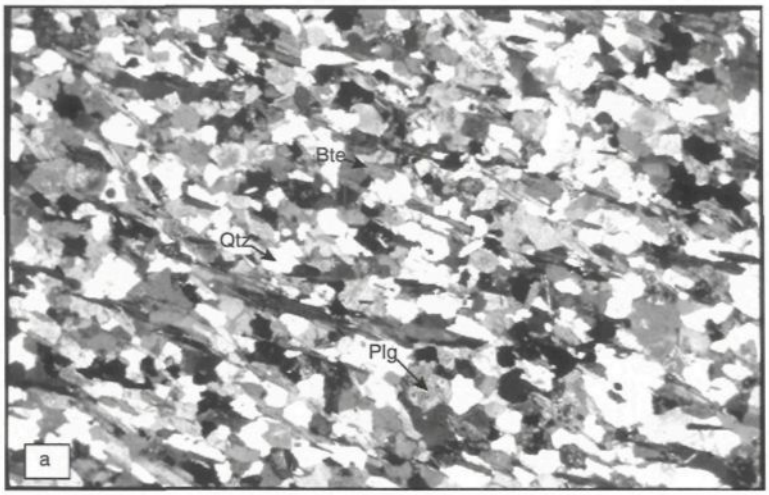

Figure 4a: Typical, non-melted, amphibolite facies metagreywacke from the Quetico subprovince showing a well developed granoblastic-polygonal microstructure.

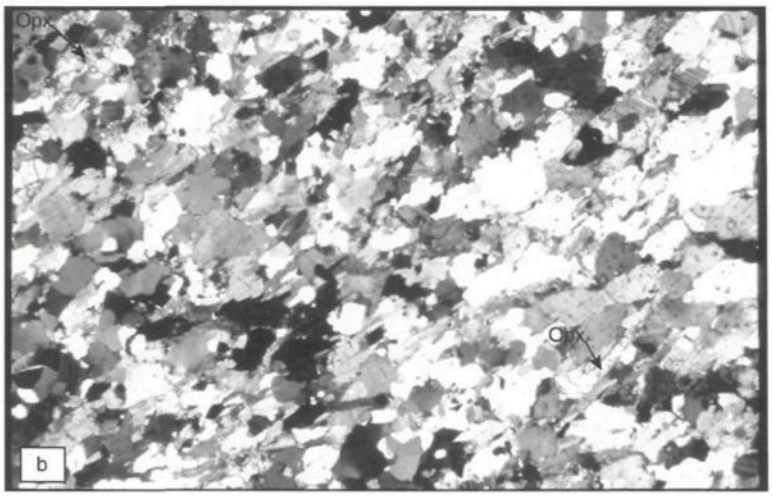

Figure 4b: Metagreywacke (227) with 8 % orthopyroxene from the Ashuanipi subprovince, note the increased grain size and greater proportion of straight grain boundaries on the plagioclase grains.

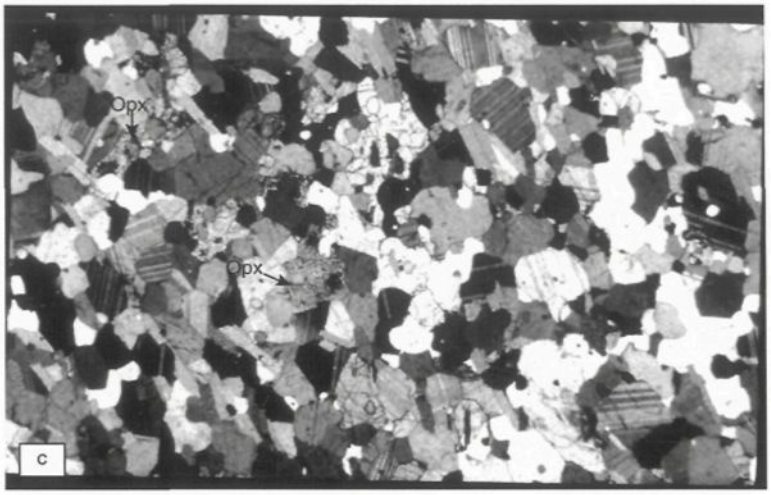

Figure 4c: Metagreywacke (5099A) with 13 % orthopyroxene from the Ashuanipi subprovince showing lower modal quartz and higher plagioclase contents in the orthopyroxene-rich parts.

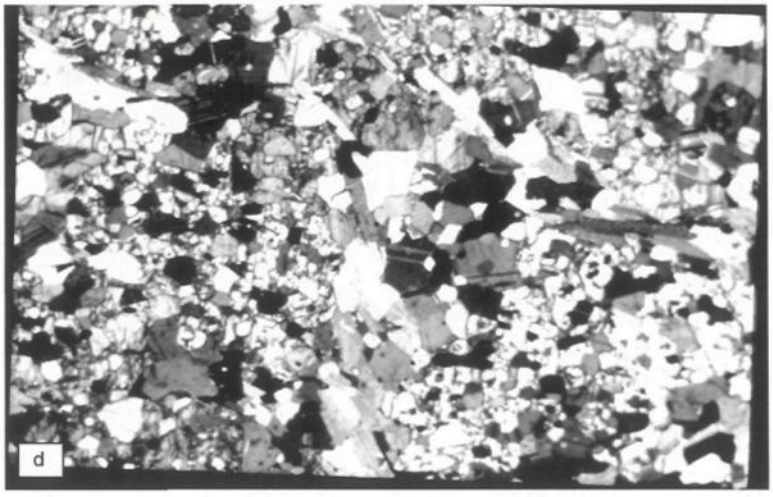

Figure 4d: Metagreywacke 5202 from the Ashuanipi subprovince which contains 3 mm orthopyroxene poikiloblasts. The matrix trapped in the poikiloblast is quartz-free and small biotite grains are included in the orthopyroxene, but quartz and biotite are still present in the matrix outside the poikiloblasts. The long side of each photomicrograph represents 4.35 mm.

The principal variation in bulk composition in the metagreywackes is manifest as a change in the modal proportions of biotite, plagioclase, quartz and orthopyroxene (see appendix VIII). Orthopyroxene content is inversely correlated with biotite and quartz (Fig. 5a), but positively correlated with plagioclase (Fig. 5b). Similar correlations can be observed in thin section in the plagioclase-rich, biotite-depletion halos around orthopyroxene. The increase in grain size, the tendency towards polygonal grain-shapes and the degradation of the foliation as orthopyroxene content increases (Fig. 4), indicates a close approach to textural equilibrium in the metagreywackes. Hunter (1987) suggested that textural equilibrium (i.e. the attainment of a low-energy grain-boundary configuration) is aided by the presence of a melt phase, which enhances grain boundary diffusion. Some metagreywacke rocks in the Ashuanipi subprovince contain microstructures interpreted (Sawyer 2001) to have formed when an intergranular anatectic melt crystallized. Figures 6a & b show mineral films with irregular shapes enveloping round, corroded grains of biotite, quartz and plagioclase.

The shape of the mineral films suggests that they replaced the corroded grains (i.e. these were the reactant minerals) and occupy their former space. The melt pools within the rocks (Figs. 6a, b & c) have crystallized to single minerals, i.e. some former melt pools are now quartz, others are plagioclase, and some K-feldspar. Many former melt pools link along the contacts between matrix grains, with the greatest interconnectivity in the foliation plane. However, there are regions where the former melt pools linked across the foliation plane (lower left on Fig. 6c).

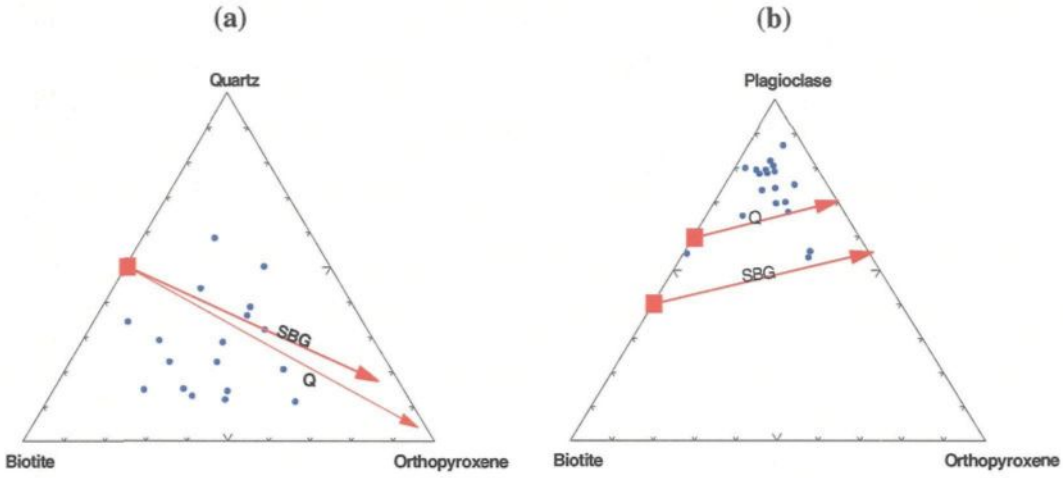

Figure 5. Variation in the modal mineralogy of metagreywacke rocks from the Ashuanipi subprovince. a) Quartz-biotite-orthopyroxene plot, and b) plagioclase-biotite-orthopyroxene plot. The squares are the composition of the average, non-melted metagreywacke from the Quetico subprovince and the composition of the SBG (Synthetic Biotite Gneiss) starting material used by Patiño Douce and Beard (1996). Arrows from the squares indicate the change in modal composition of the residuum left after extracting melt from the average Quetico (Q) and SBG starting material in the modal proportions of R4 given in the text. The blue circles are the point counted metagreywackes from the Ashuanipi subprovince.

Some grains have crystal faces at their contacts with the pore space-filling minerals; the crystal faces on plagioclase (Fig. 6d) are an overgrowth that grew from the melt and into the melt pocket. However, in the case of product orthopyroxene it does not necessarily mean it crystallized from the melt (Sawyer 2001).

3.3.2 The melting reaction in the metagreywackes

The changes in microstructure and modal mineralogy (Fig. 5), together with the grain boundary melt microstructures (Fig. 6) suggest that the melting reaction in the metagreywackes was the continuous reaction;

biotite + quartz + plagioclase = orthopyroxene + melt + Fe-Ti oxides (R1)

Moreover, the absence of biotite in some metagreywackes indicates that temperatures were locally high enough for R1 to go to completion.

Some rare mineral assemblages result from variations in the initial bulk composition of the metagreywackes. Metagreywackes with low [MgO / (MgO+FeO)] ratios may also contain minor amounts of garnet, and bulk compositions with higher (*ca.* 5 wt %) than normal (< 4 wt %) CaO contents contain clinopyroxene + orthopyroxene; both these rock types have undergone partial melting. The presence of minor amounts of K-feldspar (< 2 %) in a few metagreywackes is more problematic. The K-feldspar could have formed from biotite before the melting reaction started, as noted by Gardien *et al.* (1995) in their 10 kbar 750°C runs on the BPQII starting material. Alternatively, these rocks had slightly more aluminous compositions and, hence, a small amount of muscovite, which may have reacted with quartz and

plagioclase to produce a little melt and K-feldspar before biotite breakdown started (Thompson & Tracy 1979; Patiño Douce & Harris 1998; Pickering & Johnston 1998). Orthopyroxene is not generally altered to hydrous retrograde phases in the metagreywackes. However, some metagreywackes show minor, replacement of orthopyroxene with bladed intergrowths of biotite + quartz or biotite + plagioclase (Fig. 6e). In some rocks this reaction microstructure is clearly confined to the places where orthopyroxene is in contact with feldspar having an angular, pore-filling shape suggesting a remnant pool of melt. These microstructures are interpreted as back-reaction between orthopyroxene and residual melt left in the pore space, which reversed R1.

3.3.3 Melting reactions in the metapelites

Iron-rich pelitic rocks contain the mineral assemblage garnet + orthopyroxene + K-feldspar + quartz + plagioclase whereas the more magnesian, or aluminous, bulk compositions contain garnet + orthopyroxene + cordierite + K-feldspar + quartz + plagioclase, or garnet + cordierite + K-feldspar + quartz + plagioclase. Microstructures suggest that in cordierite-free rocks, garnet and orthopyroxene coexist stably, perhaps through a garnet + K-feldspar-forming reaction, e.g.

biotite + sillimanite + quartz = melt + garnet + orthopyroxene + K-feldspar (R2)

In a few rocks, garnet, orthopyroxene and cordierite appear to coexist stably suggesting a reaction such as,

biotite + quartz + plagioclase + sillimanite = K-feldspar + cordierite + garnet + orthopyroxene + melt (R3)

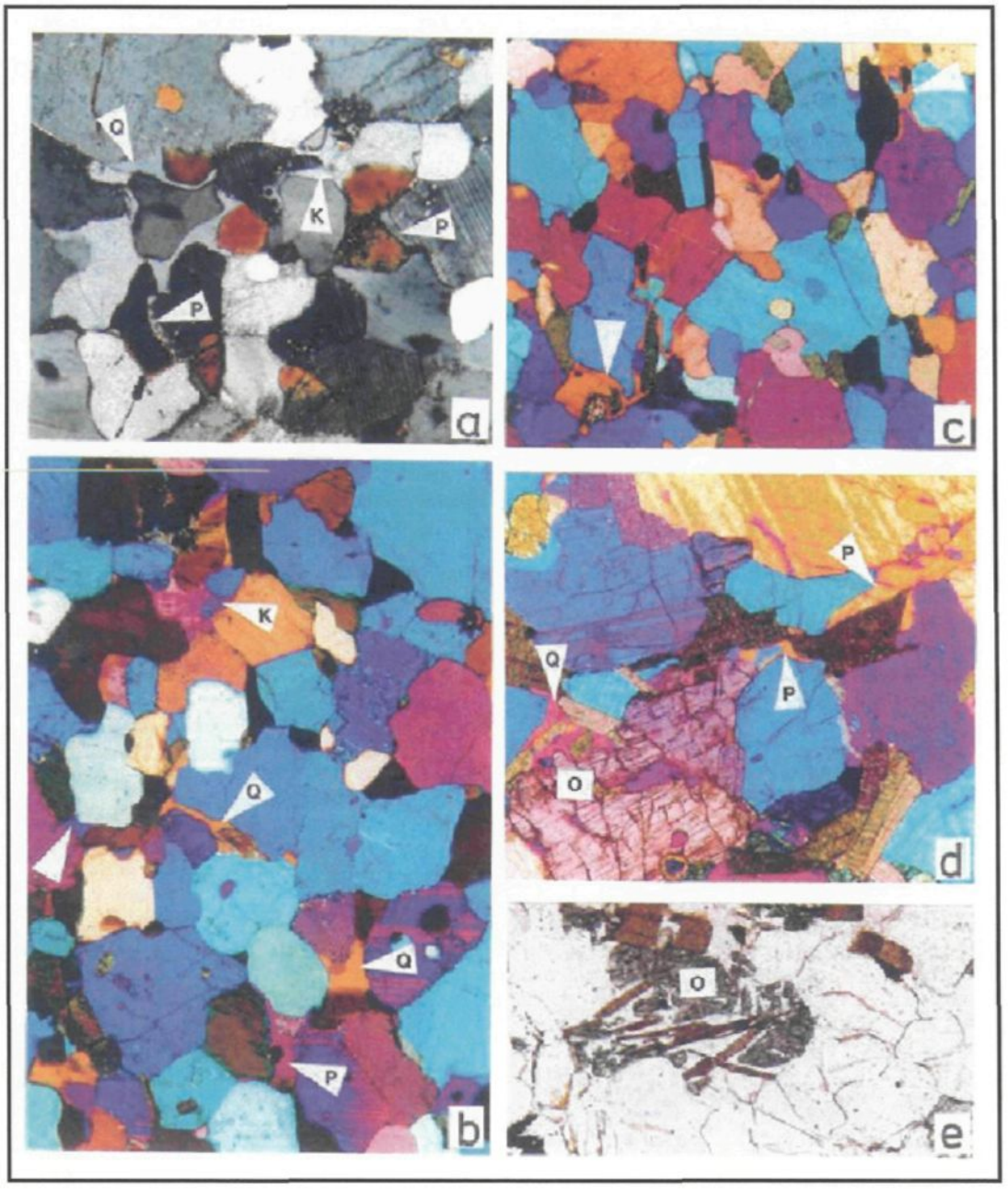
Q
K
P
P
a
c
K
Q
Q
P
b
P
Q
P
O
d
O
e

Figure 6. Photomicrographs showing the microstructures that indicate the former presence of melt in the metagreywackes from the Ashuanipi subprovince. a) Metagreywacke 7016 (5 modal % orthopyroxene) section parallel to the foliation plane, crossed polars. White triangles point to microstructures resulting from former melt; melt films along grain boundaries and melt pools at grain junctions. Note the rounded (corroded) outlines of biotite, quartz and plagioclase against former melt. Melt pools and films have crystallized to quartz (Q), plagioclase (P) and K-feldspar (K) now inverted to microcline. b) Sample 7016 section parallel to foliation, crossed polars and one lambda accessory plate ease identification of former melt microstructures. Melt has crystallized to quartz, plagioclase and K-feldspar in different parts of the rock. Note there is no strong mineral lineation, nor a preferred orientation of melt in this plane. c) Sample 5198, section perpendicular to the foliation plane which is parallel to the vertical edge of the photomicrograph. Melt films and pools occupy the space created as reactant minerals, notably biotite, are consumed and hence melt films and pools are elongated parallel to the foliation in this plane. The larger melt pool in the lower left occupies space created along grain boundaries both parallel to, and orthogonal to, the foliation. d) Sample 4174 (10 modal % orthopyroxene) section normal to the foliation plane (trace of foliation indicated in the upper left) shows a melt pool on the left which has crystallized to quartz, the plagioclase in contact with this pool has straight crystal faces, but the orthopyroxene (O) in contact with it is embayed, suggesting back reaction with the melt. The melt pool in the centre has crystallized to plagioclase (yellow) and contains a rounded, corroded plagioclase relic (blue), but the biotite has straight crystal faces and may have crystallized in the melt pool following reaction between melt and nearby orthopyroxene. The melt pool on the right crystallized to plagioclase which is in optical continuity with the adjacent, twinned matrix plagioclase (under the white triangle) crystal, but the pool-filling plagioclase is not twinned and is less calcic in composition. e) Typical, but rare, microstructure of orthopyroxene replaced by biotite blades intergrown with plagioclase (or quartz). The foliation trace is parallel to the long edge of the photomicrograph. The width of each photomicrograph corresponds to 2 mm.

described by Stevens *et al.* (1997) for magnesian bulk compositions. Garnet and orthopyroxene are partially replaced by cordierite, and contacts between garnet, orthopyroxene and K-feldspar are replaced by symplectic intergrowths of biotite, quartz and plagioclase in some Ashuanipi metapelites. These microstructures suggest back-reaction between residual minerals and interstitial melt.

3.4. PRESSURE AND TEMPERATURE CONDITIONS DURING PARTIAL MELTING

The incongruent melting of biotite with quartz and plagioclase has been investigated experimentally by many workers and enables the temperature of partial melting in the Ashuanipi subprovince to be estimated relatively well. The *Mg number* of metagreywackes from the Quetico subprovince ranges from 41 to 53 (average 47) (see appendix III), and for Quetico metapelites 45 to 51 (average 42) (see appendix IV). The range in *Mg number* for 28 partially melted metagreywackes (CaO <3.6 wt %) from the Ashuanipi subprovince used in this study is 41 to 58 (average 48); Percival (1991) reported a similar range (43 to 52, average 47) for a region 150 km farther north. The greywacke starting compositions used by Vielzeuf & Montel (1994), Patiño Douce & Beard (1995), Stevens *et al.* 1997 and Gardien *et al.* 1995 are close to the Quetico metagreywacke proxy for the Ashuanipi protolith in terms of *Mg number* (Table 1), but are richer in quartz and poorer in plagioclase. The plagioclase used in the experiments is also more calcic than that in the Quetico metagreywacke.

Table 1: Summary of bulk composition used in bte+plag+qtz melting experiments

Mineral Modes				Mg Numbers		Plagioclase	Rock	Source
Quartz	Plagioclase	Biotite	oxides	Biotite	Rock	composition	name	
34.3	26.5	37.2	2	0.5	0.5	An38	SFAG	Patino Douce and Beard (1996)
34.3	26.5	37.2	2	23	22	An38	SMAG	Patino Douce and Beard (1996)
34.3	26.5	37.2	2	54.6	52	An38	SBAG	Patino Douce and Beard (1995)
40	32	25	3	44	47	An22	CEVP	Vielzeuf and Montel (1994)
28	21	39			49	An35	A	Stevens et al., (1997)
28	21	39			58	An35	NB	Stevens et al., (1997)
28	21	39			62	An35	B	Stevens et al., (1997)
28	21	39			81	An35	C	Stevens et al., (1997)
45	28.5	26.8			41.5	An27	BPQII	Gardien et al., (1996)
28	42	30			47	An29-32	Quetico	

Figure 7 shows the location of experimentally determined phase boundaries for melting reactions using metagreywacke bulk compositions with *Mg numbers* comparable to those of the assumed protolith (Quetico) for the Ashuanipi subprovince metagreywackes. The experiments constrain the start of partial melting in the Ashuanipi subprovince metagreywackes to at least 800 to 820°C corresponding to the "orthopyroxene in" isograd. As most metagreywackes contain between 8 and 15 % orthopyroxene (Fig. 5), and some no longer contain biotite, maximum temperatures were somewhat higher. Stevens *et al.* (1997) found that biotite disappeared from TiO_2-free metagreywackes with *Mg number* 62 at about 850°C but, in TiO_2-rich (0.87 wt % TiO_2) metagreywackes with similar *Mg number* (58), "biotite out" occurred some 80°C higher. The metagreywacke studied by Vielzeuf & Montel (1994) has a lower TiO_2 content (0.7 wt %), close to that of the Quetico metagreywackes; this reached "biotite out" at between 860 and 960°C depending on the pressure. Metabasite layers in the metasediments are migmatitic and did not reach "hornblende-out", limiting the maximum temperatures to below 900 to 940°C (Fig. 7).

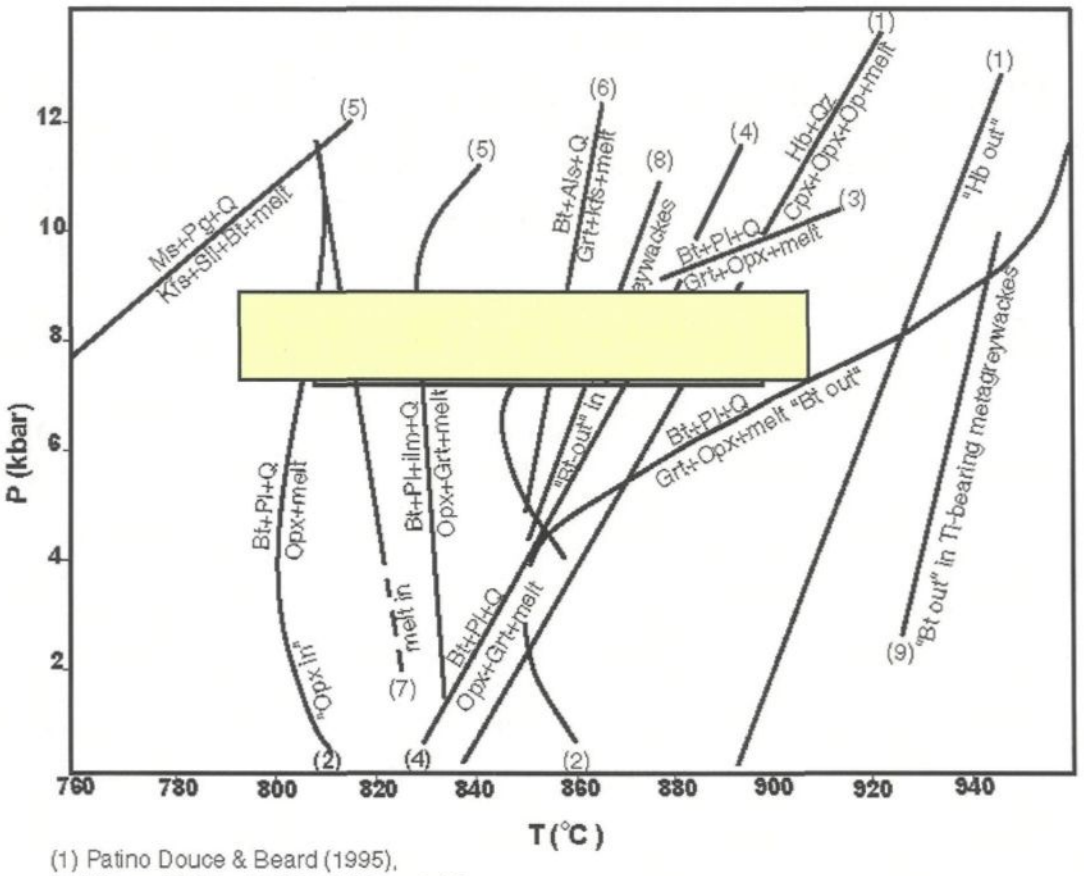

(1) Patino Douce & Beard (1995),
(2) Vielzeuf & Montel (1994), Xmg=0.47,
(3) Patino Douce and Beard (1996), Xmg=0.22,
(4) Patino Douce & Beard (1995), Xmg=0.52,
(5) Patino Douce & Harris (1998),
(6) Vielzeuf & Holloway (1988), Xmg=0.5,
(7) Stevens et al., (1997), Xmg=0.49 to 0.81,
(8) Stevens et al., (1997),
(9) Stevens et al., (1997), Xmg=0.58.
Shaded box shows temperature and pressure conditions estimated for the Ashuanipi subprovince.
Mineral abbreviations are: Quartz = Q, Muscovite = Ms, Biotite = Bt, Sillimanite = Sil, Alluminosilicate = Als, K-feldspar = Kfs, Plagioclase = Pl, Clinopyroxene = Cpx, Orthopyroxene = Opx, Ilmenite = Ilm, Garnet = Grt, Hornblende = Hb, Melt = melt.

Figure 7. Compilation of the experimentally derived dehydration melting reactions relevant to partial melting in the Ashuanipi subprovince, and to metagreywackes in particular. The box indicates the range of temperatures based on the presence of orthopyroxene in all metagreywackes and some that have passed the "biotite-out" isograd. Pressure estimate is based on the silica-Ca-Tschermakite-anorthite geobarometer of McCarthy & Patiño Douce (1998). Sources: 1, Patiño Douce & Beard (1995); 2, Vielzeuf & Montel (1994, $X_{Mg} = 0.48$); 3, Patiño Douce & Beard (1996, $X_{Mg} = 0.22$); 4, Patiño Douce & Beard (1995, $X_{Mg} = 0.52$); 5, Patiño Douce & Harris (1998); 6, Vielzeuf & Holloway (1988, $X_{Mg} = 0.41$); 7, Stevens *et al.* (1997, $X_{Mg} = 0.49$ to 0.81); 8, Stevens *et al.* (1997); 9, Stevens *et al.* (1997, $X_{Mg} = 0.58$). Mineral abbreviations after Kretz (1983).

Metamorphic pressures are more difficult to constrain. Patiño Douce & Beard (1996, Fig. 6) show that the appearance of garnet in metagreywackes occurs at progressively higher pressures as *Mg number* increases. The general absence of garnet in metagreywackes with *Mg number* around 50 is consistent with metamorphic pressures below 10 kbar in the southern Ashuanipi subprovince

The wider occurrence of garnet in metagreywackes farther north (Percival 1991b; Lapointe 1996) must, therefore, indicate some differences in metasediment bulk compositions across the Ashuanipi subprovince.

Higher metamorphic temperatures in the north would produce more garnet, but this is unlikely as it would require (R1) to have progressed farther which should be reflected in higher modal orthopyroxene + garnet and lower biotite contents, and neither can be seen in the data of Percival (1991) or Lapointe (1996).

Some Ca-rich rocks in the central Aushuanipi subprovince contain the assemblage clinopyroxene + biotite + quartz + orthopyroxene + plagioclase + opaques. Applying the silica-Ca-Tschermak - anorthite geobarometer of McCarthy & Patiño Douce (1998) to these rocks (representative mineral compositions are in Table 2) yields pressures of 6 to 7 ± 2.5 kbar for an assumed temperature of 850°C.

Thus, the peak metamorphic conditions in the Ashuanipi subprovince reached temperatures of at least 820°C, and locally exceeded 900°C, with pressure of 6 to 7 kbar (Fig. 7). Percival (1991b) obtained similar pressures (6-6.5 kbar), and peak

Table 2: Representative mineral compositions and calculated pressures for T=1123 °K

Sample 19D													
Clinopyroxene	11	12	13	14	15	16	17	18	19	20	21	23	24
SiO_2	51,95	51,68	51,71	52,24	51,93	52,14	52,44	51,99	52,03	52,29	52,30	52,19	52,09
TiO_2	0,08	0,08	0,16	0,08	0,09	0,13	0,12	0,14	0,09	0,12	0,06	0,13	0,16
Al_2O_3	1,34	1,30	1,48	1,13	1,38	1,40	1,45	1,26	1,40	1,36	1,38	1,48	1,44
FeO	7,12	7,15	7,52	6,93	7,79	7,32	7,29	7,03	7,53	7,45	7,36	7,48	7,41
MgO	14,70	14,56	14,63	14,78	14,77	14,50	14,71	14,85	14,74	14,88	14,74	14,65	14,68
CaO	22,15	22,38	22,24	22,79	21,96	22,36	22,61	22,42	22,26	22,23	22,24	21,88	21,95
Na_2O	0,42	0,45	0,47	0,42	0,48	0,51	0,47	0,46	0,51	0,45	0,51	0,52	0,48
K_2O	0,02	0,01	0,03	0,02	0,03	0,02	0,00	0,02	0,01	0,01	0,01	0,02	0,02
MnO	0,16	0,17	0,18	0,16	0,20	0,19	0,17	0,17	0,19	0,19	0,19	0,15	0,20
Cr_2O_3	0,22	0,16	0,22	0,21	0,21	0,17	0,23	0,26	0,19	0,18	0,19	0,22	0,19
Total	98,16	97,92	98,63	98,75	98,82	98,74	99,49	98,59	98,95	99,16	98,97	98,73	98,61
Structural formulae based on 6 oxygens													
Si	1,96	1,96	1,95	1,96	1,95	1,96	1,96	1,96	1,96	1,96	1,96	1,96	1,96
Ti	0,00	0,00	0,00	0,00	0,00	0,00	0,00	0,00	0,00	0,00	0,00	0,00	0,00
Al	0,06	0,06	0,07	0,05	0,06	0,06	0,06	0,06	0,06	0,06	0,06	0,07	0,06
Fe	0,22	0,23	0,24	0,22	0,25	0,23	0,23	0,22	0,24	0,23	0,23	0,24	0,23
Mg	0,83	0,82	0,82	0,83	0,83	0,81	0,82	0,83	0,83	0,83	0,82	0,82	0,82
Ca	0,90	0,91	0,90	0,92	0,89	0,90	0,90	0,90	0,90	0,89	0,89	0,88	0,89
Na	0,03	0,03	0,03	0,03	0,04	0,04	0,03	0,03	0,04	0,03	0,04	0,04	0,03
K	0,00	0,00	0,00	0,00	0,00	0,00	0,00	0,00	0,00	0,00	0,00	0,00	0,00
Mn	0,01	0,01	0,01	0,00	0,01	0,01	0,01	0,01	0,01	0,01	0,01	0,00	0,01
Cr	0,01	0,00	0,01	0,01	0,01	0,00	0,01	0,01	0,01	0,01	0,01	0,01	0,01
Plagioclase	8	9	14	15	20	21	24	25	29	30	33	40	41
SiO_2	59,46	59,83	59,22	58,93	59,42	59,50	59,10	59,44	59,72	60,02	59,78	59,75	59,31
Al_2O_3	24,78	25,03	24,96	24,68	25,05	25,02	24,95	25,15	24,99	24,80	25,01	24,76	24,88
FeO	0,07	0,06	0,07	0,08	0,09	0,12	0,08	0,10	0,09	0,09	0,13	0,06	0,09
MgO	0,00	0,01	0,00	0,00	0,01	0,00	0,01	0,01	0,00	0,00	0,00	0,00	0,01
CaO	6,72	6,77	6,72	6,65	6,80	6,75	6,88	6,96	6,77	6,82	6,95	6,72	6,58
Na_2O	7,22	7,26	7,10	7,16	7,17	7,20	7,16	7,18	7,11	7,25	7,13	7,24	7,31
K_2O	0,47	0,47	0,47	0,45	0,45	0,46	0,37	0,44	0,55	0,51	0,51	0,52	0,55
Total	98,72	99,43	98,54	97,94	98,98	99,05	98,54	99,28	99,23	99,49	99,51	99,05	98,72
Structural formulae based on 8 oxygens													
Si	2,68	2,68	2,68	2,68	2,67	2,68	2,67	2,67	2,68	2,69	2,68	2,69	2,68
Al	1,32	1,32	1,33	1,32	1,33	1,33	1,33	1,33	1,32	1,31	1,32	1,31	1,32
Fe	0,00	0,00	0,00	0,00	0,00	0,00	0,00	0,00	0,00	0,00	0,00	0,00	0,00
Mg	0,00	0,00	0,00	0,00	0,00	0,00	0,00	0,00	0,00	0,00	0,00	0,00	0,00
Ca	0,32	0,32	0,33	0,32	0,33	0,33	0,33	0,34	0,33	0,33	0,33	0,32	0,32
Na	0,63	0,63	0,62	0,63	0,63	0,63	0,63	0,62	0,62	0,63	0,62	0,63	0,64
K	0,03	0,03	0,03	0,03	0,03	0,03	0,02	0,03	0,03	0,03	0,03	0,03	0,03
Pressure(kbars)	6,50	5,94	6,24	4,56	5,80	6,75	6,62	4,89	6,07	6,10	6,46	7,27	7,05

Table 2: continued

Clinopyroxene	**90**	**91**	**92**	**93**	**94**	**95**	**96**	**97**	**103**	**104**	**105**
SiO_2	51,3	51,3	51,4	51,2	50,7	51,0	51,2	51,8	51,5	51,4	51,6
TiO_2	0,1	0,1	0,1	0,1	0,2	0,1	0,2	0,1	0,1	0,2	0,1
Al_2O_3	1,5	1,4	1,4	1,3	1,5	1,5	1,4	1,2	1,3	1,4	1,4
FeO	10,5	10,5	10,6	10,5	10,7	10,5	10,5	10,3	10,5	10,4	10,6
MgO	12,9	13,0	13,1	12,9	12,9	12,9	12,9	13,1	13,1	12,9	13,2
CaO	21,3	21,7	21,7	21,5	21,4	21,5	21,8	22,2	21,7	21,5	21,6
Na_2O	0,4	0,5	0,5	0,5	0,5	0,5	0,5	0,5	0,4	0,4	0,5
MnO	0,3	0,3	0,3	0,3	0,3	0,3	0,3	0,3	0,3	0,3	0,3
Total	98,4	98,8	99,2	98,4	98,1	98,3	98,7	99,4	98,9	98,7	99,3
Structural formulae based on 6 oxygens											
Si	1,96	1,96	1,95	1,96	1,95	1,95	1,95	1,96	1,96	1,96	1,96
Ti	0,00	0,00	0,00	0,00	0,00	0,00	0,00	0,00	0,00	0,01	0,00
Al	0,07	0,06	0,06	0,06	0,07	0,07	0,06	0,05	0,06	0,06	0,06
Fe	0,34	0,34	0,34	0,34	0,34	0,34	0,34	0,33	0,33	0,33	0,33
Mg	0,74	0,74	0,74	0,74	0,74	0,74	0,73	0,74	0,74	0,73	0,75
Ca	0,87	0,89	0,88	0,88	0,88	0,88	0,89	0,90	0,88	0,88	0,88
Na	0,03	0,03	0,04	0,04	0,04	0,04	0,04	0,03	0,03	0,03	0,03
Mn	0,01	0,01	0,01	0,01	0,01	0,01	0,01	0,01	0,01	0,01	0,01
Plagioclase	71	72	73	74	75	76	77	78	79	80	81
SiO_2	60,26	59,06	60,00	59,29	60,15	59,58	59,73	60,14	60,49	60,14	60,16
Al_2O_3	24,51	24,47	24,61	24,65	24,67	24,75	24,93	24,60	24,61	24,60	24,72
FeO	0,11	0,62	0,11	0,14	0,16	0,26	0,39	0,13	0,14	0,17	0,25
MgO	0,00	0,13	0,00	0,00	0,01	0,01	0,02	0,00	0,00	0,05	0,00
CaO	6,36	6,28	6,43	6,41	6,39	6,57	6,68	6,33	6,34	6,49	6,45
Na_2O	7,40	7,18	7,51	7,50	7,39	7,41	7,27	7,38	7,31	7,26	7,31
K_2O	0,54	0,56	0,47	0,55	0,53	0,50	0,51	0,52	0,46	0,50	0,53
Total	99,18	98,30	99,13	98,54	99,30	99,07	99,52	99,09	99,33	99,21	99,42
Structural formulae based on 8 oxygens											
Si	2,70	2,68	2,70	2,68	2,70	2,68	2,68	2,70	2,71	2,70	2,70
Al	1,30	1,31	1,30	1,32	1,30	1,31	1,32	1,30	1,30	1,30	1,31
Fe	0,00	0,02	0,00	0,01	0,01	0,01	0,01	0,00	0,01	0,01	0,01
Mg	0,00	0,01	0,00	0,00	0,00	0,00	0,00	0,00	0,00	0,00	0,00
Ca	0,31	0,31	0,31	0,31	0,31	0,32	0,32	0,30	0,30	0,31	0,31
Na	0,64	0,63	0,65	0,66	0,64	0,65	0,63	0,64	0,63	0,63	0,64
K	0,03	0,03	0,03	0,03	0,03	0,03	0,03	0,03	0,03	0,03	0,03
Pressure(kbars)	7,63	6,79	6,54	6,80	7,02	7,02	6,22	5,29	6,43	6,92	6,36

temperatures of between 700 and 835 °C for metapelites farther north, using TWEQU thermobarometry. Some of the maximum temperatures obtained by Percival (1991b) are up to 100 °C lower than suggested by the mineral assemblages and experimental calibrations of reaction R1. However, the TiO_2 contents of biotite in Percival (1991b) are between 4.62 and 6.23 wt %, which is similar to the TiO_2 contents of biotites from melting experiments carried out above 850°C (Montel & Vielzeuf 1997, Fig. 1).

3.5 THE DEGREE OF PARTIAL MELTING

The degree of partial melting can be estimated from the modal proportions of solid product minerals generated by melting reactions. This approach works if all the melting reactions which occurred in a particular rock are known. Metapelites have a complex melting sequence beginning with the breakdown of muscovite, followed by biotite + aluminosilicate and ending with biotite + quartz. Fortunately, metagreywackes have a simpler melt-generation history; their Al-poor bulk composition precludes the presence of muscovite, or one of the aluminosilicate minerals and, therefore, melting begins with (R1). Hence, if the stoichiometry of (R1) is known, the amount of melt generated is proportional to the orthopyroxene content in the rock. Patiño Douce & Beard (1995) have determined the stoichiometry of (R1) conducted with a synthetic biotite gneiss (SBG) starting material (*Mg number* 52); the stoichiometry for their 7 kbar runs was;

0.44biotite+0.11plagioclase+0.44quartz = 0.71melt+0.27orthopyroxene+0.03oxide (R4)

The ratio of product melt (M) to reactant biotite (B) is 71/44 = 1.61, and product melt to product orthopyroxene (O) is 71/27 = 2.63, averaged over the reaction interval, based of modal proportion of run products. Similar ratios are obtained from other experiments using TiO_2-bearing compositions; the 8 kbar runs of Montel & Vielzeuf (1997) yield M/B = 1.60 and M/O = 3.6; the 5 kbar NB runs of Stevens *et al.* (1997) yield M/B = 1.61, M/O = 2.67 and their 10 kbar runs M/B = 1.1 and M/O = 3.15; the BPQII starting material used by Gardien *et al.* (1995) yields M/B = 1.3. The TiO_2-free experiments of Stevens *et al.* (1997) differ; they yield M/B (0.77 to 1.02) and M/O (0.97 to 1.31) ratios for the 5 kbar runs and M/B (0.5 to 0.8) and M/O (0.83 to 1.14) ratios for the 10 kbar runs (see appendix VI).

Assuming that the stoichiometry of (R4) applied to melting of the Ashuanipi metagreywacke protolith, using only those metagreywackes with CaO < 3.5 wt % and *Mg number* 42 to 55 that are in the range of starting materials used in the experimental studies, and converting modal % to weight %, then the rocks produced from 2 to 51 wt % melt, with an average of 31 wt % (sigma = 10.7, n = 17) based on the orthopyroxene contents measured in the metagreywackes (Fig. 8). The same method yields 28 and 25 wt % melt respectively, for metagreywacke samples 216 and 266 from Percival (1991b). Similar degrees of partial melting are obtained using the melt/orthopyroxene ratios from the TiO_2-bearing experiments of Montel & Vielzeuf (1997), and Stevens *et al.* (1997). The M/B ratio indicates that the average Quetico metagreywacke could produce about 45 vol % melt, before quartz and biotite were consumed.

3.6 WHOLE ROCK GEOCHEMISTRY

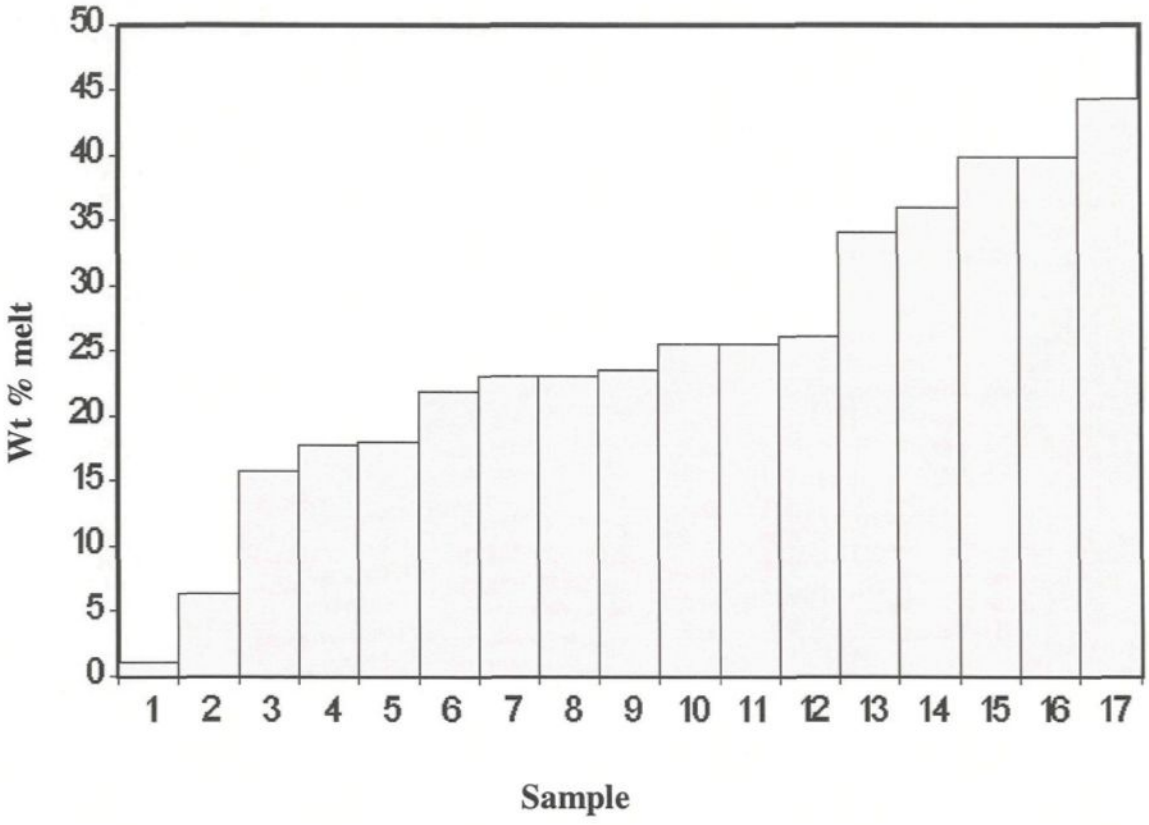

Figure 8. Melt percentages generated in metagreywackes from the Ashuanipi subprovince calculated from the modal proportion of orthopyroxene and assuming the melting reaction coefficients given in R4 (see text).

3.6.1 Analytical methods

The major oxides and trace elements Ba, Nb, Rb, Sr, Y and Zr were determined on 35 metagreywackes from the central Ashuanipi subprovince by standard XRF techniques using fused glass discs and pressed powder pellets; Cr, Cs, Hf, Sc, Th, U and the rare earth elements (REE) were determined using Instrumental Neutron Activation Analysis (INAA) at the analytical laboratories of the Ministère des Ressources Naturelles du Québec (MRNQ). Because Tb and Lu contents were close to, or below, the detection limit of the MRNQ laboratories, the REE, NaO_2, FeO, Ba, Co, Cr, Cs, Hf, Rb, Sc, Ta, Th and U were determined for 13 samples using INAA at the Université du Québec à Chicoutimi (UQAC) following irradiation in the SLOWPOKE II reactor at École Polytechnique in Montreal; Bédard & Barnes (1990) give details of the INAA method used at UQAC.

Comparison of the MRNQ and UQAC results show that they correspond closely except for Tb, Yb and Ta; the REE plots in this study use only the UQAC data. Data for the Quetico metasediments are from Sawyer (1986), plus additional unpublished data for which the major oxides and trace elements (Ba, Rb, S, Y, and Zr) were determined by XRF at McGill University and the REE, Co, Cr, Cs, Hf, Sc, Ta, Th and U determined by INAA at UQAC. Results for the metagreywackes from the Ashuanipi subprovince are given in Table 3.

3.6.2 The protolith composition

Table 3: Whole rock major and trace element compositions of 32 metagreywacke rocks and one metapelitic rock (23-A) from the Ashuanipi Subprovince

Sample	131-A	87-B	194-A	5099-A	0013-A	7016-A	7012-B	2031-B	4097-A	25-A	3095-A	3079-A	3060-B	23-A	40-C	5104-A	5109-A	AS1*
SiO_2(Wt%)	59,50	64,80	59,30	61,50	65,40	62,40	70,70	60,00	56,00	67,00	65,00	65,30	66,80	56,20	69,70	63,90	66,00	61,12
TiO_2	0,53	0,51	0,64	0,63	0,44	0,59	0,48	0,56	0,76	0,50	0,50	0,52	0,51	0,95	0,41	0,59	0,47	0,51
Al_2O_3	16,00	15,50	16,30	17,00	15,70	16,30	15,30	14,20	13,30	15,60	16,50	16,40	15,30	20,00	14,60	14,60	15,30	14,43
Fe_2O_3	1,08	0,92	1,14	1,02	0,81	1,05	0,35	1,05	1,68	0,79	0,69	0,69	0,75	1,18	0,65	1,13	0,96	1,08
FeO	5,51	4,71	5,79	5,19	4,11	5,34	1,77	5,36	8,57	4,02	3,53	3,52	3,83	6,03	3,29	5,77	4,90	5,52
MnO	0,16	0,09	0,09	0,07	0,07	0,06	0,03	0,11	0,19	0,07	0,03	0,08	0,05	0,07	0,05	0,09	0,05	0,11
MgO	4,64	2,85	4,10	4,21	2,56	3,92	1,44	7,53	8,90	2,21	3,20	2,37	2,40	4,23	1,53	4,73	2,44	7,26
CaO	7,10	3,18	3,81	3,29	3,41	3,17	2,72	5,31	6,94	3,05	2,69	4,25	2,27	2,26	3,20	3,03	3,19	3,66
Na_2O	2,69	4,10	4,40	3,78	4,77	3,94	4,44	3,08	0,69	3,74	3,45	4,58	3,77	2,38	3,66	3,71	3,73	3,56
K_2O	0,92	1,93	1,78	2,22	1,30	2,13	1,82	1,35	1,21	1,87	3,03	1,35	2,58	4,32	1,27	1,42	1,36	1,72
P_2O_5	0,17	0,12	0,05	0,07	0,14	0,10	0,14	0,12	0,23	0,12	0,10	0,15	0,09	0,09	0,12	0,11	0,15	0,22
LOI	1,13	0,49	1,57	0,13	0,64	0,65	0,71	0,72	0,86	0,50	0,84	0,64	1,23	1,01	0,91	0,37	0,99	0,34
Total	99,44	99,21	98,97	99,11	99,35	99,65	99,90	99,39	99,33	99,46	99,57	99,85	99,58	98,73	99,38	99,46	99,54	99,54
Al index	1,11	1,53	1,32	1,51	1,46	1,48	1,78	0,89	0,80	1,73	1,77	1,46	1,81	2,25	1,74	1,27	1,63	1,00
Mg #	56,03	47,82	51,75	55,11	48,52	52,66	55,14	68,02	61,15	45,46	57,84	50,50	48,68	51,50	41,34	55,37	42,98	66,57
Cr (ppm)	n.a.	n.a.	n.a.	220	150	240	54	540	420	120	130	63	160	280	140	300	150	601
Ni	142	45	125	n.a.	n.a.	n.a.	n.a.	n.a.	n.a.	n.a.	n.a.	n.a.	n.a.	n.a.	n.a.	n.a.	n.a.	195
Co	30	14	29	26	18	22	6	30	43	15	15	16	10	23	8	27	21	28
Sc	18	13	14	20	14	17	9	29	42	12	13	13	13	31	11	19	13	15
Cu	173	17	68	55	n.a.	54	17	3	3	n.a.	14	25	31	n.a.	n.a.	55	75	69
Pb	n.a.	n.a.	n.a.	21	d.l.	9	4	5	2	d.l.	17	6	19	d.l.	d.l.	8	7	10
Zn	131	84	100	82	d.l.	64	36	70	111	d.l.	61	68	43	d.l.	d.l.	90	63	n.a.
Rb	57	62	57	63	42	92	52	90	67	67	110	32	120	180	63	78	75	65
Cs	n.a.	n.a.	n.a.	0,5	0,5	2,1	2,5	2,3	0,50	0,90	5,50	0,50	2,80	4,4	0,8	0,5	0,5	1,5
Ba	540	443	524	960	390	760	460	560	390	740	950	460	730	1200	480	310	450	464
Sr	310	400	430	619	370	506	678	220	521	475	484	738	418	471	446	342	447	450
Ga	12	16	15	21	19	19	16	15	18	18	19	22	17	26	17	19	18	18
Ta	0,5	0,3	0,3	d.l.	0,7	d.l.	d.l.	0,9	0,60	d.l.	d.l.	0,90	d.l.	d.l.	0,6	d.l.	d.l.	0,2
Nb	12	12	13	5	5	4	d.l.	d.l.	d.l.	d.l.	6	d.l.	4	6	d.l.	4	5	7
Hf	2,6	3,6	3,6	4,2	3,8	4,1	3,6	2,5	2,70	5,10	3,90	3,10	3,70	4,0	4,5	3,9	5,3	3,2
Zr	86	120	120	143	113	138	129	79	99	148	122	115	124	139	148	143	153	109
Y	10	7	n.a.	9	15	9	7	14	23	12	9	9	10	10	9	12	12	13
Th	3,6	6,9	26,0	5,2	5,3	7,8	4,0	3,8	1,4	7,6	12,0	1,5	8,7	13,0	11,0	6,9	11,0	3,1
U	d.l.	d.l.	d.l.	1,0	1,4	0,7	1,5	1,2	0,9	0,9	1,4	d.l.	2,0	1,4	2,9	0,7	1,7	0,4
La	21	28	76	33	24	33	32	15	14	32	32	22	30	46	33	30	37	23
Ce	40	51	130	62	49	58	60	31	30	60	58	42	54	85	56	54	68	46
Nd	17	21	44	25	20	29	30	15	20	24	27	19	19	39	24	25	31	20
Sm	3,1	3,6	5,3	4,5	3,8	4,3	4,2	3,4	4,4	3,6	3,9	3,8	3,7	6,2	3,3	4,0	4,9	3,5
Eu	1,1	d.l.	1,2	1,2	1,3	1,2	1,0	0,7	1,1	1,2	1,1	1,0	1,0	1,6	1,0	1,0	1,0	1,3
Tb	0,4	d.l.	0,2	0,4	d.l.	0,3	d.l.	d.l.	0,5	d.l.	0,2	d.l.	0,4	d.l.	d.l.	d.l.	d.l.	0,4
Yb	1,2	1,1	0,4	1,1	1,5	0,9	0,7	1,5	2,8	1,4	0,8	1,0	1,0	1,1	1,3	1,0	1,4	1,1
Lu	0,2	0,2	0,1	0,2	0,2	d.l.	d.l.	0,2	0,4	0,2	d.l.	0,2	0,2	0,2	0,2	d.l.	d.l.	0,2

abbreviations: d.l.=detection limit; n.a.=not analysed

*samples analysed at UQAC by INAA (see text for details)

Table 3: continued

Sample	1003*	3119*	1142*	1134*	1133*	5223*	5213*	5202*	5198*	5185*	138*	5079*	213	5186a*
SiO_2 (Wt%)	64,90	68,40	71,70	64,20	64,40	67,90	67,00	60,20	66,70	65,50	65,80	67,30	67,30	65,50
TiO_2	0,50	0,43	0,35	0,56	0,54	0,44	0,48	0,49	0,49	0,53	0,43	0,49	0,47	0,49
Al_2O_3	14,40	14,70	13,90	14,80	15,80	15,30	15,50	14,50	15,30	16,70	15,90	15,10	15,30	15,20
Fe_2O_3	1,05	0,69	0,66	1,05	0,97	0,77	0,84	1,19	0,93	0,90	0,71	0,78	0,80	0,93
FeO	5,33	3,53	3,37	5,35	4,94	3,90	4,28	6,08	4,72	4,57	3,61	3,95	4,08	4,74
MnO	0,06	0,05	0,08	0,07	0,05	0,05	0,06	0,10	0,07	0,04	0,08	0,05	0,00	0,08
MgO	3,41	1,81	1,54	3,26	3,73	2,24	2,53	7,44	3,11	2,75	2,04	2,51	2,41	2,94
CaO	2,87	2,79	2,43	1,99	1,64	3,57	3,34	3,88	3,64	3,27	4,58	3,00	2,93	3,55
Na_2O	3,34	3,69	3,49	3,22	2,98	3,64	3,73	3,21	3,71	3,87	4,36	4,13	3,67	3,47
K_2O	2,29	2,64	1,64	2,65	2,65	1,20	1,72	1,62	1,26	2,13	1,03	1,63	1,94	1,34
P_2O_5	0,15	0,16	0,05	0,13	0,08	0,12	0,14	0,23	0,15	0,13	0,10	0,07	0,12	0,15
LOI	0,70	0,59	0,57	1,44	1,12	0,92	0,36	0,32	0,32	0,44	0,41	0,50	0,75	0,34
Total	99,00	99,48	99,78	98,72	98,90	100,05	99,97	99,26	100,39	100,83	99,05	99,51	99,78	98,73
Al index	1,50	1,77	1,86	1,75	1,89	1,62	1,61	1,00	1,46	1,69	1,45	1,57	1,70	1,53
Mg Number	49,21	43,74	40,94	47,98	53,35	46,52	47,27	64,95	49,96	47,66	46,12	49,02	47,20	48,43
Cr (ppm)	340	100	56	210	270	170	160	720	210	150	20	150	170	158
Ni	174	136	95	236	208	206	183	298	185	212	97	170	n.a.	n.a.
Co	16,5	14,0	9,0	21,0	27,0	17,6	15,7	30,5	14,7	16,0	17,0	17,8	n.a.	15,7
Sc	15,2	8,6	12,7	17,6	20,6	12,8	14,2	16,7	13,9	13,9	9,8	13,8	13,0	14,9
Cu	n.a.	n.a.	n.a.	n.a.	n.a.	n.a.	n.a.	n.a.	n.a.	n.a.	n.a.	n.a.	n.a.	n.a.
Pb	n.a.	n.a.	n.a.	n.a.	n.a.	n.a.	n.a.	n.a.	n.a.	n.a.	n.a.	n.a.	n.a.	n.a.
Zn	n.a.	n.a.	n.a.	n.a.	n.a.	n.a.	n.a.	n.a.	n.a.	n.a.	n.a.	n.a.	n.a.	n.a.
Rb	98	76	57	142	105	45	135	66	49	125	34	53	n.a.	61
Cs	4,0	1,4	4,3	6,5	5,5	0,4	2,9	1,7	2,5	3,0	42,6	d.l.	n.a.	2,6
Ba	670	920	350	260	480	370	490	410	420	290	340	460	n.a.	341
Sr	380	541	308	210	322	488	513	447	780	348	441	509	n.a.	218
Ga	17	17	14	20	19	17	19	18	18	19	18	18	17	18
Ta	0,4	0,2	0,3	0,7	0,4	0,5	0,5	0,2	0,4	0,4	0,4	0,1	n.a.	0,4
Nb	3	2	3	6	4	4	5	2	3	6	3	2	n.a.	4
Hf	4,5	2,1	1,6	4,9	3,8	0,4	4,4	3,4	0,4	3,8	3,1	1,5	n.a.	4,1
Zr	140	79	121	146	125	135	139	127	155	125	110	131	131	142
Y	9	3	16	12	15	12	10	11	8	5	7	5	n.a.	11
Th	7,9	0,7	9,0	14,2	10,7	9,9	13,3	3,2	10,0	10,5	3,0	12,6	7,6	10,6
U	1,1	0,2	1,7	3,7	2,3	1,5	2,0	0,6	0,8	0,8	0,8	0,5	n.a.	0,8
La	27,7	13,9	31,3	39,5	31,6	29,3	34,4	23,0	31,6	30,7	7,7	37,8	n.a.	32,2
Ce	54,3	24,6	58,5	72,2	65,8	55,0	60,0	41,2	58,0	58,7	14,5	70,4	n.a.	61,9
Nd	22,0	9,3	21,6	29,1	23,9	22,6	24,5	21,9	22,1	22,3	5,6	26,2	n.a.	24,1
Sm	3,9	1,7	3,9	5,5	4,6	3,8	4,3	3,7	3,9	3,9	1,6	3,8	n.a.	4,0
Eu	1,4	1,0	1,5	1,2	1,5	1,1	1,1	1,3	1,1	1,1	0,8	1,3	n.a.	1,3
Tb	0,5	0,2	0,5	0,6	0,6	0,4	0,4	0,4	0,4	0,4	0,3	0,3	n.a.	0,4
Yb	1,0	0,4	3,1	1,8	1,6	1,0	1,2	1,2	0,6	0,5	0,9	0,5	n.a.	0,6
Lu	0,2	0,1	0,5	0,3	0,2	0,2	0,2	0,2	0,1	0,1	0,1	0,1	n.a.	0,1

abbreviations: d.l.=detection limit; n.a.=not analysed *samples analysed at UQAC by INAA (see text for details)

The main compositional features of the assumed protolith, the greenschist to middle amphibolite facies metasediments from the Quetico subprovince will be described briefly before the granulite facies metasediments from the Ashuanipi subprovince.

The SiO_2 content of the metasediments from the Quetico subprovince ranges from 58 to 71 wt % (Fig. 9a). The pelitic layers have < 61 wt% SiO_2 and the metagreywacke layers have > 62 wt % SiO_2. The metagreywackes containing hornblende have similar K_2O, MgO, and SiO_2 contents (Figs. 9a & 9c), but higher (>3.5 wt %) CaO contents (Fig. 9b) than those containing only biotite. Metapelites have higher K_2O (Fig. 9a), MgO (Fig. 9c), TiO_2, Al_2O_3, FeO_t, Cr, (Fig. 9d), Sc and Rb, but lower CaO, Na_2O, Sr, Hf and Zr contents than the metagreywackes. There is no systematic difference between the metagreywackes and metapelites for Ba, Y, Th and the REE, principally due to the large scatter in the data. However, Y and the heavy rare earth elements (HREE) generally decrease (Figs. 9g & 9h) with SiO_2 content. The samples from the Quetico subprovince form linear arrays on many (e.g. TiO_2, MgO, FeO_t) of the major element Harker diagrams; they define a mixing line between mica + ferromagnesian minerals and quartz + plagioclase components. The intercept at zero wt % MgO is at 78 wt % SiO_2, corresponding to a quartz/plagioclase ratio of 2/3, matching the average modal composition of the metagreywackes.

On MgO *vs* K_2O and CaO *vs* K_2O plots, the metagreywackes define smaller fields with higher MgO/K_2O and CaO/K_2O ratios than the metapelites (Figs. 10a & 10b), this reflects their lower mica, and higher plagioclase contents, as also shown by a

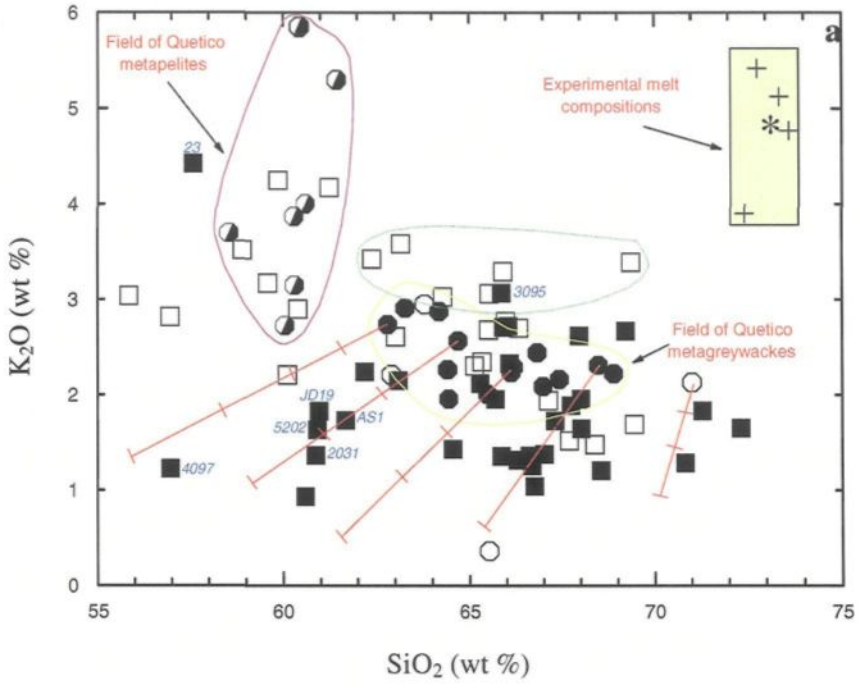
a
Field of Quetico metapelites
Experimental melt compositions
23
3095
Field of Quetico metagreywackes
JD19
AS1
5202
2031
4097
K_2O (wt %)
SiO_2 (wt %)

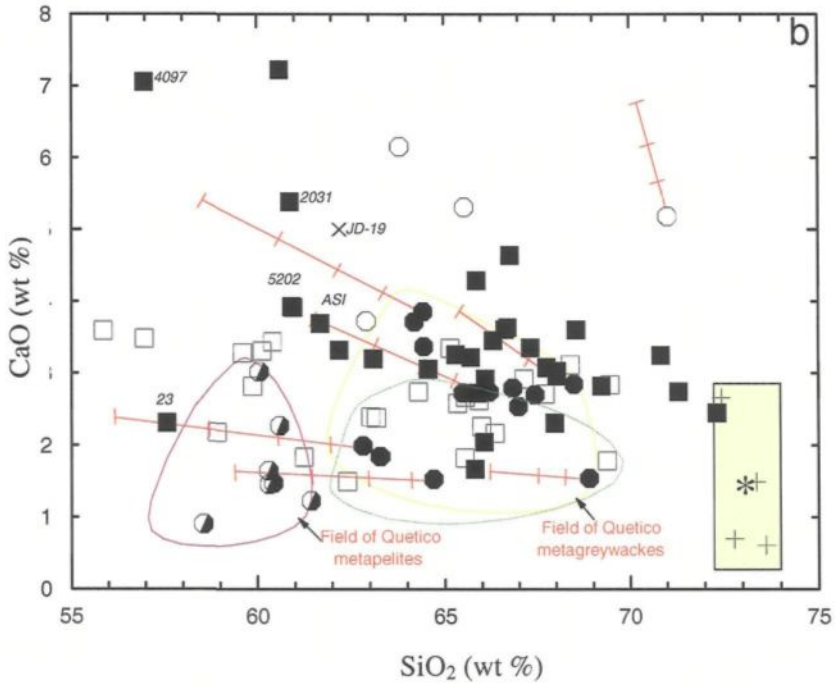
b
4097
2031
JD-19
5202
ASI
23
Field of Quetico metapelites
Field of Quetico metagreywackes
CaO (wt %)
SiO_2 (wt %)

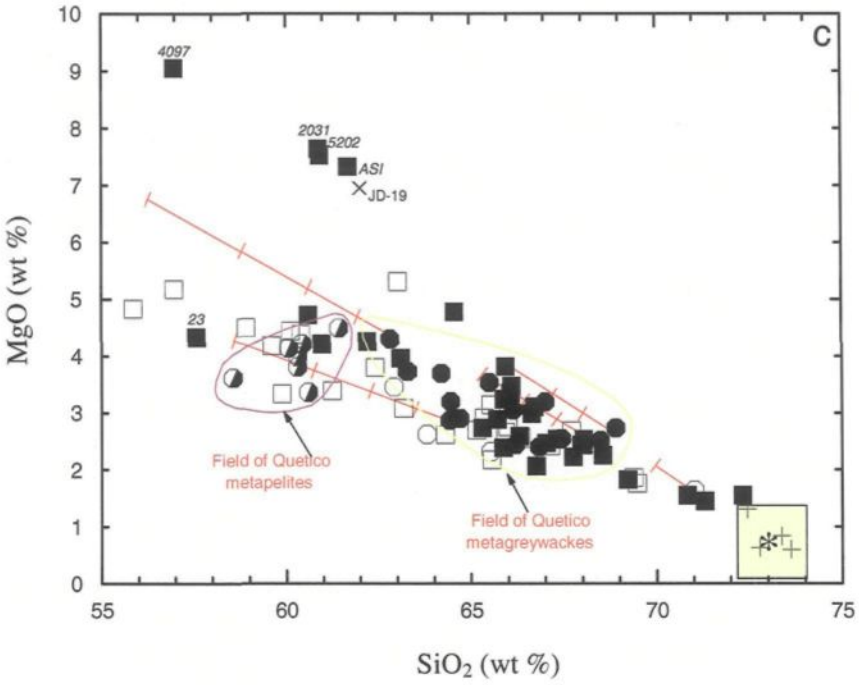
C
4097
2031
5202
ASI
JD-19
23
Field of Quetico metapelites
Field of Quetico metagreywackes
MgO (wt %)
SiO2 (wt %)

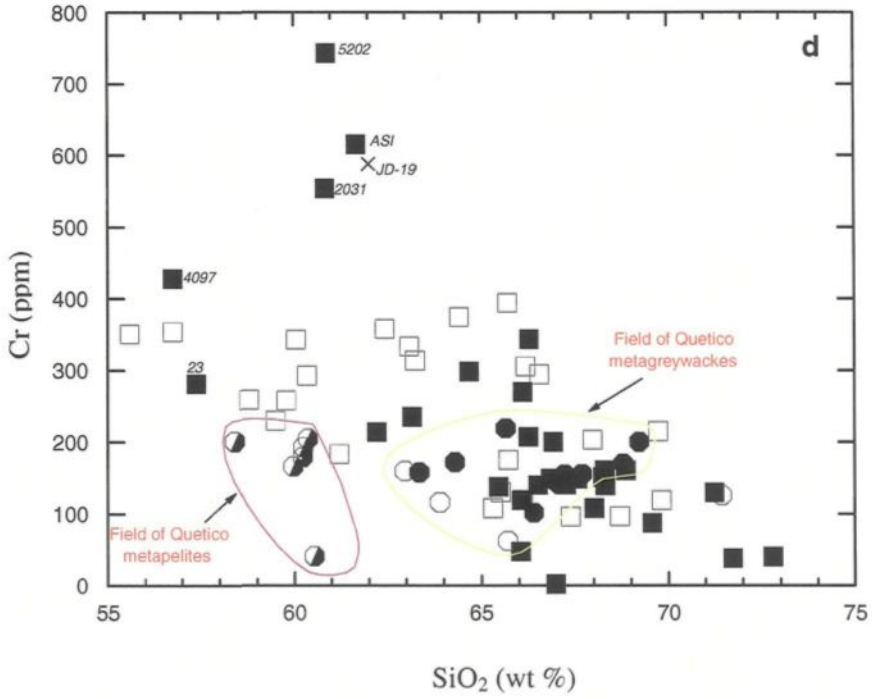
d
5202
ASI
JD-19
2031
4097
23
Field of Quetico metagreywackes
Field of Quetico metapelites
Cr (ppm)
SiO2 (wt %)

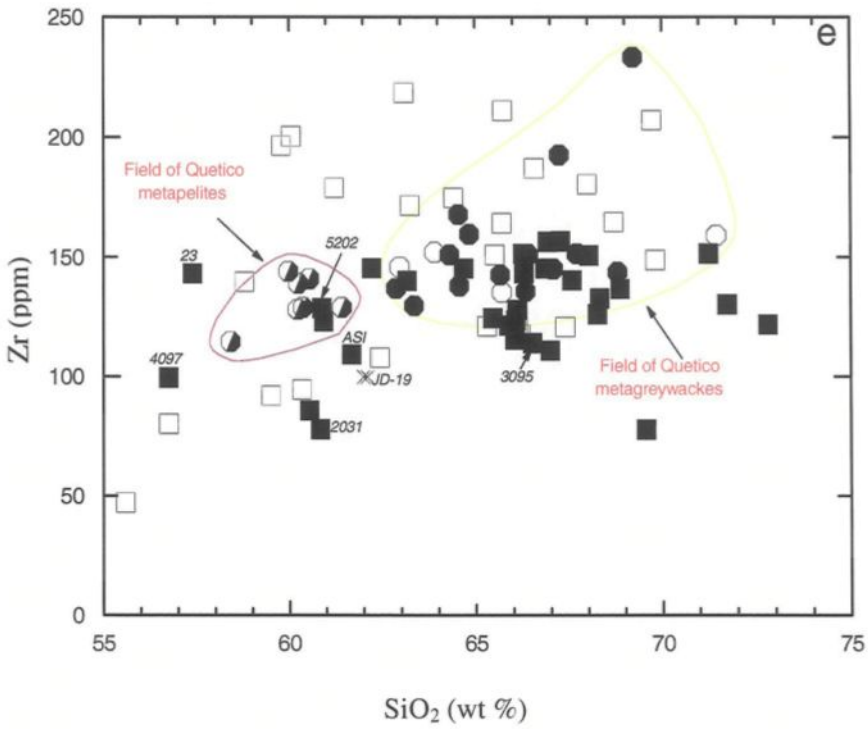
e
Zr (ppm)
SiO2 (wt %)
Field of Quetico metapelites
Field of Quetico metagreywackes
23
5202
ASI
4097
JD-19
3095
2031
250
200
150
100
50
0
55
60
65
70
75

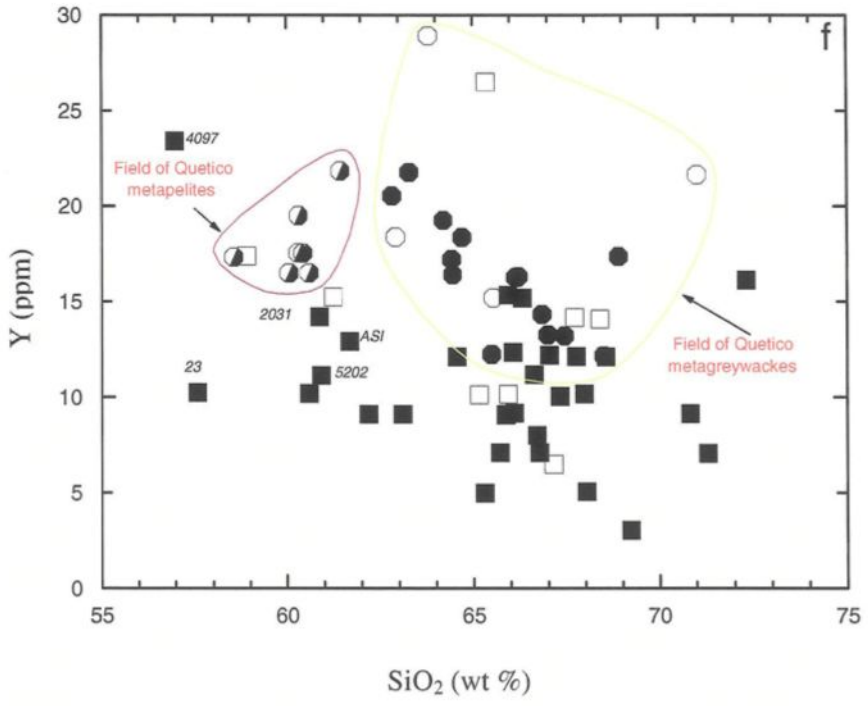
f
Y (ppm)
SiO2 (wt %)
4097
Field of Quetico metapelites
Field of Quetico metagreywackes
2031
ASI
23
5202
30
25
20
15
10
5
0
55
60
65
70
75

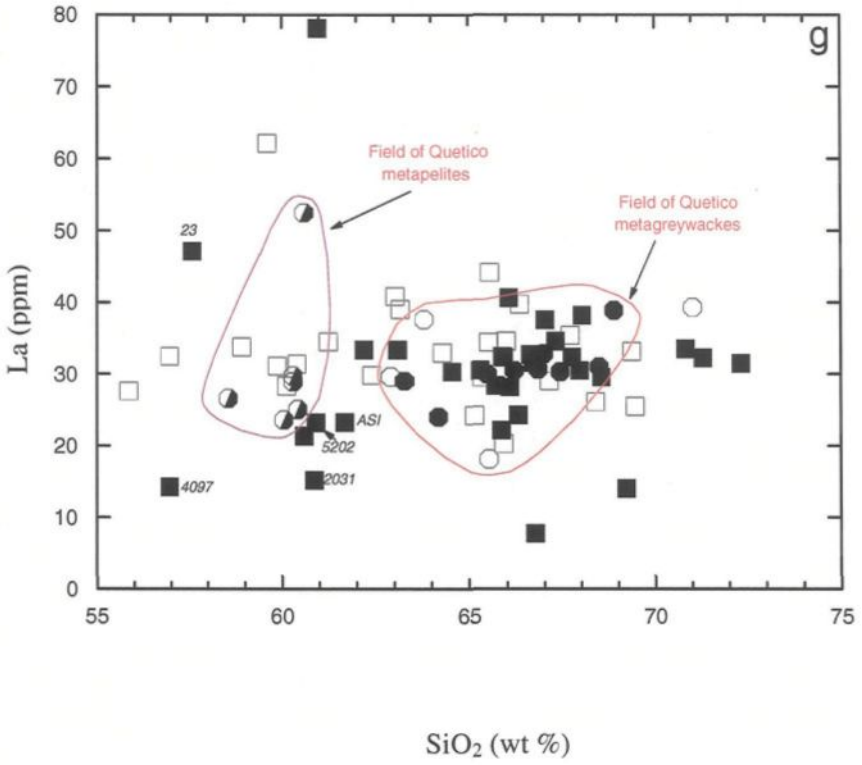
g
Field of Quetico metapelites
Field of Quetico metagreywackes
23
ASI
5202
2031
4097
La (ppm)
SiO2 (wt %)

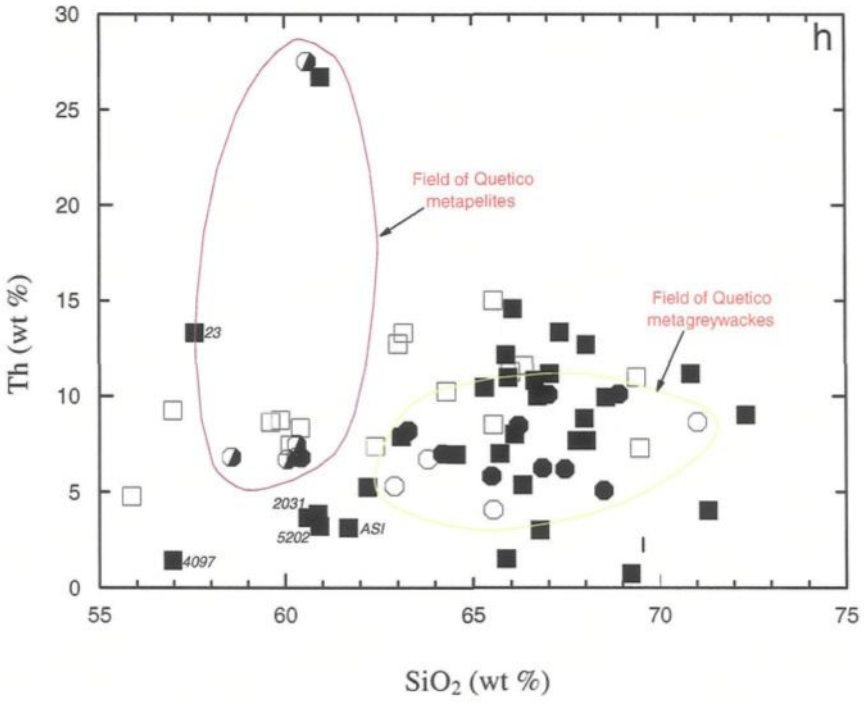
h
Field of Quetico metapelites
Field of Quetico metagreywackes
23
2031
5202
ASI
4097
Th (wt %)
SiO2 (wt %)

Figure 9. Selected Harker variation diagrams comparing the compositions of metagreywackes from the Ashuanipi subprovince (filled squares = this study; open squares = Percival (1991b) and Lapointe (1996)) with low-grade metasediments from the Quetico subprovince (filled circles = metagreywackes; half-filled circles = metapelites; open circles = hornblende-bearing metagreywackes (from Sawyer (1986) and unpublished data) and experimental melt compositions derived from greywacke starting materials (crosses = glass compositions, see text for references) and asterix = average of the experimental melt composition used for modelling). Sample JD-19 (symbol **x**) is a metagreywacke (Doyon 2004) from the Pontiac subprovince that has large component derived from an ultramafic source. Lines from some of the Quetico metagreywackes are model melt-depleted, residuum-composition trends calculated by subtracting the average melt composition; the ticks on the vectors are 10 wt % melt extraction increments.

lower average Rb/Sr ratio (Fig. 10c) in the metagreywackes. The Rb/Cs (*ca.*16.5), Sr/CaO (*ca.*146) and Th/U (*ca.*3.5) ratios are similar in both rock types (Figs. 10d, 10e & 10f), and indicates a similar ratio of minerals, clay or mica, plagioclase and accessory phases respectively, that host those elements in all the sediments.

3.6.3 Granulite facies metasediments from the Ashuanipi subprovince

All the samples collected for this study are biotite + orthopyroxene + plagioclase + quartz metagreywackes (samples 4097 and 2031 also contain trace amounts of clinopyroxene), except sample 23 which is a biotite + quartz + plagioclase + K-feldspar + garnet + cordierite metapelite. The metagreywackes contain between 56 and 73 wt % SiO_2 and overlap the field of Quetico metagreywackes to both higher and lower SiO_2 contents. They also extend towards much lower K_2O, Y, HREE, Cs, U, Zr, Ba and Th, but higher MgO, CaO and Cr than the Quetico metagraywackes, but have similar Sc, Sr, and LREE contents (Figs. 9, 10 & 11). Four samples, AS1, 2031, 4097 and 5202 have significantly higher CaO (> 3.5 %), *Mg number* (61 to 68) and high Cr contents, and will be considered separately from the other ("normal") metagreywackes.

There are significant differences in inter-element ratios compared to the Quetico metagreywackes. Although Sr/CaO ratios (Fig. 10d) are similar, the Ashuanipi metagreywackes are depleted in Rb, which generates lower average Rb/Sr ratios (Fig. 10c), and they are strongly depleted in Cs, which increases their Rb/Cs ratios markedly. The Th/U ratio is higher (7.1 *cf.* 3.5) than in the Quetico metagreywackes, because the Ashuanipi metagreywackes have lower U contents. The LREE contents are similar

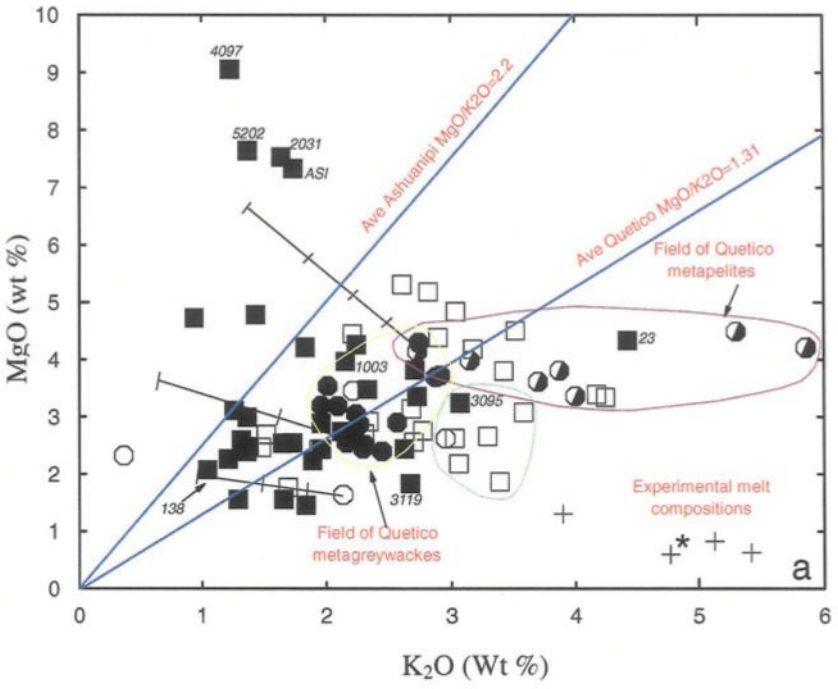
MgO (wt %)
K2O (Wt %)
Ave Ashuanipi MgO/K2O=2.2
Ave Quetico MgO/K2O=1.31
Field of Quetico metapelites
Field of Quetico metagreywackes
Experimental melt compositions
4097
5202
2031
ASI
1003
3095
23
3119
138
a

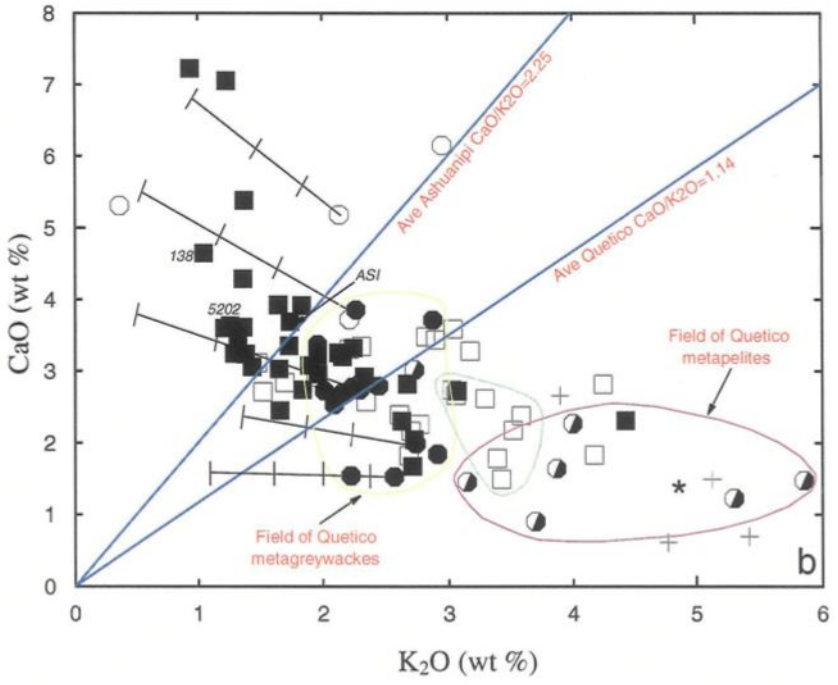
CaO (wt %)
K2O (wt %)
Ave Ashuanipi CaO/K2O=2.25
Ave Quetico CaO/K2O=1.14
Field of Quetico metapelites
Field of Quetico metagreywackes
138
ASI
5202
b

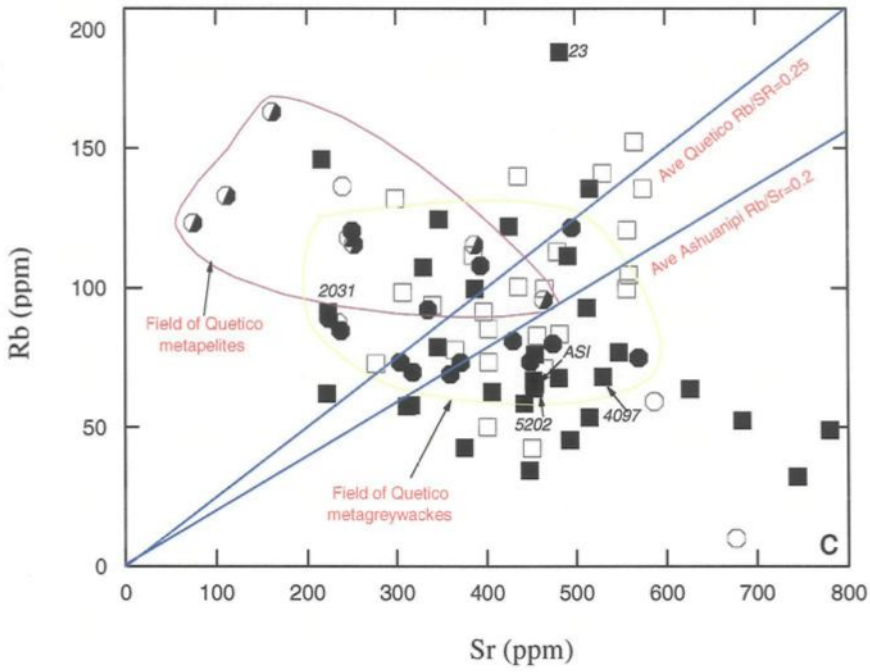
Rb (ppm)
Sr (ppm)
23
2031
ASI
5202
4097
Ave Quetico Rb/SR=0.25
Ave Ashuanipi Rb/Sr=0.2
Field of Quetico metapelites
Field of Quetico metagreywackes
c

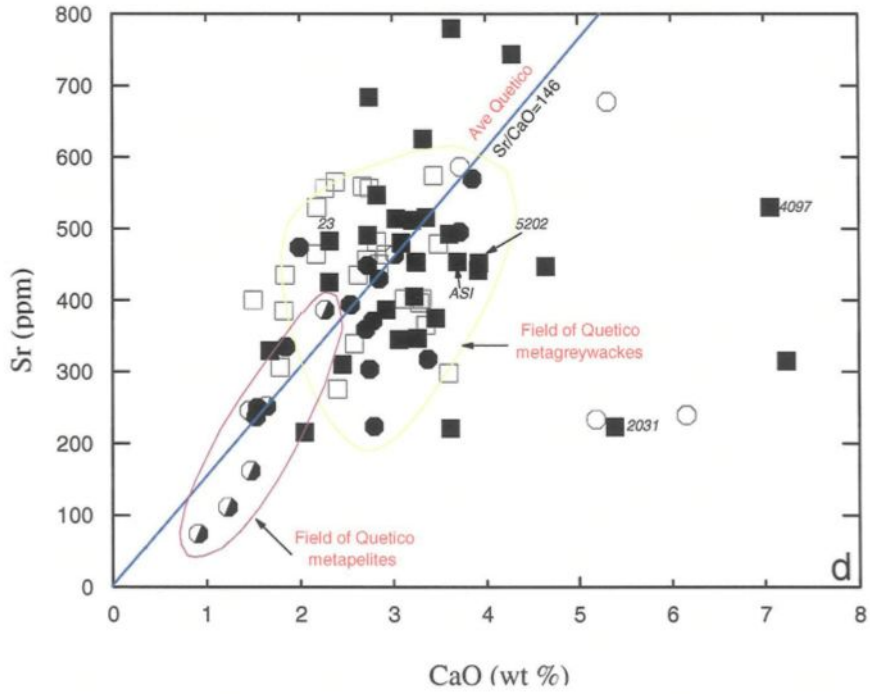
Sr (ppm)
CaO (wt %)
Ave Quetico
Sr/CaO=146
23
5202
ASI
4097
2031
Field of Quetico metagreywackes
Field of Quetico metapelites
d

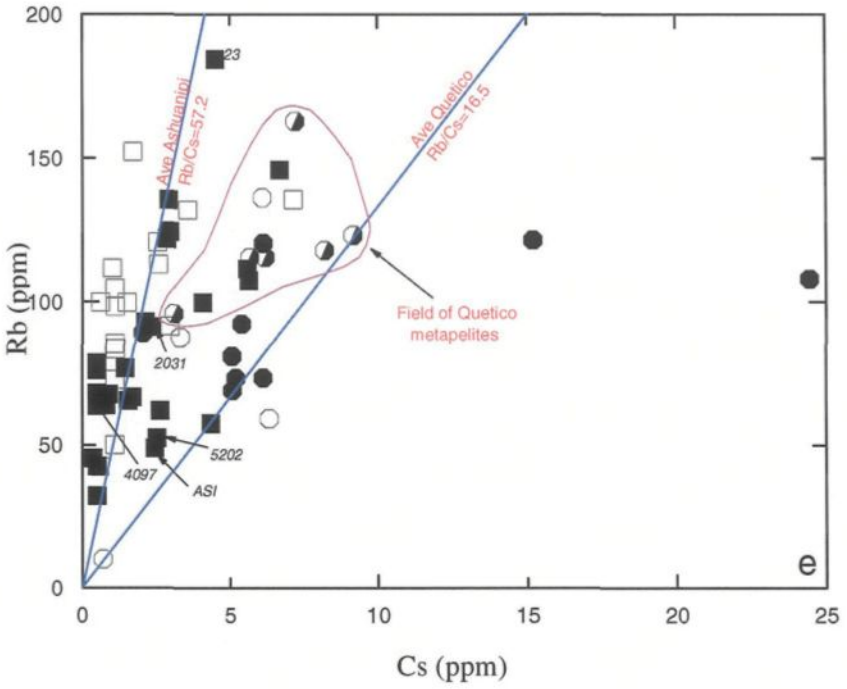
Rb (ppm)
Cs (ppm)
Ave Ashuanipi Rb/Cs=57.2
Ave Quetico Rb/Cs=16.5
Field of Quetico metapelites
23
2031
4097
5202
ASI
e

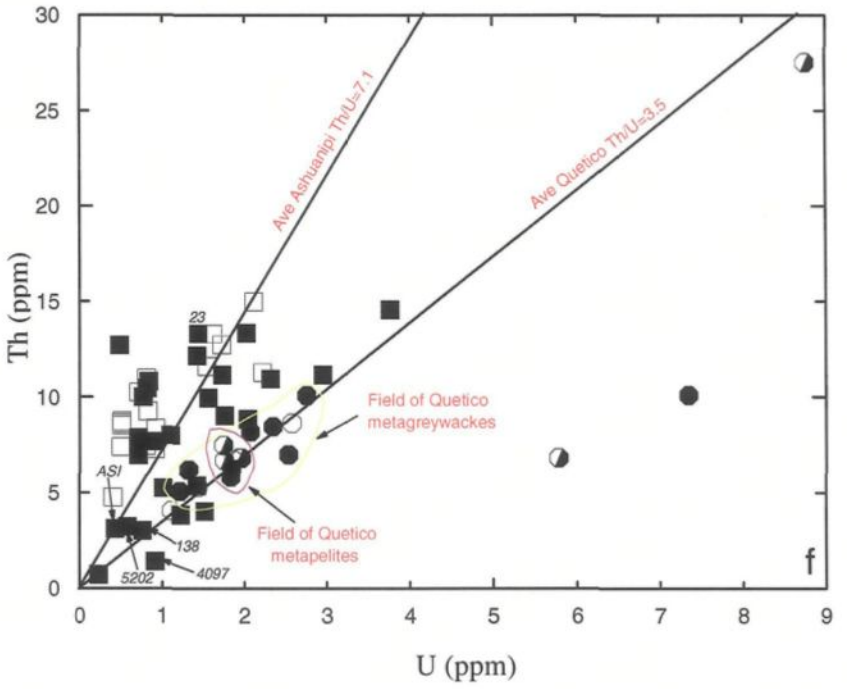
Th (ppm)
U (ppm)
Ave Ashuanipi Th/U=7.1
Ave Quetico Th/U=3.5
Field of Quetico metagreywackes
Field of Quetico metapelites
23
ASI
138
5202
4097
f

Figure 10. Major and trace element bivariant plots. a) MgO *vs* K_2O showing that the metagreywackes from the Ashuanipi subprovince are K_2O-depleted in the direction of the model melt-depletion vectors, relative to metagreywackes from the Quetico, the assumed protolith. b) CaO *vs* K_2O showing that metagreywackes from the Ashuanipi are CaO-enriched relative to those from the Quetico metagreywackes in the direction of the model residuum vectors. c) Rb *vs* Sr, showing that metagreywackes from the Ashuanipi subprovince have higher Rb/Sr ratios, d) Sr *vs* CaO, showing that Sr/CaO ratios are approximately the same for Ashuanipi and Quetico rocks. e) Rb *vs* Cs, showing a marked Cs depletion in the metagreywackes from the Ashuanipi subprovince. f) Th *vs* U, showing markedly higher Th/U ratios for the metasediments from the Ashuanipi subprovince, due to U depletion and slight Th enrichment. Symbols are as in Figure 9.

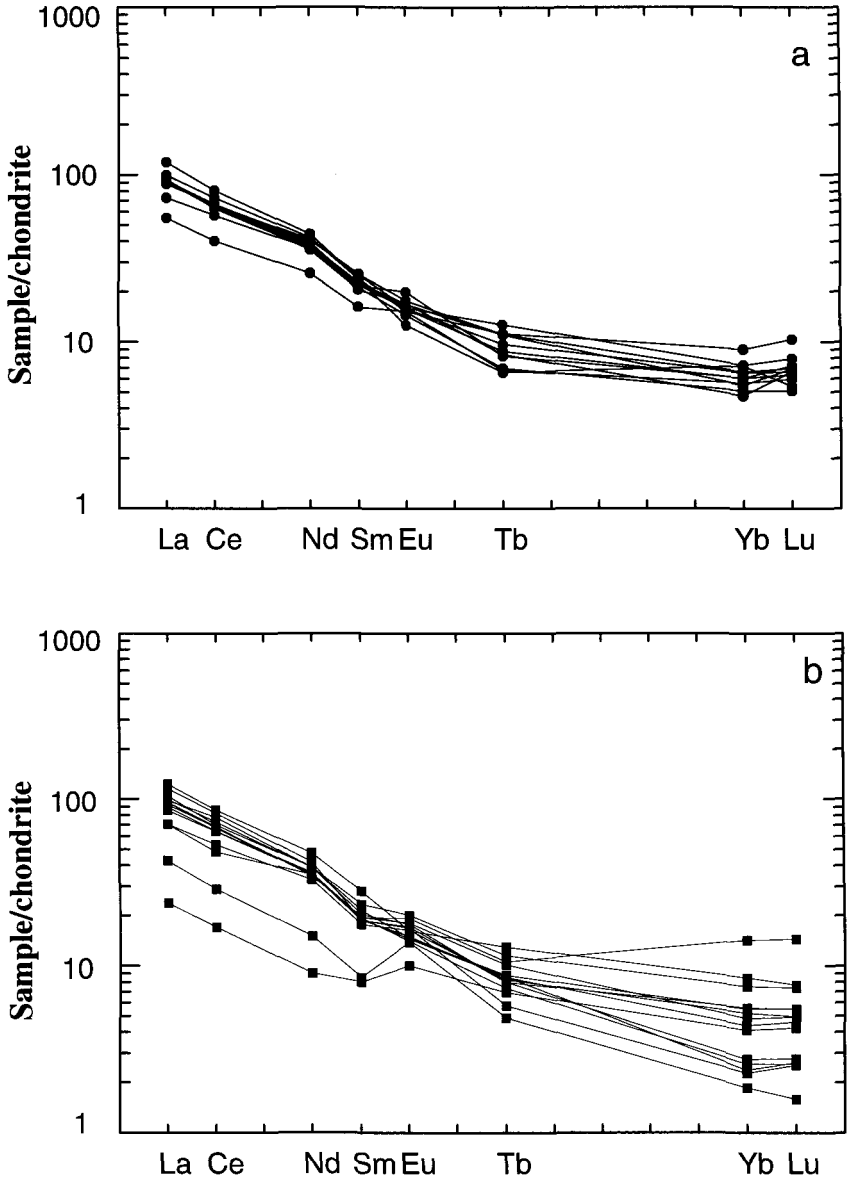

Figure 11. Chondrite normalized rare earth element diagrams; a) non-melted metagreywackes from the Quetico subprovince, and b) granulite facies metagreywackes from the Ashuanipi subprovince. The light rare earth element contents of melted and non-melted metagreywackes are similar, but the partially melted granulite facies metagreywackes have a greater range in heavy rare earth element contents. Conspicuous positive Eu anomalies are developed in the samples with the lowest total rare earth element contents from the Ashuanipi subprovince.

(Fig. 9g), but the Ashuanipi metagreywackes display a greater range in HREE abundance (Fig. 11) leading to a wider range of La/Yb_N ratios (average 19.30, sigma=10.5, n=29) compared to the Quetico (average 14.55, sigma=2.80, n=13). Europium anomalies are small, but are generally negative for the Quetico rocks and (Eu/Eu* average 0.95, sigma=0.19, 9 of 13 samples have negative Eu anomalies), and generally positive for the Ashuanipi metagreywackes (average Eu/Eu*=1.19, sigma=0.28, 11 of 13 samples have positive anomalies).

Percival (1991b) and Lapointe (1996) gave whole rock major and trace element data for Ashuanipi metasediments for an area 150 to 200 km farther north, but did not distinguish between metapelite and metagreywacke. Their data clearly contain both rock types, as some samples with high K_2O and low SiO_2 plot close to sample 23 and the field of Quetico metapelites, but others plot within the field of Quetico and Ashuanipi subprovince metagreywackes (Figs. 9 & 10). However, the metasediments reported by Percival (1991b) and Lapointe (1996) appear to be systematically poorer in CaO and richer in Zr, than our Ashuanipi metagreywackes.

3.7 DISCUSSION

The differences in composition between the metagreywackes from the Quetico and Ashuanipi subprovinces (Figs. 9 & 10) could arise if the Quetico was a reasonable estimate of the protolith composition, but that the bulk composition of the Ashuanipi metagreywackes has been modified by granulite facies metamorphism, principally by the loss of a melt fraction during anatexis or, if the Quetico metasediments are not in

fact representative of the protolith to the Ashuanipi metasediments for some elements (this would arise no matter what bulk composition the Ashuanipi metagreywackes are compared with). In order to assess these possibilities an estimate of the anatectic melt composition is required. The composition of melt rocks (i.e. leucosomes) found in the field could be used. However, leucosomes commonly have compositions that are not initial melt compositions (Sawyer 1987; Barbey *et al.* 1996, Sawyer *et al.* 1999; Solar & Brown 2001). An alternative is to use the compositions of melts derived from melting experiments done on rocks of similar bulk compositions and at the same pressures and temperatures as the natural anatexis. Melt compositions for the TiO_2-bearing metagreywacke experiments from the 7 kbar and 875°C run of Patiño Douce and Beard (1995) on the SBG starting material, the 10 kbar and 825°C experiment on BPQ material (Gardien *et al.* 1995) and the 5 kbar 851°C and 8 kbar 875°C runs of Montel and Vielzeuf (1997) are used to define the melt composition field on Figs. 9 and 10. Extraction of melt from a partially molten protolith should result in a residual rock with a bulk composition that lies on the opposite side of the protolith field to the melt field on compositional diagrams. Melt depletion effects are considered first.

3.7.1 Effect of melt extraction on composition

It is not generally possible to match a specific residual rock with the melt extracted from it for the purposes of making a mass balance, and so determine what compositional changes have occurred due to melt loss. Melt, being the mobile phase, has commonly moved from its place of formation where the immobile residuum has remained. Therefore, the approach taken here is to model general trends in residuum

composition resulting from loss of a melt fraction from its protolith, and to compare these model trends with the Ashuanipi metagreywacke compositions. The melt composition taken for calculating the melt-loss vectors is the average of the four experimental melt compositions. The Quetico metagreywackes are assumed to be the protolith, and samples representing the most siliceous, least siliceous and some typical bulk compositions (from the densest sample clustering in the protolith field) are selected for the modelling. The residuum trends are calculated at intervals of 10 wt % melt extraction. The most siliceous metagreywacke is the least fertile. It yields about 30 wt % melt before Na_2O is consumed.

The anatectic melt is richer in K_2O and SiO_2, but poorer in CaO, MgO, FeO_t, and TiO_2 than the protolith. Therefore, extraction of melt depletes the residuum in the first group, and enriches it in the second group of elements. Figure 9a shows that the position of the model K_2O- and SiO_2-depleted residuum compositions closely matches the position of the majority of the Ashuanipi metagreywackes relative to the protolith and melt fields. Because the metapelites have higher initial K_2O contents, they are principally SiO_2-depleted (e.g. sample 23); some of the metasediment samples collected by Percival (1991b) and Lapointe (1996) are evidently melt-depleted metapelites (Fig. 9). The field of Quetico metagreywackes on Fig. 9b contains two populations; one CaO-poor (< 2 wt %) and the other CaO-rich (3 to 4 wt %). Hornblende-bearing metagreywackes define a third group, at still higher CaO contents. Extraction of anatectic melt from the low-SiO_2 members of the low-CaO group yields residuum vectors that do not match the position of Ashuanipi metagreywackes when their K_2O contents (Fig. 9a) are also considered. In contrast, the residuum vectors for the CaO-

rich population match many of the Ashuanipi metagreywackes very well. Ashuanipi samples 4097 and 2031 (Fig. 9b) have very high CaO contents, and their position on Fig. 9b suggests that they could be the residuum left after melt extraction from a protolith resembling the hornblende-bearing metagreywackes of the Quetico subprovince. However, this is precluded by their high MgO and Cr contents (Fig. 9c & 9d) relative to the hornblende-bearing metagreywackes.

In MgO-SiO_2 composition space, the protolith metagreywackes and metapelites are essentially collinear, thus, many residuum vectors lie within the protolith fields, but to higher MgO and lower SiO_2 contents. The MgO-SiO_2 plot (Fig. 9c) shows a group of samples (4097 and 2031 with orthopyroxene + clinopyroxene; AS1 and 5202 with high modal orthopyroxene) forming a separate trend at high MgO contents. A tie-line from these rocks to the melt compositions indicates that they could have been derived from protoliths that had somewhat higher initial MgO contents than typical Quetico rocks. Alternatively, they could have been derived from a typical metagreywacke protolith by the extraction of 50 to 60 wt % anatectic melt, provided that the bulk composition of the extracted melt was less siliceous (*ca.* 69 wt %) and less potassic (Fig. 10a) than the four experimental melts shown (Fig. 9b). A melt with low K_2O and SiO_2 contents was obtained by Finger and Clemens (1995) from a greywacke composition (their sample 223) melted at 10 kbar and 850 °C. These four samples will be considered further in the next section.

The depletion of K_2O and enrichment in MgO and CaO (Figs. 10a &10b) shown by most of the Ashuanipi rocks can be modelled as the result of the extraction of

between 10 and 40 wt % granitic melt from a Quetico-like protolith metagreywacke. Sample 23 and those with 4 to 5 wt % MgO reported by Percival (1991b) and Lapointe (1996) were derived from metapelitic rocks following the extraction of a similar melt fraction.

Trace element modelling cannot yet be done in the same manner, because the trace element abundances in experimental melts are not known. Partition coefficients could be used (e.g. Harris & Inger 1992), but for many trace elements the mineral-melt partition coefficients are either, not well known or, vary greatly with changes in bulk composition, mineralogy, temperature and the method of measurement (Bea 1991; Harris & Inger 1992; Icenhower & London 1995).

In metamorphic rocks Rb, Ba and Cs occur principally in the micas, and Sr in plagioclase (Icenhower & London 1996). Since the plagioclase in the protolith is in excess to the reaction coefficients of R4, plagioclase content increases in the residuum (Fig. 5) as biotite and quartz decline. Thus, the Rb, Ba, and Cs contents of the residual rocks should decrease as biotite is consumed in making melt, but Sr content increases with modal plagioclase. The Ashuanipi metagreywackes have lower average Rb/Sr (0.20 *cf.* 0.25) ratios (Fig. 10c), lower average Ba (514ppm, sigma=18, n=27, *cf.* 720ppm, sigma=325, n=14), Rb (70.1ppm, sigma=26.0, n=26 *cf.* 86.4 ppm, sigma=1.0, n = 14) and Cs (2.08 ppm, sigma=1.1, n=24 *cf.* 5.67 ppm n=13) compared to the Quetico protolith. The Sr and CaO contents are higher in the Ashuanipi rocks, but the Sr/CaO ratio (Fig. 10d) remains similar to the protolith; this suggests that Sr is not fractionated from CaO during partial melting, and that neither is strongly partitioned into the melt. Icenhower and London (1996) found that during partial melting, Cs

partitioned into the melt more strongly than the Ba and Rb also hosted in the biotite, leading to a rapid depletion of Cs in the residuum; the Ashaunipi rocks have Rb/Cs ratios that are much higher than the Quetico protolith (Fig. 10e) consistent with the Cs depletion observed in experimental residua. The Ashuanipi metagreywackes are strongly depleted in U relative to the protolith (Fig. 10f) increasing their average Th/U from 3.5 to 7.1. The change from small negative Eu anomalies in the Quetico metagreywackes to small positive ones in the Ashuanipi metagreywackes is consistent with the Ashuanipi rocks being the plagioclase-rich restite left after melt extraction from a typical late Archaean metasediment (Arculus & Ruff 1990). The average Eu content in the Quetico and Ashuanipi metagreywackes is the same (1.24 ppm), hence the change from a negative to a positive Eu anomaly is due to a decrease in the abundance of the other REE in the Ashuanipi rocks. Figure 11b shows that the largest positive Eu anomalies occur in the samples with the lowest LREE abundances. The REE budget in anatectic rocks is controlled by the behaviour of REE-bearing phases during melting, e.g. HREE in zircon, LREE in monazite, Eu in plagioclase and middle REE in apatite (Miller & Mittlefehldt 1982; Bea 1991; Bea *et al.* 1994). Most of the Ashuanipi samples have Th contents similar to, or higher, than the Quetico (Fig. 9h) metagreywackes, which suggests that proportionally more monazite was retained in the residuum than dissolved into the melt. The behaviour of Zr is more complex. Our samples from the Ashuanipi subprovince are systematically depleted in Zr relative to the Quetico protolith (Fig. 9c), suggesting that much zircon dissolved into the anatectic melt, consistent with the zircon saturation data of Watson & Harrison (1983). However, there is no clear trend in the rocks from farther north, some are Zr-enriched, and others

are Zr-depleted relative to the Quetico; this may be due to initial variations in protolith Zr content.

Seven samples, 3095 and six from Percival (1991b) and Lapointe (1996) lie between the Quetico protolith and the melt fields. This group (dotted outline on Figs. 9a, 9b, 10a & 10b) has high K_2O and SiO_2, but generally low MgO, FeO_t and CaO contents and, based on sample 3095 which contains leucosomes, are interpreted as residual rocks injected by anatectic melt.

3.7.2 Protolith variations

Nearly all of the Ashuanipi metagreywackes have compositions that can be explained by melt extraction from a Quetico-like protolith, but some do not. Orthopyroxene-bearing metagreywackes (e.g. sample 1142, Table 3) with silica contents higher than the Quetico metagreywackes requires that the protolith to the Ashuanipi metasediments contained some beds richer in quartz and poorer in mica than the assumed Quetico protolith.

Samples AS1, 2031, 4097 and 5202 form a group with much higher CaO (Fig. 9b), MgO (Figs. 9c, 10a) and Cr (Fig. 9d) contents than the Quetico metagreywackes. The relatively high modal orthopyroxene content of some of these samples invites comparison with the poikilitic tonalites of the Desliens igneous suite described by Percival (1991a). Apart from the compositional banding, interpreted to be bedding in the outcrops our samples were collected from, their composition does not support

correlation with the Deslien's igneous suite. The CaO, MgO and Cr contents of the Desliens igneous suite (Percival *et al.* 2003) closely follows that of the Ashuanipi metagreywackes, the consequence of similar modal proportions of quartz, plagioclase, biotite and orthopyroxene, and the Quetico metasediments. Thus, the MgO and Cr contents of samples AS1, 2031, 4097 and 5202 are too high by a factor of two, at similar SiO2 contents, for the samples to be non-melted members of the Desliens igneous suite. If these four samples were derived from the Desliens igneous suite by removal of partial melt, then, as with derivation from a typical metagreywacke, the extraction of a large melt fraction (between 50 % and 60 wt %) is required. The combination of high CaO, MgO and Cr contents is indicative of ultramafic rocks. Metasediments with a large component derived from ultramafic sources have not yet been recognised in the Quetico subprovince, but are known from similar siliciclastic turbidites in the Pontiac subprovince (Fig. 1). A typical example of such a metasediment from the Pontiac subprovince, sample JD-19 (Doyon 2004) plots with the trend defined by samples AS1, 2031, 4097 and 5202 (Figs. 9b, c & d). Specifically, JD-19 lies between these samples and the anatectic melt field, and this suggests that the four samples were derived by the extraction of a more moderate melt fraction (< 30 wt %) from a metagreywacke that contained a large component of ultramafic detritus, rather than from the Desliens igneous suite.

3.7.3 Volume of melt generated in the Ashuanipi subprovince

The compositional characteristics (Figs. 9 & 10) of metagreywackes from the Ashuanipi subprovince indicate that they are the melt-depleted residuum left after the

extraction of anatectic melt from a protolith similar to the Quetico metagreywackes. Most Ashuanipi metagreywackes can be modelled with 20 to 40 wt % (average 31 wt %) melt loss; the average Quetico metagreywacke would yield 45 wt % melt through (R4) before quartz disappeared.

Mapping of the Ashuanipi subprovince has established that granulite facies metasedimentary rocks and migmatites derived from them, cover an area of 90 000 km^2 (Percival 1991b). The average degree of partial melting from modal analysis and supported by geochemical modelling is about 31 wt %, which corrected for the difference in density between melt (2500 kg m^{-3}) and metagreywacke (2780 kg m^{-3}), corresponds to 34 vol % (wt % x 1.112). The Ashuanipi subprovince was not part of the Lithoprobe Project, so its present thickness is unknown. However, in the comparable, but narrower Pontiac and Quetico subprovinces, the Moho is at 40 km and the metasediments extend below 30 km depth (Calvert & Ludden 1999; Hynes 1999).

A simple mass balance; 0.34 (average volume fraction partial melting) x 0.7 (volume fraction of metagreywacke i.e. excluding the metapelites (*ca.* 0.1) and the Desliens igneous suite) x 90 000 km^2 (area) x 30 km (thickness of the metasediments) yields 642 600 km^3 of granitic melt. That large volume of granitic melt was generated by biotite dehydration melting and extracted from the metagreywackes in the Ashuanipi subprovince.

3.7.4 Melt path during extraction

Several field and petrographic observations are important in understanding how such a large volume of melt separated from its source in order to create a large region of melt-depleted (residual) granulites.

1) Bedding can be traced continuously across large outcrops, even in rocks that the modal and bulk chemical compositions indicate lost *ca.* 40 wt % melt. In some melt-depleted layers, fine-scale sedimentary structures such as graded bedding, Bouma sequences and slump structures, are still visible. Furthermore, many of these melt-depleted layers have no leucosomes, or structural discontinuities (e.g. shear bands or boudins) that could have served as channels through which melt flowed. That delicate sedimentary structures survive melt extraction in granulites is not uncommon, e.g. Namaqualand (Waters & Whales 1988) and Broken Hill (Roger Powell personal communication to Sawyer 2001). The preservation of fine-scale, pre-anatectic structures in melt-depleted rocks indicates that the melt segregation process was pervasive (occurred throughout the rock volume) and non-disruptive. To achieve this, melt could not have accumulated in the matrix to pass the 20 to 25 % threshold at which magma-like flow starts (the melt escape threshold of Vigneresse *et al.* 1996) and pre-existing structures are destroyed. Hence, excess melt must have been continually drained from the matrix (Sawyer 1994) once the few percent required for permeability had formed (the liquid percolation threshold of Vigneresse et al. 1996).

2) Microstructures (Fig. 6) indicative of former melt are common in the metagreywackes of the Ashuanipi subprovince. The distribution of these microstructures mapped in thin sections reveals that the melt was; a) uniformly

distributed throughout the rock, at least at volumes required for preparing three orthogonal thin sections, b) located along the grain boundaries, most commonly those parallel to the foliation and, c) very rarely located in transgranular cracks. Melt was preferentially located in foliation planes, probably because it formed where the reactant biotite was located progressively replacing biotite as the melting reaction advanced, and in these rocks biotite defines the foliation. Since the Ashuanipi metagreywackes have lost on average 31 wt % melt, the distribution of melt revealed by the microstructures reflects the melt distribution which existed late in the melting-segregation history, and not necessarily that at the onset of melting. Point counting of the relict melt microstructures shows that between 1 and 3 vol % melt remained in the residual rocks; a little more melt may have been present if it formed overgrowths on the residual minerals that we did not recognise. The key information from these observations is that melt was distributed throughout the rock on grain boundaries, especially ones parallel to the foliation, and that even in samples without leucosomes, between 80 and 90 % of the total melt generated was extracted from the matrix of residual minerals.

3) Many outcrops do, of course, have leucosomes (Fig. 12), and in these one set generally lies parallel to bedding and/or foliation, and another less continuous, but thicker, set occurs in oblique structures; shear bands and boudin necks. Together, both sets of leucosomes form a net-like array of interconnected, melt-filled channels. A significant feature of the leucosome array in Fig. 12 is that, no point in the outcrop is more than a few tens of centimetres from a leucosome, i.e. a melt channel. This may indeed be a general feature, but probably a transient one, of partially molten rocks undergoing melt loss (see Sawyer 2000, Fig. 6; 2001, Figs. 7 & 8 for similar channel

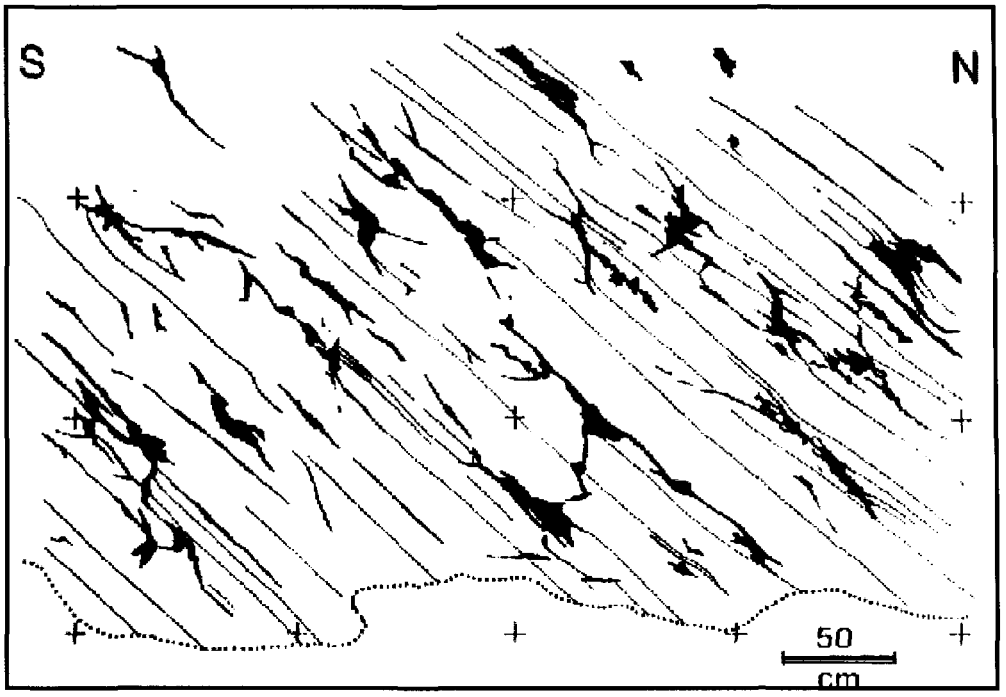

Figure 12. Outcrop map (vertical face, parallel to the stretching lineation) showing the distribution of leucosomes that are thicker than 3 mm, in a strongly melt-depleted metagreywacke. Thin, continuous leucosomes are oriented parallel to the layering (i.e. S_0, bedding) and wider discordant leucosomes in shear bands and boudin necks form a net-like array of melt channels in the outcrop. The rocks in this outcrop generated between 30 and 45 vol % melt, and about 5 vol % melt remained in the outcrop (i.e. source layer); 1 vol % on the grain boundaries in the matrix of the melt-depleted granulite and the rest as the leucosomes in the outcrop.

geometries; Brown *et al.* 1999; Marchildon & Brown 2002). Once the melt segregation process slows, or stops, the channels through which melt is flowing start to deflate (collapse), and may eventually be lost (Sawyer 2001). Unlike the leucosomes in the amphibolite facies rocks described by Sawyer (2001), the leucosomes in the granulites do not have melanosomes around them. Rather, all the rocks containing the leucosomes in Fig. 12 are residual in composition, their orthopyroxene contents and bulk compositions indicate loss of between 30 and 40 wt % melt. Hence, the channel network, preserved as the leucosome array, is the remains of that through which melt drained out of the host metasediments.

Combining these observations leads to the model of melt extraction for the Ashuanipi metagreywackes shown in Fig. 13. Melt is formed at the site of the disappearing reactant minerals and in nearby grain boundaries (Fig. 13a). When segregation starts, melt is drained from the matrix and it initially flows along all the grain boundaries commonly, but not exclusively, in the direction of the foliation in these rocks. This pervasive flow regime extends for a few to several tens of centimetres from the site where the melt formed to where the melt reaches a channel, created by either dilating bedding or foliation planes, or by the development of structures such as shear bands and boudin necks. When the melt enters these a regime of channel flow starts. Residual granulites can be generated by either, porous (grain boundary) flow draining melt into adjacent bedding planes (Fig. 13b), forming layer-parallel (stromatic) leucosomes at the boundaries of leucosome-free residual rocks or, they may form by a

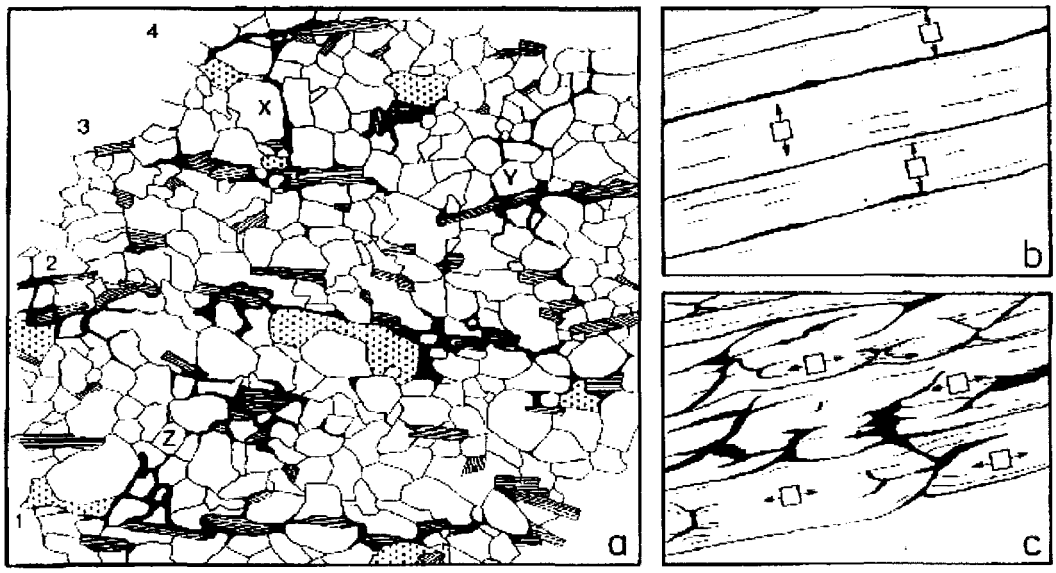

Figure 13. A model for the extraction of melt from granulites, based on the Ashuanipi subprovince. a) Distribution of melt (black), biotite (stripped), orthopyroxene (dotted), plagioclase and quartz (both unpatterned) in a typical metagreywacke rock. The melt occupies some of the space created by the destruction of reactant biotite, quartz and plagioclase. The location of melt is controlled by the distribution of biotite and is, therefore, primarily along the foliation planes. Melt pools in foliation plane 1 are better connected laterally than melt in foliation plane 2. Melt pools in foliation planes 3 and 4 are also connected along grain boundaries (X) orthogonal to the layering. Further cross-foliation interconnectivity of melt pools will occur at Y and Z when melt spreads along grain boundaries there, either because more melt is generated, or because driving forces cause melt movement. b) When melt movement (arrows) in the matrix (box) is primarily orthogonal to the layering the resulting migmatite consists of layers (beds) with residual compositions separated by layer-parallel leucosomes; note there are few leucosomes in the melt-depleted layers. c) If melt movement (arrows) in the matrix is primarily within the plane of the layer and towards dilatant sites forming as the layers deform, then the resulting migmatite consists of residual (melt-depleted) layers containing short, wide leucosomes (which drain the layer) that are linked by layer-parallel leucosomes between the layers and enable melt to be transferred out of the source region.

combination of porous flow and channel flow creating a melt-depleted granulite containing a net-like pattern of leucosomes (Fig. 13c).

The driving forces for melt segregation are the pressure gradients (Robin 1979) set up when heterogeneous (i.e. layered) rocks are subject to deviatoric stresses in a general tectonic deformation, i.e. one with both pure and simple shear components (Stevenson 1989; Sawyer 1994; Rutter 1997; Simakin & Talbot 2001). If, during deformation no strain incompatibilities develop in a particular layer, then the pressure gradients in that layer may be normal to the layering, and melt moves across the layer to its edges, accumulating between adjacent layers (Fig. 13b), much like in the metamorphic segregations described by Robin (1979). However, if strain incompatibilities develop in a particular layer, or between layers in a thinly layered sequence, then internal dilatant sites (boudinage, fractures or shear bands) develop in the layers and the direction of the pressure gradient is along the layering, and melt migrates pervasively along the layer to the dilatent sites, which if numerous, form a linked array (Fig. 13c).

3.7.5 Implication for the middle and lower crust

Vielzeuf *et al.* (1990) pointed out that there are two types of deep crustal granulite terrane. One developed from a hydrous protolith, typically a flysch-type metasedimentary sequence, metamorphosed soon after deposition and which reached temperatures of 850 to 900°C and generated large volumes of "wet S-type" granite

magma. The other type develops when already dehydrated continental crust is reworked in a second orogenic event, these typically reach higher temperatures (>1000°C) and contain "A-type" magmas. The Ashuanipi subprovince belongs to the first type, and our comment is primarily for granulites formed that way.

Rushmer (2001) has proposed that the rheological behaviour of continental crust is controlled by which melting reaction takes place, and suggests that anatectic melt generated by dehydration melting of biotite is not easily segregated from its protolith because the negligible change in volume of such reactions precludes grain cracking and hinders melt segregation. Consequently, melt accumulates in the source, leading to a weaker lower crust. In contrast, where melting occurs by muscovite dehydration, melt extraction is more rapid and efficient because of extensive cracking of protolith grains due to a large, positive volume change of reaction, consequently the upper crust is stronger because melt is not trapped in its source, but escapes (Rushmer 2001). The Ashuanipi subprovince provides a test of Rushmer's proposal. The petrographic and geochemical data shows that Ashuanipi rocks are the residuum left after an average of 31 vol % melt was extracted leaving only a few percent of melt behind in the residuum. Thus, in a regionally extensive example of natural anatexis in a contractional orogen, abundant melt generated by biotite dehydration was thoroughly extracted from its matrix. If the lower crust is weak due to melt accumulation, then the cause is not an accumulation of unsegregated melt in the matrix of the actual source itself; it must be the accumulations of segregated melt elsewhere.

3.8 CONCLUSIONS

The compositions (e.g. enrichment in MgO, FeO_t, CaO, Sr and depletion in K_2O, SiO_2, Cs and U) and orthopyroxene contents of metagreywackes in the Ashuanipi subprovince can be modelled as the result of an average loss of about 31 wt % granitic melt. Because plagioclase was present in excess during the melting, the residual rocks are very plagioclase-rich and have positive Eu anomalies. An estimated 640 000 km^3 of granitic magma was segregated from the metagreywackes. Many of the residual rocks have few leucosomes and contain, distributed throughout, microstructures that indicate the former presence of melt along grain boundaries. Melt segregation in these rocks did not destroy the bedding, and involved the dispersed flow of melt over distances of a few centimetres to several tens of centimetres, from the place of its formation to nearby dilatant structures. Thus, melt segregation began in a dispersed (or porous) flow regime on the grain boundaries and then switched to a channel melt flow regime when it entered the dilatant structures. The macroscopic melt-flow channels are visible as the linked arrays of leucosomes in some outcrops. These leucosomes contain very little residuum material and indicates that the separation of the melt fraction from the residual solid fraction was very effective. Some metagreywacke layers lost melt principally by porous or dispersed flow, but in others channel flow of melt followed the initial phase of dispersed flow. Very little melt remained in the residual rocks, which indicates that melt extraction during granulite facies metamorphism at mid-crustal levels can be, essentially, complete.

CHAPTER IV

FATE OF THE SEGREGATED ANATECTIC MELT, THE GENERATION OF THE DIATEXITE MIGMATITES

4.1 INTRODUCTION

Using petrographic and geochemical data it has been shown in chapter III that the metasedimentary rocks in the Ashuanipi subprovince are the residuum left after an average of 31 vol % granitic melt was extracted from them; only a few percent melt remained trapped in the residuum. Thus, melt extraction from the protolith layers during granulite facies metamorphism in the Ashuanipi subprovince was essentially complete. The fate of the melt that was extracted from the residuum is the subject of this chapter and the next. The microstructures present in the melt-rich rocks and their whole rock major and trace element compositions will be used to discuss the progressive changes that occurred as the melt moved through the continental crust and finally crystallized.

The creation of diatexite migmatite in anatectic terrains is the key step in the transition from a high grade metamorphic protolith to granite, indeed granitic magma can originate from such rocks (Sawyer 1996, 1998). This transition from metamorphic rocks through diatexite migmatite to granite has been well illustrated for several upper amphibolite facies anatectic terrains (Opatica subprovince, Sawyer 1998; Maine migmatites, Solar & Brown 2000; St Malo migmatite terrain, Milord *et al.* 2001). Although, partial melting in the granulite facies through the incongruent breakdown of biotite may be the principal mechanism of generating granites in the continental crust (e.g. Stevens *et al.* 1997), the petrogenetic link between melt-depleted granulite facies rocks and granites through the processes that occurr in diatexite migmatites have not yet been fully explored and are, therefore, not fully known.

Diatexite has been defined as a migmatite in which pre-existing structures are destroyed; typically a coarser grain size and flow structures are also developed (Brown 1973; Sawyer 1996). The formation of a diatexite migmatite depends strongly on the interplay between the rate of partial melting and the rate of melt segregation (Sawyer 1994). If the melt produced by anatexis is able to accumulate in the source and reaches a threshold of about 20 to 40 volume % (Wickham 1987; Vingeresse *et al.* 1996; Rosenberg & Handy 2005) a diatexite magma forms. The flow of magma occurs in response to imposed shear stresses and results in the destruction of the pre-anatectic structures in the rock (Brown 1973; Sawyer 1996, 1998; Bea 1994, White *et al.* 2005; Rosenberg & Handy 2005). We understand from this characteristic feature, that diatexite is a derivative from magma.

Field, petrographic and geochemical evidence, suggest that partial melting of the greywacke rocks in the Ashuanipi subprovince has occurred, and because a large volume of residual material remains in the Ashuanipi subprovince, that synchronous penetrative deformation and buoyancy drove the movement of granitic magma to a higher crustal level. The aim for this chapter is to identify the different processes (e.g. contamination, crystal accumulation, fractional crystallization) that occurred and modified the original composition of the anatectic melt that separated from the residuum.

The transition from metatexite to diatexite migmatite, as well as the magmatic nature of the diatexite, is well illustrated in the Ashuanipi subprovince. The metasedimentary protolith has partially melted and in places developed layer-parallel

leucosomes. In some regions, this migmatite has then been intruded by numerous, thin veins or sheets of anatectic leucogranite that are oriented at a low angle to the foliation so that, in the extreme case, the migmatite has a layered appearance in which innumerable leucocratic veins are separated by screens of residual wall rock. At their margins, many of the thin granitic veins contain elongate fragments of wall rock and biotite reaction rims derived from the wall rocks; however, the thin veins and sheets have within them few enclaves and/or schlieren, and so can be described as leucocratic veins. This is not the case for larger (metre to tens of metres) bodies of granitic magma emplaced concordant to the layering in the melt-depleted metasediments. These large bodies contain abundant enclaves of their melt-depleted host rocks as well as schlieren. Typically, the enclaves are angular at the margins of the intrusive bodies, but are rounded and smaller towards the centres, suggestive of magmatic corrosion. Concomitantly, the host magma becomes darker towards the centres of the bodies as it is progressively more contaminated with material (biotite and orthopyroxene) eroded from the rounded enclaves. This contaminated granitic magma with enclaves and schlieren is the diatexite migmatite in the Ashuanipi subprovince. Thus, in this case the transition from metatexite migmatite to diatexite migmatite is not one of a local increase in the fraction of melt present due to increased degree of partial melting. Rather, it is accomplished principally by the intrusion of anatectic leucogranite into suitable dilatant, structural sites; such as parallel and subparallel to the foliation, or in fold hinges (Stevenson 1986; Collins & Sawyer 1996; Allibone & Norris 1992) and interaction with the wall rocks.

4.2 VARIATIONS WITHIN THE DIATEXITE MIGMATITES

Diatexite migmatites occur as sheet-like bodies throughout the study area, and generally have moderate dips to the north, thus they are subparallel to the layering (bedding) in the adjacent, melt-depleted metasediments. Typically the bodies of diatexite migmatite range from several metres to several hundreds of metres in thickness. However, some diatexite bodies are laterally continuous at the regional scale (i.e. up to 100 km) and these bodies may be much thicker (in excess of a thousand metres).

All the diatexite migmatites have a medium to coarse grain size and, locally, display magmatic flow structures, such as banding and schlieren. Structures that pre-date the anatexis only occur in the metasedimentary enclaves. There is considerable diversity in the outcrop appearance of the diatexite migmatites in the Ashuanipi subprovince. Much of the variation in morphology within the diatexite migmatites can be related to the modal composition of the diatexite, principally to changes in the plagioclase / K-feldspar ratio. Systematic changes include; 1) decrease in the proportion of othopyroxene with decrease in the plagioclase / K-feldspar ratio, 2) change in the percentage of mafic minerals in from the edges of diatexite migmatite bodies, 3) changes in the size, shape, and abundance of enclaves broadly correlated to the plagioclase / K-feldspar ratio, and 4) a change in the microstructure of the diatexites with decrease in the plagioclase / K-feldspar ratio which results in a microstructure with a progressively stronger magmatic aspect.

Most of the diatexite migmatites from the Ashaunipi subprovince lie in the granodiorite field of the mesonormative QAP plot (Fig. 14), however, a few samples of diatexite migmatites lie in the monzogranite (3b) field and a few samples in the tonalite (5) field. This change can be interpreted in terms of a typical crystallization sequence for metaluminous and peraluminous granitic magmas undergoing fractional crystallization (Tuttle & Bowen 1958); plagioclase-rich rocks represent an accumulation of the early crystallized products of the melt (and possibly to some extent residual grains that did not melt), whereas the K-feldspar-rich ones represent later stages of crystallization derived from the evolved melts. In metaluminous melts quartz crystallizes with K-feldspar after plagioclase crystallization has began, however, in some peraluminous compositions, such as the Ashuanipi subprovince, quartz may begin to crystallize earlier with plagioclase, and before K-feldspar. The crystallization sequence observed in the Ashuanipi is: orthopyroxene + plagioclase; orthopyroxene + plagioclase + quartz; orthopyroxene + plagioclase + quartz + K-feldspar; plagioclase + quartz + K-feldspar ± biotite.

The systematic mineralogical and microstructural variations that occur within the diatexite migmatites will be described with the compositional framework outlined on figure 15. In the field the contacts between the three different types of diatexite migmatite are gradational due to progressive changes in the modal mineralogy. More rarely, contacts between diatexite migmatites are due to differences in mineral assemblage, principally the presence, or absence, of orthopyroxene.

4.2.1 The Plagioclase-dominated diatexite migmatites

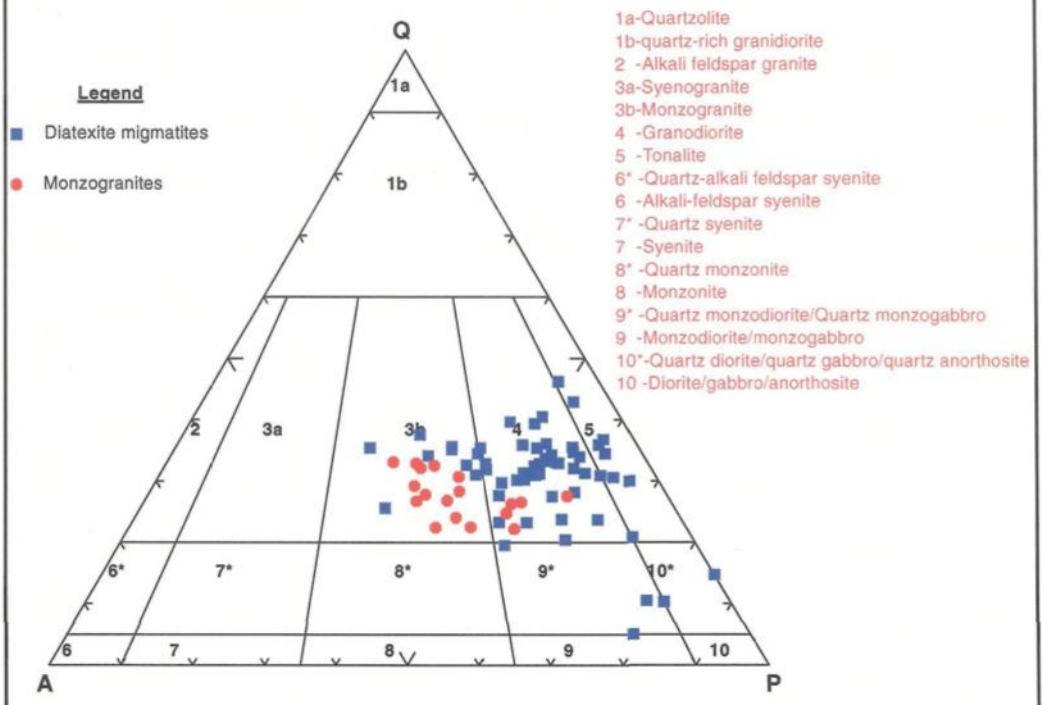

Figure 14: Quartz-Alkali-feldspar-Plagioclase (Q-A-P) mesonormative plot (Lemaitre 1989 in the Newpet software) shows that the majority of the Ashuanipi diatexite migmatite samples plot on the granodiorite field; few samples are in the monzogranite field and a few in the tonalite field. A=alkali feldspar, P=plagioclase, Q=quartz.
Symbols: blue squares are diatexite migmatites (whole rock compositions taken from table 4) and the red circles are monzogranite samples (whole rock compositions are from table 6).

Plagioclase-dominated diatexite is the most abundant type. Some plagioclase-rich diatexite migmatites have > 60 modal % plagioclase, but the average plagioclase content of the diatexites for which the point counts were made is 30 % (appendix IX). In the outcrop, this type of diatexite migmatite contains the highest proportion of enclaves, locally reaching in excess of 25 volume %. The enclaves are mostly of the melt-depleted metagreywacke, but locally enclaves consist of vein-quartz derived from the adjacent metagreywacke rocks. Rarely, enclaves derived from mafic and ultramafic layers are present, and these are interpreted to have been derived from intrusions or flows of mafic or ultramafic magma within the original sedimentary sequence in the Ashuanipi subprovince. In general, the enclaves have tabular, elongate, and rectangular shapes (Fig. 16a), with more-or-less rounded corners. In most cases the enclaves are oriented oblique to the foliation in the host diatexite that is defined by oriented tabular plagioclase. Many enclaves are sigmoidal in shape, and in places enclaves are imbricated or tiled (Blumenfeld & Bouchez 1988); these features, together with the regionally consistent orientation of the enclaves, indicates alignment during south-vergent non-coaxial shearing. Schlieren of biotite are more common in the plagioclase-dominated diatexites, than the other two types. These diatexites are generally well-foliated rocks containing oriented tabular plagioclase and biotite, and many display centimetre-scale flow banding that is most evident around the sigmoid-shaped enclaves.

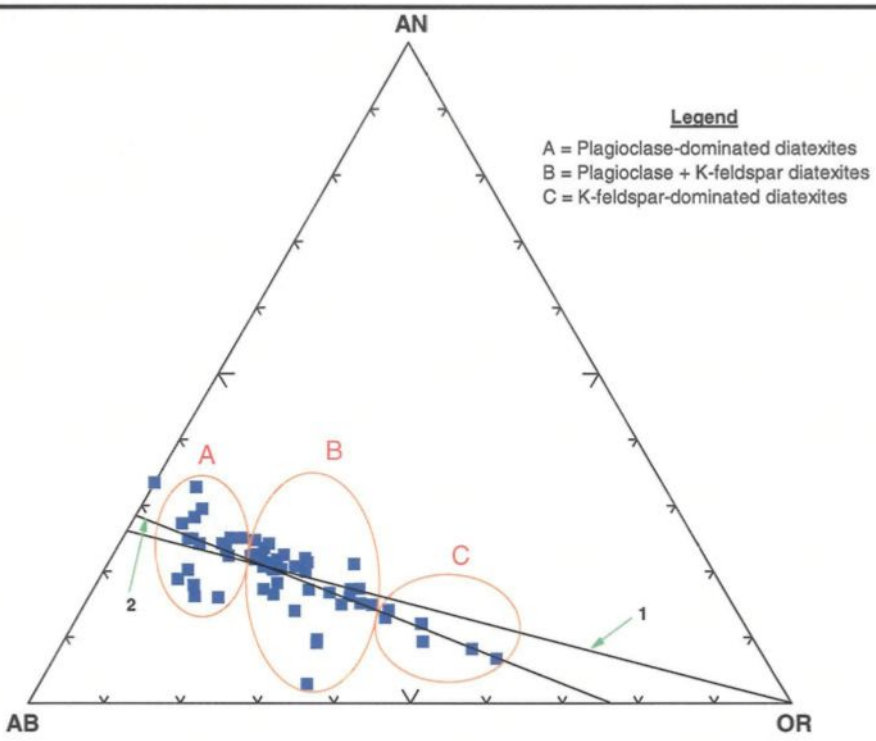

Figure 15: Albite-anorthite-orthoclase (Ab-An-Or) mesonormative plot (Kosinowski 1981, in Newpet software) showing the three main subdivisions of diatexite migmatites used in this study. A=plagioclase-dominated diatexite migmatite; B=Plagioclase+K-feldspar diatexite migmatite; C=K-feldspar-dominated diatexite migmatite. Line 1 is the line of constant Ab:An ratio; and line 2 is an oblique trend through the data which shows a decrease in anorthite content and an increase in albite content as the composition of the diatexite migmatites becomes more orthoclase-rich. AB=albite, OR=orthoclase, AN=anorthite. Symbols: blue squares, diatexite migmatites (whole rock compositions from table 4).

Plagioclase

The plagioclase in these diatexites occurs as either; 1) large euhedral or subhedral phenocrysts with straight, rational faces against quartz or, more rarely K-feldspar, this microstructure is evidence of crystallization from a melt (e.g. Platen 1982, 1983; Vernon & Collins 1988) or, 2) smaller anhedral, commonly polygonal-shaped groundmass crystals that are interstitial to the larger grains. Generally, the anorthite content of the plagioclase is uniform from the core to the rim and is typically about An_{26}. Discrete, simple zoning is developed in some of the large plagioclase crystals, and generally the cores are slightly more calcic than the rims. Some large plagioclase crystals display rounded cores that are more calcic (by 2 to 3 mol % An) than the rest of the interior. The rims of the large plagioclase grains are commonly weakly zoned from about An_{25} to An_{17} at the very edge. The small, interstitial plagioclase grains generally have compositions in the range An_{25} to An_{17} (Appendix XVII). The calcic cores could be interpreted to be residual (i.e. remnants inherited from the melt-depleted metasediments), and the more sodic plagioclase as having crystallized from the anatectic melt (e.g. Sawyer 1998), either as overgrowths on the more calcic cores, or as discrete groundmass grains.

K-feldspar

K-feldspar can be present in the plagioclase-rich diatexites, but it is always very minor (< 5 modal %). K-feldspar is typically interstitial to the subhedral plagioclase phenocrysts. However, some plagioclase-rich diatexites do not contain K-feldspar.

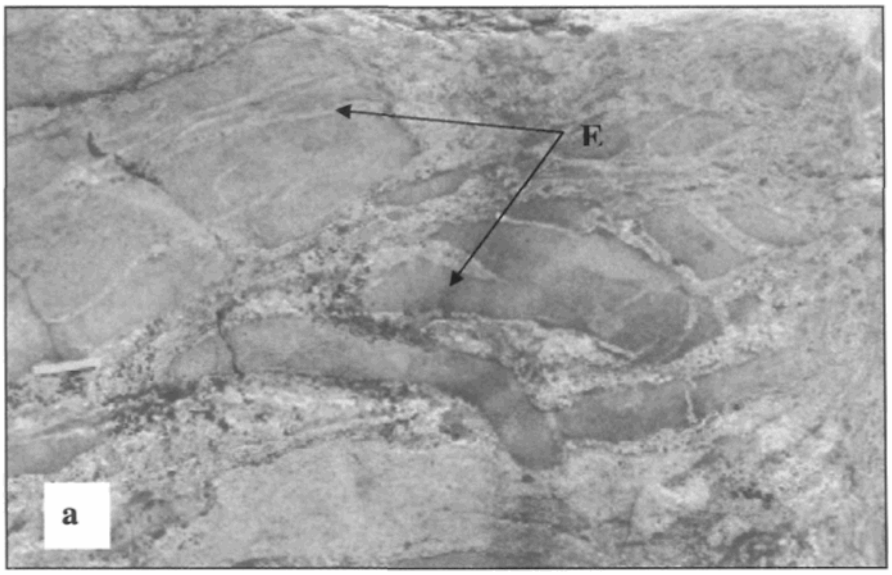

Figure 16a: Margin of a body of plagioclase-dominated diatexite migmatite that contains tabular, elongate and rectangular metasedimentary enclaves (E) spalled off from the wall rock (to the left, but out of the photograph). Note the rotation of the enclave farther into the diatexite (on the right). Note also the absence of pre-anatectic structures in the diatexite migmatite.

Quartz

The quartz is characteristically anhedral and in most of the diatexite migmatites it exhibits undulose extinction and has irregular grain boundaries; features which indicate some deformation and recrystallization.

Small rounded grains of quartz (and small euhedral biotite crystals) are present as inclusions in some of the plagioclase phenocrysts. The quartz-rich domains in most of the plagioclase-dominated diatexite migmatite are not noticeably elongate, and this indicates that the flow and formation of the foliation occurred in a magmatic state (Blumenfeld & Bouchez 1988), although some post-solidification plastic deformation has occurred in many samples (e.g. undulose extinction) it has not changed the shape of quartz domains significantly.

Ferromagnesian minerals

Biotite has, compared to the other minerals forming the groundmass, more commonly, a euhedral form. Orthopyroxene, when present in these rocks, is either subhedral, with some rational crystal faces typical of a growth in a melt (Platten 1983), or is cracked and rimmed by blades of euhedral biotite, which suggests reaction with the enclosing melt (Sawyer 1999; Waters 2001). A few of the plagioclase-rich diatexites contain small polygonal grains of orthopyroxene, and these may be grains of residual orthopyroxene derived from the melt-depleted metagreywackes. Common accessory minerals are ilmenite, zircon, magnetite, apatite, rutile, monazite and rarely tourmaline. Clinopyroxene is very rarely present in the diatexite migmatites, but in one sample attains 9 modal %. Clinopyroxene and/or hornblende crystals in the diatexites occur

where there are enclaves of mafic and ultramafic rocks, and they probably represent xenocrysts derived from the disaggregation of mafic layers (e.g. Sawyer 1998); further examination of these cpx-bearing rocks is beyond the scope of the present study.

4.2.2 The plagioclase + K-feldspar diatexite migmatites

This type of diatexite is widespread in the Ashuanipi subprovince. Enclaves within the plagioclase + K-feldspar diatexite migmatites generally have asymmetric shapes that consistently defines a south-vergent shear sense (Fig. 16 b), and is evidence for the syn-deformation flow of the diatexite magma. The foliation in these diatexite migmatites is magmatic and defined by the alignment of elongate plagioclase crystals throughout the rock, and to a lesser extent by biotite and tabular K-feldspar crystals. Biotite-rich schlieren may be present and serve to further define the foliation. Quartz forms equant domains in the rocks and indicates that the orientation of the tabular minerals occurred in a magmatic state, and not during subsequent solid state defomation.

The mineral assemblage in the plagioclase + K-feldspar diatexite rocks is the same as that in most of the plagioclase-dominated diatexites. However, as plagioclase, biotite and orthopyroxene progressively decrease in abundance, the proportion of K-feldspar and quartz increases (see Fig. 15) and the overall bulk composition extends from granodiorite to monzogranite.

4.2.3 The K-feldspar-dominated diatexites

In these diatexites there is typically a decrease in the size and the number of enclaves and schlieren, in the intensity of the flow foliation, in the abundance of schlieren, and in the proportion of mafic minerals present (to between 3 and 12 modal %). Consequently, the K-feldspar-dominated diatexite migmatites are more leucocratic and more uniform in morphology than the other types. Their overall composition is monzogranitic. The few remaining enclaves are far more rounded, and this indicates greater degree of transport, or magmatic erosion, of the enclaves in the diatexite magma (Fig. 16c).

More leucocratic melt batches poor in inclusions and schlieren, but rich in K-feldspar, commonly cross cut the flow foliation and were successively injected into pre-existing diatexites. These represent a more fractionated leucocratic melt which was emplaced after the foliation and flow banding developed in the crystal-rich portions of the diatexite. These injections of later magma have rather diffuse contacts at the grain scale, which suggests that the host was not completely solid. Since crystallization of the diatexite magmas occurred at the same time as regional deformation, it is possible that the late leucocratic melt batches represent the fractionated melt fraction segregated from the host diatexite and channelled into cross-cutting veins (e.g. Sawyer 1987). In the K-feldspar-dominated diatexites the magmatic foliation becomes less apparent, and in some examples it is absent, resulting in a massive diatexite migmatite.

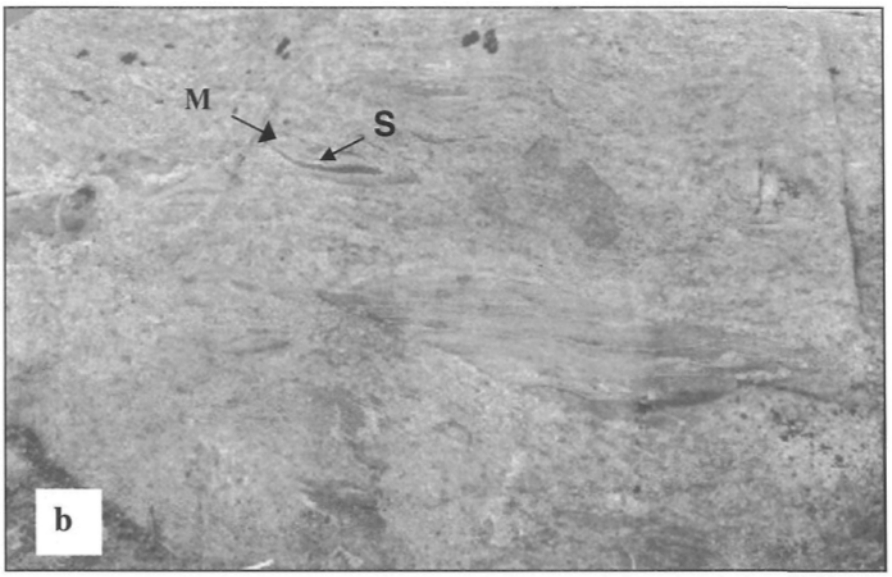

Figure 16b: Plagioclase + K-feldspar-dominated diatexite migmatite containing magma flow structures, such as schlieren (S), with melt segregation (M), the enclaves are asymmetric and indicate a consistent sense of magma flow, and are evidence for the syntectonic flow of the diatexite magma.

As the modal proportions of the mafic minerals and the plagioclase decrease, the proportion of large, euhedral feldspar crystals tends to increase (Fig. 15). Locally large K-feldspar crystals become sufficiently abundant that a leucocratic porphyritic diatexite results, this has a coarse-grained microstructure similar to the melt-rich pink diatexite described by Sawyer (1998) in the Opatica subprovince. Orthopyroxene is absent from most of the K-feldspar-rich diatexites, but in a few rocks it is present in minor amounts (6 to 8 modal %) and, typically, is partially replaced by biotite. However, some biotite grains and biotite + quartz symplectic intergrowths in the K-feldspar-dominated diatexite migmatites have conspicuously rectangular shapes, and may represent pseudomorphs after orthopyroxene.

4.3 MICROSTRUCTURES IN THE DIATEXITE MIGMATITES

Typical microstructures found in the three types of diatexite migmatite are illustrated on figure 17, and document the transition in microstructures from the plagioclase-dominated (Fig. 17a & b) through the plagioclase + K-feldspar-dominated (c, d & e) to the K-feldspar-dominated (g) diatexites.

4.3.1 Plagioclase-dominated diatexites

Figures 17a & b show that large subhedral to euhedral plagioclase is the dominant mineral in this rock, and that K-feldspar (microcline) is a minor (< 5 modal %) phase that is interstitial to the framework of crystals formed by the large plagioclase crystals.

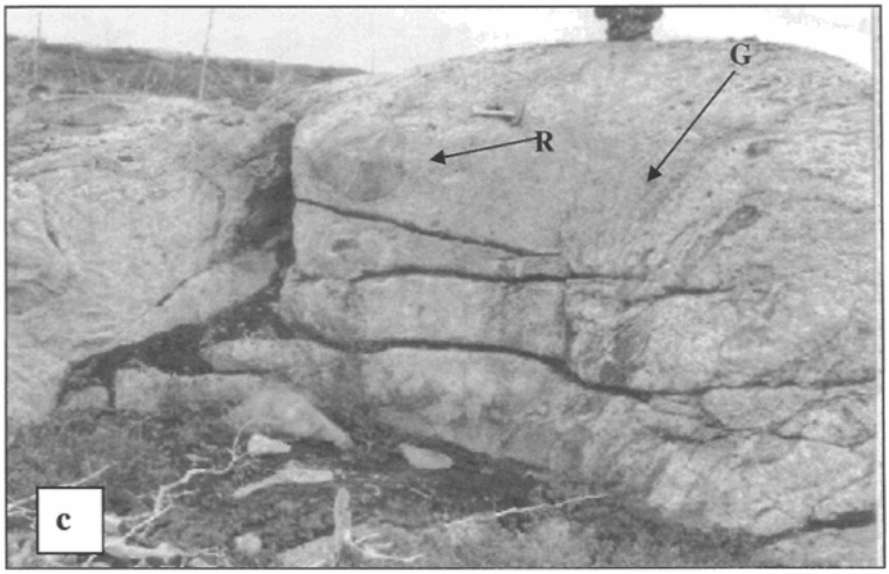

Figure 16c: K-feldspar-dominated diatexite migmatite showing a decrease in the size and number of enclaves and schlieren, note the rounded enclaves (R) and the coarse-grained microstructure (G) due to an increase in the proportion of large euhedral K-feldspar at the expense of mafic minerals and plagioclase.

However, in some rocks there are scattered individual, euhedral K-feldspar crystals that also contribute to the crystal framework structure in the rock. The matrix that fills the interstices within the plagioclase framework is fine-grained, and consists of equant, anhedral to subhedral grains of quartz and plagioclase, with bladed crystals of biotite on the grain boundaries. Large subhedral to euhedral orthopyroxene crystals may also contribute to the crystal framework structure and may compose up to 20 modal % of the rock.

4.3.2 Plagioclase + K-feldspar diatexites

The proportion of interstitial K-feldspar increases, and in some cases large K-feldspar crystals poikilitically enclose quartz and plagioclase grains, as shown in the mosaic figure 17c. In general, the grain size of the plagioclase and quartz inclusions in the K-feldspar is rather constant, but slightly smaller than the plagioclase that forms the crystal framework. Hence, plagioclase in the framework continued to grow after K-feldspar crystallized. The quartz included in the K-feldspar ranges in form from irregular to rounded, whereas the plagioclase ranges from euhedral to rounded shapes; this suggests that quartz crystallized before K-feldspar and may have contributed to the framework of large crystals. Interstitial, skeletal K-feldspar as shown in figure 17c is relatively rare, more commonly K-feldspar occurs as scattered phenocrysts as shown in figure 17d. The characteristic microstructure is a crystal framework that consists of more-or-less uniform-shaped and sized grains, some are tabular and euhedral, others anhedral. Some anhedral plagioclase is also present at the corners of the image.

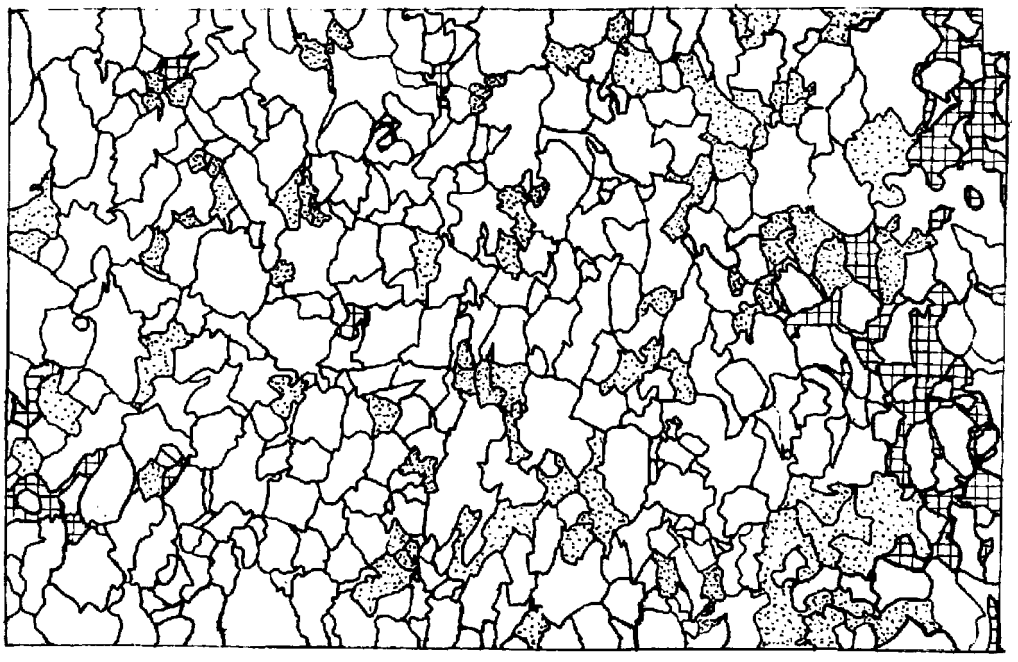

Figure 17a: Linedrawing from a photomosaic of a plagioclase-rich diatexite (sample 1085) in which the microstructure is dominated by large subhedral to euhedral plagioclase, a minor amount (< 5 modal %) of K-feldspar (microcline) is interstitial to the crystal framework comprised of plagioclase. White = plagioclase; dotted pattern = quartz; hachured = K-feldspar; black = opaque minerals.

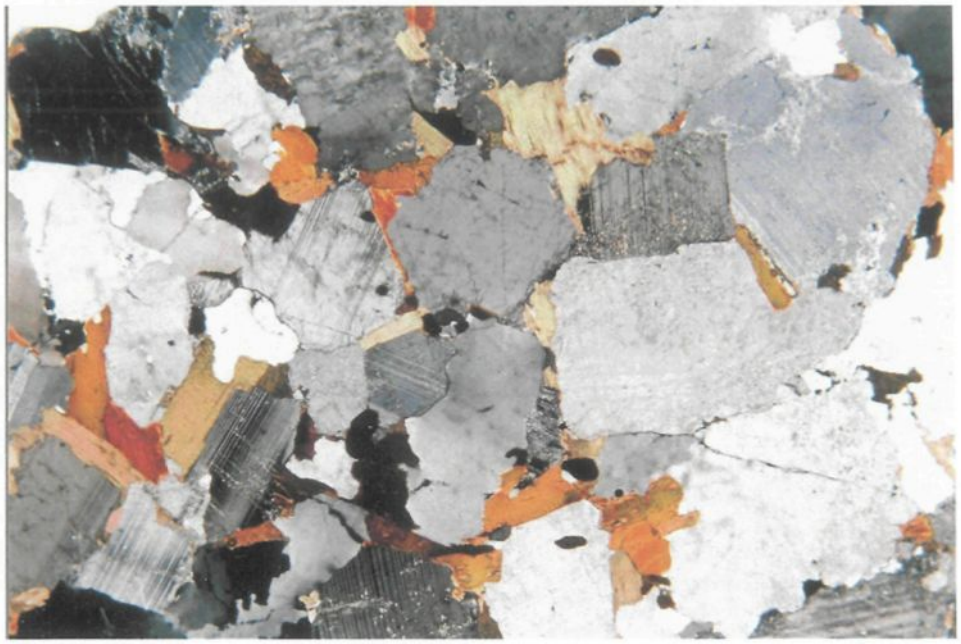

Figure 17b: Plagioclase-rich diatexite, showing a crystal framework constructed by the dense packing of the euhedral plagioclase crystals. Packing is dense because many of the plagioclase crystals are in contact along their crystal faces and not just at the corners of grains. The long side of photomicrograph is 9mm.

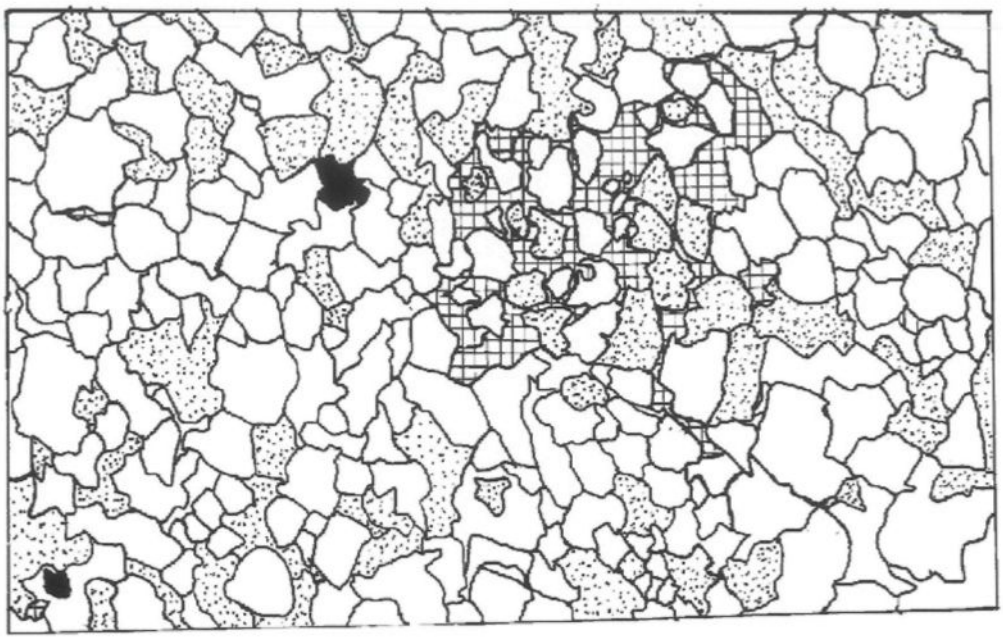

Figure 17c: Linedrawing from a photomosaic of a plagioclase-dominated diatexite (sample 5032) showing a large interstitial K-feldspar crystal that poikilitically encloses quartz and plagioclase grains. White = plagioclase; dotted pattern = quartz; hachured = K-feldspar; black = opaques minerals.

Fine-grained interstitial quartz, plagioclase and biotite located in the interstices of a crystal framework comprising large, euhedral plagioclase and K-feldspar is evident in figure 17e. Crystal faces where framework–forming plagioclase is in contact with interstitial quartz or K-feldspar is evidence for crystallization from an anatectic melt (Platten 1983; Waters 1988; Harte & Pattison 1991). The K-feldspar is, in some cases, clear and homogeneous or cryptoperthitic, but in other examples the K-feldspar is cloudy due to alteration and to perthite exsolution. In figure 17d, plagioclase and quartz form a touching framework in two dimensions. This microstructure implies that quartz also formed phenocrysts along with plagioclase and that both crystallized before K-feldspar began to form, consistent with the crystallization of magma with a peraluminous bulk composition. Few plagioclase + K-feldspar diatexite migmatites contain orthopyroxene, but in those that do, the orthopyroxene shows a far greater extent of alteration to biotite (Fig. 17f1) than orthopyroxene in the plagioclase-dominated diatexite migmatites (Fig. 17f2).

4.3.3 K-feldspar-dominated diatexites

The K-feldspar-dominated diatexite migmatites (Fig. 17g) have the coarsest grain size, and have the most granite-like, porphyritic microstructure. The examples with the highest K-feldspar contents have a distinctive, graphic intergrowth that can be seen in hand specimens. In this microstructure, large K-feldspar crystals (from 5 to 10 mm) contain aligned, elongate blebs of quartz that, from their uniform extinction, appear to be single, skeletal crystals.

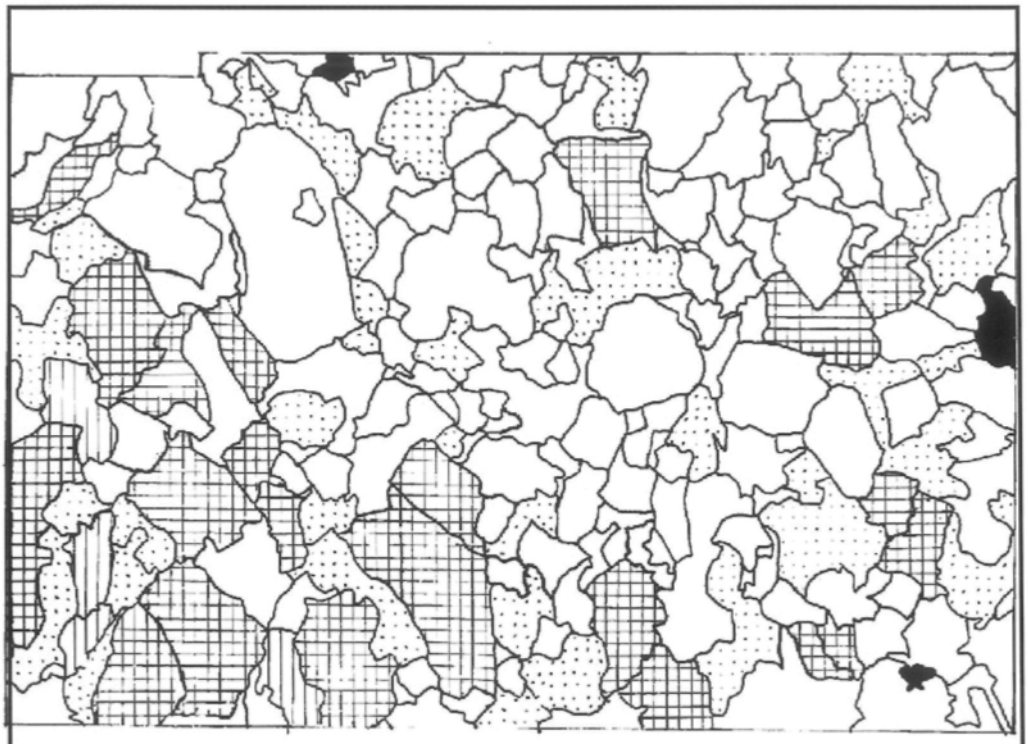

Figure 17d: Linedrawing from a photomosaic of a plagioclase + K-feldspar-dominated diatexite (sample 5016) showing that interstitial K-feldspar occurs principally as large phenocrysts that contribute to the crystal framework. White = plagioclase; dotted pattern = quartz; hachured pattern = K-feldspar; black = opaque minerals.

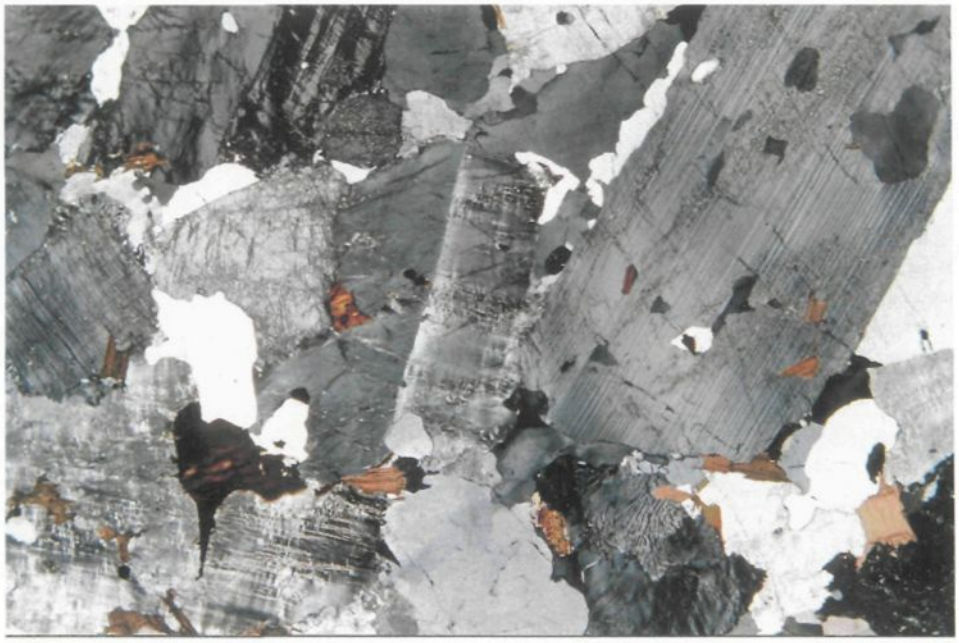

Figure 17e: Photomicrograph of a plagioclase + K-feldspar-rich diatexite migmatite showing that the plagioclase and K-feldspar form large, euhedral crystals. Crystal faces on euhedral plagioclase against K-feldspar are evidence for crystallization from an anatectic melt. The long side of photomicrograph is 13 mm

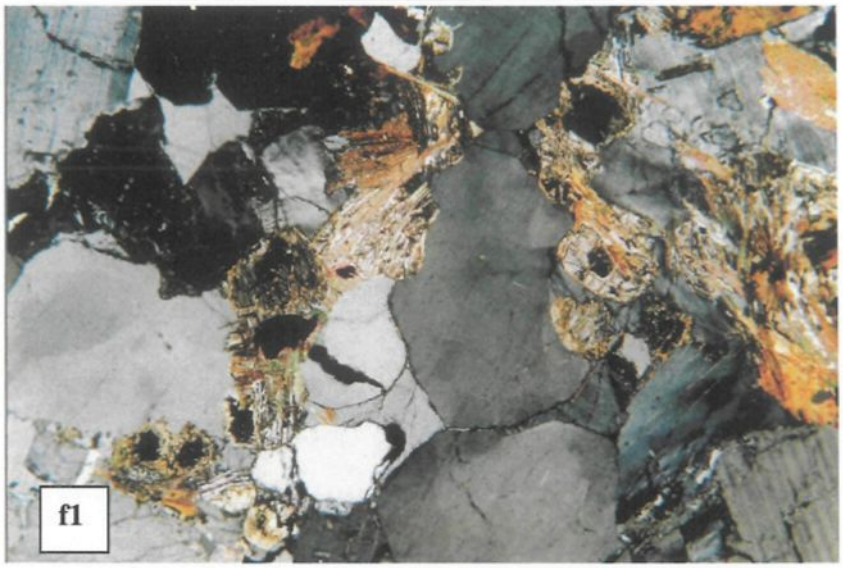

Figure 17f1: Photomicrograph of a plagioclase + K-feldspar diatexite migmatite showing extensive alteration of the orthopyroxene to biotite.

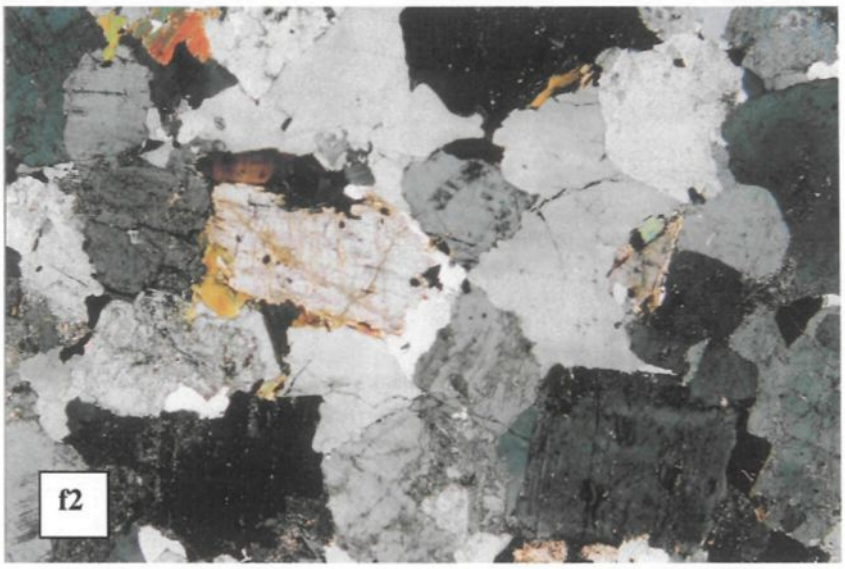

Figure 17f2: Photomicrograph of a plagioclase-dominated diatexite migmatite showing minor replacement of orthopyroxene by biotite.

Figures 17h1 & h2 show two different stages in the development of graphic intergrowths of quartz in K-feldspar; this microstructure is attributed to the reactions between cooling melts and crystals (Ashworth & McIlenan 1985; Hansen & Stuk 1993). Xenomorphic quartz is abundant in the matrix of the K-feldspar-dominated diatexite migmatites; it has irregular shapes, commonly with concave boundaries that suggest it has filled the interstitial spaces in between the other framework-forming feldspar (e.g. Hart *et al.* 1991). Plagioclase in these diatexite migmatites is more sodic than that in the plagioclase-dominated diatexite migmatites. Isolated, small elongate grains of biotite are located along quartz and feldspar grain boundaries and are interpreted to have crystallized from the anatectic melt.

4.4 INTERPRETATION OF THE PETROGRAPHIC, MICROSTRUCTURAL AND FIELD DATA

Field observations in the Ashuanipi subprovince show that there is a gradation from the plagioclase-dominated diatexite migmatite with tabular and angular enclaves to the K-feldspar-dominated diatexite which contains rounded enclaves through an intermediate plagioclase + K-feldspar-dominated diatexite. The significance of that gradation will now be discussed.

The principal variations in the microstructure of the different diatexites can be correlated with the progressive change in proportion of plagioclase to K-feldspar (Fig. 18). Unfortunately, not all of the 61 samples used for the mesonormative plot (Fig. 15)

were available for point-counting. Nevertheless, the 18 samples point counted show the general decrease in the modal abundance of plagioclase and orthopyroxene as quartz and K-feldspar increase (Figs. 18, 19 & 20). K-feldspar increases gradually to 43 modal % whereas plagioclase decreases from 70 to 20 modal % (Fig 18). The rarity of orthopyroxene in the K-feldspar-rich diatexites is in part due to its reaction with the melt to produce biotite and quartz symplectites (e.g. Fig. 17i). Modal quartz content varies from 8 to 42 %, but is generally highest in the K-feldspar-dominated diatexites (Fig. 20). The two diatexite migmatites indicated (numbers 5019 and 5016) have modal compositions that are close to the granite minimum and to the experimental melts from Patiño Douce & Harris (1998) or Stevens *et al.* (1997). Unfortunately, the whole rock chemical data of these two rocks are unavailable, hence we cannot use these two as a reference point for geochemical modelling. Instead, two alternative samples (they have mesonorms that plot near the granite cotectic) 2085 and 1054 are used for the trace element modelling. The results of this modelling will be discussed later in the section on geochemistry in Chapter V.

Percival (1991) has noted that the diatexite migmatites from the northern part of the Ashuanipi subprovince have, in general, a coarse hypidiomorphic microstructure which includes orthopyroxene, some of which is subhedral orthopyroxene, typical of magmatic crystallization. However, the microstructural study of the diatexite migmatites from the Ashuanipi subprovince (Figs. 17a to 17j) shows that there is more to the microstructure than just this.

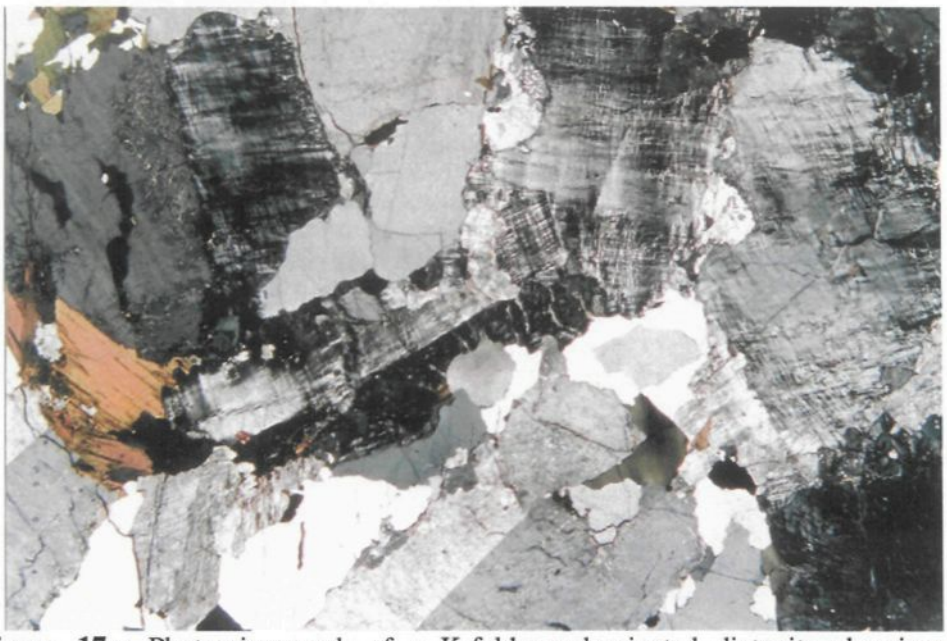

Figure 17g: Photomicrograph of a K-feldspar-dominated diatexite showing a microstructure composed of a framework of large K-feldspar (microcline) and plagioclase crystals in which the interstitial space is filled with quartz, biotite and feldspar. The long side of photomicrograph is 12 mm.

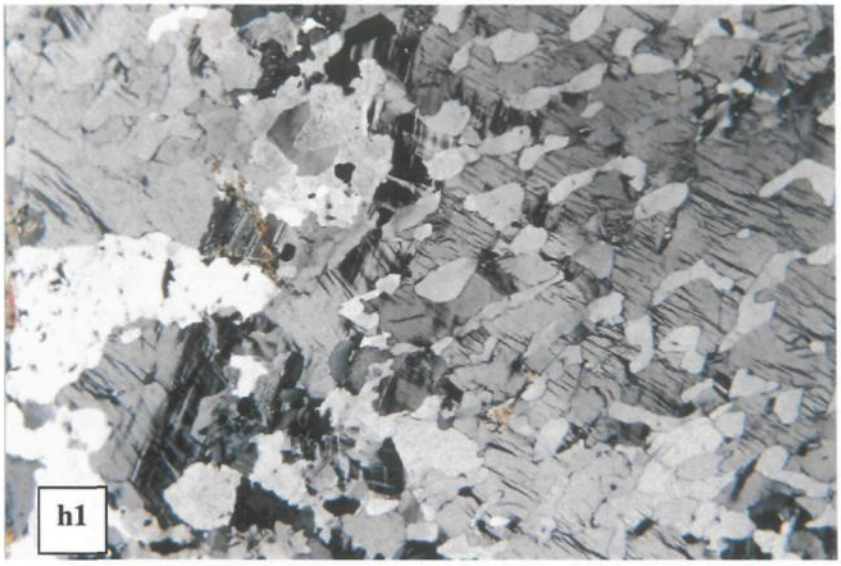

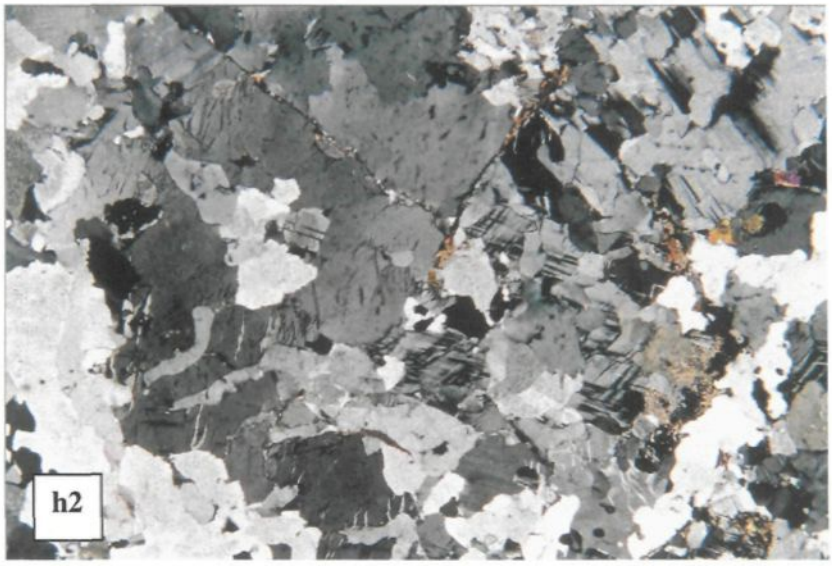

Figures 17h1 & h2: Two photomicrographs showing graphic intergrowths of quartz in K-feldspar developed in two fractionated, K-feldspar-dominated diatexite migmatites. The long side of the photomicrographs are 11 mm and 9 mm respectively.

Figure 17i: Photomicrograph of a K-feldspar-rich diatexite showing a rectangular region of biotite + quartz symplectite. The presence of relic orthopyroxene at the bottom and the rectangular shape suggest that the orthopyroxene in this diatexite has been replaced by biotite and quartz, probably because of reaction with the last increments of melt. The long side of the photomicrograph is 40 mm

There are several different types of variation in the microstructure; these can be divided into those that affect the framework structure composed of large, generally euhedral crystals (plagioclase, microcline and more rarely orthopyroxene), and those affecting the interstitial matrix material, which generally comprises smaller crystals. With respect to the crystal framework microstructure, there are two principal variations; 1) the nature of the packing density of framework-forming minerals and, 2) which minerals contribute to the framework. Variations in packing density give rise to changes in the ratio of large subhedral to euhedral crystals to matrix, and in the nature of the contacts between the large crystals. The examples of plagioclase-dominated diatexite migmatites shown in figures 17a, b & f2 have densely packed frameworks of subhedral plagioclase between in which there is relatively little matrix material. A very dense packing for the large, subhedral plagioclase crystals that form the framework is indicated by the nature of the contacts between adjacent crystals; most contacts are along crystal faces only rarely are corners touching crystal faces. This type of dense packing suggests that the crystal framework was either formed in a magmatic flow regime, or by deformation (compaction) of the magma.

In contrast the packing of the large subhedral plagioclase crystals in figure 17j is much less dense and, consequently, there is a much higher proportion of matrix. The plagioclase crystals form a framework of crystals touching at the corners which confirms that the large plagioclase crystals in this rock formed a very open framework structure in the melt. The preservation of an open crystal frameworks, such as that in figure 17j, suggests that some diatexite magmas were not subject to magma flow or to later compaction.

The progressive change in the microstructure of the feldspar framework in the diatexite migmatites can be interpreted in terms of the rheological thresholds for crystallizing magmas proposed by Vigneresse *et al.* (1996). They proposed that when about 55 volume % crystals is reached during crystallization of a magma, a rigid framework (or skeleton) of loose-packed crystals develop; they termed the point at which this occurs the rigid percolation threshold (RPT). This loose framework of crystals can support only small shear stresses, but at higher shear stresses it is deformed and compacted into a much more densely packed framework of oriented crystals. When the crystal framework is compacted its interstitial pore space is reduced, consequently, some of the melt that was trapped melt between the crystals is expelled. As progressively less melt is left between the crystals (either through advancing crystallization or through compaction), the shear strength of the crystal framework increases. When the volume of crystals surpasses 75 % further compaction of the framework cannot be accomplished without internally deforming the crystals that form the framework; Vigneresse *et al.* (1996) called this limit the particle locking threshold (PLT). Many of the diatexite migmatites sampled did not reach that stage (e.g. that in figure 17j), however, some did, and they contain feldspar crystals that contain healed cracks.

The density of packing of the feldspar crystals determines how much interstitial melt (trapped melt) the diatexite contained and consequently how close to the extremes of melt and feldspar cumulate each individual diatexite sample lies. Moreover, the composition of the trapped melt may differ from one diatexite migmatite to the next depending on how much interstitial melt there was, how much melt has been lost, and

how far down the crystallization sequence each diatexite progressed before the trapped melt was frozen in.

The mineralogical constituents of the crystal framework, and of the matrix, also contain important petrological information. None of the plagioclase-dominated diatexite migmatites have compositions that are close to the initial anatectic melt composition. The most extreme deviation from the anatectic melt composition is shown by those with a densely-packed, plagioclase framework (e.g. Figs. 17b & f2) and with only minor amounts of interstitial material; these rocks contain far too much plagioclase to be a primary anatectic melt; they are in effect accumulations of plagioclase. They may have formed by normal igneous accumulation processes, such as crystal settling, but the deformation structures that they contain argue for some compaction and the consequent expulsion of a large volume of evolved melt, i.e. anatectic melt that has already crystallized and had plagioclase removed from it. However, there is considerable variation within the group of samples that show dense packing. The interstitial material in some is mostly quartz and biotite, but in other examples some K-feldspar is present, either as large interstitial grains, or as small grains distributed throughout the groundmass. The interstitial melt in the latter group may have been more evolved. The plagioclase-dominated diatexite migmatites with loose-packed plagioclase framework structures may have bulk compositions somewhat closer to that of the anatectic melt because of the quartz + K-feldspar in the interstitial space, however, these rocks too, are essentially accumulations of plagioclase. The crystal framework structure in the plagioclase-dominated diatexite migmatites formed before K-feldspar started to crystallize. In contrast, the framework structure of large crystals in

the plagioclase + K-feldspar diatexite migmatites contains both plagioclase and K-feldspar. Thus, the microstructure present in these diatexite migmatites must have formed later in the crystallization sequence when both K-feldspar and plagioclase crystallized. Consequently, some of these diatexite migmatites could have compositions that are similar to the anatectic melt extracted from the melt-depleted metatexite migmatites. The plagioclase in the matrix is slightly more sodic than in the larger, subhedral plagioclase in the framework. In most cases the interstitial quartz, biotite, plagioclase and K-feldspar are evenly distributed and suggests that they crystallized together, but in some cases K-feldspar formed a partial rim around the interstitial pores between the framework crystals before quartz crystallized. The diatexite migmatites in which the crystal framework structure is dominated by K-feldspar must have formed later in the magma evolution sequence than the other diatexites, when K-feldspar was the principal crystallizing phase. This could be because either; a) the initial anatectic melt was very potassic, perhaps derived from a pelitic source that was plagioclase-poor (e.g. Grant 2004), b) these represent the crystallization product of an evolved anatectic melt (i.e. an anatectic melt that had already crystallized large amounts of plagioclase), such as may have been expelled from some of the plagioclase-dominated diatexites during compaction or, c) these rocks are K-feldspar accumulations. Generally, the K-feldspar dominated diatexite migmatites have a much coarser grain size, and their interstitial space is dominated by quartz and a fine-grained plagioclase that is considerably more sodic (An_{17} *cf* An_{25}) than the large plagioclase crystals in the framework structure. In some cases the framework K-feldspar is intergrown with quartz to form a graphic microstructure (Fig. 17f). These matrix characteristics are also consistent with the formation of the K-feldspar-rich

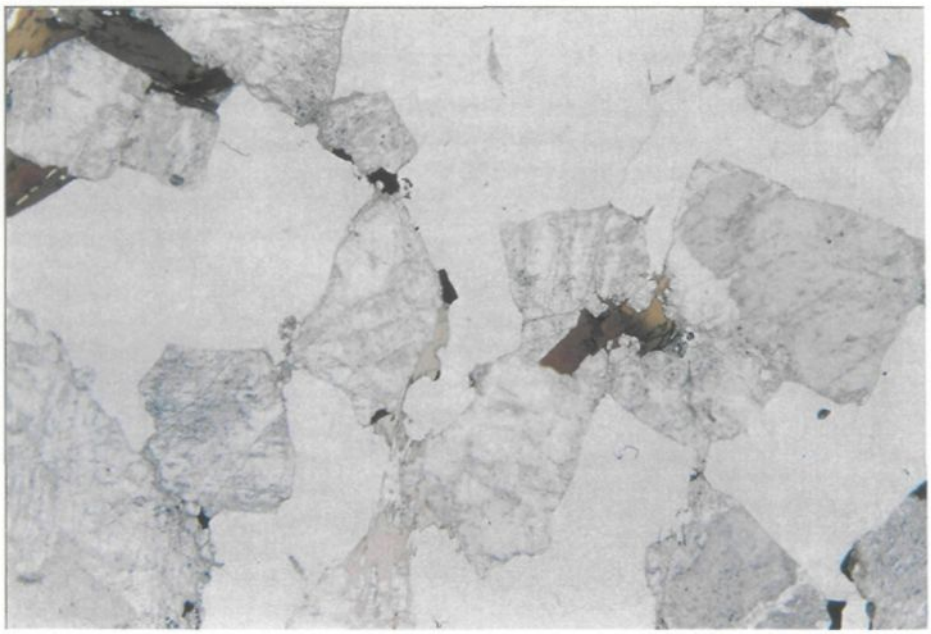

Figure 17j: Photomicrograph of a plagioclase-dominated diatexite migmatite showing a very open (or loose packed) crystal framework of touching, subhedral plagioclase crystals (cloudy). The loose packing is illustrated by the plagioclase crystals touching mostly at the corners, and by the high fraction of matrix (clear). The long side of the photomicrograph is 12 mm.

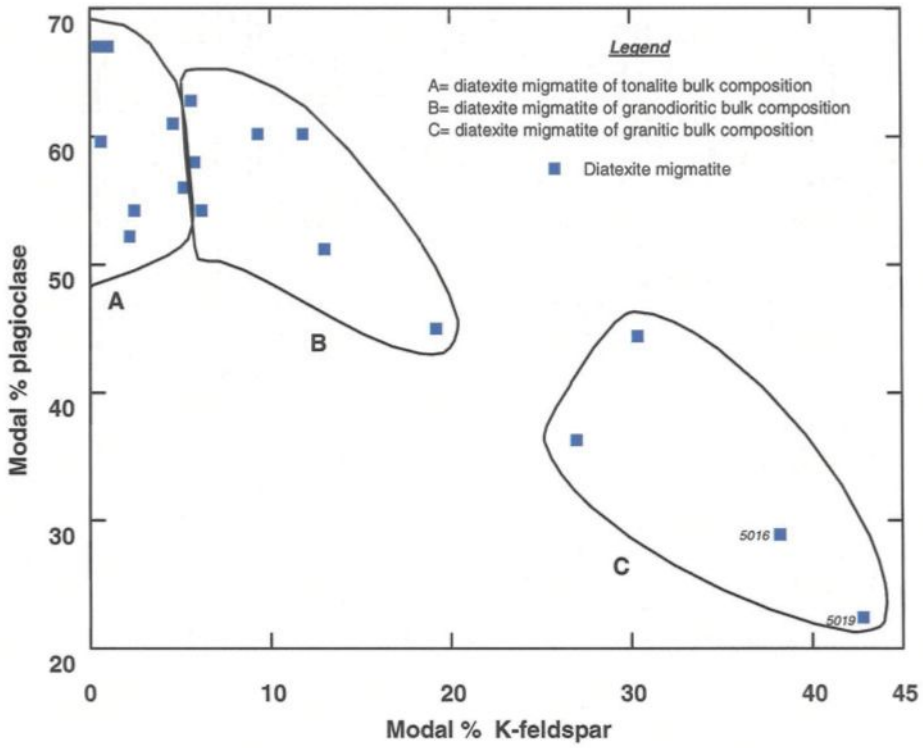

Figure 18: Modal % plagioclase *versus* modal % K-feldspar showing a negative correlation between modal plagioclase and modal K-feldspar determined for 18 diatexite migmatites from the Ashuanipi subprovince by point counting.

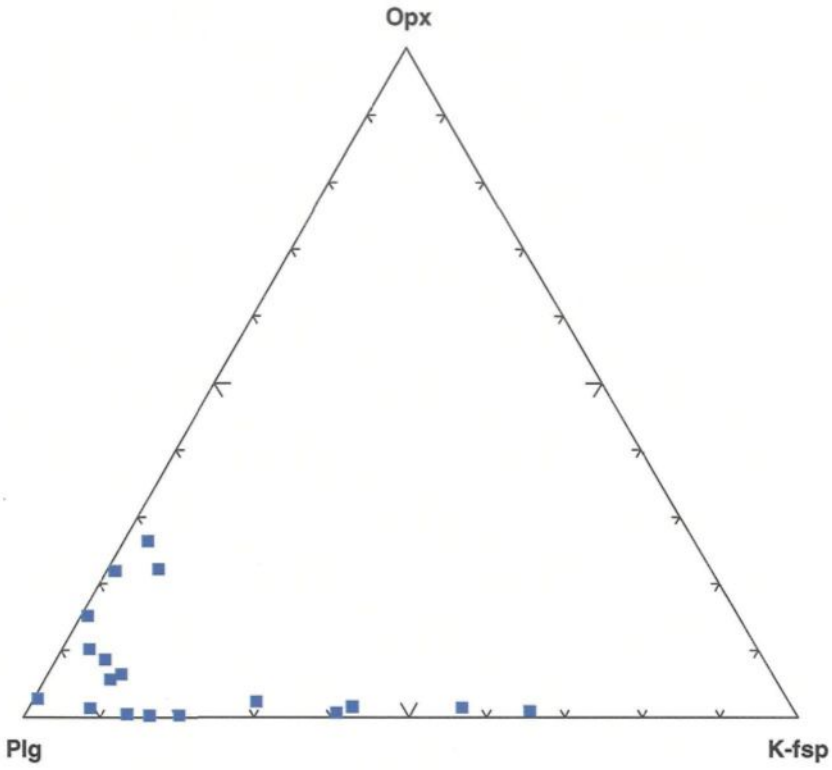

Figure 19: Ternary plot showing the variation in modal plagioclase, orthopyroxene, and K-feldspar based on point counts of the diatexite migmatites from the Ashuanipi subprovince. Orthopyroxene is more abundant in the plagioclase-dominated diatexites compared to the K-feldspar-rich diatexites. Plg = plagioclase, K-fsp = K-feldspar, Opx = orthopyroxene.

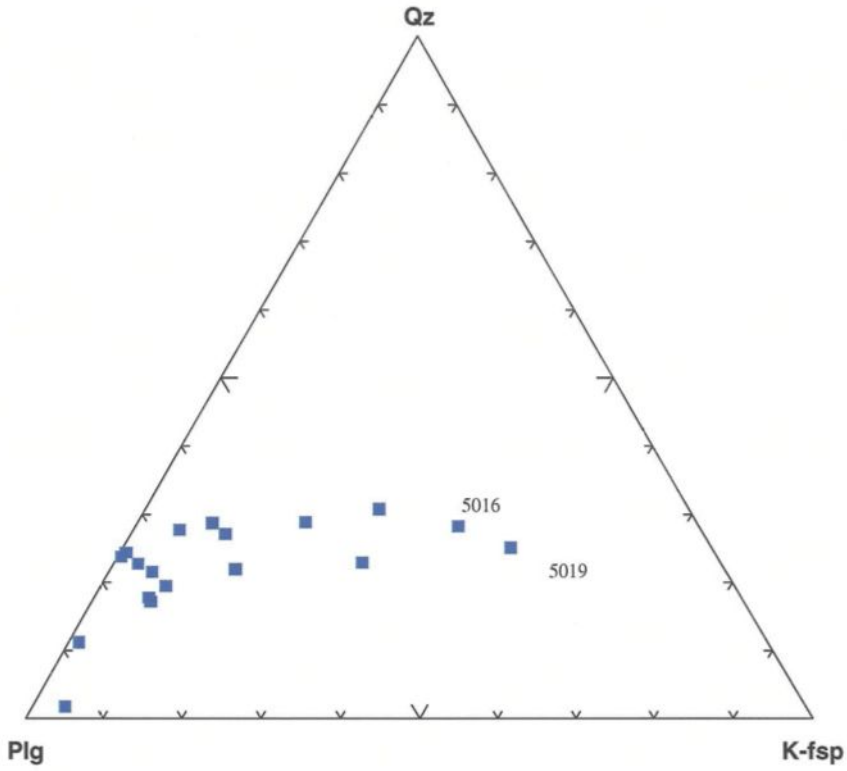

Figure 20: Ternary plot showing the variation in modal plagioclase, quartz, and K-feldspar contents in the diatexite migmatites from the Ashuanipi subprovince.

diatexite migmatites at a late stage in the crystallization history of the diatexite magma. Small, up to metre-scale, pockets of very leucocratic monzogranite, typically with graphic quartz-feldspar intergrowths, also occur in many outcrops and indicate that most of the diatexite migmatites, even the plagioclase-dominated ones locally underwent the final stages fractional crystallization *in situ*.

4.5 GEOCHEMISTRY OF THE DIATEXITE MIGMATITES

4.5.1 Analytical procedure

The major and selected trace element contents of some 61 diatexite migmatites (table 4) and 18 monzogranites (table 6, Chapter V) from the Ashuanipi subprovince were determined. The major oxides, except Na_2O and FeO were determined on fused glass discs; and the trace elements Nb, Ba, Rb, Sr, Y and Zr on pressed powder pellets, whereas Cs, U, Hf, Sc, Th, Cr and the rare earth elements (REE) were determined using Instrumental Neutral Activation Analysis (INAA) at the analytical laboratories of the Ministere des Ressources naturelles du Québec (MRNQ). Because the Tb and Lu contents of the rocks are below the INAA detection limit of the MRNQ laboratories for many samples the REE, Na_2O, FeO, Th, U, Ta, Rb, Sc, Cs, Hf, Co, Cr and Ba were redetermined on 22 diatexite and 10 monzogranite samples at the Université du Québec à Chicoutimi (UQAC) where the detection level using INAA is significantly lower (Bedard & Barnes 2002). These samples were irradiated in the Slowpoke II reactor at École Polytechnique in Montreal.

The geochemical variation diagrams also contain data from the 18 diatexites given in Percival (1992) and 6 from Lapointe (1996), which were sampled further north in the Ashuanipi (see appendix VII). First of all, general trends that represent the Ashuanipi diatexites will be described, then particular compositional peculiarities will be discussed. The geochemistry of the monzogranites and their relationship to the diatexite migmatites will be discussed in chapter V.

4.5.2 Major element compositions of the diatexite migmatites

4.5.2.1 Some reference compositions

The singular feature about the anatexis and the formation of migmatites in the Ashuanipi subprovince is that the separation of the melt fraction from the residual solid fraction was virtually complete (Chap III). The extracted melt probably had a very low fraction of entrained residual material when it left its source rock. However, as it migrated through the arrays of veins in the melt-depleted metatexite migmatites described in Chapter III and by Sawyer (2001) it became contaminated by spalled-off pieces of the wall rock and by minerals disaggregated from the wall rocks.

In order to understand the geochemical evolution of the anatectic melt after it was segregated from the metasediments and collected to form bodies of diatexite migmatite, it is necessary to include on the various compositional diagrams; a) the starting point from which diatexite migmatite composition evolved, i.e. the composition of the initial, or starting anatectic melt, b) the composition of the possible contaminant

Table 4: Whole rock major and trace element compositions of 61 diatexite migmatite rocks from the Ashuanipi Subprovince

Sample	3311-A	3035A2+	1061-A	3012A2	3237-A+	2171-A+	3155-A+	1181-A+	5103A+	2085	5098A+	5095A+	1059A	5109A1+	1056A+	2081A1+	1054	5109A5+	5109A6+	5109A2+
SiO_2 (Wt%)	70,20	66,71	65,99	54,05	69,39	66,23	68,87	72,92	58,20	65,78	60,04	66,57	62,83	71,32	67,07	66,79	67,70	66,05	65,74	70,03
TiO_2	0,22	0,50	0,50	0,68	0,43	0,86	0,48	0,06	0,39	0,50	0,69	0,46	0,66	0,17	0,59	0,46	0,59	0,42	0,49	0,20
Al_2O_3	15,94	15,64	17,08	15,56	16,13	15,10	14,54	15,33	19,96	16,07	17,43	14,68	16,17	16,37	15,48	15,89	14,53	16,34	16,18	16,67
Fe_2O_{3t}	1,28	4,44	3,77	9,34	3,02	5,86	4,79	0,84	6,04	4,40	7,94	5,88	6,82	1,38	4,85	5,22	5,24	5,22	5,51	1,78
MnO	0,03	0,03	0,08	0,17	0,04	0,08	0,07	0,04	0,10	0,04	0,07	0,06	0,06	0,01	0,07	0,03	0,04	0,04	0,04	0,01
MgO	0,85	2,59	2,21	7,23	1,16	1,01	2,44	0,55	3,17	2,63	4,96	2,88	3,15	0,98	2,42	2,53	2,56	2,59	2,74	1,20
CaO	1,45	2,76	4,26	7,86	2,28	3,23	2,31	2,10	5,27	2,81	2,71	2,50	3,17	2,28	2,64	3,28	2,75	2,84	2,56	2,35
Na_2O	3,10	3,63	4,40	3,81	4,38	3,52	3,16	4,61	5,36	4,18	3,48	3,74	3,91	3,41	3,97	3,95	4,07	3,49	3,50	3,60
K_2O	6,72	3,56	1,52	1,00	3,01	3,87	3,24	3,40	1,18	3,35	2,62	3,11	2,99	3,95	2,81	1,78	2,40	2,78	3,05	4,01
P_2O_5	0,22	0,13	0,19	0,30	0,16	0,25	0,09	0,15	0,33	0,23	0,07	0,11	0,23	0,12	0,11	0,06	0,13	0,21	0,19	0,14
LOI	0,82	0,79	0,55	0,56	1,05	0,38	0,83	0,77	0,09	0,89	0,72	0,44	1,15	1,05	0,91	0,51	1,01	1,07	1,14	1,05
Total	100,8	100,8	100,5	100,6	101,0	100,4	100,8	100,8	100,1	100,9	100,7	100,4	101,1	101,0	100,9	100,5	101,0	101,1	101,1	101,1
Al index	1,41	1,57	1,68	1,23	1,67	1,42	1,67	1,52	1,69	1,55	1,98	1,57	1,60	1,70	1,64	1,76	1,58	1,79	1,78	1,67
Mg #.	56,71	53,63	53,76	60,55	43,10	25,39	50,28	56,75	51,00	54,23	55,29	49,19	47,78	58,37	49,70	49,02	49,22	49,56	49,62	57,25
Cr (ppm)	n.a.	n.a.	n.a.	n.a.	n.a.	n.a.	n.a.	n.a.	100	100	282	151	183	31	132	131	131	131	162	36
Ni	20	81	25	91	21	19	86	12	n.a.	n.a.	n.a.	n.a.	n.a.	n.a.	n.a.	n.a.	n.a.	n.a.	n.a.	n.a.
Co	7,1	19,2	11,1	33,3	7,1	11,1	19,2	4,0	17,0	15,1	28,2	21,1	19,3	5,1	16,2	14,1	16,1	18,2	20,2	5,1
Sc	3,0	10,1	8,1	33,3	4,1	12,1	10,1	1,0	41,9	13,1	22,2	15,1	15,3	3,8	16,2	11,1	12,1	12,1	11,1	4,5
Cu	9	36	15	53	12	15	40	12	21	36	43	62	38	5	32	31	28	35	48	7
Pb	n.a.	n.a.	n.a.	n.a.	n.a.	n.a.	n.a.	n.a.	16	9	6	32	8	13	12	13	8	11	9	17
Zn	30	73	74	109	28	119	148	27	76	57	88	67	68	16	55	52	63	55	57	21
Rb	202	111	39	8	75	131	111	46	29	121	86	67	163	131	142	92	172	101	131	141
Cs	0,00	0,00	0,00	0,00	0,00	0,00	0,00	0,00	0,90	1,51	1,31	0,50	0,92	0,71	0,61	1,91	1,82	0,50	1,01	0,71
Ba	1916	909	1011	374	840	1107	860	1412	329	673	987	935	610	1111	496	201	626	837	718	1112
Sr	545	484	990	586	568	352	454	726	567	424	486	452	454	458	374	361	437	471	452	471
Ga	9	14	15	16	13	18	10	13	27	19	22	17	22	16	20	21	19	19	20	16
Ta	dl	0,40	dl	0,40	0,30	dl	0,40	dl	0,90	dl	0,91	dl	dl	0,71	dl	1,21	dl	0,61	dl	dl
Nb	9,1	14,1	3,0	12,1	11,2	22,1	12,1	4,0	7,0	9,0	4,0	dl	14,2	dl	11,1	6,0	8,1	4,0	9,1	4,0
Hf	2,32	3,13	3,23	2,63	1,12	9,36	3,43	1,11	4,79	4,62	4,03	4,42	4,88	1,92	4,35	4,33	4,44	3,53	4,35	2,12
Zr	74	101	90	69	19	312	90	18	188	160	138	144	166	63	153	141	184	117	152	69
Y	dl	4	dl	32	dl	32	dl	dl	45	12	9	11	7	5	12	7	6	10	13	7
Th	7,77	2,72	0,97	0,31	0,42	1,11	2,63	0,56	3,29	5,42	5,74	7,04	3,66	4,14	24,28	29,17	16,14	0,20	0,91	1,72
U	dl	dl	dl	0,20	dl	dl	dl	dl	dl	dl	0,81	dl	0,61	dl	dl	0,80	dl	dl	dl	dl
La	30,26	15,14	22,23	20,21	15,22	48,31	14,14	14,12	31,94	26,11	33,25	32,18	18,30	17,17	49,57	68,40	55,49	12,10	13,15	14,15
Ce	57,49	27,25	44,47	51,53	27,39	97,63	24,24	25,21	73,87	48,21	60,45	56,32	30,50	30,31	95,09	120,70	99,88	22,19	23,26	24,25
Nd	23,20	12,11	20,21	34,35	10,14	53,35	7,07	13,11	51,91	23,10	29,22	26,15	13,22	13,13	31,36	42,25	36,32	9,08	13,15	11,12
Sm	4,54	3,03	3,44	8,28	1,83	11,07	1,11	2,42	12,98	4,22	4,63	4,12	2,85	2,42	5,36	5,43	5,65	2,52	3,24	2,32
Eu	dl	0,91	1,01	1,62	1,01	2,11	0,91	0,71	1,00	1,21	1,31	1,21	1,02	0,91	1,01	0,91	1,21	1,01	1,01	1,01
Tb	0,30	0,40	0,20	0,81	0,10	1,11	0,10	0,20	1,60	0,50	0,20	0,50	0,20	0,20	0,20	0,20	0,20	0,30	0,40	0,20
Yb	0,40	0,91	0,91	2,73	0,20	3,12	0,30	0,30	4,49	1,00	0,91	1,51	dl	0,61	2,33	0,40	0,30	0,81	0,91	0,51
Lu	0,050	0,091	0,051	0,465	0,000	0,483	0,050	0,050	0,499	dl	dl	0,201	dl	dl	0,303	dl	dl	dl	dl	dl

Table 4: continued

Sample	6017A	2013A+	1041A+	3012A+	0030A+	37A+	3128A	36A+	4025A	4020A+	3127B	4049A	2040A+	1044A	3024A+	1029A+	5034A+	3056A+	5079	5110*	5078*	5020*
SiO_2 (Wt%)	76,42	63,70	64,33	59,44	65,11	64,50	69,87	65,12	72,95	65,66	77,08	65,82	68,57	67,77	67,43	71,01	63,25	65,00	67,67	68,03	62,58	68,59
TiO_2	0,05	0,71	0,82	0,59	0,59	0,56	0,33	0,78	0,23	0,39	0,25	0,63	0,42	0,63	0,40	0,47	0,30	0,43	0,49	0,45	1,15	0,48
Al_2O_3	12,67	16,68	16,43	18,54	15,59	16,33	15,51	16,08	13,27	16,44	13,01	15,37	15,16	15,27	15,84	14,73	15,86	15,19	15,18	15,60	15,24	15,29
Fe_2O_3	1,06	5,66	6,13	6,18	6,44	6,72	3,27	5,70	3,92	5,39	1,72	5,57	4,33	4,84	4,43	3,77	5,24	4,12	5,20	4,24	7,08	4,03
MnO	0,01	0,04	0,06	0,12	0,05	0,12	0,01	0,03	0,04	0,06	0,01	0,04	0,04	0,03	0,04	0,07	0,11	0,08	0,05	0,03	0,07	0,02
MgO	0,42	2,54	3,01	2,60	2,88	2,64	1,64	2,67	1,90	2,53	1,02	2,80	1,95	2,36	2,04	1,52	3,75	3,39	2,52	2,10	2,42	1,69
CaO	1,42	2,35	2,51	3,48	2,52	2,63	1,72	2,39	2,37	2,96	1,97	2,35	2,26	2,83	2,58	2,42	4,82	3,99	3,02	3,01	4,35	1,94
Na_2O	3,12	4,12	3,73	6,17	3,73	3,58	3,06	3,56	3,65	3,96	3,09	3,67	4,05	3,93	3,98	3,70	5,02	4,22	4,15	4,21	4,10	3,51
K_2O	4,83	4,11	2,91	2,38	2,99	2,82	4,51	3,61	1,61	2,53	1,83	3,74	3,15	2,29	3,16	2,26	1,35	3,42	1,64	2,16	2,57	4,40
P_2O_5	0,01	0,10	0,06	0,51	0,10	0,09	0,08	0,06	0,05	0,07	0,01	0,01	0,07	0,05	0,10	0,04	0,28	0,16	0,07	0,17	0,45	0,06
LOI	0,52	1,07	0,94	0,69	1,21	0,74	-0,52	0,95	1,32	0,86	0,60	1,26	1,65	1,07	1,51	0,74	0,96	0,62	0,50	0,79	0,88	0,88
Total	100,5	101,1	100,9	100,7	101,2	100,7	99,5	101,0	101,3	100,9	100,6	101,3	101,6	101,1	101,5	100,7	101,0	100,6	100,5	100,8	100,9	100,9
Al index	1,35	1,58	1,80	1,54	1,69	1,81	1,67	1,68	1,74	1,74	1,89	1,58	1,60	1,69	1,63	1,76	1,42	1,31	1,72	1,66	1,38	1,55
Mg N.	44,20	47,02	49,34	45,46	46,93	43,75	49,83	48,11	49,03	48,21	54,01	49,89	47,16	49,12	47,73	44,43	58,60	62,00	49,02	49,58	40,34	45,42
Cr (ppm)	23	131	202	95	152	171	71	142	101	101	24	172	112	162	132	98	192	221	151	111	52	108
Ni	n.a.	n.a.	n.a.	n.a.	n.a.	n.a.	n.a.	n.a.	0	0	0	0	0	0	0	0	0	0	0	154	99	97
Co	5,0	18,2	19,2	14,1	18,2	14,1	8,9	19,2	11,1	16,1	5,0	19,2	13,2	16,2	16,2	10,1	17,2	18,1	0,0	16,2	17,2	12,1
Sc	2,2	14,2	17,1	12,1	12,2	22,2	6,0	12,1	8,5	14,1	2,3	12,1	12,2	9,8	11,2	14,1	43,4	12,1	13,1	11,1	10,8	8,8
Cu	4	n.a.	n.a.	n.a.	n.a.	n.a.	n.a.	n.a.	n.a.	n.a.	7	36	21	12	n.a.	n.a.	27	10	n.a.	n.a.	n.a.	n.a.
Pb	18	dl	dl	dl	dl	dl	24	dl	n.a.	n.a.	8	13	13	n.a.	n.a.	n.a.	5	12	n.a.	n.a.	n.a.	n.a.
Zn	12	dl	dl	dl	dl	dl	32	dl	n.a.	n.a.	14	68	48	n.a.	n.a.	n.a.	79	60	n.a.	n.a.	n.a.	n.a.
Rb	111	182	192	23	182	131	159	172	59	78	80	142	132	152	142	131	39	111	53	106	85	196
Cs	0,90	0,81	2,82	0,50	0,71	0,91	0,50	1,42	0,51	0,71	0,50	0,51	0,92	1,11	1,02	0,91	0,51	0,50	0,00	1,59	0,48	1,18
Ba	1307	1112	595	443	739	716	1392	930	486	686	561	1213	549	516	873	434	323	1308	463	292	965	1019
Sr	431	406	352	969	541	406	444	400	384	471	401	460	383	390	431	373	435	730	512	402	530	410
Ga	13	20	21	21	21	20	18	21	15	19	15	18	19	21	19	18	19	19	18	19	21	17
Ta	dl	0,71	dl	2,01	1,42	dl	1,19	0,81	dl	dl	dl	dl	dl	0,81	dl	dl	dl	dl	0,00	0,21	0,40	0,22
Nb	dl	13,1	9,1	10,1	8,1	5,0	5,0	12,1	dl	4,0	dl	6,1	10,2	8,1	9,1	7,1	6,1	dl	2,0	3,0	11,2	4,1
Hf	4,22	5,76	5,85	0,60	4,86	5,74	6,16	5,66	6,59	5,04	3,70	4,75	4,58	6,47	5,89	4,94	5,25	4,13	0,00	4,22	8,60	7,06
Zr	116	153	142	39	159	162	191	183	195	177	107	147	154	155	148	162	156	146	132	125	330	200
Y	dl	7	13	19	4	24	9	dl	4	15	dl	dl	5	dl	6	23	52	11	5	10	20	3
Th	6,84	12,13	10,08	0,81	14,18	16,13	45,72	8,60	5,98	19,16	10,01	12,13	20,35	16,18	13,20	20,17	3,44	1,61	9,95	6,13	1,34	60,35
U	dl	dl	0,71	dl	dl	1,21	dl	0,71	dl	0,81	dl	0,61	0,81	dl	0,61	dl	dl	dl	0,70	0,63	0,20	0,85
La	26,14	38,42	28,23	32,24	50,63	40,31	109,33	26,29	23,30	50,43	37,04	42,47	53,92	33,38	40,62	37,32	28,29	27,17	n.a.	20,97	55,55	92,64
Ce	41,23	70,78	53,44	65,48	88,10	78,61	208,73	45,51	39,51	95,82	71,07	71,79	101,73	64,74	76,17	72,62	70,73	50,31	n.a.	39,01	116,43	174,56
Nd	14,08	27,30	20,17	31,23	35,44	28,22	78,52	18,20	16,21	40,35	24,02	23,26	36,62	27,31	29,45	31,27	45,47	27,17	n.a.	17,48	54,92	69,88
Sm	1,31	3,64	3,13	7,76	3,85	3,63	9,94	2,33	2,13	6,35	3,10	2,63	5,29	4,25	3,35	4,44	12,12	4,93	n.a.	3,53	7,85	8,22
Eu	1,41	1,11	1,01	1,11	1,11	1,21	0,89	0,91	1,11	1,41	0,80	1,42	1,02	1,11	1,22	1,01	1,41	1,11	n.a.	0,86	2,14	1,23
Tb	0,20	0,20	0,20	0,71	0,20	0,20	0,20	0,20	0,20	0,20	0,20	0,20	0,20	0,20	0,20	0,20	1,52	0,50	n.a.	0,48	0,79	0,54
Yb	dl	0,51	2,22	1,31	0,41	4,23	0,30	0,40	dl	1,51	dl	dl	0,41	dl	0,41	6,25	4,85	1,31	n.a.	0,80	1,66	0,45
Lu	dl	dl	0,302	0,201	dl	0,605	dl	dl	dl	0,202	dl	dl	dl	dl	dl	1,009	0,606	0,201	n.a.	0,121	0,244	0,069

Table 4: continued

Sample	5074*	5076*	5186*	5224*	1052*	123*	71*	1035*	1040*	1047*	2047*	3071*	3095*	5093*	1118*	1017*	57*	64*	5028*
SiO_2 (Wt%)	74,08	71,16	69,37	69,38	66,28	70,05	60,95	69,30	66,25	68,06	68,61	71,65	56,01	65,04	73,93	73,31	75,03	64,01	64,22
TiO_2	0,27	0,71	0,22	0,35	0,45	0,35	0,77	0,21	0,64	0,44	0,60	0,50	1,02	0,56	0,17	0,16	0,11	0,77	0,54
Al_2O_3	13,98	14,23	15,48	15,67	14,30	15,44	17,81	15,50	15,30	15,35	14,88	14,03	16,37	16,24	14,16	14,38	13,29	16,46	14,18
Fe_2O_3	2,56	3,85	3,62	3,84	6,13	3,68	5,69	3,17	5,62	4,15	4,82	3,28	7,02	4,43	1,43	1,69	1,19	5,31	5,81
MnO	0,01	0,01	0,04	0,02	0,08	0,04	0,07	0,05	0,04	0,06	0,04	0,03	0,09	0,05	0,01	0,01	0,01	0,05	0,08
MgO	0,97	1,50	1,76	1,50	2,92	1,12	2,71	1,30	2,57	1,94	1,21	0,47	5,18	2,05	0,60	0,60	0,50	2,14	3,86
CaO	2,73	2,26	2,61	1,96	3,50	2,14	4,14	2,44	2,66	3,53	2,11	2,09	6,34	3,43	1,74	1,59	0,93	3,48	4,04
Na_2O	4,11	3,74	3,63	3,33	4,52	5,15	5,88	3,92	3,65	4,77	3,59	3,55	4,65	4,86	3,42	3,14	2,59	4,78	3,84
K_2O	1,23	2,52	3,06	3,88	1,65	1,94	1,90	3,89	3,18	1,54	3,90	4,26	2,89	3,04	4,46	5,06	6,29	2,57	3,22
P_2O_5	0,05	0,01	0,20	0,07	0,15	0,08	0,07	0,21	0,09	0,15	0,24	0,14	0,44	0,29	0,09	0,05	0,06	0,42	0,21
LOI	0,88	0,73	0,43	0,79	0,62	0,58	0,92	0,60	0,74	0,77	0,62	0,25	0,73	0,95	0,52	0,59	0,33	0,67	0,85
Total	100,9	100,7	100,4	100,8	100,6	100,6	100,9	100,6	100,7	100,8	100,6	100,3	100,7	100,9	100,5	100,6	100,3	100,7	100,9
Al index	1,73	1,67	1,66	1,71	1,48	1,67	1,49	1,51	1,61	1,56	1,55	1,42	1,18	1,43	1,47	1,47	1,35	1,52	1,28
Mg N.	42,90	43,61	49,05	43,55	48,53	37,59	48,52	44,75	47,54	48,06	33,30	22,16	59,38	47,79	45,32	41,31	45,42	44,39	56,79
Cr (ppm)	90	68	88	94	224	56	63	43	148	82	47	10	135	57	22	31	21	39	234
Ni	190	100	104	119	191	15	134	37	119	95	76	67	117	83	84	89	81	91	139
Co	8,7	10,7	10,0	9,6	19,3	6,7	16,7	6,0	18,3	10,5	8,4	4,5	26,2	11,0	4,2	5,3	3,2	12,9	18,2
Sc	5,5	4,2	8,4	6,5	16,6	1,8	5,5	8,3	14,8	5,5	7,2	5,7	24,3	12,6	1,7	3,0	1,6	6,7	14,9
Cu	n.a.	n.a.	n.a.	n.a.	n.a.	n.a.	n.a.	n.a.	n.a.	n.a.	n.a.	n.a.	n.a.	n.a.	n.a.	n.a.	n.a.	n.a.	n.a.
Pb	n.a.	n.a.	n.a.	n.a.	n.a.	n.a.	n.a.	n.a.	n.a.	n.a.	n.a.	n.a.	n.a.	n.a.	n.a.	n.a.	n.a.	n.a.	n.a.
Zn	n.a.	n.a.	n.a.	n.a.	n.a.	n.a.	n.a.	n.a.	n.a.	n.a.	n.a.	n.a.	n.a.	n.a.	n.a.	n.a.	n.a.	n.a.	n.a.
Rb	40	102	90	139	66	117	71	203	157	65	128	124	102	87	105	121	147	73	102
Cs	dl	0,42	0,75	0,61	0,66	6,13	1,30	1,40	1,80	0,89	0,59	0,37	0,83	0,73	0,42	0,60	2,46	0,55	1,89
Ba	263	889	955	908	373	696	387	902	851	50	648	892	813	629	1214	1530	1798	545	1114
Sr	407	387	432	390	474	252	679	476	468	345	332	261	822	464	620	449	506	521	671
Ga	16	19	17	18	18	22	23	20	19	22	20	17	22	21	16	13	13	21	17
Ta	dl	0,10	0,11	0,17	0,38	0,63	0,68	0,32	0,21	0,08	0,19	0,47	0,11	0,05	0,80	0,07	0,06	0,28	0,11
Nb	2,0	3,0	3,0	5,0	5,0	4,0	10,2	12,2	6,1	3,0	10,1	8,0	6,1	3,0	2,0	2,0	2,0	7,1	2,0
Hf	15,37	32,94	5,67	3,10	3,41	4,75	11,43	5,28	5,57	3,53	12,78	5,35	4,77	5,16	3,70	4,59	0,71	5,17	3,00
Zr	449	889	181	117	122	124	355	112	169	110	437	175	171	184	111	145	39	178	98
Y	4	6	19	3	14	13	15	24	5	7	15	13	24	17	3	7	3	11	9
Th	6,65	2,13	17,14	11,38	5,19	104,79	5,70	83,12	27,06	4,31	26,01	1,00	2,26	5,13	0,41	27,06	0,95	6,28	1,22
U	1,00	0,49	0,81	0,39	1,37	175,87	1,82	1,75	0,59	0,27	0,72	0,41	0,33	0,68	0,31	0,98	0,21	0,77	0,31
La	22,20	20,83	45,29	30,16	23,43	146,51	58,13	158,52	53,30	36,16	73,22	29,79	39,41	31,44	10,41	47,65	8,26	49,61	18,10
Ce	40,73	32,46	84,27	51,81	45,73	194,20	115,54	257,55	99,33	64,80	146,63	61,42	83,06	72,59	17,43	95,35	13,61	95,97	39,91
Nd	13,98	11,38	35,72	19,93	21,51	86,30	50,60	79,11	40,16	23,43	62,51	29,45	48,34	33,09	5,88	39,96	4,68	42,03	22,33
Sm	2,08	1,33	5,47	2,57	3,74	20,88	7,24	9,53	4,94	3,28	9,17	4,86	9,24	5,43	0,94	6,28	0,94	5,85	3,86
Eu	1,06	1,03	1,06	0,93	0,90	1,36	1,85	1,24	1,34	0,99	1,47	1,74	1,62	1,12	0,85	1,39	0,86	1,05	1,20
Tb	0,19	0,23	0,71	0,24	0,47	1,09	0,70	1,01	0,37	0,28	0,79	0,54	0,94	0,49	0,09	0,56	0,10	0,50	0,43
Yb	0,69	0,87	1,39	0,26	1,31	1,16	1,40	1,84	0,73	0,57	1,06	1,14	2,11	0,88	0,20	0,46	0,21	0,75	0,87
Lu	0,108	0,144	0,207	0,042	0,195	0,149	0,208	0,259	0,103	0,083	0,146	0,168	0,282	0,119	0,029	0,068	0,026	0,113	0,124

Abbreviations: n.a.= not analyzed, dl = below detection limit, * = samples analyzed at UQAC

wall rocks (e.g. the melt-depleted metasediments) and minerals that could have been derived from the wall rocks (e.g. quartz, plagioclase, biotite and orthopyroxene) and, c) the composition of the major phases that crystallized from the contaminated anatectic magma (e.g. quartz, plagioclase, K-feldspar, orthopyroxene), so that the effects of fractional crystallization can be examined.

The initial melt composition is unlikely to be found in the field, because leucosomes usually have compositions which are not that of the initial melt (Sawyer 1987; Barbey *et al.* 1996; Sawyer *et al.* 1999; Solar & Brown 2001). For this purpose the same anatectic melt composition used for the chemical modelling of the melt-depleted granulites (Chapter III) will be used. This anatectic melt composition is the average of the four melt compositions obtained from the experimental studies by Patiño Douce & Beard (1995), Gardien *et al.* (1995), and Montel & Vielzeuf (1997) carried out on bulk compositions that are similar to those of the protolith of Ashuanipi migmatites and at *P-T* conditions comparable to those under which anatexis occurred in the Ashuanipi subprovince (*P* 7±2 kbar and *T* 850±50°C, Chapter III). The representative mineral composition (e.g. symbols bte, opx, plg, qtz, and K-fsp) used to define the vectors indicated by the various arrows on the composition diagrams (e.g. Fig. 21), were determined by electron microprobe. The geochemical variation in any suite of rock is reflected by changes in the modal and mineralogical compositions in the suite. However, the interpretation of rocks that were dominantly melt becomes more complicated because they represent the result of a series of combined sequential and concurrent processes during the segregation of melt from residuum, contamination by the host rock as the melt moved in leucosome or vein arrays, and later when

crystallization began and the separation of accumulated solid phases from the magma (melt + solid) occured and formed an evolved liquid, i.e. the various processes associated with fractional crystallization (Tindle 1988; Sawyer 1987, 1998).

Most of the major oxides and trace elements are plotted on diagrams such that a component that partitions into the melt, such as SiO_2 and K_2O is plotted against one that partitions into the residuum, or early crystallized phases; such elements are MgO, and CaO. In general, the elements such as MgO, CaO, FeO, TiO_2, Al_2O_3, Cr, Sc, Y and Sr all show negative correlations when plotted against either SiO_2 content or K_2O content (e.g. Figs. 21, 22, 23 & 24), similar to results from other migmatites (Sawyer 1998; Solar & Brown 2001; Milord *et al.* 2001).

The SiO_2 content of the diatexite migmatites ranges between 53 and 78 wt % (Fig. 21), and the K_2O content from 1 to 7 wt %. K_2O shows a positive correlation with SiO_2. Most of the diatexite migmatites have lower SiO_2 and K_2O contents than the plausible initial anatectic melt composition. Similarly, the diatexite migmatites have higher MgO (Fig. 22) and CaO contents (Fig. 23) than the assumed initial melt composition. These features could indicate either contamination, or fractional crystallization (or both) of the initial melt. The distribution of samples on figure 21 shows several trends; but most samples define a trend (trend 1) that shows a decrease in K_2O and SiO_2 from the initial anatectic melt composition; this trend coincides with a mixing line between the anatectic melt and orthopyroxene, which could mean that the melt has been contaminated by orthopyroxene from the wall rocks, or it could mean that

orthopyroxene that crystallized from the melt had accumulated. However, those same samples define a trend on figure 22 in which MgO increases with decreasing SiO_2, and this cannot be due to adding just orthopyroxene, rather biotite and or orthopyroxene + plagioclase had to have been added to the melt. The main trend on figure 23 indicates that plagioclase was the principal phase added to the melt. Trend 2 on figure 21 is outlined by a subset of samples that define a steeper decrease in K_2O; this could be interpreted as the result of adding only plagioclase to the initial melt composition, however these samples have a higher MgO content than the initial melt, so they too must contain some additional orthopyroxene. A weak trend (trend 3) towards high K_2O contents and moderate SiO_2 contents is attributed to the addition of K-feldspar to the initial anatectic melt. A few samples could be modelled as the addition of biotite (e.g. BL17), or of quartz, to the starting melt composition. However, most of the data is clustered at around 66 to 67 wt % SiO_2, and trends towards plagioclase and quartz emanate from that point (Fig. 21).

Most of the samples with SiO_2 lower than the initial melt composition, lie between the vectors for initial melt + plagioclase and initial melt + orthopyroxene compositions; these correspond to initial melt + orthopyroxene + plagioclase or initial melt + biotite on figure 22. However this does not distinguish between residual biotite, quartz, plagioclase and orthopyroxene and biotite, plagioclase quartz and orthopyroxene that crystallized from the melt; the former implies contamination of the melt by the wall rocks, whereas, the latter implies fractional crystallization. Mass balance calculations indicate that much more plagioclase has to be added than orthopyroxene (see also the modal mineralogy, figure 19), and this displaces the trend of samples to lower SiO_2 and

higher CaO contents; as can be seen on figure 23, where the sample trend is dominated by plagioclase relative to the orthopyroxene – melt, or the biotite – melt, mixing lines.

A few samples (5074, 6017, & 57) plot on the high silica side of the initial melt composition on figures 21, 22 and 23; these represent the addition of silica component to the melt. Quartz is certainly a residual phase, but it is anticipated that the addition of residual quartz would be accompanied by even greater amounts of plagioclase and orthopyroxene. However, the addition of quartz derived from quartz veins in the melt-depleted metasediments would be accompanied by the addition of plagioclase. Samples with K_2O contents lower than the initial melt formed in some of the diatexites (presumably the most peraluminous), thus samples with high silica contents could represent quartz crystallized from the peraluminous melt which was later concentrated by accumulation.

Samples with K_2O contents lower than the proposed initial melt composition and located on the high silica side of the melt + orthopyroxene and the melt + plagioclase lines on figure 21, are the result of orthopyroxene, plagioclase and quartz being added to the melt, as they have somewhat higher CaO and MgO contents than the average anatectic melt composition. Only a few diatexite migmatites (e.g. samples 1017*, 2085, 1054) have bulk compositions that are compatible with a primary anatectic melt.

4.5.3 Interpretation of the geochemical trends of the diatexite migmatites

4.5.3.1 The major elements

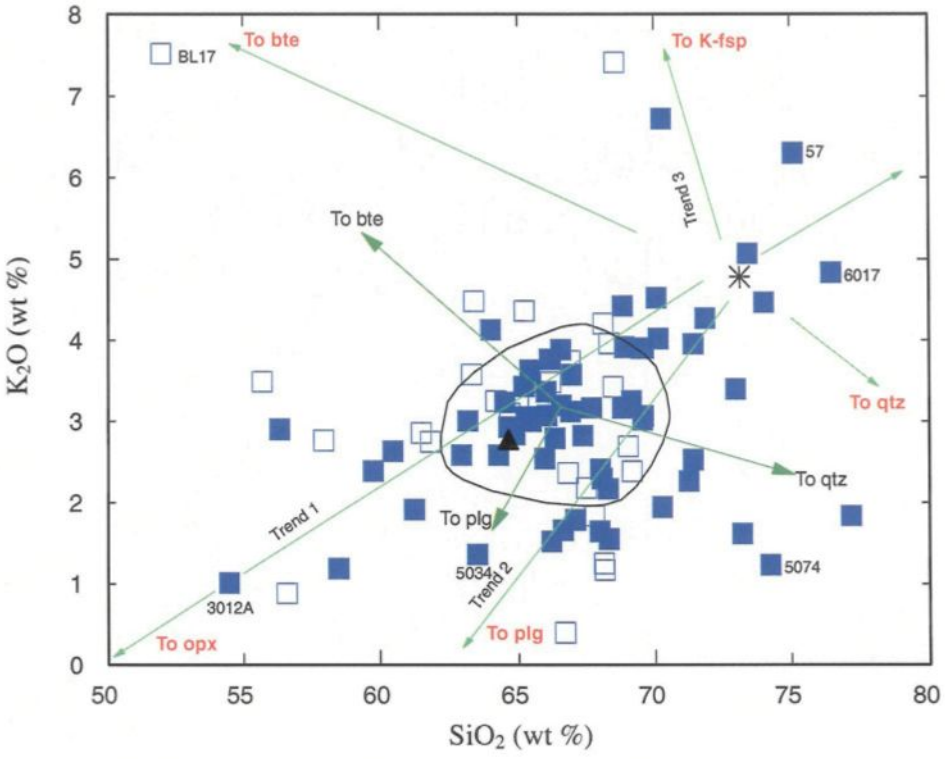

Figure 21: Plot of K_2O *versus* SiO_2 for diatexite migmatites from the Ashaunipi subprovince. K_2O shows a positive correlation with SiO_2, but there are several trends. Trend 1 could be modelled as the addition of orthopyroxene to the initial melt (asterix). Trend 2 shows a steeper decrease in K_2O and SiO_2, and can be modelled as the result of adding plagioclase to the melt. The weak trend 3 has the highest K_2O contents but moderate SiO_2 content and could be attributed to the addition of K-feldspar to the melt. A few samples could be modelled as the addition of biotite (sample BL17) or quartz (sample 5074) to the melt composition. Also shown are the vectors (arrows) for plagioclase, quartz, orthopyroxene, biotite, and K-feldspar. The orthopyroxene and biotite compositions used are from Percival (1991) and ideal plagioclase compositions from table 5. The filled blue squares represent the diatexite migmatites from this study and open squares are the diatexite migmatites from the north Ashuanipi (Percival 1991b & Lapointe 1996), The asterix represents the average experimental melt composition, the filled triangle is an estimate of the average protolith composition using data from the Quetico subprovince. Plg = plagioclase, bte = biotite, qtz = quartz, opx = orthopyroxene, K-fsp = K-feldspar.

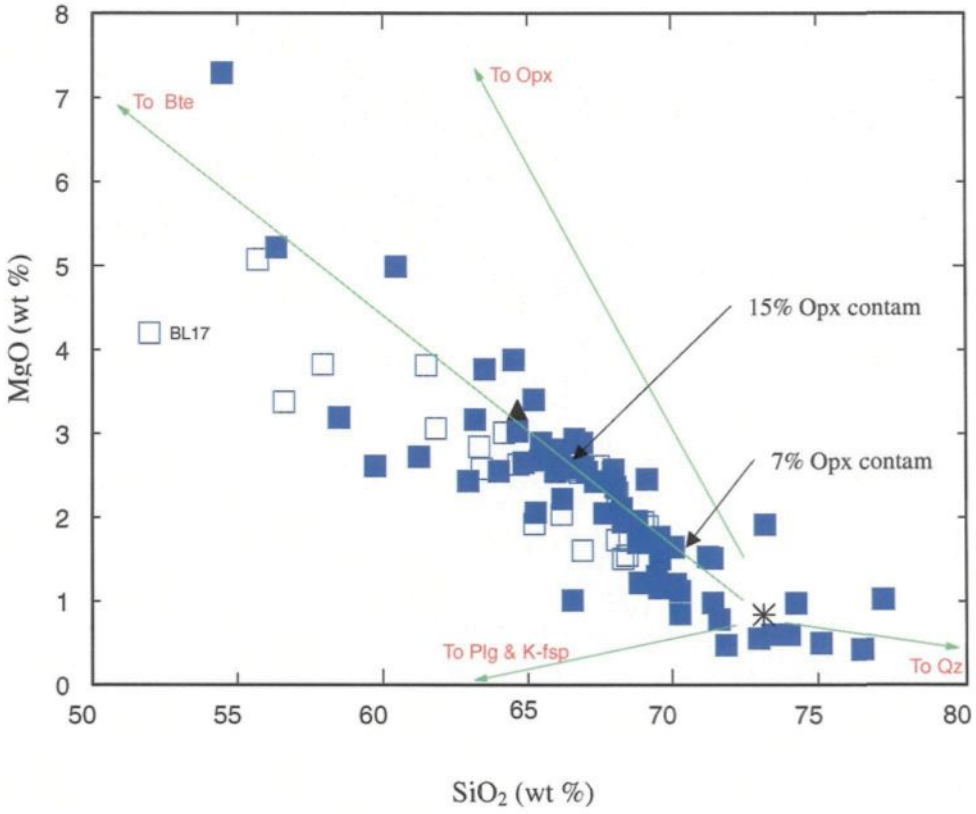

Figure 22: MgO *versus* SiO_2 Harker variation diagram for the Ashuanipi diatexite migmatites showing a decrease in MgO as SiO_2 increases. The main trend shows a decrease in MgO with increasing SiO_2 along the mixing line melt + biotite. However, based on figure 21, this trend is better explained as the addition of orthopyroxene + plagioclase to the melt. Another trend towards high SiO_2 is due to the addition of silica to the melt; these could be samples derived from fractionated anatectic melts. Symbols are as in Fig. 21.

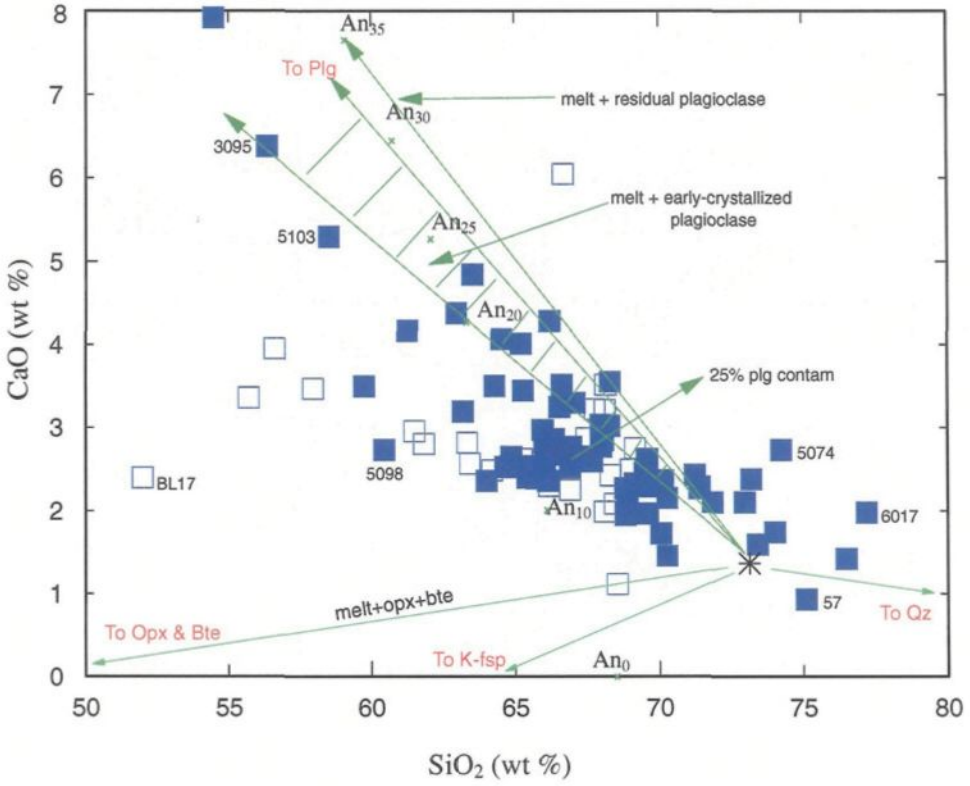

Figure 23: CaO *versus* SiO_2 Harker variation diagram for the Ashuanipi diatexite migmatites illustrating that the majority of samples with SiO_2 lower than the assumed initial melt lie between the vectors for melt + plagioclase and melt + opx + bte. Because the trend of samples is displaced to lower SiO_2 and higher CaO more plagioclase has been added to the melt than orthopyroxene, or opx + bte. Plagioclase of different compositions (An_0 to An_{35}) is shown on the diagram. Samples with SiO_2 contents higher than the anatectic melt, but with higher CaO contents may be evolved anatectic melts that contain crystals of earlier-formed calcic plagioclase. Residual plagioclase has composition of about An_{30}, early-crystallized plagioclase about An_{25}, and the late-crystallized plagioclase about An_{17}. Symbols are as on figure 21.

The major element variation diagrams show that various combinations of quartz, plagioclase, orthopyroxene, biotite and K-feldspar may have been added to the anatectic melt in order to derive each of the trends present on the diagrams. K-feldspar is not generally a residual phase in the partially melted metagreywacke rocks in the Ashuanipi subprovince (although it is in the residual rocks derived from metapelitic protoliths). Therefore, addition of K-feldspar to the melt implies the addition of a phase that had crystallized from the melt, and hence the process of fractional crystallization in the diatexite magma. Alternatively, these melts could have been derived from the metapelitic layers and were more potassic to start with (e.g. Grant 2004). Most of the quartz, orthopyroxene and plagioclase enrichment could be due to crystal accumulation. Reaction of early-crystallized orthopyroxene with the evolved melt in a diatexite to make the texturally late biotite (e.g. Fig 17i), should not change either the K_2O, or the MgO, contents of the bulk rock. Hence any biotite added to the diatexite migmatites is most likely derived from the residuum, albeit by destruction of residual orthopyroxene. Fractional crystallization in a granitic melt commonly increases the SiO_2 content of the evolved melt, typically, the K_2O and Na_2O contents are also increased and some of the samples are enriched in these elements beyond the average initial melt composition, consequently, they must be considered as the likely products of a fractionated anatectic melt.

However, for most SiO_2-rich samples there is no increase in K_2O (e.g. Fig. 21) and Na_2O, hence the additional SiO_2 in these diatexites indicates some addition of silica, perhaps by contamination with the quartz from the residuum, or accumulation of previously crystallized quartz phenocrysts. High CaO contents for the SiO_2-rich

samples (e.g. 5074) could indicate the presence of either early-formed plagioclase, or of residual plagioclase. However, the generally low MgO contents of the high SiO_2 samples (e.g. Fig 22) suggests that contamination of an evolved anatectic melt by orthopyroxene, or biotite, was negligible, but it is difficult to see how, if the residuum was the contaminant, that orthopyroxene and biotite were not added along with plagioclase. The position of various plagioclase compositions (An_0 to An_{35}, see Table 5 for compositions) are shown on figure 23. The trends present on figure 23 indicate that residual plagioclase (An_{30}) plays only a very minor part in determining the composition of the diatexite migmatites. However, the addition of plagioclase with a composition between An_{20} and An_{25} to an initial granitic melt could be a major factor in explaining the compositional trends in the diatexite migmatites. The progression to more sodic plagioclase compositions within samples and in the diatexite migmatite suite in general, together with the large size and euhedral form, indicates that most plagioclase in the diatexite migmatites crystallized from the anatectic melt and was locally accumulated. Similarly, orthopyroxene in the diatexite migmatites could have been derived from the residuum, but the large size and euhedral form of the orthopyroxene crystals in the diatexite migmatites suggests that they grew in the melt either as a liquidus, or possibly, as a peritectic phase. There is some microstructural evidence that plagioclase from the residuum acted as nuclei for the growth of plagioclase from the melt. Hence, the compositional range of the diatexite migmatites in the Ashuanipi subprovince is due fractional crystallization and some contamination by its residuum. A maximum of about 60 % contamination with the residuum occurred in some samples, most-likely during the stage of channelled flow in dykes, and when the anatectic melt accumulated

in dilatant sites to form large diatexite sheets. However, for most samples the fraction of residuum that contaminated the melt was considerably lower (<< 40 %).

Table 5: Plagioclase compositions calculated from ideal stoichiometry

Oxides	An_0	An_5	An_{10}	An_{15}	An_{20}	An_{25}	An_{30}	An_{35}	An_{50}	An_{100}
SiO_2	68.74	67.39	66.05	64.72	63.39	62.07	60.76	59.46	55.60	43.20
Al_2O_3	19.44	20.35	21.25	22.16	23.04	23.93	24.82	25.69	28.29	36.64
Na_2O	11.82	11.19	10.57	9.95	9.34	8.73	8.12	7.52	5.73	0
CaO	0	1.07	2.13	3.17	4.23	5.27	6.30	7.33	10.38	20.16
Na_2O/CaO	0	10.46	4.96	3.14	2.21	1.66	1.29	1.03	0.55	0

4.5.3.2 The trace elements

The Cr *vs* SiO_2 diagram (Fig. 24), shows a negative Cr trend at high SiO_2 contents, but there are several trends. Of the two principal trends, one is towards high Cr contents and one to lower Cr contents. The high Cr could be due to the addition of a Cr-rich phase, such as orthopyroxene, to the melt, however, the MgO and CaO contents seem to rule that out. High and low Cr trends that are negatively correlated with silica are found in many Archaean metasediments of the Superior province, thus the two trends may simply reflect different protoliths for the respective diatexite migmatites, one with a high Cr content and the other with a low Cr content. The addition of quartz to the melt, or the effects of fractional crystallization could have produced the negative low Cr trend for the samples with $SiO_2 > 72$ %.

There is no well-defined pattern for Rb content with SiO_2 in the diatexites (Fig. 25), but overall the Rb concentration shows the same behaviour as K_2O, and increases with SiO_2 content up to about 70 % SiO_2. The Rb contents of the diatexite migmatites are, on average, higher than in the melt-depleted metasediments, at the same SiO_2 contents. The mobile element Cs shows two trends on a plot against K_2O, and figure 26 (Rb *vs* Cs) shows that most of the diatexite migmatites have very low Cs contents relative to Rb (Rb/Cs ratios of about 175). However, some diatexite migmatites have higher Cs contents that yield Rb/Cs ratios of about 63, which is similar to the average Rb/Cs ratio of the melt-depleted metagreywackes (residuum from the melting).

Most diatexite migmatites are strongly depleted in Cs relative to, the residuum left after melting (Rb/Cs $\approx$ 16.5), if the average for the Quetico metasediments is representative of the protolith.

The trace elements Zr, La and Th show broadly similar patterns against SiO_2 on figures 27a, b and c. All show a nearly flat, or weakly, increasing contents up to about 65 to 70 wt % SiO_2, followed by a decrease to slightly lower concentrations as SiO_2 content increases. This type of pattern is a very common feature in felsic magma suites, and is generally attributed to the crystallization of accessory phases such as zircon, monazite and allanite (Hoskin et al. 2000).

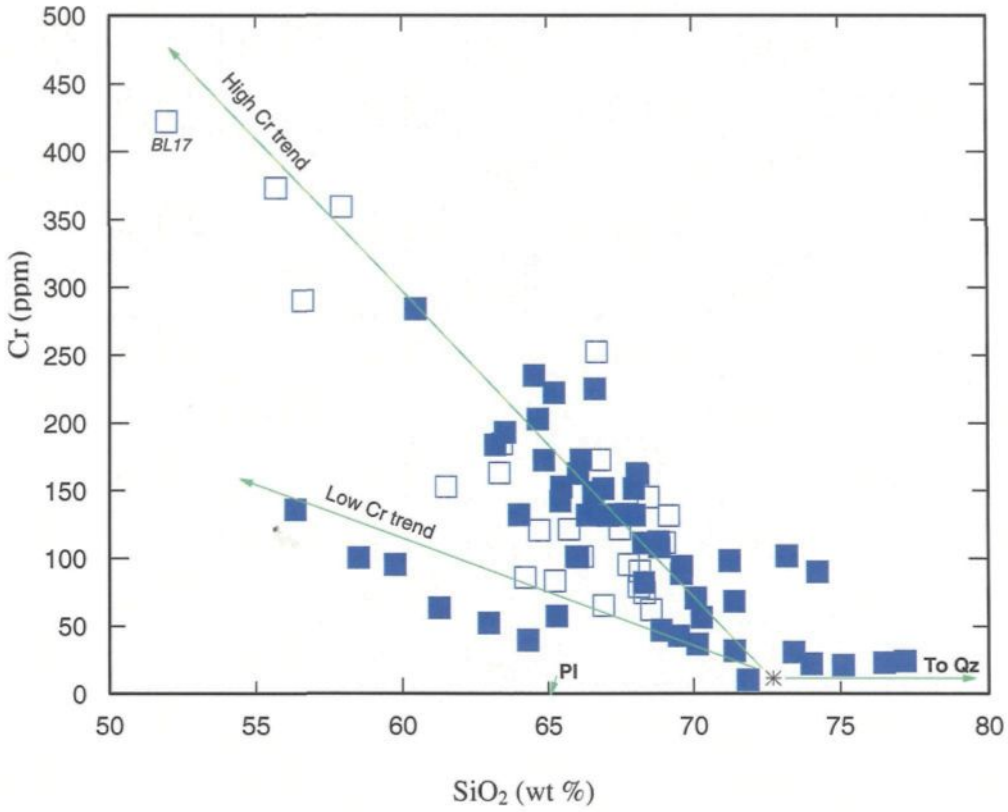

Figure 24: Cr *versus* SiO_2 variation diagram showing the different trends for the Ashuanipi diatexite migmatites. Samples that define the high-Cr trend towards biotite-rich sample BL17 contain about three times as much Cr as the samples that define the low Cr trend. Symbols are as on Fig. 21.

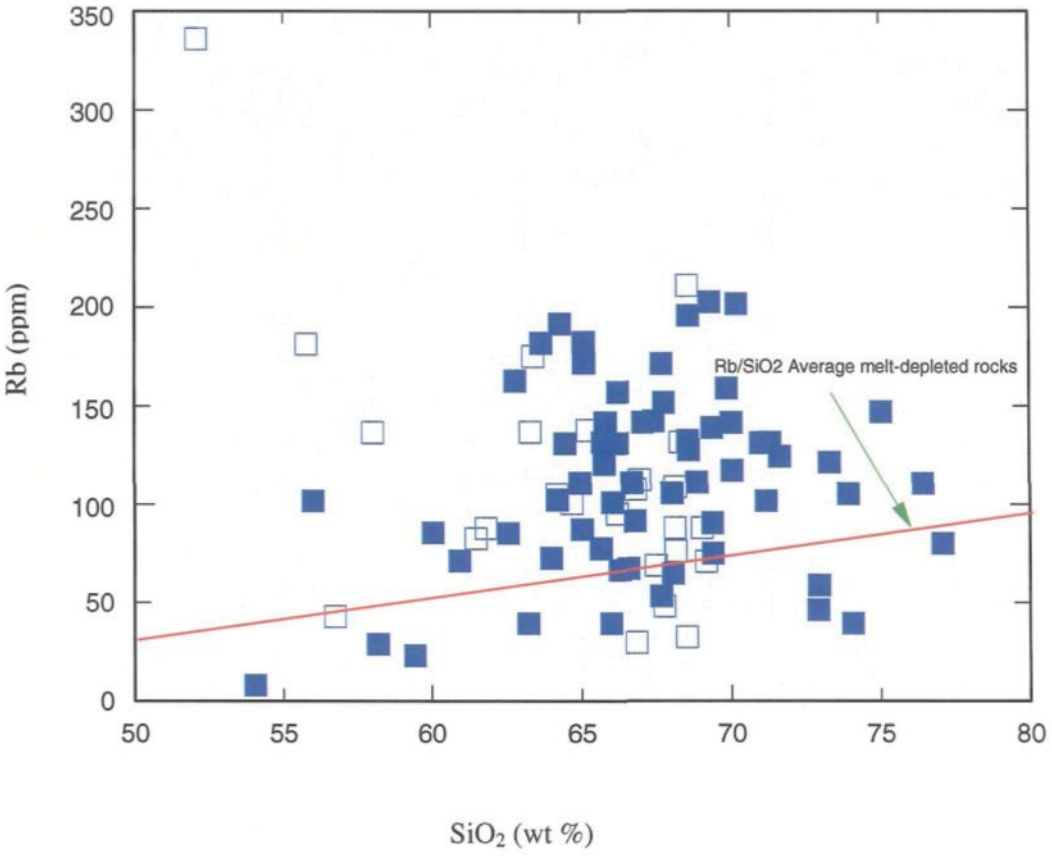

Figure 25: Rb *versus* SiO_2 variation diagram for the Ashuanipi diatexite migmatite showing little correlation between the two elements. The Rb contents in the diatexite migmatites are higher than in the residual, melt-depleted metasediments. Symbols are as on Fig. 21.

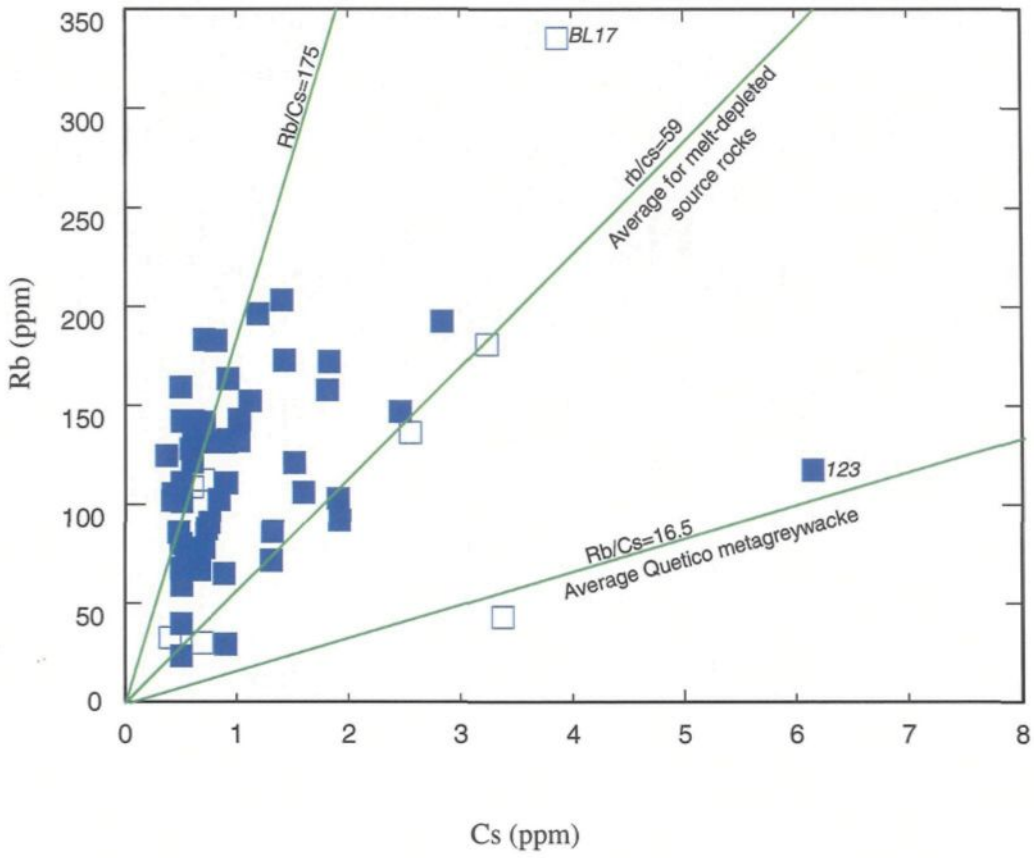

Figure 26: Rb *versus* Cs variation diagram shows that the Cs content in the diatexite migmatites is considerably lower relative to Rb than in rocks that may be representative of the protolith. Most of the samples have less than 1 ppm Cs, the detection limit is at about 0.3 ppm. Symbols are as on Fig. 21.

The extraction (i.e. fractionation) of an accessory phase results in depletion of residual melt in the appropriate trace element, as the magma evolves to high SiO_2 content, but at the place where the accessory minerals are accumulated whole rock compositions are highly enriched in the appropriate trace elements. However, some samples with around 70 wt % SiO_2 show a considerable enrichment in Zr, Th and La. There is no systematic correlation of high Zr with high La and/or Th in the sample set, and neither is there a correlation between high Zr, La, or Th with high Y, Nb, Ta or the HREE (see Table 2). Thus the variation in Zr, La and Th within the diatexite migmatites appears to be due to a unique accessory mineral assemblage in each rock, rather than to a systematic increase in the modal abundance of the same accessory mineral assemblage.

The average Zr, Th and La contents (164 ppm, 12.51 ppm and 37.95 ppm respectively) in the diatexites is high compared to the possible protolith. The samples 123 and 1035 have the highest contents of La and Th, but have low concentrations of Zr and, therefore, their respective origins will be discussed later in the trace element modelling section. Accessory minerals such as apatite, zircon, titanite, and more rarely allanite, monazite and xenotime are more important than the major phases in controlling the concentrations of some trace elements (e.g. Y, Zr, Hf, REE, U and Th) during fractional crystallization (Dodge & Mays 1972; Condie 1978; McCarthy & Kable 1978).

The abundance of Sr shows a very weak positive correlation with CaO content (Fig. 28), and hence highest modal plagioclase. The Sr/CaO ratio is similar to that of

the possible protolith and to the melt-depleted residuum (metagreywackes) in the Ashaunipi subprovince. Thus, Sr and CaO do not appear to be fractionated from one another during anatexis and the formation of diatexite migmatites. However, the diatexite migmatites have, on average, slightly lower CaO contents and form a tighter cluster in Sr-CaO composition space than the residual rocks do.

The samples with the highest K_2O abundances have the greatest Ba (Fig. 29) and Rb concentrations (Fig. 30). However, compared to the average for the melt-depleted metasediment, the diatexite migmatites have similar Ba/K_2O and Rb/K_2O ratios, but markedly higher Ba, K_2O and Rb contents (Table 3). Therefore, Ba, K_2O and Rb have not become fractionated from one another during anatexis, and have partitioned into the anatectic melt.

The trace elements that are compatible with the major mafic phases (i.e. Sc, Cr, and Y), biotite and orthopyroxene, show a negative correlation with SiO_2. The average Rb/Sr (0.13), Th/U (4.27) and Rb/Cs (100) ratios for diatexite migmatites in the Ashuanipi subprovince (see appendix VIII) are different to those in the protolith (averages 0.25, 3.5 and 16.5 respectively) and the average melt-depleted residuum (0.2, 7.1 and 57.2 respectively). Thus, the U and Cs are both strongly depleted in the diatexite migmatites relative to the protolith suggesting either that; 1) the primary melt from which the diatexites were derived was strongly depleted in Cs and U relative to its source material or, 2) that crystallization of the diatexite magma occurred in an open system where the accumulated crystals became separated from their corresponding, or

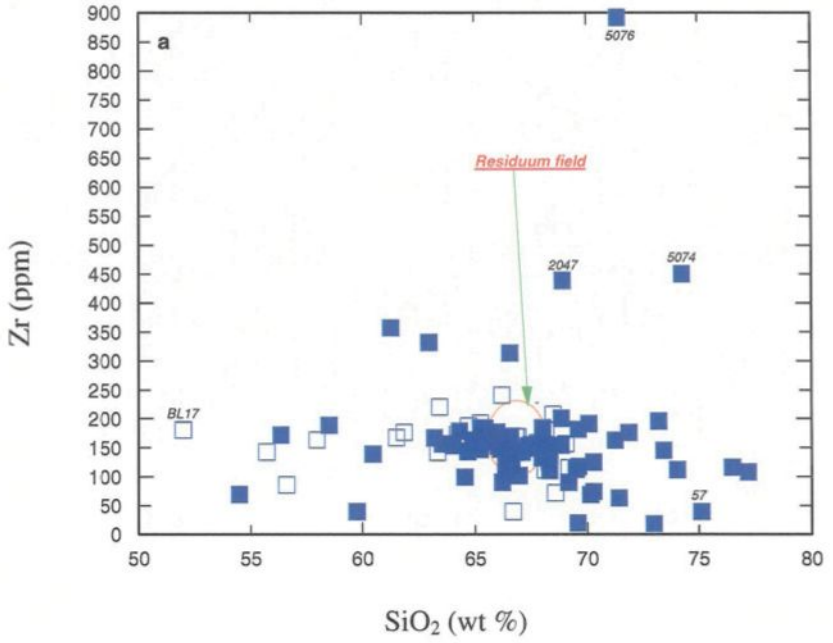
a
Zr (ppm)
SiO2 (wt %)
Residuum field
5076
2047
5074
BL17
57
900
850
800
750
700
650
600
550
500
450
400
350
300
250
200
150
100
50
0
50
55
60
65
70
75
80

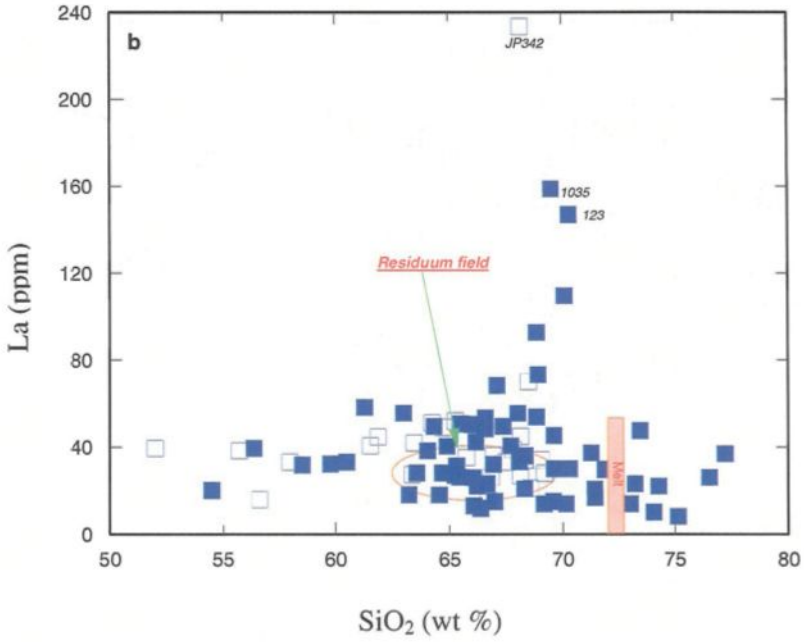
b
La (ppm)
SiO2 (wt %)
Residuum field
JP342
1035
123
240
200
160
120
80
40
0
50
55
60
65
70
75
80

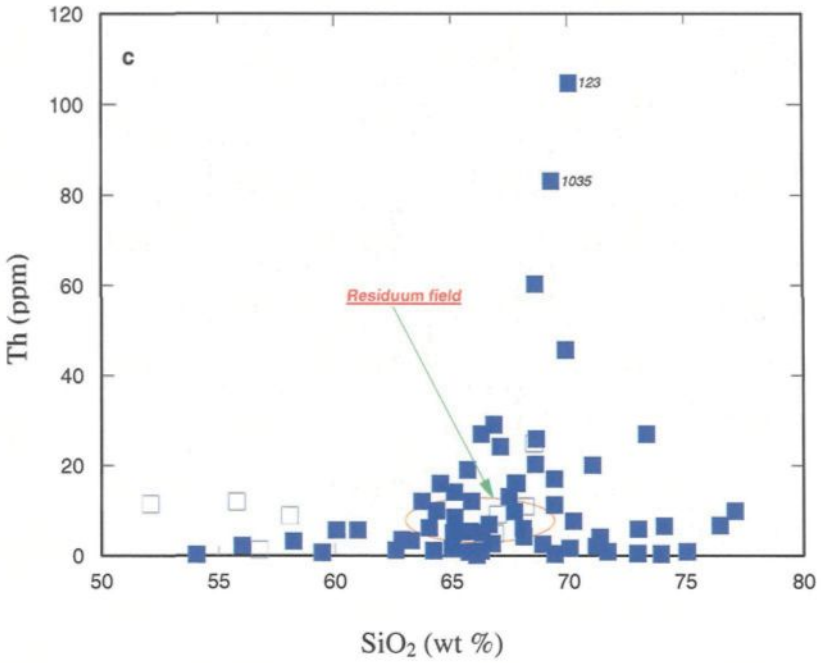

Figure 27: Trace element variation plots; (a) Zr *versus* SiO_2, (b) La *versus* SiO_2 and, (c) Th *versus* SiO_2 showing that in the diatexite migmatites from the Ashaunipi subprovince the maximum concentrations of Zr, La and Th occur at around 70 wt % SiO_2. Symbols are as on Fig. 21.

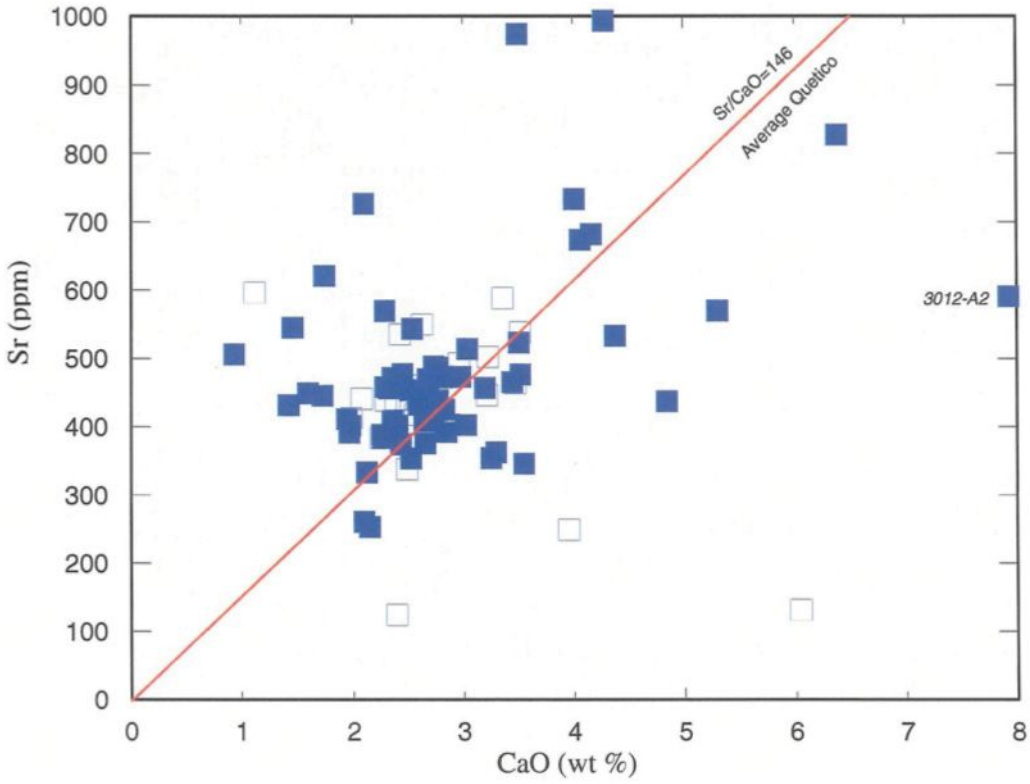

Figure 28: Sr *versus* CaO variation diagram showing a weak positive correlation. The samples with the highest CaO, and hence modal plagioclase content, have the greatest Sr content. Symbols are as on Fig. 21.

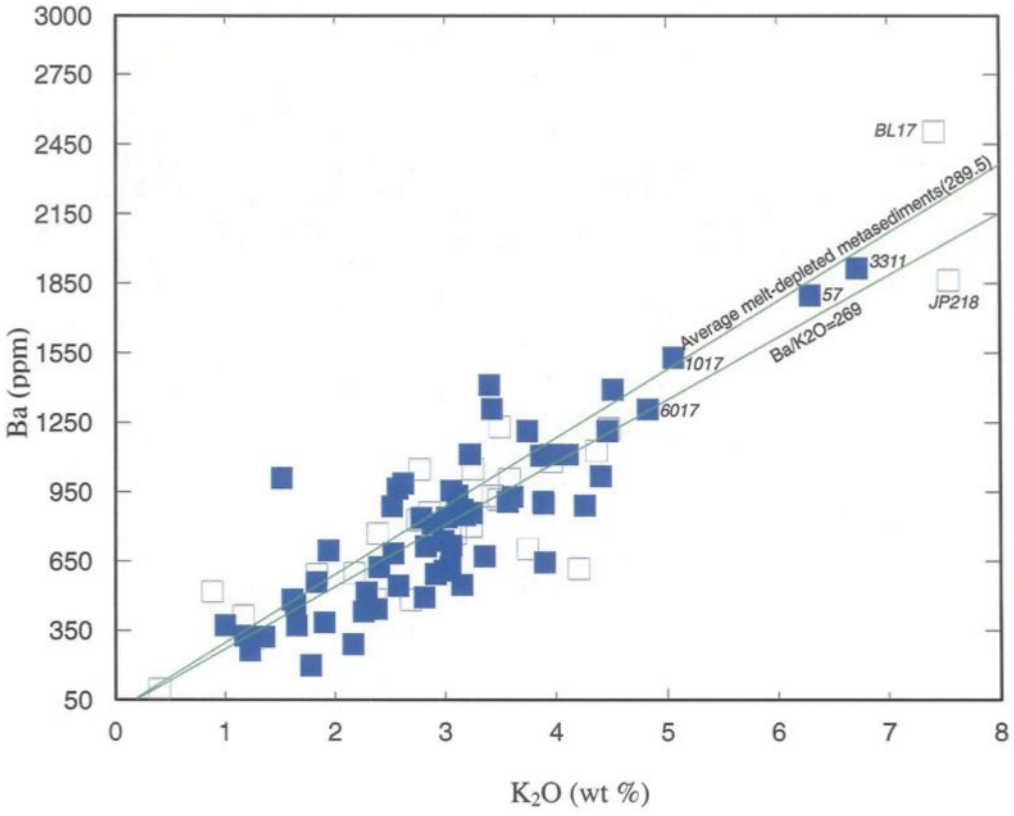

Figure 29: Ba *versus* K_2O variation diagram showing a good positive correlation between the two elements for the diatexite migmatites. The samples with the highest K_2O abundances have the greatest Ba contents and are those with the highest modal K-feldspar. Symbols are as on Fig. 21.

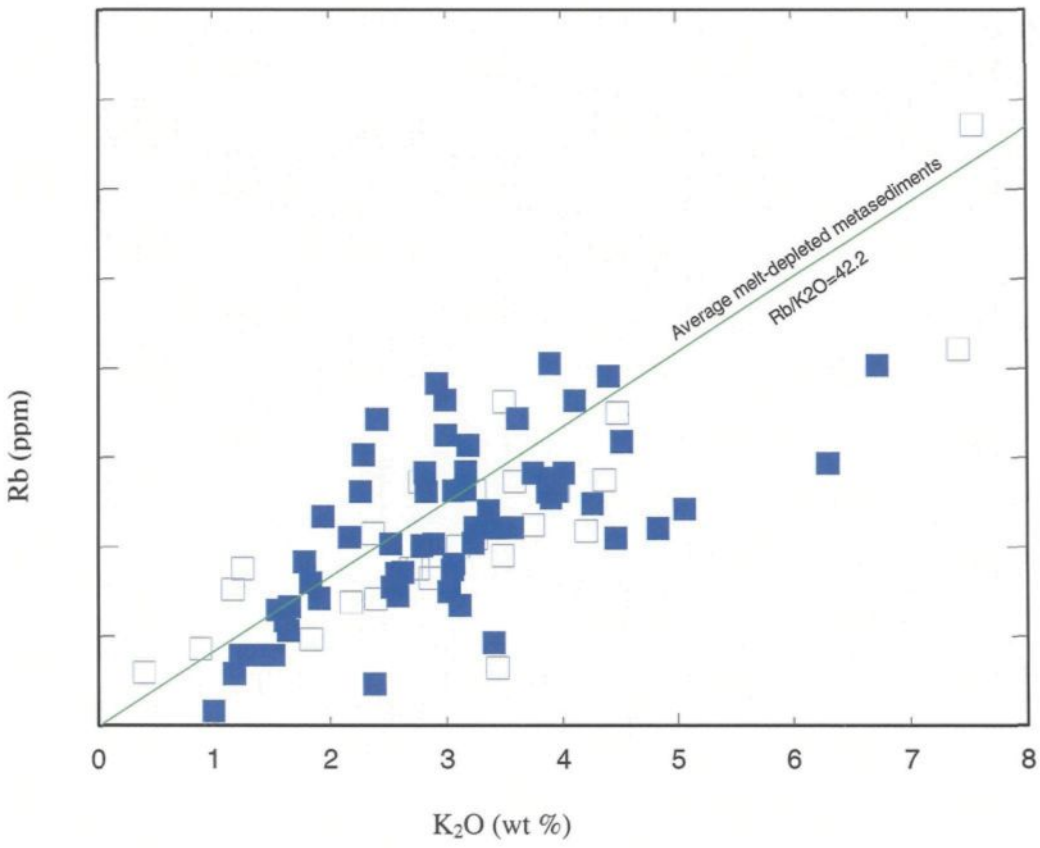

Figure 30: Rb *versus* K_2O variation diagram showing that the Rb content increases proportionally with K_2O, and that the Rb concentration is higher in the diatexite samples that have the highest modal K-feldspar. Symbols are as on Fig. 21.

complementary, fractionated melt which was enriched in elements such as Cs and U. Since the melt-depleted residuum left after the extraction of melt is depleted in U and Cs relative to the potential protolith, both trace elements were concentrated in the anatectic melt that was removed from the residuum; the second alternative seems the most likely explanation.

4.5.3.3 The rare earth elements

In order to better show the behaviour of the rare earth elements (REE) in the diatexite migmatites, the samples have been divided into three groups; those with a low SiO_2 (56-68 wt%), with intermediate SiO_2 (68-73 wt%), and with high SiO_2 (>73 wt%) on figures 31. This division corresponds approximately to the divisions of plagioclase-dominated, plagioclase + K-feldspar and K-feldspar-dominated diatexites respectively. All the diatexite migmatites have whole rock REE patterns that are LREE enriched relative to chondritic values, and are typical of upper crustal rocks derived from metasedimentary protoliths (e.g. Taylor & McLennan 1985). Relative to the plagioclase-dominated and K-feldspar-dominated, the plagioclase + K-feldspar diatexite migmatites have higher total REE abundances (Figs. 31a, b & c), and this is consistent with the trends shown on the La *vs* SiO_2 plot (Fig. 27b) which shows enrichment of LREE at intermediate silica contents.

The plagioclase-dominated diatexite migmatites (Fig. 31a) have LREE enriched patterns with an average La/Yb_N ratio of 24.15, (1 sigma = 12.88, n = 5). The europium

anomalies for these samples are generally very small, and some samples display small negative Eu anomalies (average Eu/Eu* 0.88, 1 sigma = 0.20, n = 5; see appendix XIII).

The plagioclase + K-feldspar diatexite migmatites (Fig. 31b) are also enriched in LREE, but they have steeper patterns with an average La/Yb_N ratios of 42.38 (1 sigma = 25.64, n = 10). The samples with the highest REE abundances display small negative Eu anomalies, whereas, those with the lowest REE abundances have positive Eu anomalies; this combination of these patterns is evidence for the effect of fractional crystallization of feldspar within this group of migmatites (e.g. Sawyer 1987, 1998). The range of Eu/Eu* in these rocks is between 0.28 and 2.30.

The K-feldspar-dominated diatexite migmatites (Fig. 31c) have lower levels of HREE enrichment than the other two groups, but also have patterns that show an overall enrichment of the LREE. Most samples have slopes similar to the plagioclase-dominated diatexites, but one sample raises the group average La/Yb_N ratio to 37.93 (1 sigma = 21.87, n = 4). Three of the samples show positive Eu anomalies (average Eu/Eu* 2.34, 1 sigma = 1.04, n = 4) that is consistent with an enrichment in feldspar (the principal Eu-bearing mineral) for three of them (see appendix XIII). Samples 1118 and 57* have high SiO_2 and high K_2O, and are enriched in K-feldspar, whereas sample 5074* is an example of high-SiO_2 diatexite migmatite with low K_2O contents and a positive Eu anomaly, consistent with enrichment of plagioclase. The fourth sample (1017, 74 wt% SiO_2; 5.06 wt % K_2O) shows a smooth REE pattern with a weak negative Eu anomaly, and it is interpreted as the crystallization product of a fractionated anatectic melt.

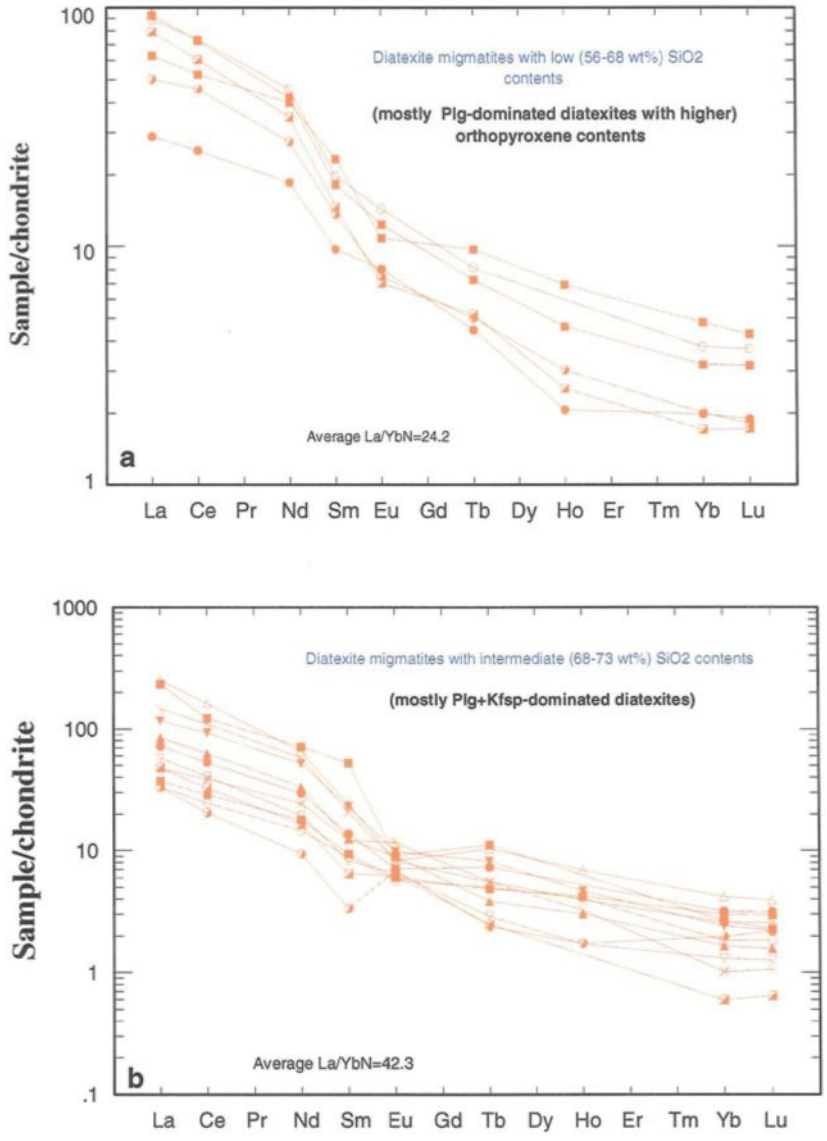
Diatexite migmatites with low (56-68 wt%) SiO2 contents
(mostly Plg-dominated diatexites with higher) orthopyroxene contents
Average La/YbN=24.2
a
Sample/chondrite
100
10
1
La Ce Pr Nd Sm Eu Gd Tb Dy Ho Er Tm Yb Lu
Diatexite migmatites with intermediate (68-73 wt%) SiO2 contents
(mostly Plg+Kfsp-dominated diatexites)
Average La/YbN=42.3
b
Sample/chondrite
1000
100
10
1
.1
La Ce Pr Nd Sm Eu Gd Tb Dy Ho Er Tm Yb Lu

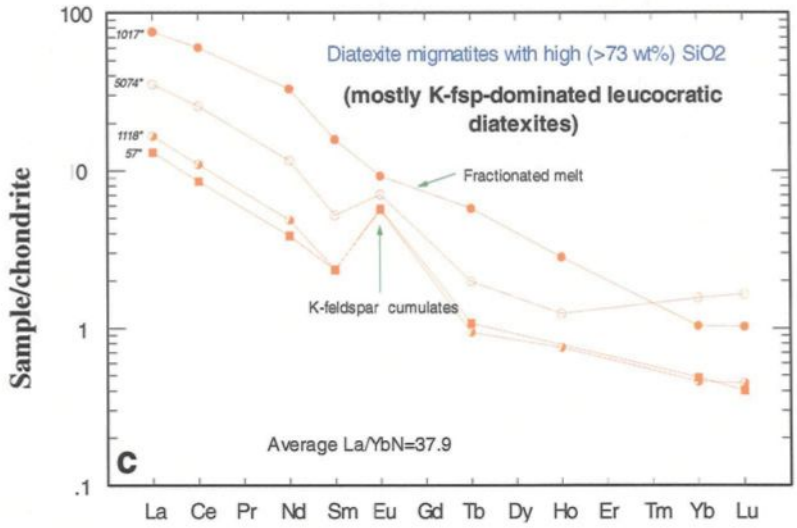

Figure 31: Rare earth element diagrams normalized to the chondrite values of Taylor and Mclennan (1985). a) Diatexite migmatites with low (56-68 wt %) SiO_2 contents, b) diatexite migmatite with intermediate (68-73 wt %) SiO_2 contents and c) diatexite migmatite with high (> 73 wt %) SiO_2 contents. The light rare earth element contents in a) and c) are similar, whereas in b) they are slightly higher. The range of heavy rare earth elements is greater in a) and c), compared to in b). Negative Eu anomalies are developed in samples with the highest LREE, and positive Eu anomalies in samples with the lowest LREE contents.

4.6 CONCLUSIONS

The transition from metatexite to diatexite migmatite and the essentially magmatic processes that occur in the diatexites are well illustrated in the Ashuanipi subprovince. The metasedimentary protolith has partially melted throughout, although a large volume of anatectic melt was generated and extracted, leucosomes are not particularly common. However, in some regions, this melt-depleted migmatite has been intruded by numerous veins or sheets of the anatectic leucogranite, so that, in extreme cases, the resulting migmatite has a layered, or stromatic, appearance. Elsewhere the sheets of anatectic granite are much thicker. The margins of the granitic veins contain screens of residual wall rock that exhibit various stages of transformation to schlieren and schollen diatexite migmatite. The transition from metatextite to diatexite migmatite can arise through several different factors such as; 1) the injection of melt magma from elsewhere to increase melt content (e.g. Greenfield *et al.* 1996), 2) a simple increase in the fraction of melt as temperature increases, and 3) by the local redistribution of anatectic melt. The anatectic melt extracted from the metasediments migrated into large, low pressure (dilatant) structural sites, such as parallel or subparallel to the foliation or bedding, or in fold hinges (Stevenson 1986; Collins & Sawyer 1996; Allibone & Norris 1992); the melt become contaminated with some of residual material it passed through. These bodies of contaminated anatectic melt form diatexite migmatites. Plagioclase-rich diatexite is a contaminated cumulate rock composed principally of plagioclase that crystallized from the anatectic melt, whereas the K-feldspar rich diatexite is derived from the putative liquid lost from the plagioclase-rich diatexite, and consequently has much less residual rock material in it. The plagioclase +

K-feldspar diatexite migmatite approximate the contaminated anatectic melt composition. Most of the diatexite magmas in the Ashuanipi subprovince are modified by the effects of fractional crystallization, and very few actually represent primary melt compositions.

CHAPTER V

MONZOGRANITE: THE END PRODUCT OF THE FRACTIONATION OF DIATEXITE MAGMA

5.1 INTRODUCTION

That migmatites are the source for granite was considered to be far from substantiated by some authors (e.g. Ashworth 1985, Olsen 1985, 1991, White & Chappell 1990, Clemens & Mawer 1992) because, in their studies, there appeared to be a discrepancy between the composition of granite and that of the leucosomes in the associated migmatites (see Olsen 1991). However, an intimate genetic connection between migmatites and granites was found by Read (1956), Wickham (1987), Sawyer (1998), Brown & Solar (1999), Castro *et al.* (2000), Vanderhaeghe (2000, 2001), Solar & Brown (2001), Ledru (2001), Milord *et al.* (2001) and Slagstad *et al.* (2005) who demonstrate that the partial melts formed in migmatites were able to segregate and coalesce to form a granitic magma, from which a granite pluton crystallized.

This chapter reports variations in morphology, petrography and geochemistry of a suite of monzogranites from the Ashuanipi subprovince. The Ashuanipi subprovince is a large natural laboratory which shows that "monzogranites" are magmas that originated from diatexite migmatites. Chapter IV showed that the separation of the crystallized fraction from the remaining melt occurred at various stages during the crystallization of the diatexite magma, and generated a suite of diatexite rocks ranging from plagioclase-rich cumulates to fractionated, K_2O-rich melts. This chapter is concerned with the relationship between the diatexite migmatites and the monzogranites. The field and petrological characteristics of the monzogranites are described first, then, the geochemistry of the diatexite migmatites and the monzogranites are described and compared in order to evaluate the hypothesis that the

monzogranites are, indeed, the end product of the fractional crystallization of the diatexite magma. In other words, that the diatexite magma was "parental" to the monzogranites found in the Ashuanipi subprovince. The conclusions confirm recent studies that there is a genetic link between migmatites and granites.

5.2 MORPHOLOGY AND PETROGRAPHY OF THE MONZOGRANITES

Bodies of monzogranite occur at all scales throughout the Ashuanipi subprovince. Figure 32 shows that most samples lie in the compositional field of monzogranite, but a few plot on the granodiorite field, consequently, there is a wide range in plagioclase / K-feldspar ratio. Monzogranite *senso stricto* applies to about 75 % of the samples, the remainder are either granodiorite or syenogranite; nevertheless, the term monzogranite suite is used as a field term to describe the overall characteristics of this suite of leucogranitic rocks.

Monzogranite occurs in two different settings, and rocks from each provide crucial evidence towards the petrogenetic interpretation of this suite of rocks. 1) Monzogranite occurs as small, centimetre to metre-scale patches within many of the types of diatexite migmatite, except the most plagioclase-rich varieties, but the patches are most common in the K-feldspar-rich diatexite migmatites. The patches have diffuse, gradational contacts with the host diatexite migmatite, and this suggests that the patches formed *in situ*. 2) Monzogranite also occurs as larger, metre- to kilometre-scale discordant, intrusive bodies (e.g. veins, stocks and plutons) within both the diatexite migmatites and the melt-depleted metasedimentary rocks. In most cases the

location of the intrusions of monzogranite is structurally controlled, typically by a shear zone, or by a fold hinge.

Irrespective of their location and mode of occurrence, the monzogranites are leucocratic, pink to pale grey rocks that weather to a whitish colour; they are generally massive, or weakly foliated. A magmatic foliation is locally present in the monzogranite, most commonly in the more biotite-rich (*ca.* 10 %) varieties, and is defined by the preferred orientation of biotite, although in some cases tabular feldspar crystals are also aligned. Biotite schlieren are very rare.

Although the composition and microstructures of the monzogranites from the gradational patches and the intrusive bodies have many similarities, there are some important differences that are crucial to the interpretation of the whole rock geochemistry. These will be described next.

5.2.1 Monzogranite in the diffuse patches

Because the contacts of the monzogranite patches are gradational with the host diatexite migmatite, the monzogranite that is sampled is necessarily that which is considerably different from the host diatexite, both in modal proportions and microstructure. The less obvious part of the patch that more closely resembles the diatexite host in terms of modal proportions and microstructures were sampled less. Consequently, the sample set from the monzogranite patches is likely biased towards the extreme varieties, and the transitional rocks are severely under-represented. Given

the likelihood of a bias in the sample suite the gradational patches are, nevertheless, all coarser grained and more leucocratic compared to the host diatexite migmatites. Many examples of the patches are compositionally and microstructurally zoned. The outer parts have a grain size of 5 to 15 mm (compared to 5 to 7 mm for the host diatexite) and a composition that is leucogranite; K-feldspar is slightly more abundant than plagioclase, and there is less than 2 or 3 % biotite, and no orthopyroxene. The crystal framework in these rocks comprises euhedral to subhedral crystals of K-feldspar and sodic plagioclase; the K-feldspar crystals are consistently larger (5 to 15 mm) than the plagioclase (5 to 8 mm). The interstities of the feldspar framework structure are lined with equant, fine-grained, anhedral, sodic plagioclase and K-feldspar and the interior filled with larger, anhedral crystals of quartz. Myrmekite is commonly developed between the large subhedral K-feldspar crystals and the matrix plagioclase. The K-feldspar is a microcline microperthite in which the plagioclase exsolution form fine strings and stringlets. Biotite occurs as bladed grains located along the edges of the framework feldspars, and is commonly altered to chlorite.

The patches are progressively coarser-grained (up to 50 mm) and have different modal proportions and microstructures in the centres of the patches. The mineral assemblage becomes dominated by K-feldspar (> 40 %) and quartz (25 to 30 %) with a significant decrease in the plagioclase content to about 20 %, and biotite to less than 3%; there is no orthopyroxene. Consequently, the bulk composition changes from leucogranodiorite or leucomonzogranite to leucosyenogranite. A characteristic microstructure of the central parts of the patches is a graphic (symplectite) intergrowth of quartz in the K-feldspar. Quartz forms stringers or blebs up to 50 mm long and 1 to 5

mm wide in large (up to 50 mm) subhedral crystals of microcline perthite that contain 20 to 25 % exsolved sodic plagioclase in wide sinuous ribbons. Plagioclase occurs as euhedral to anhedral crystals that are up to 6 mm across, and these have scattered K-feldspar exsolutions (i.e. they are antiperthite), and smaller (0.5 mm) groundmass grains. Myrmekite is developed in the small groundmass plagioclase crystals where they are close to the large K-feldspar crystals.

5.2.2 Intrusive monzogranite bodies

Because the contacts are sharp, there is no doubt where the intrusive bodies of monzogranite begin, and sampling is easier. Therefore, more petrological variety is represented in the sample set from the intrusive bodies. Many intrusive monzogranite bodies contain rocks with up to 15 % mafic minerals; in most cases this is predominately biotite with a subordinate amount (typically < 5 %) of orthopyroxene, but some samples contain as much as 13 modal % orthopyroxene (see appendix X). Orthopyroxene occurs as 5 mm euhedral to subhedral crystals that are part of the crystal framework composed of slightly larger (4 to 8 mm) subidioblastic crystals of plagioclase and K-feldspar. The biotite-rich parts are typically medium to coarse-grained (3 to 8 mm) and range in composition from granodioritic (40 % plagioclase, 25 % quartz and 20 to 25 % K-feldspar) to monzogranitic in composition. K-feldspar is a microcline microperthite that contains scattered stringlets of sodic plagioclase. The interstitial space of the crystal framework is filled with finer-grained (0.5mm) K-feldspar and plagioclase however, the interstitial anhedral quartz crystals are much larger (5 mm). Some of these monzogranite rocks resemble the plagioclase + K-

feldspar diatexite migmatites in composition and in appearance at outcrop. However, they have very different microstructures; the K-feldspar present in the monzogranite suite rocks forms part of the crystal framework, it does not occur solely as an interstitial phase, and the magmatic foliation due to the orientation of tabular minerals is much weaker than in the diatexite migmatites.

There is a progressive decrease in the modal proportion of biotite, orthopyroxene and plagioclase as the K-feldspar content increases in the other rocks found in the intrusive bodies. The majority of rocks are leucomonzogranites; typically containing 40 to 45 % K-feldspar, 25 to 30 % quartz, 20 to 30 % plagioclase and > 2 % biotite, however, a few are leucosyenogranites. As the modal proportion of plagioclase decreases the K-feldspar crystals tend to become systematically larger and increasingly perthitic, only rarely does the grain size reach that found in the monzogranite patches hosted by the diatexite migmatites, although the graphic intergrowth of quartz in K-feldspar occurs in most of the leucocratic, K-feldspar-rich rocks.

5.2.3 Other petrographic features of the monzogranite suite

Of the 21 thin sections examined from the monzogranite suite, only five rocks contain orthopyroxene. The highest modal proportion (13 %) occurred in a granodiorite with a plagioclase / K-feldspar ratio of 1.73, and the others (5 % and three with < 1%) are leucomonzogranites with plagioclase / K-feldspar ratio of between 1.3 and 1. None of the biotite shows microstructural evidence similar to that shown in figure 17j that indicate it has replaced orthopyroxene. However, all the monzogranite samples for

which whole rock geochemical data are available, contain orthopyroxene in the calculated norm (see appendix XI). The normative abundance of orthopyroxene is small; it varies from a high of 15 % in sample 1011 (which has 42 normative % plagioclase) to 1 % in sample 2180 which contains 35 normative % K-feldspar (Figs. 32, 33 & 34). The discrepancy between the modal and normative orthopyroxenes is small, and could be interpreted as evidence that orthopyroxene was present but has been largely replaced.

The majority of samples from the monzogranite suite are coarse grained leucocratic rocks and have a noticeable scarcity of the accessory minerals, zircon, monazite, titanite and apatite. The few accessory minerals that are present occur as very small grains located along the borders of the large feldspar grains, that is, in the matrix. However, a few samples are different, they contain crystals of zircon, monazite and titanite (but not apatite) that are conspicuously larger, by a factor of 5 or more, which results in a significantly higher modal abundance of these minerals.

5.3 THE GEOCHEMISTRY OF THE MONZOGRANITE SUITE AND ITS RELATIONSHIP TO THE DIATEXITE MIGMATITES

The major and selected trace element contents of some 18 intrusive monzogranites from the Ashuanipi subprovince are given in table 6. The suite of monzogranites can be divided in two groups; 1) a high silica (69 wt % to 76 wt % SiO_2), high potassium (3.73 wt % to 6.56 wt % K_2O) group (HSHP) which have monzogranite

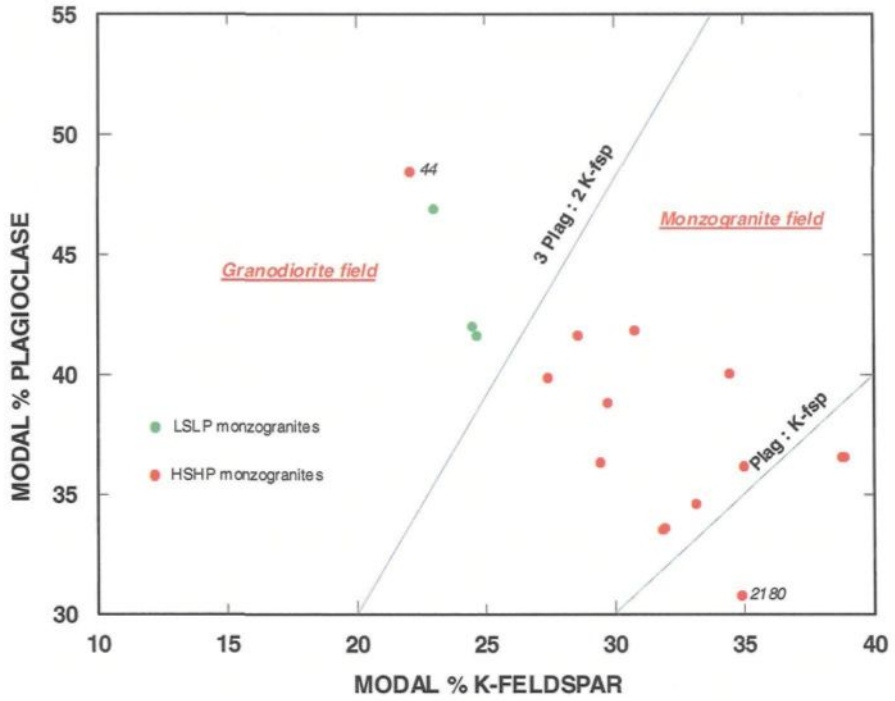

Figure 32: Normative % plagioclase *versus* normative % K-feldspar in the monzogranites showing a negative correlation between the plagioclase and K-feldspar contents. The low silica, low potassium (LSLP) samples plot in the granodiorite field, whereas the high silica, high potassium (HSHP) samples plot in the monzogranite field. The green circles are the LSLP granites and the red circles are the HSHP granites.

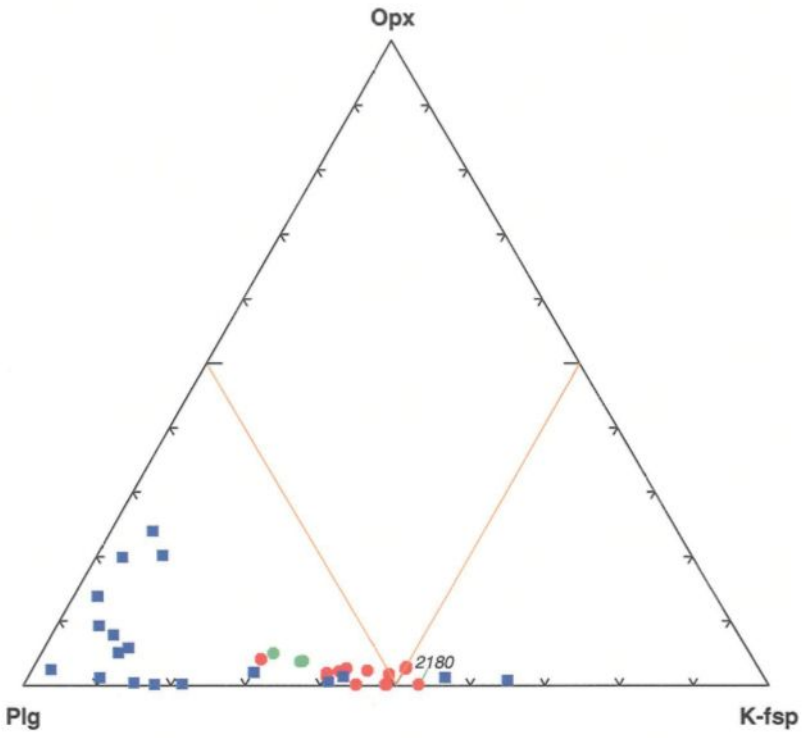

Figure 33: Ternary plot showing the variation in normative plagioclase, orthopyroxene, and K-feldspar for the monzogranites and diatexite migmatites (blue squares) from the Ashuanipi subprovince. The green circles are the LSLP granites which contain more orthopyroxene compared to HSHP granites represented by the red circles. Plg = plagioclase, K-fsp = K-feldspar and Opx = orthopyroxene

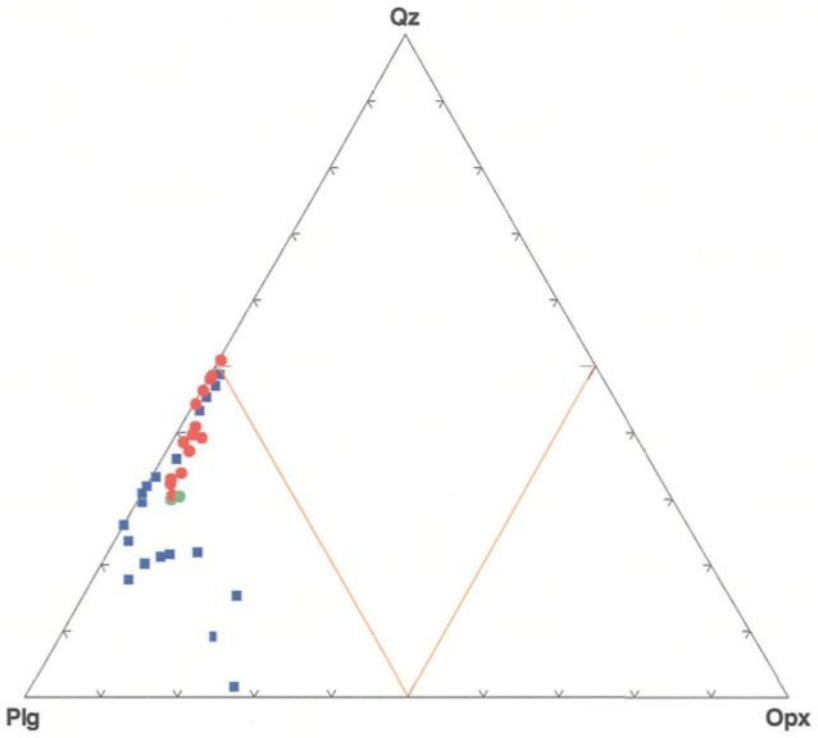

Figure 34: Ternary plot showing the variation in normative plagioclase, quartz, and orthopyroxene for the monzogranite suite and the diatexite migmatites from the Ashuanipi subprovince. Normative quartz is higher in the HSHP granites relative to the LSLP granites. Plg = plagioclase, Opx = orthopyroxene and Qz = quartz. Symbols are as on figure 22.

Table 6: Whole rock major and trace element compositions of 18 monzogranite rocks from the Ashuanipi subprovince

Sample	2066A	2074A	2176A	2180A	44	6016A	5096A	3014*	1009*	1023	1049*	1115	1117*	1025*	2009*	1011*	33*	1114
SiO2	76,34	74,58	74,69	75,27	69,57	71,34	71,98	69,62	69,09	69,23	72,99	71,42	69,50	72,71	68,25	63,42	68,73	66,58
TiO2	0,02	0,06	0,14	0,08	0,42	0,20	0,24	0,30	0,79	0,32	0,17	0,54	0,13	0,22	0,41	1,04	0,28	0,87
Al2O3	13,58	14,53	14,11	13,97	15,11	15,70	14,60	15,97	14,18	15,95	14,72	14,20	16,22	14,60	16,00	14,69	15,19	14,92
Fe2O3	0,22	0,92	0,98	0,63	3,18	1,30	1,70	2,44	4,08	2,34	1,25	3,07	1,56	1,78	2,92	7,54	3,34	5,63
FeO	0,00	0,00	0,00	0,00	0,00	0,00	0,00	0,00	0,00	0,00	0,00	0,00	0,00	0,00	0,00	0,00	0,00	0,00
MnO	0,01	0,03	0,03	0,01	0,03	0,01	0,01	0,01	0,05	0,02	0,01	0,03	0,02	0,01	0,03	0,11	0,04	0,08
MgO	0,05	0,12	0,33	0,17	1,22	0,55	0,92	0,69	0,84	0,73	0,42	0,06	0,83	0,54	1,06	1,48	1,57	0,57
CaO	0,45	1,00	0,69	0,67	2,05	1,39	1,10	1,39	1,88	1,47	1,27	1,50	1,50	1,47	2,12	3,57	2,52	3,41
Na2O	3,94	3,75	3,60	3,27	4,59	3,52	3,70	4,23	3,77	3,98	4,24	3,36	3,54	3,93	4,81	3,57	4,27	3,68
K2O	5,38	4,98	5,39	5,90	3,73	5,92	5,73	5,20	5,02	5,82	4,83	5,60	6,56	4,63	4,17	4,14	3,89	3,90
P2O5	0,01	0,03	0,04	0,03	0,09	0,08	0,03	0,14	0,28	0,14	0,09	0,20	0,15	0,10	0,24	0,44	0,17	0,35
LOI	0,43	0,50	0,77	0,38	0,43	0,65	0,62	0,89	0,46	0,54	0,04	0,36	0,45	0,30	0,40	0,78	0,62	0,16
Total	100,43	100,50	100,77	100,38	100,43	100,65	100,62	100,89	100,46	100,54	100,04	100,36	100,45	100,30	100,40	100,78	100,62	100,16
MgN	31,04	20,71	40,25	34,83	43,08	45,78	51,73	35,85	28,97	38,07	40,15	33,93	51,16	37.66	41,93	27,99	48,20	16,73
Cr	n.a	n.a	n.a	n.a	38	20	20	24	17	25	18	12	25	15,21	25	24	46	7
Ni	8	4	9	6	n.a	n.a	n.a	n.a	n.a	n.a	n.a	n.a	n.a	n.a	n.a	n.a	n.a	n.a
Co	3,0	3,0	3,0	3,0	7,0	5,0	5,0	4,4	3,0	5,0	2,8	3,9	6,0	3,0	6,6	10,0	7,9	5,3
Sc	n.a.	n.a.	n.a.	n.a.	5,0	2,5	5,1	1,8	8,9	2,0	0,6	3,4	3,6	1,0	3,7	16,2	4,5	11,6
Pb	25	51	21	29	n.a.	n.a.	n.a.	n.a.	n.a.	n.a.	n.a.	n.a.	n.a.	n.a.	n.a.	n.a.	n.a.	n.a.
Zn	12	12	22	10	n.a.	n.a.	n.a.	n.a.	n.a.	n.a.	n.a.	n.a.	n.a.	n.a.	n.a.	n.a.	n.a.	n.a.
Rb	101	161	161	191	105	137	140	133	214	127	129	276	151	117,82	179	179	104	124
Cs	n.a	n.a	n.a	n.a	1,44	0,70	0,50	0,47	1,24	1,24	0,47	0,47	0,55	0,84	5,14	3,32	1,13	1,11
Ba	111	256	680	547	781	1610	810	1415	1722	1514	776	1108	2115	1107,75	1215	1114	1006	1602
Sr	37	95	121	151	516	477	247	773	369	603	446	254	700	464,25	771	343	609	481
Ga	11	12	11	8	18	0	0	18	21	17	17	20	15	16,11	21	23	17	23
Ta	dl	dl	0,20	dl	0,24	dl	0,60	0,02	1,32	0,07	0,06	0,99	0,12	0,07	1,21	1,34	0,15	0,75
Nb	9,1	10,1	13,1	11,1	2,0	5,0	0,0	2,0	27,4	2,0	2,0	18,1	2,0	2,01	12,2	19,3	2,0	11,0
Hf	1,41	3,33	3,02	2,71	4,70	6,34	0,00	8,42	16,14	3,67	3,35	10,99	8,42	3,12	4,19	16,83	2,98	9,72
Zr	32	81	96	76	159	203	314	293	519	139	102	373	257	105,74	150	505	111	312
Y	dl	22,20	dl	dl	8,11	4,02	13,00	4,04	42,55	3,03	3,02	30,22	6,04	3,02	18,23	66,87	7,04	39,05
Th	1,61	22,20	10,08	36,18	4,70	32,20	49,99	64,55	14,24	16,78	0,97	20,12	25,78	7,62	6,37	16,18	3,29	8,81
U	dl	dl	dl	29,14	0,51	dl	1,70	0,18	1,93	0,51	0,36	1,34	0,54	0,38	1,96	2,06	0,76	1,09
La	7,04	32,29	28,22	39,19	27,34	100,61	76,98	218,16	73,24	92,14	11,53	132,57	113,29	32,64	17,60	135,45	26,67	59,42
Ce	9,05	61,56	51,41	80,39	54,20	0,00	0,00	378,78	183,97	160,98	19,96	248,13	205,61	59,18	42,46	290,64	51,81	132,79
Nd	2,01	22,20	18,14	30,15	21,94	62,38	64,98	115,96	96,44	46,23	6,68	87,66	58,88	20,13	20,52	137,67	21,08	65,15
Sm	0,40	5,35	3,02	6,43	3,33	5,84	11,00	10,08	15,05	4,34	1,07	11,18	5,93	2,28	4,42	20,90	3,07	11,48
Eu	0,10	0,30	0,50	0,50	1,07	1,21	0,80	1,51	3,01	1,27	0,93	1,73	1,46	0,88	1,01	2,90	1,18	3,62
Tb	0,10	0,71	0,30	0,04	0,35	0,20	1,00	0,58	1,45	0,24	0,10	1,00	0,42	0,19	0,53	2,31	0,28	1,48
Yb	0,40	3,73	1,01	0,00	0,64	0,00	0,90	0,48	3,27	0,24	0,17	2,10	0,67	0,26	1,32	5,24	0,64	3,63
Lu	0,050	0,656	0,141	0,000	0,089	0,000	0,000	0,062	0,483	0,038	0,028	0,307	0,094	0,032	0,177	0,759	0,094	0,542

Abbreviations: n.a.= not analyzed, dl = below detection limit, * = samples analyzed at UQAC

(*senso stricto*) compositions and, 2) a low silica (63 to 68 wt % SiO_2), low potassium (3.89 to 4.17 wt % K_2O) group (LSLP), which generally have granodioritic bulk composition (Figs. 35).

The composition of the LSLP group just partially overlaps the composition field of plagioclase-dominated diatexite migmatites; whereas, the compositional field of the HSHP group corresponds quite closely with the field of K-feldspar-rich (i.e. evolved) diatexite migmatites (Fig. 34). The oxides and elements CaO, MgO, TiO_2, Al_2O_3, Sc, Cr, Y, Sr and Eu in the monzogranite suite samples all show negative correlations with SiO_2 , as they do for the diatexite migmatites. However, K_2O, Ba and Rb do not show strong positive correlation with SiO_2, but are nevertheless interpreted to have been incompatible with the crystallized phases. The lowest concentrations of MgO, CaO, FeO_t, TiO_2, Sr and Ba all occur in the HSHP monzogranite samples.

There is a systematic difference in bulk composition between the HSHP samples and the LSLP samples of the monzogranite suite, that is similar to the changes shown in the diatexite migmatites, and is related to the changes in their respective modal mineralogies. The MgO and CaO contents attain their maximum (1.57 wt %, sample 33* and 3.57 wt %, sample 1011* respectively; Figs. 36a & b). The LSLP monzogranite group and the plagioclase-dominated diatexites have higher MgO + FeO_t = (up to 8.28 wt %) and CaO + Na_2O = (7.35 wt %) abundances than the HSHP group (MgO + FeO_t = 2.35 wt % and CaO + Na_2O = 5.09 wt % respectively) and the K-feldspar-dominated diatexites, which are both markedly leucocratic rocks

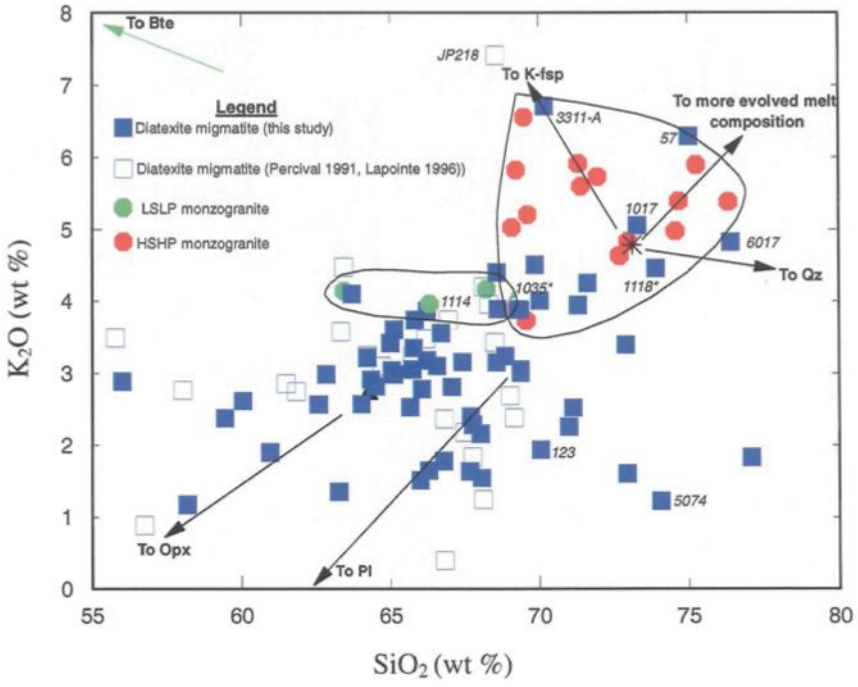

Figure 35: K_2O *versus* SiO_2 variation diagram showing the position of the two types of monzogranites (LSLP and HSHP) relative to the diatexite migmatites. The samples with low silica and low potassium (green) partially overlap the field of plagioclase-rich diatexites, and samples with high silica and high potassium (red) overlap the field of K-feldspar-rich diatexites; diatexite migmatites are shown in blue. The vectors (arrows) for quartz, orthopyroxene, biotite, K-feldspar and evolved melt composition are also shown. Asterisk = the average composition for the experimental melts discussed in Chapters III and IV.

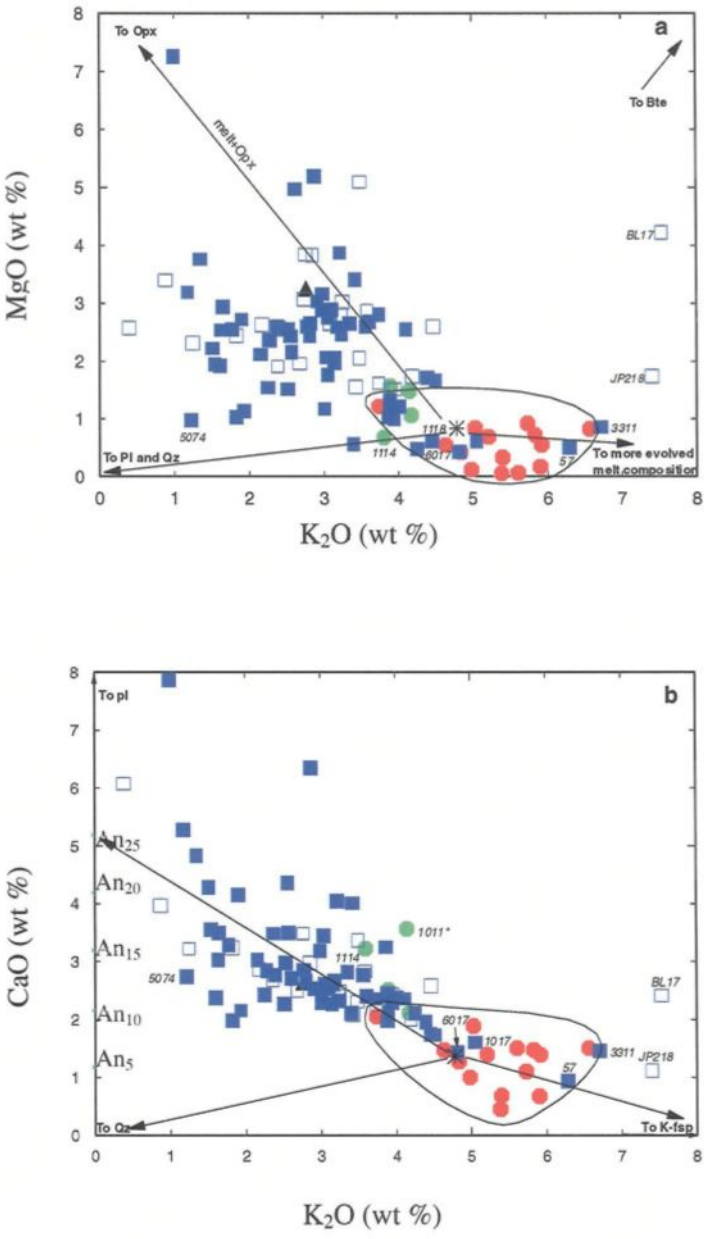

Figure 36: Harker variation diagrams; a) MgO *versus* K_2O, and b) CaO *versus* K_2O showing that the HSHP monzogranites have lower MgO and CaO contents relative to the LSLP monzogranites. Vectors for quartz (Qz), orthopyroxene (opx), plagioclase (plg), K-feldspar (K-fsp) are also shown. Symbols are as in figure 35.

These values indicate higher plagioclase, and orthopyroxene and/or biotite contents in the LSLP samples (Figs. 32, 33 & 34), and in the plagioclase-rich diatexite migmatites this is consistent with the calculated mineral norms.

Both Ba and Rb are enriched in the HSHP monzogranites and the K-feldspar-dominated diatexite migmatites relative to the LSLP samples and the plagioclase-rich diatexites. This is due essentially to the greater abundance of K-feldspar in the HSHP monzogranites and the K-feldspar-rich diatexite migmatites (Figs. 37 & 38). The LSLP samples of the monzogranite suite have the same Ba and K_2O contents as the plagioclase and plagioclase + K-feldspar-dominated diatexite migmatites. However, the HSHP samples show a different behaviour, some HSHP samples follow the trend of the K-feldspar-dominated diatexite migmatites and have, therefore, similar Ba, K_2O contents and Ba / K_2O ratios; however, about half of the samples are depleted in Ba relative to the trend defined by the diatexite migmatites. These rocks may have crystallized from melts that were already depleted in Ba, probably by the prior crystallization of K-feldspar.

Samples from the monzogranite suite overlap the Rb-K_2O compositional field of the diatexite migmatites. However, the distribution of the HSHP samples within their field suggests that most (80 %) of the HSHP samples have Rb / K_2O ratios that are lower than that typical for the diatexite migmatites (Fig. 38). Since the HSHP samples have higher K_2O contents, they have, therefore, generally lower Rb contents than the diatexite migmatites.

Figure 39 shows that the highest Rb / Sr ratios occur in the HSHP monzogranites, but that, overall, the monzogranite suite has a similarly large range of Rb / Sr ratios as the diatexite migmatites, but is displaced to somewhat higher ratios. The diagram also shows an overall higher Rb and lower Sr contents in the monzogranite suite, suggesting that they were derived by the crystallization of a magma that had already crystallized substantial amounts of plagioclase. The HSHP group has the highest Rb content (Fig. 39) whereas the LSLP group and most of the diatexite samples have the highest Sr concentrations. Figures 37, 38 and 39 show that, when compared to the diatexite migmatites, the LSLP monzogranites plot in the plagioclase-rich diatexites field, whereas, the HSHP monzogranites lay beyond the K-feldspar-rich diatexites.

The Rb / Cs ratios change progressively from 55 in the LSLP group to 270 in HSHP group, a range that closely follows the diatexite migmatites (e.g. Fig. 26). The average Th / U ratio is 5.9 in LSLP group, but it increases to 8.39 for the HSHP group (see appendix XIV).

The abundances of trace elements Th, La, Y, Ce and Zr (Figs. 40a, b, c, d & e) within the monzogranite suite reach their maximum in the rocks with SiO_2 contents of about 70 wt % and, thereafter, progressively decrease to higher SiO_2 contents in a manner similar to that displayed by the diatexite migmatites. However, the rocks from the monzogranite suite show a more gradual decline from the peak trace element contents, whereas, the diatexite migmatites which show a much sharper decline in trace element contents above 71 wt % SiO_2. This pattern suggests that these trace elements are controlled by the saturation of the accessory minerals zircon, monazite and / or

allanite in the felsic melt; these accessory minerals have been observed in the monzogranite samples. The average Zr content is higher in the LSLP group (269 ppm) than in the HSHP group (196 ppm), this is because of the low Zr contents of the HSHP samples that have about 75 wt % SiO_2. However, the average Th and La concentrations are higher in the HSHP group (21.9 ppm and 70.4 ppm respectively) than the LSLP group (8.7 ppm and 59.8 ppm respectively). In general, Th, La, Ce and Zr attain slightly higher concentrations in the diatexite migmatites than in the monzogranite samples.

The HSHP group is enriched in the LREE relative to the diatexite migmatites and the LSLP group (Fig. 40b). The REE patterns (Fig. 41) of the monzogranite suite rocks are all LREE enriched, and they display a wide range of La / Yb_N ratios (average 47.8, 1 sigma=5.23, n=14) and their Eu / Eu* values are between 0.19 and 3.27 (see appendix XIV). The samples with the highest LREE contents display marked negative Eu anomalies, whereas, those with the lowest LREE contents display positive Eu anomalies; such a pattern suggests that most samples were also derived from fractionated anatectic melts, but some are accumulations of feldspar, and based on the mineral modes, accumulations of K-feldspar specifically.

In contrast, the LSLP group (Fig. 41b) has slightly lower LREE contents, and flatter REE patterns that have lower La / Yb_N ratios (average 14.3, 1 sigma=8, n=4) compared to the HSHP group. The europium anomaly is negative for two samples (2009 and 1011, Eu / Eu* = 0.82, 0.51 respectively), but weakly positive for the other two samples (33* and 1114; Eu / Eu* = 1.50 and 1.09 respectively) (see appendix XIV).

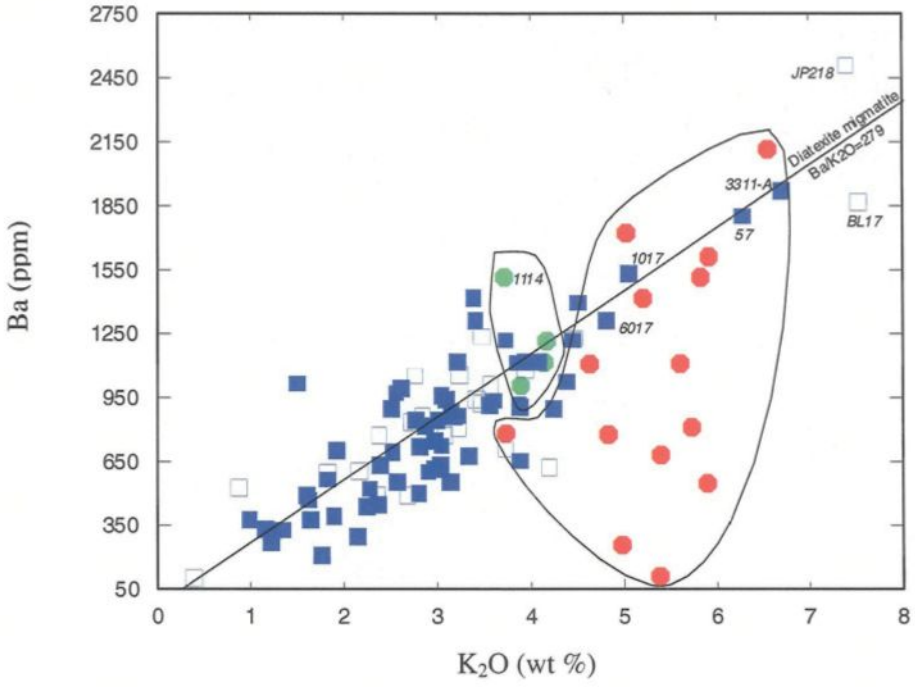

Figure 37: Ba *versus* K_2O variation diagram shows that the LSLP samples of the monzogranite suite have the same Ba and K_2O contents as the diatexite migmatites. However, the HSHP samples show a different behaviour, some samples follow the trend of the diatexite migmatites and, therefore, have similar Ba, K_2O contents and Ba / K_2O ratios, but about half of the samples are depleted in Ba relative to the trend defined by the diatexite migmatites. Symbols are same as figure 35.

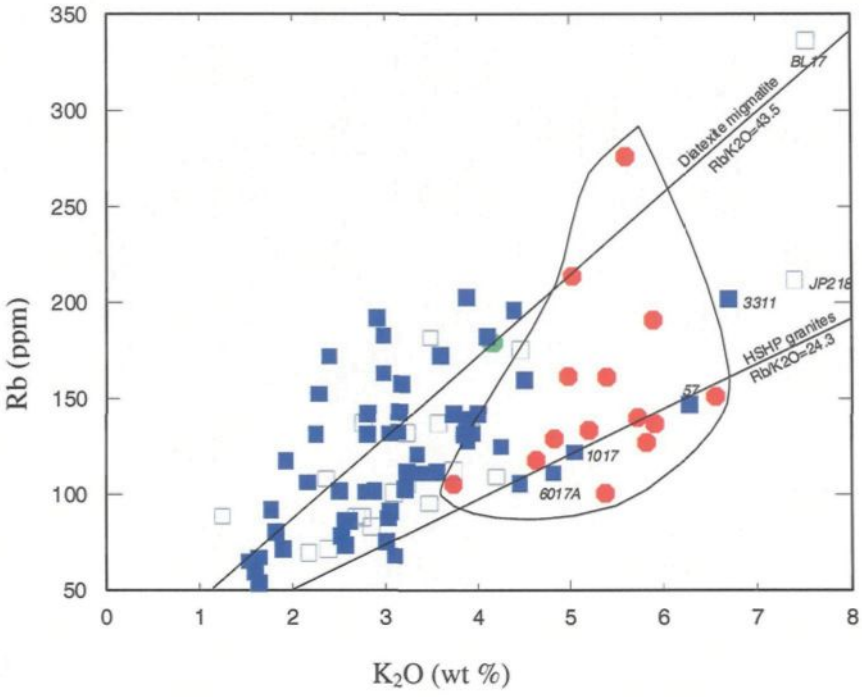

Figure 38: Rb *versus* K_2O variation diagram shows that the monzogranite suite overlaps the compositional field of the diatexite migmatites. However, the distribution of the HSHP samples within their field suggests that most of the HSHP (80 % of samples) have Rb / K_2O ratios that are lower than is typical for the diatexite migmatites. Symbols are same as for figure 35.

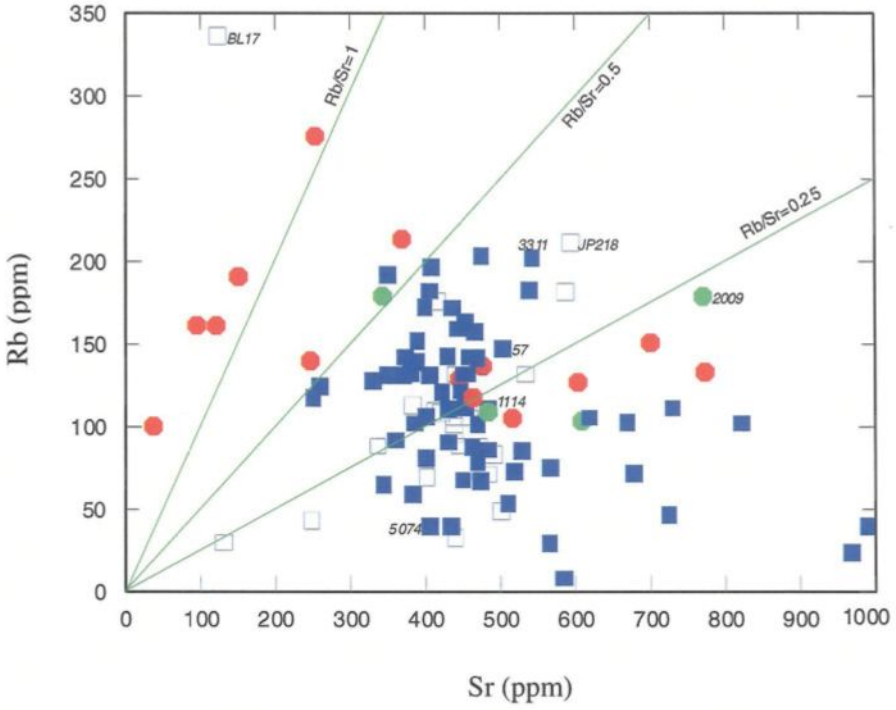

Figure 39: Rb *versus* Sr variation diagram shows that the LSLP and some of the HSHP samples partially overlap the field of the diatexite migmatites. However, some of the HSHP monzogranites are significantly depleted in Sr relative to the diatexite migmatites. The average Rb content of the monzogranite suite samples is greater than the average for the diatexite migmatites. Symbols are same as on figure 35.

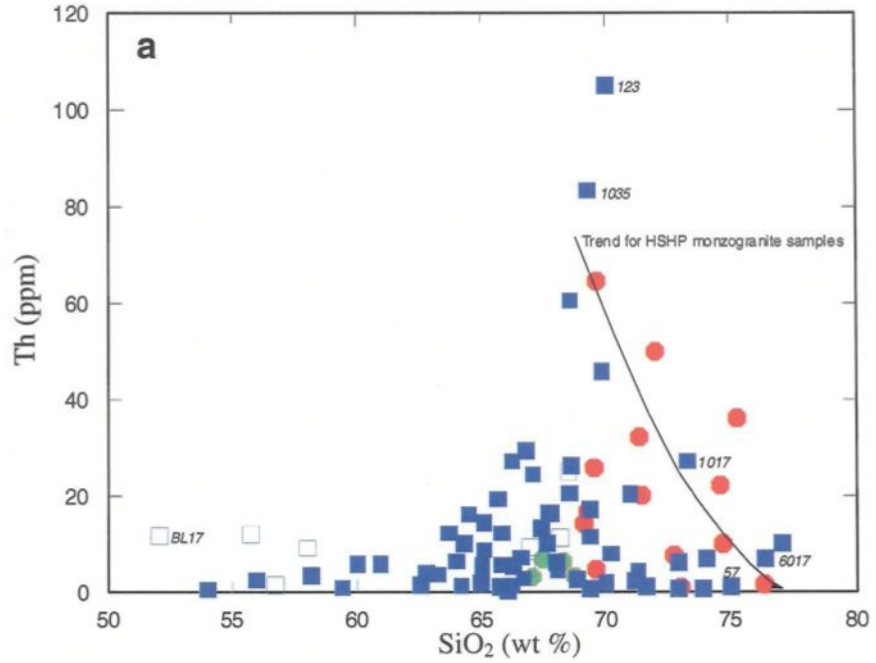
a
123
1035
Trend for HSHP monzogranite samples
1017
BL17
57
6017
Th (ppm)
SiO2 (wt %)
0
20
40
60
80
100
120
50
55
60
65
70
75
80

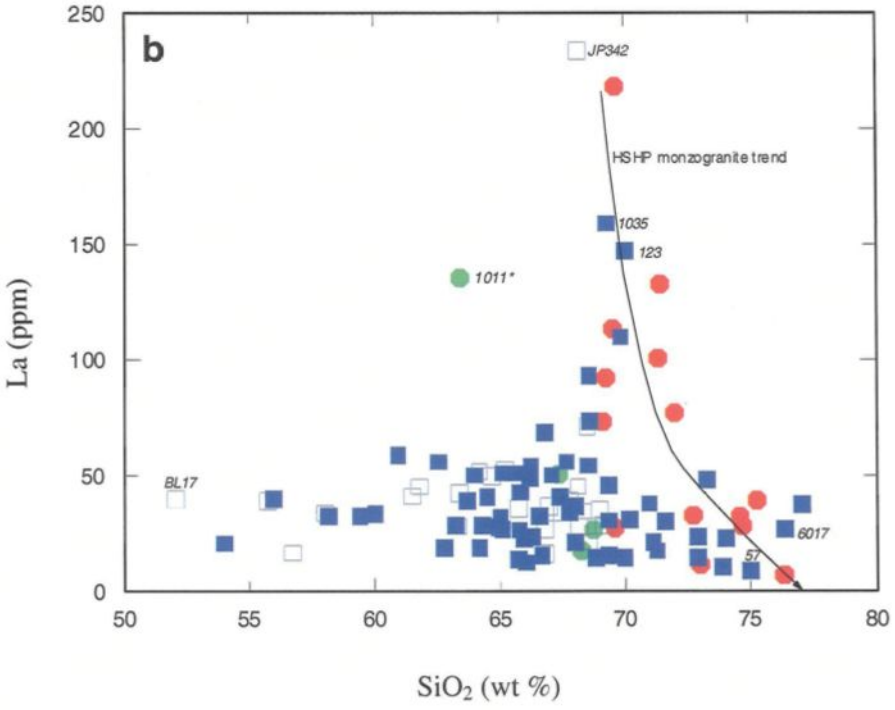
b
JP342
HSHP monzogranite trend
1035
123
1011*
BL17
6017
57
La (ppm)
SiO2 (wt %)
0
50
100
150
200
250
50
55
60
65
70
75
80

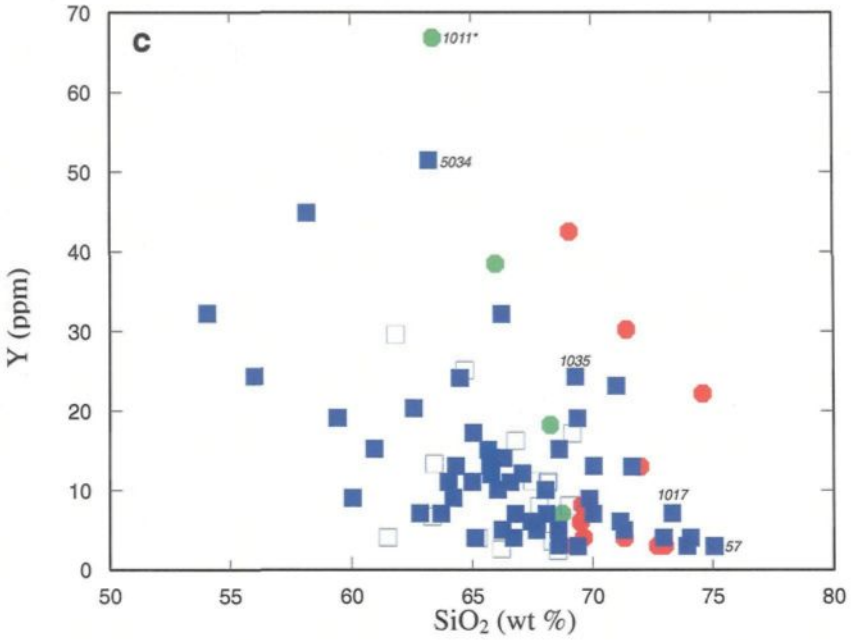
c
1011*
5034
1035
1017
57
Y (ppm)
SiO2 (wt %)
0
10
20
30
40
50
60
70
50
55
60
65
70
75
80

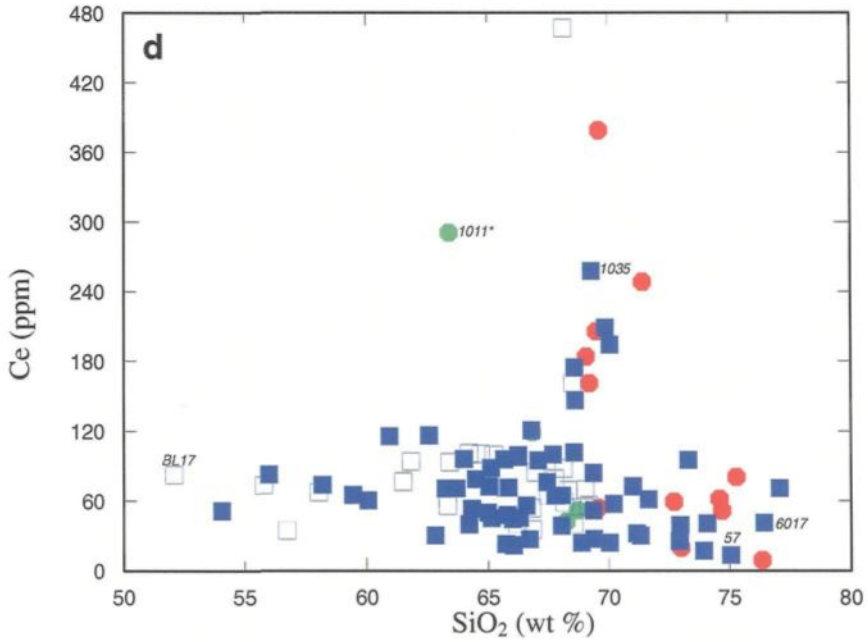
d
1011*
1035
BL17
6017
57
Ce (ppm)
SiO2 (wt %)
0
60
120
180
240
300
360
420
480
50
55
60
65
70
75
80

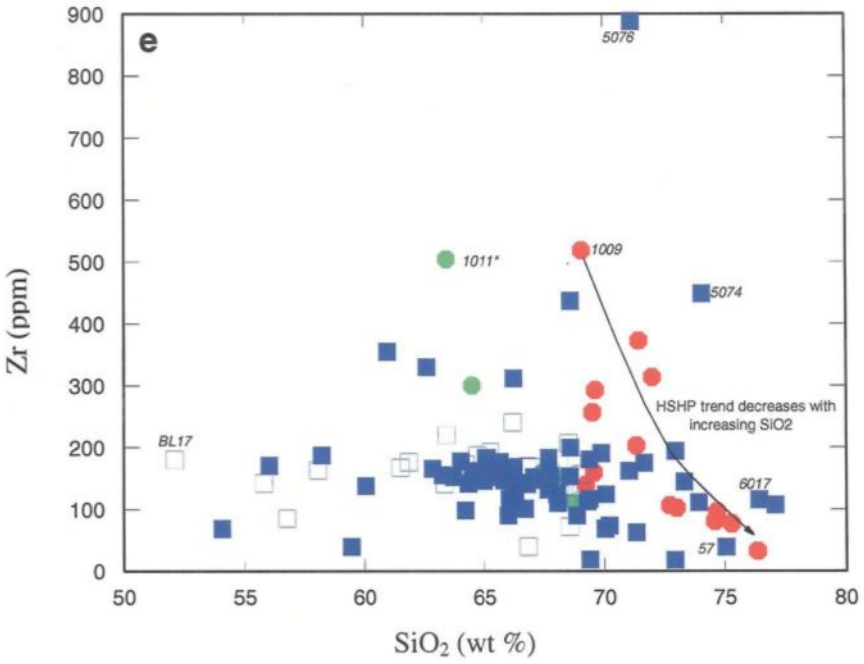

Figure 40: Trace element bivariant plots for the Ashuanipi monzogranites. a) Th *versus* SiO_2, b) La *versus* SiO_2, c) Y *versus* SiO_2, d) Ce *versus* SiO_2, and e) Zr *versus* SiO_2. Th, La, Y, Ce and Zr all decrease from maximum values at 69-70 wt % SiO_2, a pattern which suggests that the concentration of these trace elements are controlled by the saturation of accessory minerals in the felsic melt. Symbols are the same as on figure 35.

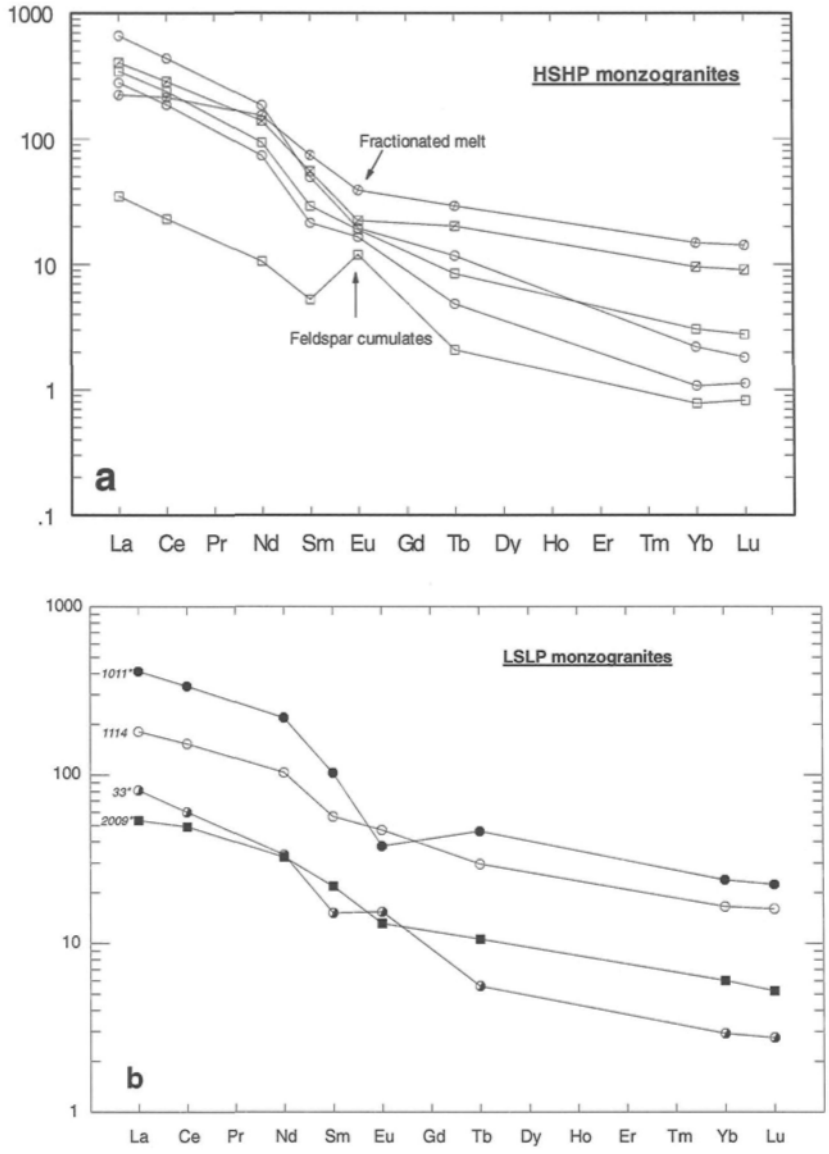

Figure 41: Rare earth element variation diagrams normalised to the chondritic values of Taylor & McLennan (1985). Both the HSHP and LSLP groups are enriched in the light rare earth elements (LREE) relative to the heavy rare earth elements (HREE), and show positive europium anomalies for the samples with the lowest total REE contents and negative anomalies for those with the highest total REE contents.

The sample with the highest total REE content has a negative europium anomaly and the sample with the lowest total REE content has a positive anomaly. Such a relationship also suggests that some samples were derived from fractionated anatectic melts that had already crystalized feldspar.

As the SiO_2 and K_2O contents and the Rb / Sr ratios (from 0.22 in LSLP samples to 0.41 in HSHP samples) of monzogranite samples increase, the total REE contents, and the La / Yb_N ratios (14 in LSLP samples and 47 in HSHP samples) also tend to increase (see appendix XIV). Such behaviour is similar to that shown by the diatexite migmatites.

5.4 THE CONTRIBUTION OF ACCESSORY PHASES TO THE COMPOSITION OF DIATEXITE MIGMATITES AND THE MONZOGRANITES

Accessory minerals are thought to exert a strong control on the composition of granitic rocks (e.g. Sawka 1988; Miller *et al.* 1982; Miller *et al.* 1992); first at partial melting, and then during crystallization, especially at in its later stages. Accessory minerals in high grade metamorphic rocks commonly occur as inclusions in the major phases, for example biotite (e.g. Bea 1996), and this can control how the accessory phases participate in the process of partial melting. The metamorphic reactions that result in partial melting have an important effect on how much of the REE and high field strength elements (HFSE), such as Hf, Th and Zr, enter the melt. If the accessory

phases held as inclusions in a reactant phase are able to come into contact with the anatectic melt as their host dissolves, then the melt can, potentially, become saturated in the trace elements contained in the accessory minerals as they dissolve into the melt. Once saturated in the dissolving phase the melt may then contain the available, undissolved accessory minerals as xenocrysts. However, if the accessory phases in the hosting reactant phases are not able to come into contact with the melt because the host does not dissolve sufficiently to release them, then they remain as inclusions in the residuum, and the melt has, correspondingly, a low content of the trace elements that are hosted in the accessory phases (Rapp & Watson 1986; Sevigny 1993; Watt & Harley 1993; Nabelek & Glascock 1995). Of course, the particular accessory phases included in the reactant phase, say in biotite, will control what the effect of the addition, or subtraction, of residual biotite from the melt has on the trace element bulk composition of migmatites (Milord *et al.* 2001).

During crystallization the magma may become saturated in zircon, monazite and the other accessory phases, which will then start to crystallize in exactly the same manner as the major phases. As the accessory phases crystallize, the magma always remains saturated in the accessory phase, although the concentration of the accessory phase required to maintain saturation drops rapidly as temperature decreases (e.g. Watson & Harrison 1983; Harrison & Watson 1983, 1984). Fractional crystallization of the accessory phases can also occur and, hence, some samples can contain accumulations of the crystallized accessory phases; this results in those samples having high concentrations of the REE and the appropriate HFSE (e.g. Th, Hf, and Zr). If accumulation processes occurred, then it is possible that some samples will contain

accumulations of any xenocrystic accessory phases that have remained in the melt since partial melting. These samples too, may contain high concentrations of the REE and the appropriate HFSE.

5.5 FORMATION OF THE DIATEXITE MIGMATITES AND MONZOGRANITE SUITE

5.5.1 Modelling the major element compositions

Some compositional variation in the anatectic melts produced from the Ashuanipi metagreywackes is to be expected, and may have resulted from; 1) compositional differences between the individual beds undergoing partial melting, 2) differences in the temperature at which the partial melts formed (partial melting may have occurred over an interval of 100 degrees Celsius or more, from the "*opx in*" isograd to the "*biotite out*" isograd, 3) differences in the degree of partial melting, 4) variable degrees of separation of the melt from the residual solids and, 5) crystal fractionation as the anatectic melt begins to crystallize.

The diatexite and monzogranite samples lie between the plagioclase and/or quartz and orthopyroxene, and the orthopyroxene and / or quartz and plagioclase vectors respectively (see figures 42a & b). Very few samples lie in the direction of the biotite vector, and this indicates that biotite is either absent, or not a major constituent in most of the diatexites and monzogranites. One trend in the data can be modelled by adding residuum to the composition of the average experimental melt (appendix XII); the

residuum composition is based on sample 5104 (appendix VIII) and is 0.55 plagioclase + 0.16 orthopyroxene + 0.17 quartz + 0.12 biotite (mineral compositions given in appendix XVI); the mixture of melt and residuum is shown as trend 1 on figures 42a & b. The other trends shown were obtained by adding residual plagioclase An_{31} (trend 2), residual orthopyroxene (trend 3) to the average experimental melt composition (asterisk).

On the plot MgO *versus* K_2O (Fig. 42a), trends 1 and 3 can be used to investigate the origin of samples that are enriched in MgO as the result of contamination of the melt by residuum, or by residual orthopyroxene. The mineral vectors show that few of the diatexites can be modelled as anatectic melt contaminated by a single residual phase alone, be it plagioclase, biotite, quartz or orthopyroxene. The majority of samples are best explained by wholesale contamination of the anatectic melt with the plagioclase + biotite + orthopyroxene + quartz, as in the residual metasediments. A few samples of diatexite migmatite (open squares) could be considered as anatectic melt contaminated with up to 30 vol % orthopyroxene. This also means that if the orthopyroxene had crystallized from the melt, then few, if any, of the diatexite migmatites are accumulations of only crystallized orthopyroxene. Most of the diatexites might be modelled as an anatectic melt contaminated by its residuum (trend 1). In that case most samples would contain between 30 and 55 vol % residuum, and this amounts to 8 to 10 vol % residual orthopyroxene. However, petrographic observations suggest that little of the orthopyroxene, or plagioclase, is in fact residual. The large size of the crystals is more consistent with crystallization from the diatexite magma; this is investigated on figure 42b.

Plagioclase is the principal reservoir of CaO in the diatexite migmatites. Figure 42b shows that very few of the diatexite migmatites lie along trend 2 and so can be considered to be melt contaminated by residual plagioclase only. Rather, many of the samples lie along the trend 1 for wholesale contamination of the melt by the adjacent residual rocks. However, many of the samples that follow trend 2 on figure 42b, in fact lie to higher MgO contents than the trend 2 on figure 42a, so these samples are interpreted to contain a non MgO-bearing phase, such as plagioclase, but it must be a plagioclase that is less calcic than the residual plagioclase. These samples lie on a trend that projects to plagioclase of about composition An_{22}. This suggests that most of the diatexite migmatites are accumulations of plagioclase that crystallized from the diatexite magma, an interpretation that is consistent with the petrographic interpretation of the plagioclase framework structures and crystallization sequence in these rocks (Chapter IV). The more calcic plagioclase crystals could be residual, or they could be early crystallization products of the melt; the large euhedral grains that form the framework structure are certainly crystallization products of the melt. The more sodic plagioclases are crystals that grew later from a more evolved melt composition. Diatexite samples show a range in SiO_2 content, contamination of the anatectic melt with the residuum results in SiO_2 contents of about 68 to 70 wt % melt (Fig. 43), most samples are more calcic and less siliceous than this, consistent with a high modal fraction of plagioclase in the composition range An_{17} to An_{20}.

The LSLP monzogranite samples have lower MgO contents, but similar CaO contents, to the diatexite migmatites (Figs. 42 & 43) and, therefore, could be interpreted to have a lower biotite and orthopyroxene component. Their relatively high silica

content combined with relatively low CaO content indicates that they contain a large component of sodic plagioclase (in the range An_{17} to An_{20}).

The diatexite and monzogranite samples with high K_2O (> 4.5 wt %), low MgO and CaO (< 2 wt %) were derived from magmas that had more evolved compositions, and they lie along the trend towards fractionated melt compositions located between the K-feldspar and quartz vectors. Some samples lie along the K-feldspar + melt mixing line, and these represent K-feldspar accumulations with (more fractionated) interstitial melt (Figs. 42a & b and Fig. 43). However, the principal characteristic of most of these samples is that have very leucocratic (low MgO + FeO) compositions indicating that previous crystallization and crystal fractionation has removed the crystallized ferromagnesian minerals, and any entrained residual, ferromagnesian minerals; a feature also noted in the diatexite migmatites from the Opatica subprovince (Sawyer 1998). The major element geochemical features indicate that the principal processes involved in controlling the composition of the diatexite migmatites are contamination of the anatectic melt with residuum to create the diatexite magma, followed by crystallization of the melt fraction and separation of entrained residuum together with any crystallization products. The question that arises now is; how do we distinguish contamination from fractional crystallization, when plagioclase could be an important phase in both processes? If the diatexite migmatites have formed at sites where the melt accumulated (e.g. Sawyer 1994, 1998) then the way to separate the contaminants from the evolved melt is by either a filter-pressing mechanism in which the remaining, evolved residual melt is squeezed out from the crystal framework, or when the diatexite cools and begins to crystallize and the contaminant crystals are trapped in the growing

plagioclase crystal framework (Sawyer 1998). Once the contaminants are removed, therefore, fractional crystallization becomes the principal factor changing the composition of the melt, and hence, controlling the composition of the resulting migmatites. The same processes have been described in diatexite migmatites from the Opatica subprovince (Sawyer 1998), and the St Malo Migmatite Terrane (Milord *et al.* 2001).

5.5.2 Crystallization of the melt

The compositional trends observed in many granites (e.g. McCarthy & Groves 1979; Tindle & Pearce 1981; Sawyer 1998; Solar 2001) are commonly ascribed to fractional crystallization. McCarthy and Groves (1979) described most granitic rocks as 'mushes' comprising mixtures of cumulate crystals and trapped interstitial melt in various proportions. Later, Tindle and Pearce (1981) took into account in their fractional crystallization modelling, the probability that many granite plutons should be treated as crystal mushes, rather than pure melts, or pure "cumulates". They also considered that accumulations of crystals could arise from processes other than crystal settling, and developed a filter pressing model in which the liquid phase moved inwards, towards the centre of the pluton, leaving a melt-poor outer part.

5.5.3 Modelling of Rb, Sr, Ba, and Eu

In principle, it should be possible to test the results of the modelling of the major element compositions against results obtained from trace elements, such as the Rb, Sr

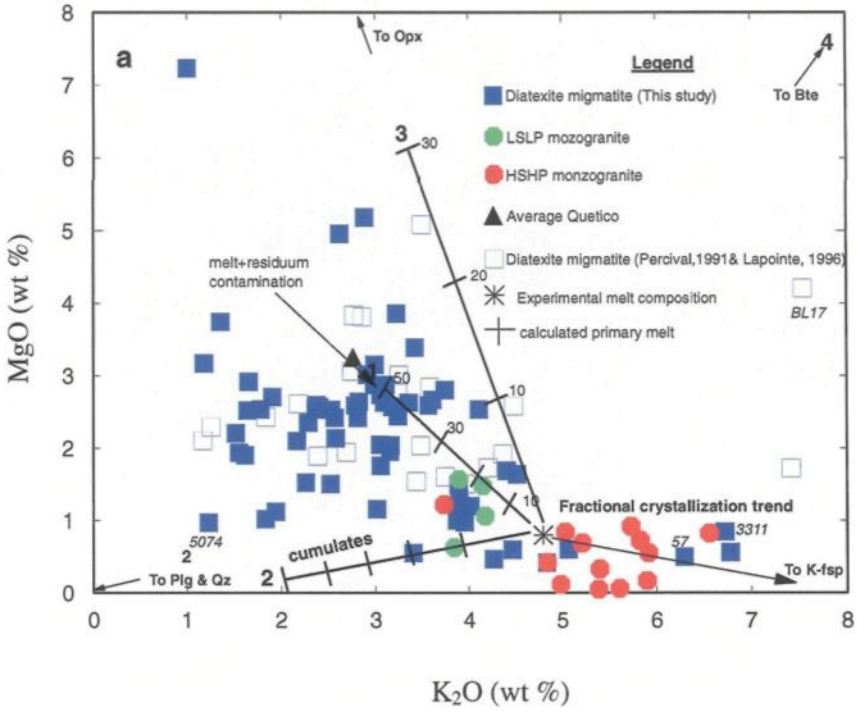
a
To Opx
Legend
Diatexite migmatite (This study)
LSLP mozogranite
HSHP monzogranite
Average Quetico
Diatexite migmatite (Percival,1991& Lapointe, 1996)
Experimental melt composition
calculated primary melt
To Bte
4
3
30
20
10
melt+residuum contamination
50
30
10
Fractional crystallization trend
BL17
5074
3311
57
cumulates
2
2
To Plg & Qz
To K-fsp
MgO (wt %)
K2O (wt %)

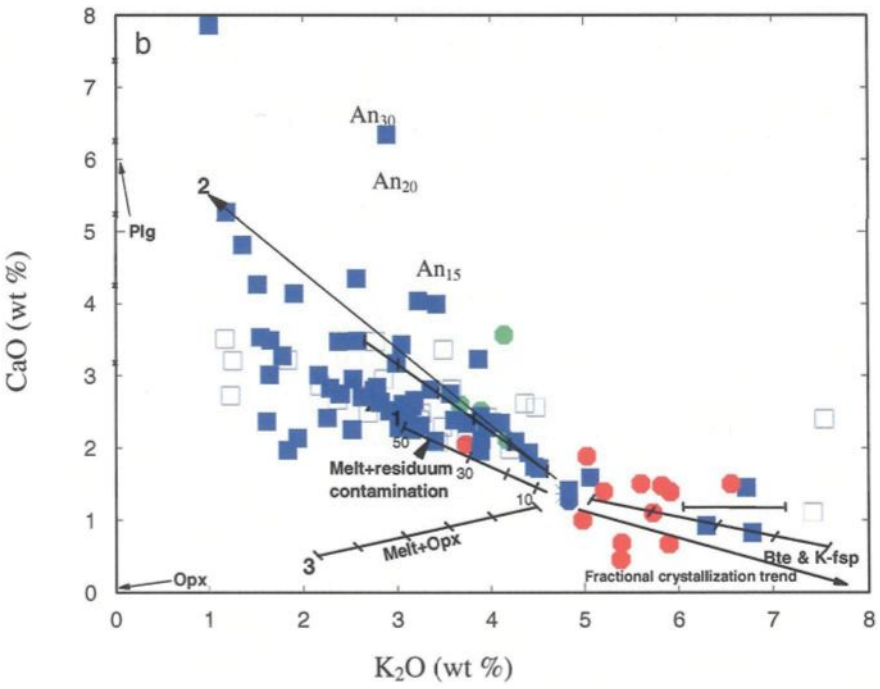
b
An30
An20
An15
2
Plg
1
50
Melt+residuum contamination
30
10
3
Melt+Opx
Opx
Bte & K-fsp
Fractional crystallization trend
CaO (wt %)
K2O (wt %)

Figure 42: Plots of a) MgO *versus* K_2O, and b) CaO *versus* K_2O for the diatexite migmatites and monzogranites from the Ashuanipi subprovince. The vectors for; contamination of the anatectic melt by the residuum, plagioclase (Plg), orthopyroxene (Opx), biotite (Bte), quartz (Qz), K-feldspar (K-fsp) and fractional crystallization are shown. The lines extending from the experimental melt composition (asterisk) represent model mixing between the experimental melt and whole rock residuum (trend 1), residual plagioclase (trend 2), orthopyroxene (trend 3) and biotite (trend 4). Ticks on the line are at 10 vol % intervals of mixture with melt. The symbols are as in Fig. 35.

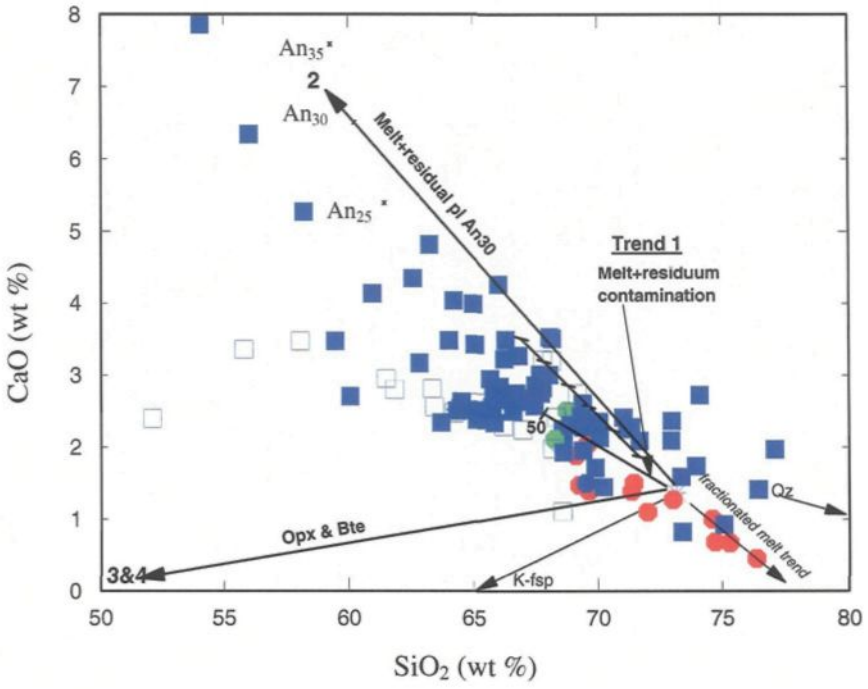

Figure 43: Plot of CaO *versus* SiO_2 for the diatexite migmatites and monzogranite suite samples. Symbols are the same as on Fig. 35.

The third point is that the mineral-melt distribution coefficients vary considerably during fractional crystallization as the temperature and melt composition change (Watson 1976). Further complications for the partition of the trace elements may arise during the final stages of crystallization, if an aqueous magmatic fluid (Hanson 1978) is exsolved. A final concern is the difficulty of incorporating the effects of accessory minerals into petrogenetic models, because of their very low abundances and the poorly determined trace element distribution coefficients into them (Tindle & Pearce 1981; Bea 1991, 1994, 1996).

5.5.3.1 Method of modelling

Two basic equations describe the extremes of behaviour of trace elements during crystallization:

1) $C_l/C_0 = F(D_a-1)$

For Rayleigh fractional crystallization, and

2) $C_l/C_0 = 1/(F+D_a(1-F))$

For equilibrium crystallization;

Where C_0 = concentration of element a in the original melt

C_l = concentration of element a in the residual melt

F = weight fraction of melt remaining

D_a = bulk distribution coefficient for element a in the phases crystallized

$D_a = \mathrm{Sum}D_{ai}X_i$ where,

D_{ai} = partition coefficient of element a between mineral i and melt

X_i = Weight fraction of phase i crystallized

The first problem is to decide on the likely trace elements content of the parent magma. Three diatexite migmatite samples (71*, 1054 and 2085) have smooth REE patterns (Eu / Eu*= 0.95, 0.99 & 1.01 respectively, Fig. 44) and could, therefore, be considered close to a primary, unfractionated melt composition from which the Ashuanipi diatexite migmatites and monzogranites were derived. Moreover, an initial, or starting melt, composition should be granitic in its modal mineralogy. Melt compositions obtained from biotite dehydration melting of plagioclase + biotite + quartz metapsammitic protoliths are relatively potassic (e.g. Patiño Douce & Beard 1996, Stevens *et al.* 1997). Therefore, it is unlikely that sample 71*, which is plagioclase-rich (*ca.* 60 modal %) represents a primary melt compositions (Sawyer 1999). Thus, samples 2085 and 1054 are the best remaining candidates, and are used as the starting compositions from which to model the crystallization.

The cooling of migmatites in granulite facies regional metamorphic terranes is slow (Sawyer 1987; Sawyer *et al.* 1999) and the Ashuanipi subprovince may have been at temperatures above the solidus (i.e. T > 650°C) for 40 Ma (chapter III). Therefore, cooling may well have been slow enough that equilibrium between the melt and the whole volume of the crystals was maintained, consequently, the equilibrium crystallization model is preferred. The projection of the two primary melts on to the quartz – albite – anorthite - orthoclase tetrahedron of Kosinowski (1981), shows that they plot close to the quartz-albite-anorthite side and, therefore, they will crystallize quartz and plagioclase before K-feldspar (Fig. 45).

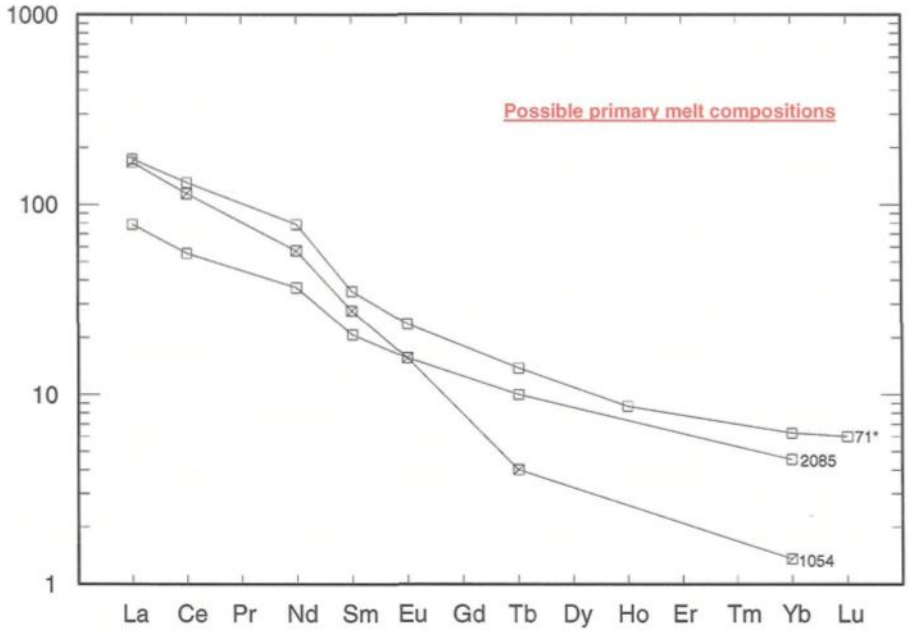

Figure 44: Chondrite normalized rare earth element diagram for the samples of diatexite migmatite that may represent primary melt compositions. Sample 71* has a modal composition that is too plagioclase rich. Therefore, samples 1054 and 2085 are used for the trace elements modelling.

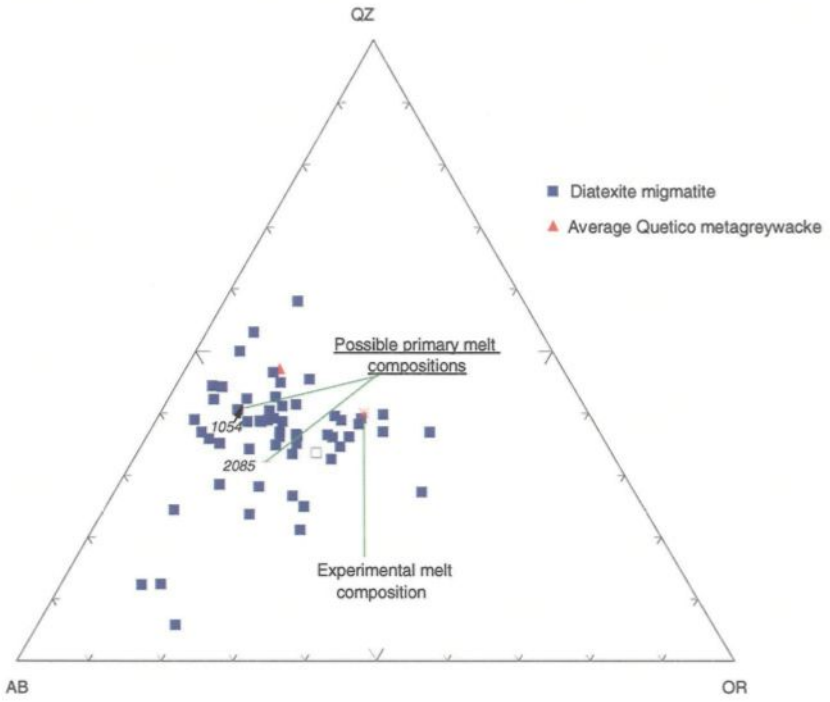

Figure 45: Composition of diatexite migmatites that are without Eu anomalies plotted on projection within quartz-albite-anorthite-orthoclase tetrahedron of Kosinowski (1981). Both samples plot close to the quartz-albite side and will, therefore, crystallize quartz and plagioclase before K-feldspar.

The early stages of crystallization (up to 70 %) are modelled (Fig. 46) without K-feldspar on the liquidus, but the final stages are modelled with quartz, plagioclase, K-feldspar and orthopyroxene present in their calculated CIPW, normative proportions for each sample.

The mineral proportions of the two primary melts were also calculated by the least squares solution to the overestimated mass-balance constraints (Bryan *et al.* 1969) (see appendix XI); the results were almost identical to the CIPW normative calculations. The mineral-melt partition coefficients of Arth (1976) have been used for the modelling, and they are given in appendix XV.

5.5.3.2 Interpretation of the trace element modelling results

Some samples on figures 46b, c & d, plot to the right of the primary melt composition; these samples (e.g. 1035 and 5020) represent the fractionated melt compositions. In contrast, the samples that represent cumulate compositions plot on the opposite side of the starting compositions to the fractionated melts.

Modelling of the trace elements Ba, Rb, Sr and Eu yield trends that do not lie near to the majority of the Ashuanipi diatexite migmatites and monzogranite samples, only a few samples plot close to the model curves on figures 46a, b, c and d. The effect of the onset of the crystallization of K-feldspar on the model curves is considerable for Ba (Fig. 46a), but for Rb (Fig. 46b), Sr (Fig. 46c) and Eu (Fig. 46d) its effect on the model curves is negligible. The model trend for fractionated melt is displaced to higher

Rb contents in figure 46b, and this could be due to the high initial Rb content in the assumed primary melt composition. Most of the diatexite migmatite and monzogranite samples plot on the opposite side to the model curves and may, therefore, be interpreted to be cumulates rather than fractionated melts, and such an interpretation is consistent with their microstructure (Figs. 17a & b, chapter IV).

In general, the majority of samples of diatexite migmatite and monzogranite have higher concentrations of Sr and Ba than either of the two samples interpreted to be the primary melts used as starting points for the modelling. This suggests that feldspar accumulation has occurred in many of the diatexite migmatites and monzogranites. However, more than half of the samples have Eu contents that are lower than the samples chosen as potential primary melts and this may mean that the "primary melts" were, in fact, feldspar cumulates. The Rb concentrations are highest in the fractionated melts (Fig. 46b), and these samples plot closer to the model curve than the majority of the cumulate diatexites. Such a trace element relationship indicates that most of the Ashuanipi diatexites are a mixture of accumulated crystals and more fractionated interstitial melt. The Rb *versus* Sr diagram (Fig. 47) shows that all the diatexite migmatites and a majority of the monzogranite samples plot on the model curves, since the plagioclase is a principal crystallizing phase in the cumulates, the contaminated magmas and even some of the fractionated magmas. The samples (5020, 1035 and 2047) have high SiO_2, K_2O, Ba and Rb concentrations (see table 4 and chapter IV). They are also LREE-enriched and have small negative Eu anomalies. These samples plot close to all the model melt curves, hence they represent rocks derived from fractionated melts. However, sample (123) has a high SiO_2 content, but low K_2O, Ba,

and Rb contents, suggesting that quartz and plagioclase are the dominant minerals in it, and that some accumulation of plagioclase crystals has occurred. However, its high LREE and Th contents imply that the trapped liquid may have been extremely fractionated.

Although the modelling reproduced realistic Rb, Sr, Ba and Eu concentrations in the diatexite migmatites, it is concluded that modelling of the trace element distributions in granulite facies migmatite terrains, where multiple processes of crustal melting and fractional crystallization occurred in an open-system is indeed a very complex matter.

5.6. CONCLUSIONS

The generation of granitic magma in the Ashuanipi subprovince was an open system processes at the regional scale, starting with contamination of the segregated melt fraction by the residuum it passed through as it moved into low pressure structural sites where the diatexite migmatites and granites later crystallized. However, fractional crystallization was the most important process, and evidence for this is the presence of outcrop-scale, *in situ* bodies of monzogranite with diffuse, gradational contacts within the diatexite migmatites.

The field relationships and compositional range of monzogranite compositions from LSLP to HSHP is consistent with a derivation from a common parent magma that resembled the evolved K-feldspar-rich diatexites.

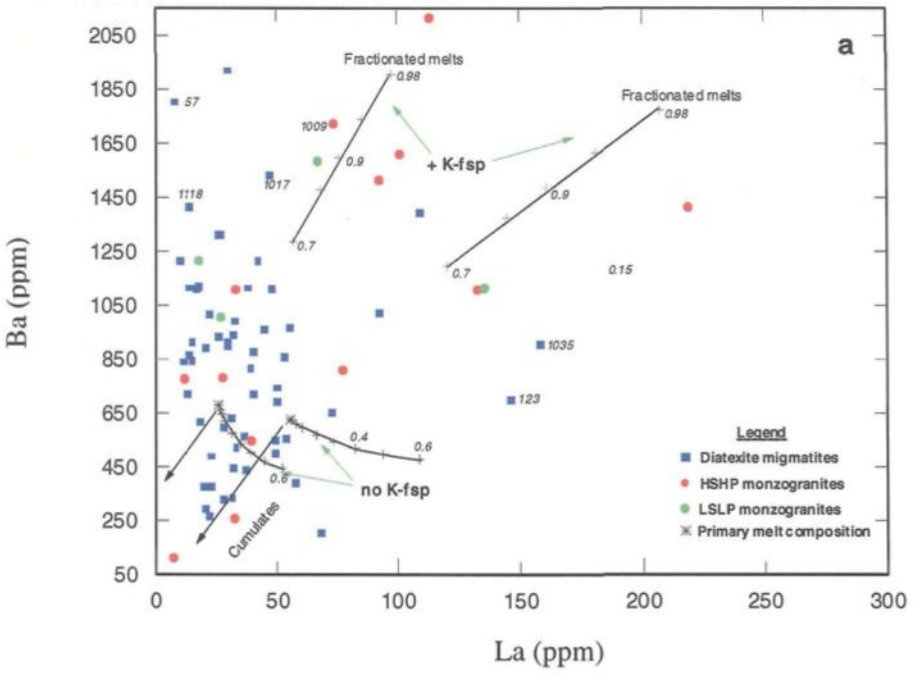
a
Fractionated melts
0.98
0.9
0.7
+ K-fsp
Fractionated melts
0.98
0.9
0.7
0.15
57
1009
1017
1118
1035
123
0.4
0.6
0.8
no K-fsp
Cumulates
Legend
Diatexite migmatites
HSHP monzogranites
LSLP monzogranites
Primary melt composition
Ba (ppm)
La (ppm)
2050
1850
1650
1450
1250
1050
850
650
450
250
50
0
50
100
150
200
250
300

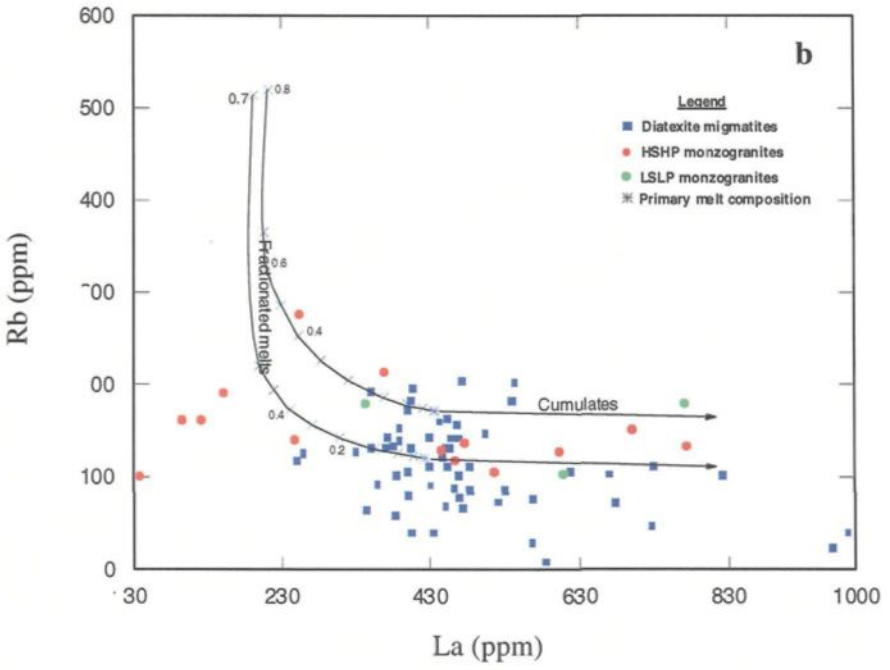
b
0.7
0.8
0.6
0.4
0.4
0.2
Fractionated melts
Cumulates
Legend
Diatexite migmatites
HSHP monzogranites
LSLP monzogranites
Primary melt composition
Rb (ppm)
La (ppm)
600
500
400
00
00
100
0
30
230
430
630
830
1000

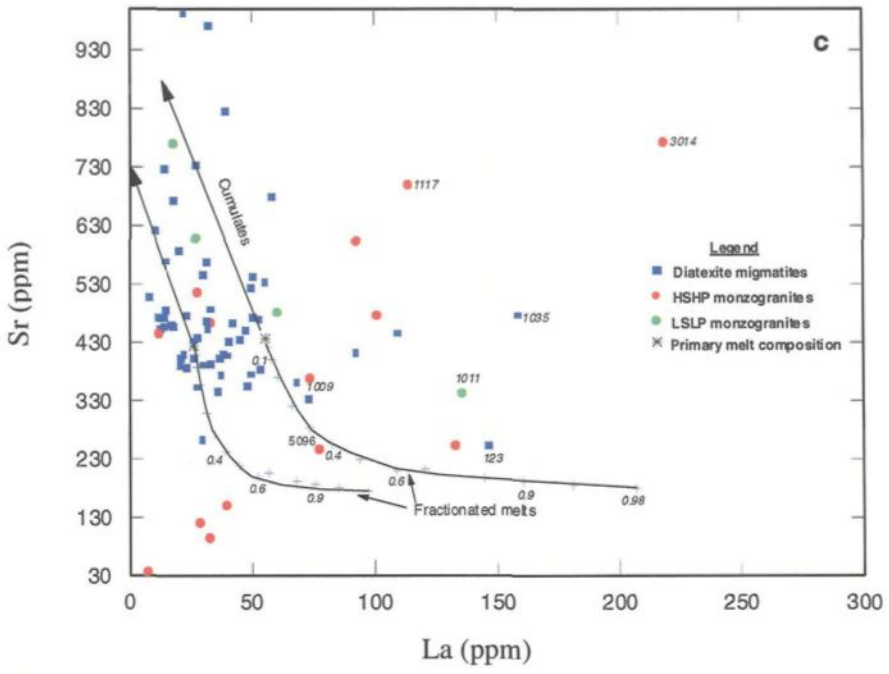
c
Sr (ppm)
La (ppm)
Cumulates
Fractionated melts
Legend
Diatexite migmatites
HSHP monzogranites
LSLP monzogranites
Primary melt composition
3014
1117
1035
1009
1011
5096
123
0.1
0.4
0.6
0.9
0.98

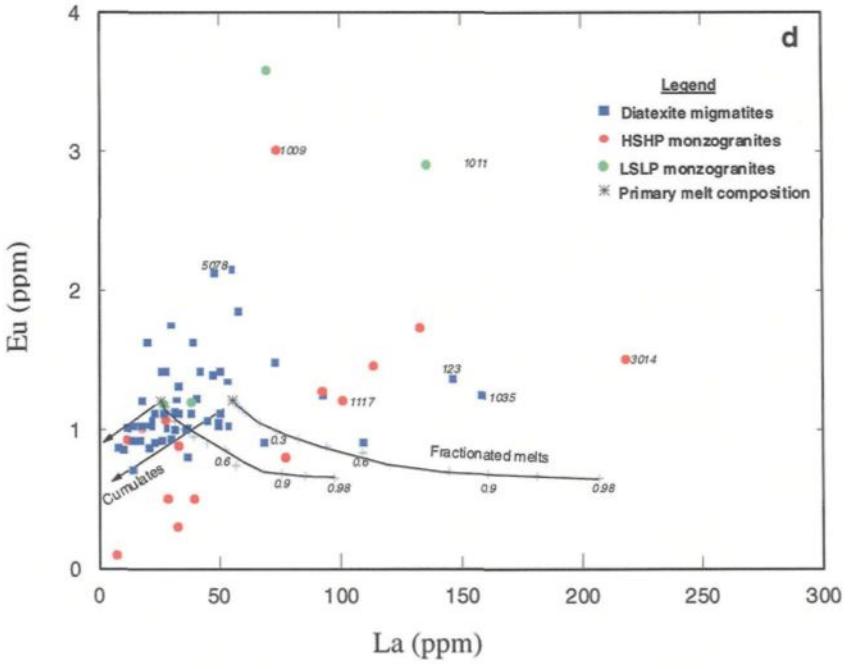
d
Eu (ppm)
La (ppm)
Cumulates
Fractionated melts
Legend
Diatexite migmatites
HSHP monzogranites
LSLP monzogranites
Primary melt composition
1009
1011
5078
123
3014
1117
1035
0.3
0.6
0.9
0.98

Figure 46: Results of equilibrium crystallization models for compatible elements. All model curves from 0.98 to 0.7 weight fraction crystallization (F=0.3) are calculated without K-feldspar. The portion between 0.6 and 0.08 crystallization is calculated with the phases present in proportion to their modal abundance in the diatexite migmatites. Crosses on the model curves indicate degree of crystallization in 0.05 increments for the first 0.2 weight fraction crystallization, then 0.1 increments to 0.9 weight fraction crystallization. The location of model curves depends strongly upon when K-feldspar starts to crystallize. For Rb (b), Sr (c) and Eu (d) the effect of K-feldspar on the model curves is negligible, whereas for Ba (a) the difference is considerable. Note the curves where no K-feldspar crystallized and the curves where K-feldspar started to crystallize at 0.6 (F=0.4) crystallization.

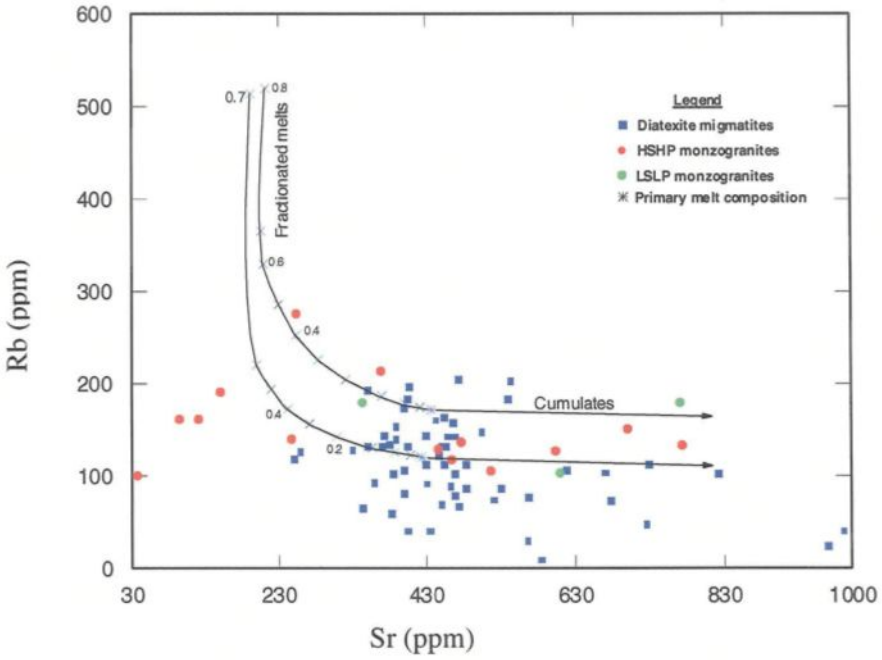

Figure 47: Rb *versus* Sr diagram shows that all the diatexites and the majority of monzogranites plot on the model curves, since the plagioclase is a principal phase that crystallized in both the diatexite migmatites and the monzogranite suite.

The LSLP group of samples represents the cumulate members of the monzogranite suite formed from a magma containing orthopyroxene and early-crystallized plagioclase. The HSHP monzogranites are the complement to the LSLP rocks and represent the highly fractionated end product magma derived from the parental, evolved, K-feldspar-rich diatexite magma after formation of the LSLP monzogranites. The concentration of K-feldspar is a significant feature of the HSHP rocks.

CHAPTER VI

THE SIGNIFICANCE OF MIGMATITE TERRANES IN THE EVOLUTION OF THE CONTINENTAL CRUST

6.1 INTRODUCTION

One of the fundamental geophysical (Drummond 1988; Christensen & Mooney 1995) and geochemical (Lambert & Heier 1968; Fyfe 1973; Taylor & McLennan 1985) observations made of the earth is the stratified and differentiated, nature of the continental crust. The lower part comprises denser, more mafic material, whereas the upper part comprises less dense, more felsic material. If the continental crust was formed predominantly in volcanic / plutonic arcs, then one hypothesis is that this chemically differentiated, layered structure developed through partial melting in the lower crust. The melt fraction generated by anatexis ascends to shallow crustal levels where it forms granite plutons (or erupts), whereas the dense, residual fraction remains in the lower crust and the result is an overall differentiation of the continental crust into a melt-depleted lower crust and a melt-enriched upper crust (e.g. Fyfe 1973; Brown *et al.* 1995). In a competing model the layered structure of the crust is created when dense material is added to a crust of intermediate bulk composition, either by the underplating of mafic magma, or by the underplating of cumulate mafic material during episodes of continental flood basalt outpouring at the surface. Needless to say, the underplating, or intraplating, of large volumes of hot mantle-derived mafic magma into the crust, also adds a significant quantity of heat to it, and this heat may provoke extensive high temperature, or ultra high temperature metamorphism and partial melting (Clemens 1990).

The transition from metatexite to diatexite migmatite is arguably the most important of all processes to affect the lower and middle crust, and should not be

neglected. The transition from metatexite migmatite to diatexite magma reworks the continental crust, not only does this process produce the vertical compositional fractionation well documented by geochemists and geophysists, but it also gives rise to a structural and deformational style. Anatexis at all scales in the continental crust, from the small-scale effects present in migmatites to the large-scale, regional metamorphic terranes has a great impact on the rheology of the continental crust and in particular how the weak, melt-bearing regions of the continental crust influence, or control, the geometry and tectonic evolution of orogens (Beaumont & Jamieson 2005). Since the progression from migmatite to granite can be observed throughout the high-grade metamorphic terranes of the world; the Cooma area of the Lachlan Fold Belt of Australia, the Black Forest in Germany, the Himalayas, East Greenland, the European Alps, and in Spain, one can expect that the rheological consequences of crustal anatexis are also of major importance on a global scale.

Rosenberg & Handy (2005) have reinterpreted the experimental data on the strength of partially molten rocks and have concluded that there are two major transitions. One at low melt contents (*ca.* 7 vol %), which they termed the "melt connectivity transition" (MCT), marks a rapid loss in strength once a sufficient proportion of grain boundaries become melt-bearing so that rapid deformation can occur. The other, which occurs at higher (40 to 60 vol %) melt fractions, they termed the "solid to liquid transition" (SLT) marks the transition from a solid-framework to a liquid with crystals. The SLT of Rosenberg & Handy (2005) corresponds to the "rheologically critical melt percentage" (RCMP) of Arzi (1978) and to the "melt escape threshold" (MET) of Vigneresse *et al.* (1996). Rosenberg & Handy's (2005) analysis of

the experimental data shows that the largest, most dramatic drop in the strength of a partially molten rock occurs at the MCT and, although there is a decrease in strength at the SLT (equivalent to the RCMP and MET), it is minor in comparison.

This chapter investigates the relationship between granites and diatexite migmatites and between diatexite migmatites and melt-depleted, lower-crustal, metatexite migmatites during large-scale anatexis of the crust. Then, some of the important questions relating to the significance of granulite terranes in the evolution of continental crust will be addressed. The Ashuanipi subprovince is one of the best terranes for this because it contains several fundamental petrological transitions which may be key factors in producing the major, crustal scale rheological transitions that control the way the continental crust behaves during major deformational events.

6.2 THE PROGRESSION FROM MIGMATITE TO GRANITE IN THE ASHUANIPI SUBPROVINCE

The segregation of anatectic melt in the Ashuanipi subprovince started when connectivity was established between the pockets of melt formed at the innumerable sites where the melt-producing reaction occurred. The first few centimeters of melt movement occurred in the regime of dispersed flow (also called porous flow), in which melt moved along the edges of the solid grains in the partially melted rock. After an initial phase of porous flow, melt movement became concentrated along fewer, but larger and wider channels, this phase of the flow of melt is called the channel flow regime and it resulted in the collection of anatectic melt into structurally-controlled sites

(Stevenson 1986; Sawyer 1991; Collins & Sawyer 1996; Brown *et al.* 1999), most commonly these sites are dilated foliation planes, but also the interpartitions between boudins (see figure 13 in chapter III). The widespread presence of residual rocks that have few, or no, leucosomes in the Ashuanipi subprovince, is good evidence that the process by which anatectic melt was segregated was effective enough to extract a very high proportion of the melt generated and, moreover, affected a very large volume of the middle crust. The highly effective segregation and removal of melt from its source in the Ashuanipi subprovince means that, even at extreme temperatures and degrees of partial melting, most of the migmatites retain their pre-anatexis structures, such as bedding, graded bedding and cross laminations, and because of this the rocks can be termed metatexite migmatites, albeit ones that have experienced considerable melt-depletion.

In metasedimentary, and other layered protoliths, the anatectic melt generally flows out, from the grain boundaries where it formed, into bedding-parallel dilatant sites that become the leucosomes. It collects and remains in these sites until suitable pressure gradients develop which enable it to migrate out of the rock altogether (Sawyer *et al.* 1998), typically through a system of fractures that have been termed the melt transfer network (Brown *et al.* 1999; Sawyer 2001). Very similar features are observed across the spectrum of anatectic rocks; from those formed at the onset of muscovite dehydration melting in the middle amphibolite facies (low melt loss, mildly residual rocks, e.g. Milord *et al.* 2001; Solar & Brown 2001) to ultra-high temperature metamorphic conditions (high melt loss, strongly residual rocks, e.g. Raith *et al.* 1997; Sawyer 2001). However, the microstructural and geochemical development that occurs

in partially molten rocks will be entirely different if this normal pattern of melt migration leading to melt-depletion does not occur; other processes, such as bulk flow (Sawyer 1996) may occur and involves other deformation mechanisms, such as grain boundary sliding, that disrupt the primary structures and result in a rock with a morphology that is entirely syn-anatectic.

6.2.1 The transition from metatexite migmatite to diatexite migmatite

The transition from a continuous, layered metatexite migmatite containing very few leucosomes to a migmatite consisting of disrupted blocks, or enclaves, floating in a melt-enriched matrix (i.e. a diatexite migmatite) in the Ashuanipi subprovince is a consequence of a locally higher fraction of melt. The fraction of melt required for this to happen must locally be sufficiently high locally, that the contiguous framework of touching crystals in the metatexite migmatite is no longer maintained. This could occur pervasively through the rock detaching each individual grain contact, but more likely it occurs on a much smaller fraction of grain contacts and detaches aggregates of grains, nevertheless, the proportion of melt must be sufficient for the overall coherence of pre-anatectic planar structures in the rocks to be lost, and the fragments to be able to rotate with respect to one another. Alternatively, the contiguity of pre-anatectic structures could be lost when the blocks of country rock isolated by veining become sufficiently widely spaced that the volume of melt filled veins becomes large enough that the detached blocks of country rock do not touch, and can rotate freely in the anatectic melt.

Field observations in the Ashuanipi subprovince indicate that the diatexite migmatites were dominated by a granitic magma fraction in which the ferromagnesian mineral-rich solid fraction is represented by schlieren that indicate the magmatic flow structure, and by enclaves of metatexite migmatite. In contrast, the metatexite migmatites preserve the compositional layering (bedding) and fine-scale sedimentary structures of their protolith and have relatively few leucosomes (see Fig 3 in chapter III). In the Ashuanipi subprovince the loss of continuity of pre-anatectic structures appears to be the result of the injection of anatectic melt by dyking and veining of the metatexite in and around the structural sites where melt collected, because in many outcrops there are sharp cross-cutting contacts between veins and dykes of anatectic granite and the host metatexite migmatite (see Fig. 3b in chapter III). The transition from metatexite to diatexite migmatite is, therefore, typically abrupt, and occurs over a few metres. Moreover, there is a consistent morphological and mineralogical progression across the transition from metatexite to diatexite migmatite; the metatexite migmatite contains progressively more granitic veins until the metatexite occurs only as detached blocks within a net-like array of anatectic granite. In the next zone the enclaves become progressively rounder and smaller and the enclosing anatectic granite progressively more contaminated with ferromagnesian minerals derived from the magmatically eroded enclaves.

6.2.2 The transition from diatexite migmatite to monzogranite

Metre-scale bodies of homogeneous, leucocratic monzogranite occur in outcrops of heterogeneous diatexite migmatite. Some have sharp, discordant boundaries, and this suggests the intrusion of the leucocratic magma. However, most metre-scale bodies of leucocratic monzogranite have diffuse boundaries that are transitional to a K-feldspar-rich diatexite migmatite host that has an evolved composition; this field relationship is interpreted to indicate *in situ* segregation of a fractionated, residual granite melt from the already largely-crystallized host diatexite migmatite. The much larger (tens to hundreds of metres across) bodies of leucomonzogranite have intruded into the metatexite and diatexite migmatites, but are also interpreted to have been derived from the diatexite magma by fractionational crystallization and segregation of the late, evolved melt fraction.

The compositional range found within the diatexite migmatites provides good evidence for fractional crystallization of the diatexite magma as it crystallized. Most of the diatexite migmatite has far too much plagioclase to be the crystallized anatectic melt that was extracted from the metatexite migmatites, therefore, this portion of the diatexite migmatite may represent a cumulate fraction of early crystallized minerals, mostly plagioclase fractionated from the anatectic melt removed from the melt-depleted metatexite migmatites. The complementary, evolved melt to the plagioclase-rich diatexite migmatite may have gone on to form some of the larger bodies of leucocratic monzogranite that are intrusive into the migmatites of the Ashuanipi subprovince. Within the diatexite migmatites, there are smaller volumes of plagioclase + K-feldspar

diatexite and more evolved K-feldspar-rich diatexites, these rocks may represent the initial bulk composition of the diatexite magma (i.e. the anatectic melt extracted from the melt-depleted metatexite migmatites plus some contamination by the wall rocks) and an evolved diatexite magma compositions, respectively. The *in situ* leucocratic monzogranite patches found within the diatexite migmatites are rather similar in composition to some of the K-feldspar-rich diatexites, but they differ in several significant ways. They have a lower modal proportion of biotite, they contain the distinctive quartz-K-feldspar graphic intergrowth, they have a slightly coarser grain size, and they locally develop an incipient pegmatite microstructure. Consequently, they are interpreted to be the last pockets of magma to crystallize within the diatexite migmatites.

6.3 A MODEL FOR THE FORMATION OF MIGMATITES AND GRANITE IN THE ASHUANIPI SUBPROVINCE

The diatexite migmatites in the Opatica subprovince (Sawyer 1998) and in the St. Malo Migmatite Belt (Milord *et al.* 2001) were formed by a progressive increase in the fraction of melt in the source that enabled a change in the deformation mechanisms to occur from those applicable to a solid containing melt, to those allowing the magma-like flow behaviour of a suspension of solids in a melt. The diatexite migmatites in the Ashuanipi subprovince did not form in this way, and the critical evidence for this is the widespread occurrence of the melt-depleted metatexite migmatites. Their presence in the Ashuanipi subprovince indicates that the melt fraction did not remain in the source, and so could not have built up to the level required to cause magma-like flow there.

Consequently, this section outlines a model that explains how the diatexite migmatites in the Ashuanipi subprovince were formed. Contrary to the model developed by Milord *et al.* (2001) for the St Malo migmatites, this model is applicable to melt-depleted, granulite facies terranes in general.

Alumina-poor psammitic metagreywacke is the most abundant rock type in the Ashuanipi subprovince. Melting in these rocks began with the breakdown of biotite + plagioclase + quartz, and produced an average of 31 vol. % granitic melt. Unlike anatexis in the Opatica subprovince, the melt fraction that was produced in the Ashuanipi subprovince was segregated from its residuum as it formed (see steps 1 and 2, Fig. 48). The segregated anatectic melt is the source material (or feed stock) for the development of melt-rich rocks, such as the diatexite migmatites and monzogranites, in the Ashuanipi subprovince. The immediate segregation of anatectic melt from its residuum implies that the melt segregation rate equaled the melt generation rate (Sawyer 1994) throughout the Ashuanipi subprovince; this observation suggests that this may, indeed, be the general case for anatexis in an orogenic setting. The typical outcrop of metagreywacke in the Ashuanipi subprovince is without, or contains few, leucosomes and, based on their mineral paragenesis and bulk compositions, they are residual rocks from which virtually all the anatectic melt that was produced in them, has been removed. These rocks are the melt-depleted metatexite migmatites.

The anatectic melt expelled from the melt-depleted parts of a migmatite has been shown to move from one structurally favourable low-pressure site to the next, as a migmatite terrain undergoes progressive regional deformation (e.g. Sawyer *et al.* 1999). Thus, the anatectic melt expelled from the Al-poor metagreywackes would have moved to the nearest suitable low-pressure sites within the Ashuanipi subprovince. The map pattern suggests that these sites were parallel to the regional foliation, or bedding, and notably in the hinge region of very large-scale open folds formed during the regional, south-vergent thrusting event that affected the subprovince. Flow of the anatectic melt was along a network of dykes and sills that crossed the melt-depleted metatexite migmatites. Field observations of the dykes, and especially at the edges of the bodies of diatexite migmatite, show that the anatectic melt became contaminated with its wall rocks as it moved towards and occupied the most stable, low-pressure dilatant sites in the Ashuanipi subprovince. Hence, step 3 of the model is transport, and contamination of the expelled anatectic melt with its wall rocks. Step 4 is the accumulation of melt in the largest of the structural sites to produce the layers of diatexite magma so evident in the field; the layers range from a few metres to many hundreds of metres in thickness. The evidence that the melt-rich diatexite migmatites either, grew in, or developed into, major south-vergent thrusts, is the ubiquitous and consistent asymmetry of the metatexite enclaves, and the presence of a strong magmatic alignment of platy minerals such as plagioclase, orthopyroxene and biotite in the layers of diatexite migmatite.

The diatexite magma contained crystals derived from the wall rocks, but as it started to crystallize, large tabular plagioclase crystals became abundant. Evolution of the diatexite magma starts at stage 5 (Fig. 48) with the separation of crystals from the

diatexite magma as it cools. The separation of crystals from the remaining melt may occur in response to pressure gradients and strain-rate discontinuities that develop as the diatexite magma flowed (Sawyer 1996; Milord & Sawyer 2003). A variety of rock types were generated depending upon when in the crystallization sequence of the diatexite magma the melt and crystal fractions were separated. The plagioclase-rich diatexite migmatites represent accumulations of up to 60 vol. % of early-crystallized plagioclase. Some of these diatexite migmatites must have formed early in the crystallization history, or else contained very little trapped, evolved liquid, as they have very little interstitial K-feldspar. Some of the K-feldspar-dominated diatexites have a cumulate microstructure, and they are interpreted to have formed later by the accumulation of K-feldspar when that mineral began to crystallize as subhedral grains from an evolved melt. However, other K-feldspar-rich diatexites do not have microstructures that are indicative of feldspar accumulation, and these rocks may represent crystallized evolved melts. In some of the plagioclase + K-feldspar diatexites the plagioclase defines a cumulate microstructure, and the K-feldspar in the rocks is interstitial to the plagioclase framework, thus, these rocks are interpreted to be accumulations of plagioclase that contained a trapped, and somewhat evolved, melt. However, other plagioclase + K-feldspar diatexite migmatites have a granitic composition, and do not have conspicuous cumulate microstructures; these rocks may represent crystallized diatexite magma which did not undergo significant fractional crystallization.

The field work shows a close spatial relationship between the monzogranites and the K-feldspar-rich diatexite migmatites. Moreover, the geochemical data (chapter V) indicates that the two are related by fractional crystallization of a common diatexite magma. Thus, step 6 of figure 48 shows the monzogranites found in situ or, as intrusions, within migmatites of the Ashuanipi subprovince as derived from a K-feldspar-rich diatexite magma by fractional crystallization. By analogy with observations in the crustal section exposed in the Opatica subprovince (Sawyer 1998) and inferred from the geochemical data from the diatexite migmatites at St Malo (Brown 1979; Milord *et al.* 2001) the last step in the evolution of the anatectic magma in the Ashuanipi subprovince is ascent to higher crystal levels and continued fractional crystallization of the evolved monzogranitic magma as it rises (step 7, Fig. 48). Unfortunately, the Ashuanipi subprovince has been deeply eroded, and the crustal levels that were above the exposed granulite facies terrane are not preserved, therefore, there is no direct evidence for the loss of large volumes of anatectic melt. However, the lack of extensive rehydration of the granulites in the Ashuanipi can be taken as evidence for the desiccation of the terrain by the removal of H_2O with the anatectic melt (*e.g.* Powell 1983; Powell & Downes 1990; Spear *et al.* 1999, White *et al.* 2001). Higher crustal levels are preserved in some of the adjacent metasedimentary subprovinces (*i.e.* the La Guiche and Nemiscau subprovinces); both of these contain allochthonous granites that have highly evolved compositions that could represent the evolved, highly fractionated melts that were derived from a granulite facies, diatexite magma.

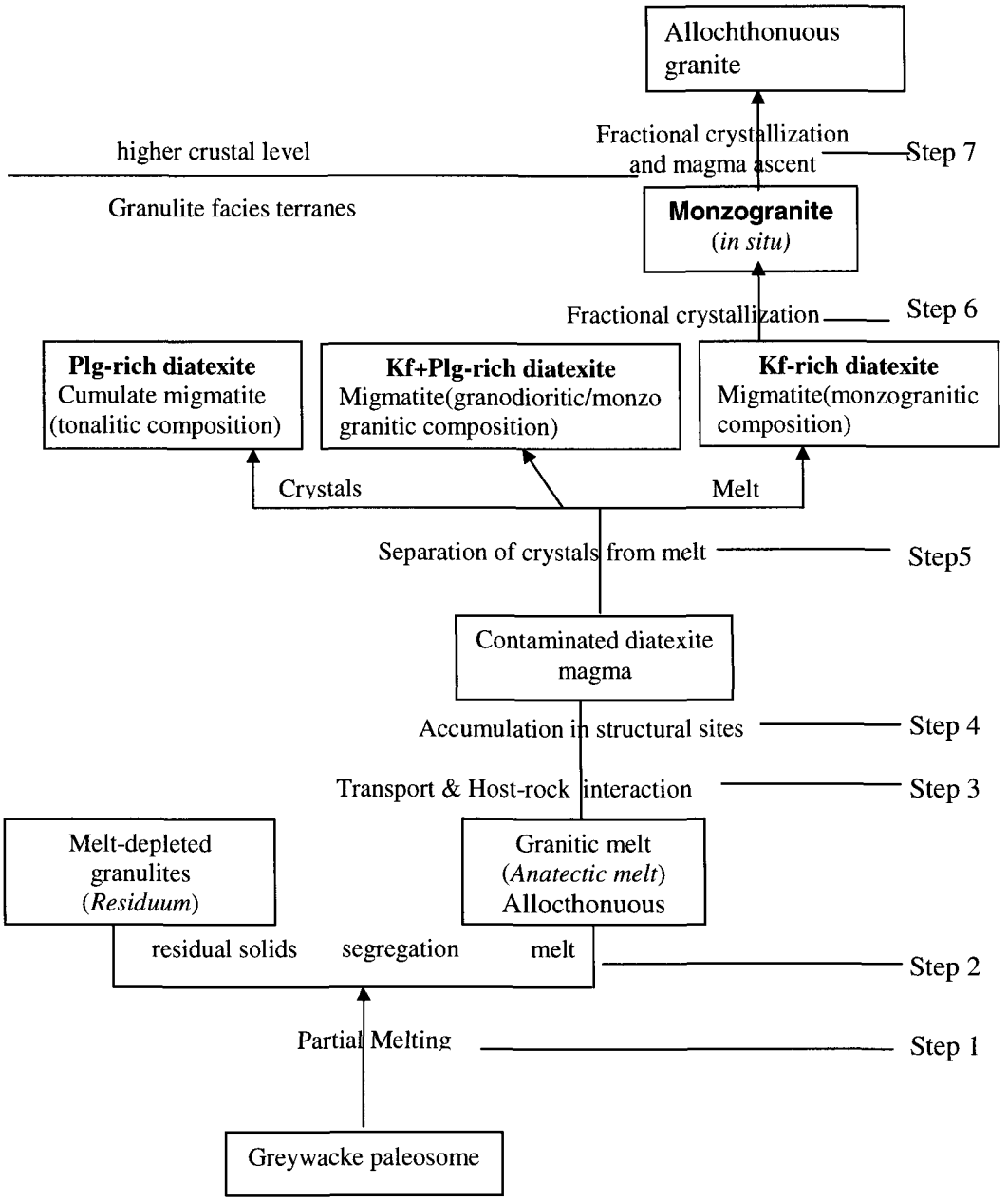

Figure 48: A model for the formation of migmatites and granitic magmas in melt-depleted, granulite facies terranes, such as the Ashuanipi subprovince.

6.4 THE OPEN SYSTEM BEHAVIOUR IN THE ASHUANIPI AND THE EFFECT OF FLUIDS ON GRANULITIC ROCKS

Some migmatites evidently formed as crustal-scale, closed systems (e.g. Dougan 1981; Olsen 1982; Sawyer & Barnes 1988; Sawyer 1998; Milord *et al.* 2001), whereas others formed in open systems at smaller scales, recording petrological and / or geochemical evidence of melt loss (e.g. Weber *et al.* 1985; Barbey *et al.* 1990; Hansen & Stuk 1993; Nyman *et al.* 1995; Hartel & Pattison 1996; Sawyer 1998; Kriegsman 2001; Solar & Brown 2001). For crustal differentiation to occur, open system behaviour is required, with transport of substantial melt volumes on a scale of kilometers (Droop *et al.* 2003). If no melt is lost from granulite facies rocks, high-grade anhydrous assemblages may very well be completely retrogressed on cooling and converted to hydrous ones typical of the upper amphibolite facies (Powell 1983; Powell & Downes 1990; Spear *et al.* 1999; White *et al.* 2001).

Although, a minor degree of hydrous retrogression is common in the Ashuanipi granulites, the extent of such retrogression is very small, thus, anatexis and crustal reworking in the Ashuanipi was an open system process with the loss of water presumably in the felsic melt. Melt loss may also have a profound effect on the response of lower crustal rocks to deformation.

The absence of melt at high temperatures will inevitably affect the rheology of the lower crust, making it stronger than melt bearing equivalents (van der Molen & Patterson 1978; White & Powell 2002). In contrast, if the melt accumulates in the

source, this will lead to a weaker lower crust (Huerta *et al.* 1996; Ellis *et al.* 1998; Rushmer 2001). However, the recent study by Rosenberg & Handy (2005) indicates that the major decrease in the strength of the continental crust as it undergoes anatexis likely does not occur when the morphological transition from metatexite-diatexite happens, but occurs beforehand, at much lower fractions of melt. This may mean that the loss of strength occurs ubiquitously soon after partial melting has started and is not limited to the cases where anatexis advances to 0.25 melt fraction or higher.

The distribution of melt within the rocks of the Ashuanipi subprovince has some interesting implications for understanding the behaviour of the lower crust during orogenic deformation. The melt-depleted rocks contain only about 2 % melt that is located on their grain boundaries (see chapter III). Since this is just below the melt connectivity transition (7 % melt) defined by Rosenberg & Handy (2005), the melt-depleted metatexite migmatites were probably still mechanically strong layers. However, the diatexite migmatites form laterally continuous layers that contained in excess of 25 vol. % melt (some may even have been essentially 100 % melt). These layers had a melt fraction above both the melt connectivity transition and the solid-to-liquid transition (about 35 % melt) of Rosenberg & Handy (2005), therefore, they would have had only a tiny fraction of the strength of the metatexite migmatites, at least until they were nearly fully crystallized. Consequently, the overall deformational style of the granulite facies crust in the Ashuanipi subprovince must have been controlled by the layers of weak diatexite migmatite. Strain would have been strongly partitioned into the weaker diatexite layers. This indeed appears to have been the case, because the evidence for syn-anatectic deformation is widely preserved in the diatexite migmatites

as a syn-magmatic foliation, as asymmetric enclaves, as foliation fish and as rotated and tiled enclaves. In contrast, evidence for syn-anatectic deformation is exceedingly rare in the metatexite migmatites.

6.5 CONCLUSIONS

This study has demonstrated that the granulite facies Ashuanipi subprovince of northern Quebec produced a very large volume of granite melt. Field and petrographic observations combined with geochemical data indicates an initially simple history with the nearly complete extraction of the anatectic melt from its metagreyacke source, leaving behind a melt-depleted plagioclase + orthopyroxene granulite. However, the fate of the anatectic melt, and the sequence by which it evolves to monzogranite is much more complex. Initially, the composition of the magma was modified by contamination with the wall rocks of the dykes that it flowed through. Then, as crystallization began, separation of the crystals from the magma contributed to further diversity in magma composition and to the microstructure of the rocks derived from it, notably producing a variety of feldspar cumulates. The final stages of the evolution of the anatectic rocks are dominated by fractional crystallization that yields leucomonzogranite.

CHAPTER VII

GENERAL CONCLUSIONS

The objective from this study was to document the formation and the evolution of anatectic melt derived from a granulite facies, psammitic protolith that shows the transition from metatexite to diatexite migmatite and through to granite. The example used is the Ashuanipi subprovince of the Superior Province in northern Quebec. Field, petrographic and geochemical methods were used to; 1) define the protolith and to determine how much granitic melt formed and was then extracted from the residual rocks in the granulite facies terrane, 2) determine how the anatectic melt moved out of the source and what the length-scale of the flow paths were during the melt extraction stage, 3) determine which processes, such as contamination, crystal accumulation, fractional crystallization may have modified the initial composition of the anatectic melt that was extracted from the residuum and, 4) determine the genetic relationship between migmatites and granites in the region. The main findings and contributions from this study can be summarized as follows:

1. The Ashuanipi subprovince is a large, high-grade, granulite facies terrane; containing abundant partially melted metagreywackes that contain the paragenesis orthopyroxene + biotite + plagioclase + quartz + former melt +/- garnet.

2. Anatexis occurred principally through the dehydration melting reaction:

biotite + quartz + plagioclase = melt + orthopyroxene + oxides

In the simple plagioclase + biotite + quartz protoliths, the modal orthopyroxene content can be used to constrain the degree of partial melting.

3. The peak metamorphic conditions at anatexis in the Ashuanipi subprovince reached temperatures of at least 820°C (opx-in), and may have locally exceeded 900°C (biotite-out), with pressure in the range of 6 to 7 kbar.

4. An estimated 640 000 km^3 (based on an average of 31 wt % partial melting) of garnitic magma was segregated from the metagreywackes leaving behind melt-depleted residual rocks that are enriched in MgO, FeO, CaO and Sr, but depleted in K_2O, SiO_2, Cs and U.

5. The presence of layers of residual metagreywacke that are without leucosomes indicates that the melt extraction process occurred without destroying the bedding in the protolith and hence involved the pervasive grain boundary (porous) flow of melt over short (up to 50 cm) distances from the site of melting to nearby dilatant structures. In some outcrops, the nature and distribution of leucosomes is interpreted to show that melt moved through a network of interconnected and structurally controlled conduits. Thus, segregation of melt began in a dispersed flow regime on the grain boundaries then, switched to a channel flow regime when it entered dilatant structures.

6. Only minor amounts of residuum material remained in the leucosomes found in the residual metatexite migmatites and this indicates that the separation of the melt fraction from its residual solid fraction in the Ashuanipi subprovince was a very effective process. Furthermore, petrographic evidence in the melt-depleted rocks (residual metagreywackes) show that very little (only a few percent) anatectic melt

remained on the grain boundaries, evidence that melt extraction during granulite facies biotite-dehydration melting at mid-crustal levels can be, essentially, complete even if the ΔV of the reaction is zero.

7. As the extracted anatectic melt moved through the source region and pooled or was redistributed into large low pressure sites it became contaminated with some of the residuum that it passed through. These bodies of contaminated anatectic melt formed the diatexite magma from which the diatexite migmatites were formed. The solid and melt fractions in the diatexite magma became progressively separated during flow and crystallization of the diatexite magma and so generated crystal-enriched and a melt-enriched diatexites. Plagioclase-rich diatexites are contaminated cumulate rocks composed principally of plagioclase crystallized from the anatectic melt, whereas the K-feldspar rich diatexite is consistent with the putative liquid lost from these rocks. Plagioclase + K-feldspar-rich diatexites are approximately the composition of the contaminated anatectic melt.

8. The diatexite magma was also parental to the monzogranites, as can be readily inferred from the *in situ* patches in the larger bodies of diatexite migmatite. The range of monzogranite is consistent with a derivation from a common parent that resembled the evolved diatexite migmatites.

9. Most of the diatexite magmas in the Ashuanipi are modified by the effects of fractional crystallization and very few actually preserve primary melt compositions. Geochemical modelling of the diatexite migmatites and monzogranites show that for

both major and trace elements, most diatexites and few granites have the geochemistry of contaminated cumulates (accumulations of plagioclase + quartz plus a trapped liquid), whereas, others represent fractionated or, evolved granitic melts.

10. There is a morphological, mineralogical and geochemical continuity from metatexite migmatite (depleted granulites, chapter III) to diatexite migmatites and anatectic granites in the Ashuanipi subprovince (chapters IV and V). The effects of hydrous retrogression are very minor in the granulites of the Ashuanipi subprovince, consistent with the loss of water with the anatectic melt. However, anatexis and crustal reworking in the Ashuanipi were open system process.

APPENDIX I

ABBREVIATIONS FOR MINERALS USED IN THE TEXT AND THE FIGURES

Abbreviation	Mineral
Ab	Albite
An	Anorthite
Bte	Biotite
Cpx	Clinopyroxene
K-fsp	Feldspar
Opx	Orthopyroxene
Or	Orthoclase
Plg	Plagioclase
Qtz	Quartz

APPENDIX II

LIST FOR ABBREVIATIONS USED IN TEXT, FIGURES AND TABLES

Abbreviation	Meaning
A	Metagreywacke (Mg # =49)
B	Metagreywacke (Mg # =62)
BPQII	Biotite+ Plagiocalse +Quartz II
C	Metagreywacke (Mg # =81)
CEVP	Starting glass
HFSE	High Field Strength Elements
HREE	Heavy Rare Earth Elements
HSHP	High silica High Potassium
INAA	Instrumental Neutral Activation Analysis
LILE	Large Ion Lithophile Elements
LREE	Light Rare Earth Elements
LSLP	Low Silica Low Potassium
M/B	Melt-Biotite ratio
M/O	Melt-Orthopyroxene ratio
Ma	Million Years
MCT	Melt Connectivity Transition
MRNQ	Ministère des Ressources Naturelles du Québec
NB	Natural Biotite
Q	Quetico
RCMP	Rheological Critical Melt Percentage
SBAG	Synthetic Biotite Annite Gneiss
SBG	Synthetic Biotite Gneiss
SFAG	Synthetic F-annite Gneiss
SHRIMP	Sensitive High Resolution Ion MicroProbe
SLT	Solid to Liquid Transition
SMAG	Synthetic Magnesian-Annite Gneiss
UQAC	Universitédu Québec a Chicoutimi
XRF	X Ray Fluorescence

APPENDIX III

THE QUETICO METAGREYWACKE WHOLE ROCK COMPOSITIONS

(from Sawyer (1986) and unpublished data)

Whole rock major and trace element compositions of 13 metagreywacke rocks from the Quetico subprovince

Sample	es356	es357	es360	es362	es363	es36	es353	es366	es367	es98	es373	es126	es280A
SiO2(Wt %)	65,49	66,14	63,28	64,44	66,20	68,49	67,44	64,70	66,84	71,02	64,42	67,00	64,20
TiO2	0,57	0,52	0,69	0,58	0,56	0,51	0,53	0,66	0,56	0,46	0,65	0,58	0,75
Al2O3	15,73	15,60	17,71	15,98	15,74	14,86	15,09	16,51	15,58	13,95	16,31	15,65	15,42
FeO*	5,69	5,56	7,30	6,66	5,99	4,62	5,74	7,42	5,79	4,40	5,29	5,13	6,12
MnO	0,09	0,09	0,06	0,09	0,09	0,07	0,09	0,08	0,10	0,12	0,08	0,08	0,08
MgO	3,54	3,05	3,73	3,20	2,45	2,51	2,55	2,91	2,40	1,64	2,87	3,19	3,70
CaO	2,72	2,78	1,84	3,37	2,74	2,85	2,70	1,53	2,79	5,18	3,86	2,54	3,72
Na2O	3,96	3,87	2,31	3,57	3,79	3,62	3,55	3,49	3,36	0,94	4,02	3,55	2,94
K2O	2,01	2,24	2,91	1,96	2,29	2,31	2,16	2,57	2,44	2,13	2,27	2,09	2,88
P2O5	0,19	0,15	0,15	0,14	0,14	0,16	0,15	0,13	0,13	0,14	0,23	0,19	0,20
LOI	1,66	0,79	2,58	1,79	1,18	1,45	1,62	0,80	1,15	2,31	0,70	1,65	0,63
Total	101,66	100,79	102,58	101,79	101,18	101,45	101,62	100,80	101,15	102,31	100,70	101,65	100,63
Mg Number	52,57	49,42	53,00	47,66	46,11	42,13	49,21	41,10	42,53	44,18	49,19	52,58	51,82
Cr (ppm)	228	dl	169	dl	115	180	166	dl	153	138	dl	166	182
Ni	dl	55	89	58	44	dl	dl	70	dl	45	59	dl	92
Co	dl	dl	27,1	dl	20,1	dl	dl	dl	dl	15,9	dl	dl	30,0
Sc	14,6	dl	22,8	dl	13,1	12,0	12,3	dl	14,0	13,4	dl	12,0	19,0
Ba	524	604	690	517	469	634	554	857	588	382	809	846	1514
Rb	73	73	92	70	73	81	69	85	89	88	75	108	122
Sr	449	371	335	318	304	430	359	238	224	234	570	394	495
Y	12	16	22	16	16	12	13	18	14	22	17	13	19
Zr	142	135	130	137	150	143	150	158	144	158	166	190	150
Nb	dl	5,1	8,3	6,2	6,1	dl	dl	dl	dl	6,2	dl	dl	7,1
Hf	3,16	dl	3,32	dl	3,67	3,24	3,05	dl	3,68	3,71	dl	3,36	3,55
Cs	6,12	dl	5,39	dl	5,20	5,07	5,08	dl	2,05	3,30	dl	24,47	15,19
Ta	0,41	dl	0,41	dl	0,41	0,30	0,61	dl	0,72	0,52	dl	0,20	0,41
U	1,84	dl	2,07	dl	2,34	1,22	1,32	dl	1,84	2,58	dl	2,75	2,53
Th	5,82	dl	8,19	dl	8,46	5,07	6,19	dl	6,24	8,65	dl	10,09	6,99
La	29,99	dl	29,02	dl	30,48	31,01	30,36	dl	30,69	39,26	dl	32,83	24,01
Ce	55,09	dl	57,52	dl	56,27	54,73	57,87	dl	56,26	69,75	dl	63,11	49,53
Nd	23,97	dl	25,60	dl	22,32	22,90	23,15	dl	24,75	27,92	dl	26,51	22,89
Sm	4,59	dl	5,14	dl	4,17	4,32	4,49	dl	4,39	4,84	dl	4,81	4,58
Eu	1,22	dl	1,23	dl	1,31	1,11	1,22	dl	1,53	1,17	dl	0,97	1,30
Tb	0,48	dl	0,63	dl	0,42	0,34	0,44	dl	0,41	0,56	dl	0,33	0,55
Yb	1,43	dl	1,59	dl	1,04	1,11	1,32	dl	1,33	1,98	dl	1,57	1,21
Lu	0,22	dl	0,27	dl	0,22	0,17	0,24	dl	0,21	0,35	dl	0,18	0,23

abbreviations: dl=below detection limit,

APPENDIX IV

THE QUETICO METAPELITE WHOLE ROCK COMPOSITIONS

(data from Sawyer (1986) and unpublished data)

Whole rock major and trace element compositions of 7 metapelite rocks from the Quetico subprovince

Sample	es358	es361	es364	es365	es82	es103	es306A
SiO2 (Wt %	58,29	58,42	58,63	59,13	58,80	57,48	58,78
TiO2	0,68	0,69	0,69	0,67	0,62	0,63	0,43
Al2O3	17,63	18,14	17,47	16,82	16,50	16,77	19,55
Fe2O3	1,15	1,32	1,28	1,28	1,75	2,38	0,90
FeO	5,86	6,71	6,52	6,52	8,90	12,14	4,58
MnO	0,11	0,09	0,08	0,08	0,11	0,11	0,08
MgO	4,02	3,69	4,09	4,32	3,89	3,55	3,26
CaO	2,93	1,59	1,43	1,18	1,42	0,89	2,20
Na2O	3,66	2,47	1,11	1,13	2,42	0,61	3,25
K2O	2,65	3,75	5,68	5,10	3,07	3,63	3,88
P2O5	0,19	0,15	0,17	0,13	0,20	0,20	0,19
LOI	1,82	3,03	2,57	2,46	2,04	1,78	2,34
Total	98,99	100,04	99,71	98,82	99,72	100,17	99,44
Mg Number	50,96	45,45	48,74	50,07	39,83	30,70	51,87
Cr (ppm)	171	183	207	dl	197	206	56
Ni	dl	dl	dl	91	dl	dl	31
Co	dl	dl	dl	dl	dl	dl	12,5
Sc	20,4	23,1	23,3	dl	20,7	21,4	8,0
Cu	dl	dl	dl	29	dl	dl	23
Pb	n.a.	n.a.	n.a.	n.a.	n.a.	n.a.	n.a.
Zn	dl	102	100	dl	137	86	dl
Rb	93	112	158	128	115	121	112
Cs	3,00	6,00	7,00	dl	8,00	9,00	5,50
Ba	610	717	572	692	846	563	1280
Sr	450	244	157	107	240	73	375
Ga	n.a.	n.a.	n.a.	n.a.	n.a.	n.a.	n.a.
Ta	0,70	0,40	0,40	dl	0,30	0,52	0,60
Nb	dl	dl	dl	7,0	dl	dl	8,0
Hf	2,90	2,90	2,90	dl	3,00	2,70	4,00
Zr	139	124	125	124	135	113	136
Y	16	17	17	21	19	17	16
Th	6,50	6,60	6,60	dl	7,30	6,70	26,70
U	1,70	5,60	1,90	dl	1,70	1,90	8,50
La	22,90	28,80	24,30	dl	28,20	26,10	50,90
Ce	48,00	59,00	54,00	dl	64,00	56,00	84,80
Nd	21,50	28,30	41,70	dl	29,80	24,20	29,90
Sm	4,53	4,69	4,76	dl	5,39	4,98	5,31
Eu	1,30	1,10	1,00	dl	1,60	1,40	1,33
Tb	0,41	0,50	0,47	dl	0,69	0,42	0,41
Yb	1,40	1,80	1,90	dl	2,00	1,60	1,01
Lu	0,25	0,22	0,22	dl	0,34	0,28	0,18

abbreviations: dl=below detection limit, n.a.=not analyzed

APPENDIX V

WHOLE ROCK COMPOSITIONS OF METAGREYWACKE ROCKS FROM THE ASHUANIPI SUBPROVINCE

(from Percival, 1991b and Lapointe, 1996)

Whole rock compositions of metagreywacke rocks from the Ashuanipi subprovince (Percival, 1991b and Lapointe, 1996)

Sample	JP76	JP157	JP184	JP199	JP248	JP266	JP297	JP343	BL18	BL19	BL21	BL22	BL29	BL34	BL35	BL38	BL39	BL45	BL54	BL56	BL58	BL65	BL66	BL75
SiO2 (Wt%)	57,60	64,90	60,30	64,10	64,40	68,00	66,90	67,10	65,10	65,10	64,50	65,50	62,60	62,50	58,80	55,40	62,30	55,00	63,30	58,60	68,80	59,20	59,80	68,60
TiO2	0,83	0,55	0,72	0,54	0,55	0,48	0,55	0,52	0,53	0,58	0,57	0,60	0,67	0,70	0,72	0,81	0,72	0,89	0,59	0,74	0,43	0,71	0,69	0,44
Al2O3	18,10	15,80	19,00	16,00	16,30	15,00	14,70	16,30	16,50	16,60	16,60	16,30	17,00	17,60	17,80	17,20	14,90	17,10	16,30	17,10	15,20	15,80	16,20	15,40
Fe2O3	2,20	1,10	1,70	1,70	0,90	0,70	1,50	0,90	0,83	0,81	1,01	0,93	1,00	1,26	1,16	1,51	1,31	1,87	1,06	1,25	0,73	1,38	1,48	0,65
FeO	6,00	4,00	4,10	4,90	4,40	4,70	4,80	3,70	4,21	4,11	5,15	4,72	5,10	6,41	5,91	7,71	6,66	9,52	5,42	6,36	3,72	7,05	7,54	3,31
MnO	0,10	0,06	0,07	0,01	0,06	0,08	0,08	0,04	0,05	0,04	0,05	0,06	0,06	0,07	0,09	0,10	0,09	0,11	0,11	0,06	0,04	0,09	0,09	0,04
MgO	4,40	2,62	3,34	2,86	2,67	2,45	2,66	2,43	2,17	2,51	3,09	2,74	3,05	3,81	3,28	5,04	5,25	4,76	2,58	4,11	1,85	4,30	4,42	1,74
CaO	2,13	2,58	1,81	2,53	3,31	3,10	2,68	2,92	2,65	2,13	1,80	2,25	2,36	1,50	2,77	3,39	2,37	3,54	2,70	3,23	1,77	3,37	3,29	2,81
Na2O	3,10	3,60	3,40	3,30	3,90	3,40	3,50	4,10	4,20	3,61	3,06	3,42	3,72	2,96	3,46	3,37	2,72	2,67	3,35	3,73	3,29	3,32	3,81	4,11
K2O	3,44	3,24	4,11	2,30	2,28	1,47	1,50	1,94	3,04	2,65	2,64	2,75	3,55	3,43	4,17	2,74	2,58	2,99	2,98	3,12	3,36	2,84	2,20	1,67
P2O5	0,09	0,10	0,09	0,01	0,17	0,11	0,09	0,08	0,12	0,06	0,05	0,08	0,08	0,05	0,16	0,13	0,07	0,20	0,15	0,14	0,05	0,09	0,09	0,05
LOI	1,60	0,80	1,30	1,10	1,10	0,70	0,90	0,70	0,55	0,20	0,14	0,44	0,37	0,55	0,39	0,85	0,35	0,73	1,11	0,21	0,52	1,67	0,27	0,41
Total	99,59	99,35	99,94	99,35	100,04	100,19	99,86	100,73	99,94	98,39	98,66	99,78	99,56	100,84	98,71	98,25	99,32	99,38	99,66	98,64	99,76	99,82	99,88	99,22
Mg Number	49,56	48,34	51,39	44,22	47,73	45,03	43,53	48,98	43,86	48,08	47,61	46,80	47,53	47,38	45,68	49,75	54,41	43,10	41,88	49,47	42,94	48,03	47,03	44,35
Cr (ppm)	260	130	190	140	120	110	210	110	184	294	389	308	315	361	260	347	333	348	370	234	222	292	344	130
Ni	100	21	30	54	75	30	70	44	28	22	53	42	60	85	107	180	55	197	102	124	74	181	140	66
Co	30,0	14,0	15,0	20,0	22,0	16,0	26,0	18,0	20,2	14,5	15,0	21,2	29,6	28,0	26,0	35,0	26,7	33,4	22,0	27,0	19,8	33,0	31,0	18,0
Sc	n.a.	n.a.	n.a.	n.a.	n.a.	n.a.	n.a.	n.a.	13,6	14,5	18,0	15,4	17,1	20,9	21,2	23,7	21,8	25,2	19,7	18,6	10,0	20,0	21,0	11,7
Cu	63	29	12	34	61	35	100	25	n.a.	n.a.	n.a.	n.a.	n.a.	n.a.	n.a.	n.a.	n.a.	n.a.	n.a.	n.a.	n.a.	n.a.	n.a.	n.a.
Pb	n.a.	n.a.	n.a.	n.a.	n.a.	n.a.	n.a.	n.a.	n.a.	n.a.	n.a.	n.a.	n.a.	n.a.	n.a.	n.a.	n.a.	n.a.	n.a.	n.a.	n.a.	n.a.	n.a.	n.a.
Zn	73	57	0	58	64	50	63	86	n.a.	n.a.	n.a.	n.a.	n.a.	n.a.	n.a.	n.a.	n.a.	n.a.	n.a.	n.a.	n.a.	n.a.	n.a.	n.a.
Rb	138	99	138	92	77	73	82	71	104	98	110	99	151	50	82	110	72	130	119	90	98	133	85	42
Cs	n.a.	n.a.	n.a.	n.a.	n.a.	n.a.	n.a.	n.a.	1,1	0,6	1	1,5	1,7	1,1	1,10	2,50	1,10	3,50	2,50	2,90	1,10	7,00	1,10	0,60
Ba	994	861	784	521	661	371	584	561	1108	998	991	894	1089	941	1201	687	335	907	880	588	699	860	708	303
Sr	518	429	429	333	361	400	451	464	555	456	379	552	560	401	473	466	273	294	548	390	304	563	400	445
Ga	n.a.	n.a.	n.a.	n.a.	n.a.	n.a.	n.a.	n.a.	n.a.	n.a.	n.a.	n.a.	n.a.	n.a.	n.a.	n.a.	n.a.	n.a.	n.a.	n.a.	n.a.	n.a.	n.a.	n.a.
Li	n.a.	n.a.	n.a.	n.a.	n.a.	n.a.	n.a.	n.a.	n.a.	n.a.	n.a.	n.a.	n.a.	n.a.	n.a.	n.a.	n.a.	n.a.	n.a.	n.a.	n.a.	n.a.	n.a.	n.a.
Ta	n.a.	n.a.	n.a.	n.a.	n.a.	n.a.	n.a.	n.a.	0,3	0,4	0,3	0,5	0,5	0,3	0,7	0,5	0,5	0,6	0,4	0,4	0,3	0,7	0,4	0,4
Nb	n.a.	n.a.	n.a.	n.a.	n.a.	n.a.	n.a.	n.a.	n.a.	n.a.	n.a.	n.a.	n.a.	n.a.	n.a.	n.a.	n.a.	n.a.	n.a.	n.a.	n.a.	n.a.	n.a.	n.a.
Hf	n.a.	n.a.	n.a.	n.a.	n.a.	n.a.	n.a.	n.a.	5,8	4,6	5,3	4,5	4,9	4,3	3,7	3,8	4,6	4,0	4,3	3,7	4,9	3,9	3,7	3,8
Zr	136	120	174	147	120	162	176	121	206	181	160	117	168	109	190	80	212	50	170	92	202	94	196	146
Y	17	10	15	26	10	14	14	6,5	n.a.	n.a.	n.a.	n.a.	n.a.	n.a.	n.a.	n.a.	n.a.	n.a.	n.a.	n.a.	n.a.	n.a.	n.a.	n.a.
Th	n.a.	n.a.	n.a.	n.a.	n.a.	n.a.	n.a.	n.a.	14,9	11,4	8,40	11,2	13,2	7,40	8,6	9,0	12,6	4,7	10,1	8,5	10,90	8,20	7,40	7,20
U	n.a.	n.a.	n.a.	n.a.	n.a.	n.a.	n.a.	n.a.	2,10	1,51	0,5	2,2	1,6	0,5	0,5	0,8	1,7	0,4	0,7	0,5	0,80	0,90	0,80	0,90
La	33	20	34	29	24	26	35	29	44	39	34	34	39	30	30,6	31,6	40,4	27,2	32,5	61,10	32,90	30,80	28,20	25,20
Ce	71	48	77	61	57	62	73	58	88	81	66	68	77	63	66,5	69,3	83,9	54,7	67,9	64,20	68,70	67,00	61,60	51,90
Nd	35	23	36	27	27	27	30	26	34	31	25	27	31	17	14,0	23,6	23,8	24,2	30,1	19,30	24,20	24,60	23,90	18,70
Sm	5,3	3,8	4,7	3,7	4	3,8	3,9	2,7	4,7	4,5	3,8	3,8	4,2	3,7	4,3	4,3	4,6	4,0	4,2	7,00	3,20	4,10	3,80	2,80
Eu	1,3	1	1,4	0,9	1,2	1	1,1	1,2	1,3	1,5	1,4	1,2	1,3	1,3	1,4	1,5	1,3	1,5	1,3	1,50	1,10	1,50	1,40	1,20
Tb	0	0	0	0	0	0	0	0	0,4	0,4	0,5	0,4	0,4	0,6	0,6	0,6	0,7	0,6	0,6	0,40	0,40	0,40	0,40	0,40
Yb	1,4	1,1	1,3	2,9	0,8	1,2	1,4	0,5	1,5	1,3	1,9	1,6	1,5	1,3	0,9	1,4	1,4	1,9	2,3	0,50	1,00	0,70	1,00	1,30
Lu	n.a.	n.a.	n.a.	n.a.	n.a.	n.a.	n.a.	n.a.	0,2	0,2	0,3	0,2	0,2	0,2	0,2	0,2	0,3	0,3	0,3	0,10	0,20	0,10	0,10	0,20

Abbreviations: n.a.=not analyzed, JP=John percival samples, BL=Bernard Lapointe samples

APPENDIX VI

MELT-BIOTITE (M/B) AND MELT-ORTHOPYROXENE (M/O) RATIOS FROM DIFFERENT EXPERIMENTAL RUNS (CHAPTER III)

Starting composition	Pressure	M/B	M/O	Author
SBG	7 kbars	1,61	2,63	Patiño Douce & Beard (1995)
TiO_2 bearing compositions	8 kbars	1,60	3,60	Montel & Vielzeuf (1997)
NB	5 kbars	1,61	2,67	Stevens *et al.*, (1997)
NB	10 kbars	1,10	3,15	Stevens *et al.*, (1997)
BPQII	10 kbars	1,30		Gardien *et al.*, (1995)
TiO_2 free compositions	5 kbars	(0,77-1,3)	(0,97-1,3)	Stevens *et al.*, (1997)
TiO_2 free compositions	10 kbars	(0,5-0,8)	(0,83-1,14)	Stevens *et al.*, (1997)

APPENDIX VII

WHOLE ROCK COMPOSITIONS OF DIATEXITE MIGMATITE ROCKS FROM THE ASHUANIPI SUBPROVINCE

(from Percival, 1991b and Lapointe, 1996)

Whoe rock major and trace elements of diatexite migmatites from the Ashuanipi subprovince (Percival, 1991b, and Lapointe, 1996)

Sample	JP18	JP52	JP126	JP160	JP179	JP189	JP198	JP230	JP285	JP334	JP338	JP54	JP99	JP121	JP163	JP218	JP337	JP342	BL1	BL17	BL20	BL30	BL33	BL36
SiO2(wt%)	61,50	61,84	66,81	65,74	67,49	64,71	69,17	64,22	69,02	67,77	68,13	66,19	63,34	63,43	68,32	68,56	65,25	68,15	55,70	51,99	66,68	57,95	68,47	56,60
TiO2	0,67	0,81	0,64	0,71	0,61	0,63	0,41	0,51	0,47	0,48	0,38	0,86	0,71	1,14	0,47	0,41	0,40	0,44	0,91	1,01	0,24	0,73	0,44	0,65
Al2O3	16,93	17,48	16,14	16,08	15,30	16,58	15,67	16,76	15,59	15,44	15,91	15,79	16,93	16,60	16,48	15,42	17,89	15,84	18,30	18,86	8,99	18,67	15,62	15,29
Fe2O3	1,53	1,02	0,81	1,01	0,61	1,41	0,40	0,91	0,61	1,00	0,60	1,72	1,53	0,20	0,50	0,41	0,40	0,91	1,48	2,04	2,23	1,45	0,67	2,70
FeO	5,71	6,34	3,96	4,35	4,46	4,62	3,34	5,15	3,04	3,81	4,00	3,74	4,08	5,02	2,41	2,43	2,81	3,35	7,55	10,40	11,35	7,41	3,41	13,76
MnO	0,07	0,14	0,05	0,06	0,06	0,10	0,06	0,09	0,04	0,05	0,07	0,06	0,03	0,03	0,02	0,02	0,04	0,05	0,08	0,08	0,11	0,12	0,06	0,12
MgO	3,81	3,07	2,54	2,79	2,61	2,63	1,89	3,01	1,94	2,43	2,29	2,03	2,85	2,58	1,51	1,72	1,92	2,10	5,07	4,20	2,56	3,83	1,54	3,38
CaO	2,96	2,80	2,67	2,39	2,87	2,52	2,75	2,48	2,49	3,22	3,21	2,30	2,81	2,56	2,42	1,12	2,62	3,51	3,36	2,40	6,04	3,47	2,08	3,95
Na2O	3,88	3,68	3,86	3,54	3,75	3,62	3,84	3,53	4,05	3,91	4,10	3,74	3,98	3,48	3,82	2,43	4,22	4,37	3,93	1,42	1,21	3,47	4,25	2,46
K2O	2,86	2,75	2,37	3,24	2,18	3,09	2,39	3,25	2,69	1,83	1,25	3,48	3,58	4,48	3,96	7,41	4,36	1,17	3,49	7,52	0,40	2,76	3,43	0,88
P2O5	0,08	0,07	0,15	0,09	0,06	0,08	0,07	0,08	0,07	0,06	0,06	0,08	0,16	0,47	0,09	0,07	0,07	0,10	0,12	0,08	0,19	0,13	0,03	0,21
LOI	1,20	0,80	1,20	1,00	1,00	1,10	1,00	0,90	1,00	0,80	0,80	1,00	0,90	1,10	0,80	0,90	0,70	0,70	0,67	1,22	0,35	0,56	0,56	0,64
Total	101,20	100,80	101,20	101,00	101,00	101,10	101,00	100,90	101,00	100,80	100,80	101,00	100,90	101,10	100,80	100,90	100,70	100,70	100,67	101,22	100,35	100,56	100,56	100,64
Mg Number	48,95	42,95	49,09	48,61	48,21	44,34	47,66	47,33	49,15	47,85	47,34	40,65	48,17	46,92	48,40	52,33	51,86	47,30	50,44	37,96	25,48	43,90	40,62	27,10
Cr(ppm)	153	n.a.	173	121	122	121	131	86	111	95	79	101	163	184	74	62	83	90	373	422	252	359	145	290
Ni	40	75	46	54	55	55	32	55	43	63	41	48	44	57	20	23	28	46	169	170	26	39	32	90
Co	20	24	16	18	20	21	15	22	16	20	18	19	19	22	11	13	14	18	27	37	12	22	10	19
Sc	n.a	n.a	n.a	n.a	n.a	n.a	n.a	n.a	n.a	n.a	n.a	n.a	n.a	n.a	n.a	n.a	n.a	n.a	16	26	11	24	8	21
Cu	57	55	34	32	52	48	21	30	27	46	53	52	33	35	17	8	10	33	n.a	n.a	n.a	n.a	n.a	n.a
Zn	83	63	61	71	64	74	36	72	56	72	64	80	74	123	34	38	54	64	n.a	n.a	n.a	n.a	n.a	n.a
Rb	83	88	108	131	69	100	71	105	88	48	88	95	137	175	132	211	138	76	181	335	30	136	32	43
Cs	n.a	n.a	n.a	n.a	n.a	n.a	n.a	n.a	n.a	n.a	n.a	n.a	n.a	n.a	n.a	n.a	n.a	n.a	3,24	3,87	0,69	2,55	0,41	3,38
Ba	862	829	485	800	600	770	771	1048	484	594	314	918	1007	1223	1080	2504	1129	413	1228	1859	98	1045	933	517
Sr	493	472	421	441	403	440	485	460	338	502	446	439	474	418	536	596	550	538	588	124	132	464	441	249
Ta	n.a	n.a	n.a	n.a	n.a	n.a	n.a	n.a	n.a	n.a	n.a	n.a	n.a	n.a	n.a	n.a	n.a	n.a	0,71	0,51	0,30	0,71	0,10	0,70
Hf	n.a	n.a	n.a	n.a	n.a	n.a	n.a	n.a	n.a	n.a	n.a	n.a	n.a	n.a	n.a	n.a	n.a	n.a	4,65	4,89	2,08	4,39	5,48	3,18
Zr	167	177	170	155	155	188	115	173	157	158	181	241	142	220	137	72	193	137	143	180	40	163	207	85
Y	4	30	16	14	11	25	17	9	8	8	11	3	7	13	4	2	4	11	n.a	n.a	n.a	n.a	n.a	n.a
Th	n.a	n.a	n.a	n.a	n.a	n.a	n.a	n.a	n.a	n.a	n.a	n.a	n.a	n.a	n.a	n.a	n.a	n.a	12,03	11,52	4,95	8,98	24,95	1,39
U	n.a	n.a	n.a	n.a	n.a	n.a	n.a	n.a	n.a	n.a	n.a	n.a	n.a	n.a	n.a	n.a	n.a	n.a	1,01	0,92	0,89	0,51	0,25	0,50
La	40,80	44,98	26,40	35,40	33,44	49,24	28,31	51,49	34,41	39,10	45,02	23,28	27,54	42,01	34,16	21,30	52,28	233,60	38,52	39,66	15,83	33,47	70,29	16,19
Ce	76,49	94,04	53,81	71,81	64,86	100,48	56,63	100,97	69,83	79,20	88,04	40,48	56,09	93,25	69,33	40,57	99,53	467,19	73,50	82,27	35,52	67,24	161,28	34,76
Nd	32,64	42,93	25,38	33,38	29,39	44,21	25,28	43,42	31,37	36,09	37,01	16,19	27,54	49,19	32,15	18,26	39,21	182,82	29,62	37,01	21,07	25,10	23,74	14,20
Sm	4,28	6,13	1,83	5,97	3,55	6,43	3,34	3,43	4,25	5,01	3,90	1,62	3,06	6,05	5,22	0,00	3,52	17,27	4,14	5,20	3,26	3,67	4,56	4,07
Eu	1,12	1,23	0,91	0,91	1,11	1,11	1,11	1,31	0,81	1,20	1,30	1,11	1,02	1,33	1,11	1,12	1,41	2,03	1,82	2,45	1,19	1,63	1,22	1,59
Gd	2,45	5,21	3,35	3,24	2,53	4,32	2,83	3,74	3,24	3,41	2,90	1,11	2,86	6,25	2,71	1,12	2,31	10,05	n.a	n.a	n.a	n.a	n.a	n.a
Tb	n.a	n.a	n.a	n.a	n.a	n.a	n.a	n.a	n.a	n.a	n.a	n.a	n.a	n.a	n.a	n.a	n.a	n.a	0,20	0,31	0,59	0,61	0,20	0,79
Yb	0,20	2,15	1,42	1,62	1,22	3,22	2,02	0,50	0,51	0,50	1,00	0,20	0,31	0,51	0,10	0,10	0,20	0,41	0,40	0,31	2,08	3,57	0,10	2,09
Lu	n.a	n.a	n.a	n.a	n.a	n.a	n.a	n.a	n.a	n.a	n.a	n.a	n.a	n.a	n.a	n.a	n.a	n.a	0,10	0,10	0,30	0,51	0,00	0,30

Abbreviations: n.a.=not analyzed, JP=John percival samples, BL=Bernard Lapointe samples

APPENDICE VIII

RESULTS OF MODAL POINT COUNTING OF THE METAGREYWACKES FROM THE ASHUANIPI SUBPROVINCE (CHAPTER III)

Sample	%plg	%Qz	%Kf	%Opx	%Bte
5185	34,80	28,80	7,80	0,50	28,10
5016	71,80	9,40	0,00	2,30	15,70
5223	61,80	18,90	4,60	5,70	7,80
4019	73,10	6,00	0,00	6,40	13,90
5109	65,80	13,40	0,90	6,50	10,60
7012	80,60	5,90	0,80	7,90	4,60
4169	76,00	3,10	0,00	8,30	12,50
8024	62,30	5,60	0,00	8,30	23,80
227	75,80	5,40	0,00	8,50	9,80
6031	71,70	7,60	0,00	9,20	9,90
7016	72,00	7,60	0,30	4,90	13,70
4174	69,90	4,50	0,30	9,40	15,90
5213	71,60	3,40	0,00	12,30	12,70
5099	57,80	19,40	2,40	13,00	6,20
5213	58,60	14,20	1,70	14,40	10,70
8025	66,20	4,90	0,00	14,40	14,50
5104	55,40	17,10	2,70	16,00	11,20
As-1A	46,90	10,50	0,40	27,00	13,30
5202	52,70	5,40	0,00	28,80	13,30
As-1B	48,60	9,00	0,00	29,00	12,00

APPENDIX IX

RESULTS OF MODAL POINT COUNTING OF THE DIATEXITE MIGMATITES FROM THE ASHUANIPI SUBPROVINCE (CHAPTER IV)

Sample	%plg	%Qz	%Kf	%Opx	%Bte
5032	62,80	26,20	5,60	0,00	5,80
5078	58,00	13,20	5,80	3,80	13,40
5079	59,60	19,40	0,60	10,80	8,40
5095	67,00	8,60	1,00	19,00	3,20
5105	44,40	22,20	30,40	0,00	3,00
5110	54,20	14,60	6,20	0,00	25,00
5186	51,20	18,00	13,00	0,20	16,60
5224	61,00	18,00	4,60	6,20	9,60
5196	54,19	1,00	2,47	20,25	12,34
5109A2	56,00	13,20	5,20	17,40	7,60
5039	60,20	26,80	11,80	0,20	0,60
5022	52,20	16,00	2,20	6,20	16,00
5019	22,40	21,80	42,80	0,60	12,20
5074	67,00	21,00	0,40	0,00	11,40
5076	49,50	42,00	0,00	0,00	8,00
5020	45,00	26,00	19,20	0,00	9,60
1085	60,20	28,00	9,30	0,00	2,20
5016	29,00	26,40	38,20	0,00	6,30
6017	36,30	28,10	27,01	0,10	0,90

APPENDIX X

RESULTS OF MODAL COMPOSITIONS OF THE MONZOGRANITES FROM THE ASHUANIPI SUBPROVINCE (CHAPTER V)

(Eyeball estimates of the modes by Sawyer, unpublished data)

Sample	%Qz	%Pl	%K-fsp	%Bte	%Opx
DL98-5192A	25	25	47	3	0
5029A	27	22	50	1	0
DL98-522A	27	27	42	1	0
DL97-5095C	37	33	30	tr	0
5044A	27	27	41	4	0
60-A	20	15	65	tr	0
2051A	30	37	27	6	0
5109A8	30	35	30	4	1
5003A	25	45	25	5	0
5038A	30	15	55	tr	0
98-5028A	40	15	45	tr	0
97-6016A	27	40	27	6	0
97-6051B	25	35	40	1	0
126-A	28	37	33	2	0
97-6017A	35	33	30	2	tr
RT99-4001-A2	22	35	35	2	5
RT99-3057A	20	40	30	10	tr
RT99-2267A	30	35	25	10	0
RT99-1172A	22	35	35	7	0
RT99-2287A1	22	38	22	5	13

APPENDIX XI

RESULTS OF NORMATIVE COMPOSITIONS OF THE MONZOGRANITES FROM THE ASHUANIPI SUBPROVINCE (CHAPTER V)

calculated by the least square solution to the overestimated mass-balance constraints (Bryan *et al.* 1969)

Sample	Qz	Pl	K-fsp	Opx
2066A	36,22	34,21	30,50	
2074A	33,00	38,47	27,49	
2176A	33,82	34,90	29,46	
2180A	33,41	31,99	34,60	1,08
6016A	24,32	38,52	34,99	2,97
5096A2	27,19	34,91	33,77	4,49
124A	36,48	36,52	24,45	3,34
3014	21,67	42,72	30,78	5,15
1009	24,58	37,46	28,71	7,57
1023	20,72	40,02	34,36	5,03
44	23,98	47,06	20,96	7,60
1025	29,37	40,00	27,13	3,80
1049	29,56	40,09	28,03	2,64
1115	27,88	34,09	32,92	4,34
1117	20,01	37,31	39,11	4,22
2009	20,33	48,92	23,51	6,72
33	22,15	46,70	21,78	8,98
1011	15,35	42,60	23,84	14,92
1054	25,53	47,24	14,18	6,3
2085	19,38	47,82	19,8	6,48

APPENDIX XII

AVERAGE EXPERIMENTAL MELT COMPOSITION FROM GREYWACKE PROTOLITHS

from Patinõ Douce & Beard (1995); Gardien *et al.* (1995) ; Montel & Vielzeuf (1997)

Oxides	Wt %
SiO_2	73,15
TiO_2	0,28
Al_2O_3	14,67
Fe_2O_3	0,00
FeO	1,71
MnO	0,06
MgO	0,84
CaO	1,37
Na_2O	3,14
K_2O	4,78
Total	100,00
Mg Number	46,53

APPENDIX XIII

CALCULATED ELEMENT RATIOS FOR DIATEXITE MIGMATITES (ALL SAMPLES WERE ANALYSED AT UQAC)

Plagioclase-dominated diatexite migmatites

Sample	Rb/Sr	Rb/Cs	Th/U	Eu/Eu*	La/ybN
5078*	0,16	178,72	6,60	1,00	18,84
3095*	0,12	121,95	6,94	0,64	10,55
64*	0,14	133,33	8,18	0,69	37,39
5028*	0,15	54,01	3,87	1,10	11,74
71*	0,10	54,69	3,13	0,95	23,36

Plagioclase+K-feldspar-dominated diatexite migmatites

Sample	Rb/Sr	Rb/Cs	Th/U	Eu/Eu*	La/ybN
5110*	0,26	66,46	9,67	0,80	17,53
5076*	0,26	243,90	4,40	2,30	16,02
5186*	0,21	120,00	21,05	0,65	21,71
5224*	0,36	227,87	29,23	1,36	77,16
1052*	0,14	100,00	3,79	0,82	11,95
123*	0,46	19,09	0,60	0,28	84,18
1035*	0,43	144,93	47,42	0,47	57,61
1040*	0,34	87,08	46,05	1,08	49,16
1047*	0,19	72,98	15,81	1,16	42,10
2047*	0,38	217,24	36,20	0,62	46,37

K-feldspar-dominated diatexite migmatites

Sample	Rb/Sr	Rb/Cs	Th/U	Eu/Eu*	La/YbN
5074*	0,10	0	6,63	1,92	21,63
1118*	0,17	247,62	1,32	3,36	34,56
1017*	0,27	201,69	27,66	0,84	69,73
57*	0,29	59,76	4,52	3,26	25,81

APPENDIX XIV

CALCULATED ELEMENT RATIOS FOR THE MONZOGRANITES

HSHP monzogranites (MgO + FeOt = 2.35 wt % and CaO + Na2O = 5.09 wt %)					
Sample	**Rb/Sr**	**Rb/Cs**	**Th/U**	**EuN/Eu***	**LaN/YbN**
2066A	2,70	0	0	0,65	11,70
2074A	1,70	0	0	0,19	5,78
2176A	1,33	0	0	0,62	18,72
2180A	1,27	0	1,24	0,40	0,00
44*	0,20	73,24	9,26	1,19	28,73
6016A	0,29	194,29	0,00	0,96	0,00
5096A2	0,57	280,00	29,41	0,28	57,21
3014*	0,17	280,85	354,89	0,64	301,01
1009*	0,58	172,95	7,36	0,76	15,00
1023*	0,21	102,44	32,61	1,26	259,79
1049*	0,29	272,34	2,68	3,27	44,81
1115	1,09	585,47	15,02	0,60	42,12
1117*	0,22	272,73	47,39	1,00	112,67
1025*	0,25	140,96	19,92	1,53	82,88
LSLP monzogranites (MgO + FeO = up to 8.28 wt % and CaO + Na2O = 7.35 wt %)					
Sample	**Rb/Sr**	**Rb/Cs**	**Th/U**	**EuN/Eu***	**LaN/YbN**
2009*	0,23	34,84	3,24	1,01	8,91
1011*	0,52	53,96	7,87	0,51	17,28
33*	0,17	91,96	4,30	1,48	27,69
1114	0,26	111,71	8,07	1,09	10,94

APPENDIX XV

PARTITION COEFFICIENTS USED IN CRYSTAL FRACTIONATION MODELS IN DIATEXITE MIGMATITES AND MONZOGRANITES (CHAPTER V)

	Pl (An_{30})	Opx	K-fsp
Ba	0,36	0,02	6,00
Sr	2,84	0,03	3,87
Rb	0,05	0,02	0,80
La	0,26	0,01	n.d
Yb	0,08	0,46	0,01
Eu	2,15	0,07	1,13

Data from Arth (1976). n.d.=no (or limited) data

APPENDIX XVI

MINERAL COMPOSITIONS USED IN MAJOR AND TRACE ELEMENTS MODELLING IN DIATEXITE MIGMATITES AND MONZOGRANITES (CHAPTERS IV & V)

Oxides	Pl (An_{30})	Opx	K-fsp	Bte
SiO_2	61,16	50,62	63,02	36,42
TiO_2		0,03		4,52
Al_2O_3	23,92	2,04	18,44	14,247
FeO	0,06	27,80	0,24	17,53
MgO	0,01	18,90	0,08	12,76
CaO	5,51	0,20	0,01	0,01
Na_2O	8,01	0,01	0,60	0,04
K_2O	0,38	0,02	16,53	10,36
Total	99,06	99,62	98,92	95,89

APPENDIX XVII

MICROPROBE ANALYSES OF PLAGIOCLASE

Carried out at McGill University

Thin sections # 19D, 227, and 5219: metagreywackes from the Ashuanipi subprovince

Thin section # 5212, 5186, and 5042: Diatexite migmatites from the Ashuanipi subprovince

(Acc. Voltage : 15 Kv, Probe Dia : 5, Beam Current: 1.959E-08)

Standard Data for plagioclase

Element	Standard name	Wt.(%)	ZAF Fac.	Z	A	F
1 Na2O	Albite	11.4300	5.4858	10.7252	0.5094	1.0041
2 MgO	Diopside	17.9400	4.7341	7.8691	0.5985	1.0051
3 K2O	Orthoclase	16.9100	1.0758	1.2033	0.8940	1.0001
4 FeO	Fe2O3m	89.9830	0.2140	0.2170	0.9864	1.0000
5 SiO2	Orthoclase	65.0300	3.2797	4.4186	0.7415	1.0011
6 Al2O3	Orthoclase	16.9800	4.3209	5.8692	0.7244	1.0163
7 CaO	Diopside	25.1800	0.8662	0.9351	0.9261	1.0002

#	Na2O(wt%)	MgO(wt%)	K2O(wt%)	FeO(wt%)	SiO2(wt%)	Al2O3(wt%)	CaO(wt%)	Total	Comment
1	7,22	0,00	0,47	0,07	59,46	24,78	6,72	98,72	19dplg-acore1
2	7,26	0,01	0,47	0,06	59,83	25,03	6,77	99,43	19dplg-acore2
3	7,04	0,00	0,48	0,08	59,33	25,03	6,78	98,74	19dplg-acore3
4	7,05	0,00	0,50	0,10	59,46	24,95	6,77	98,83	19dplg-acore4
5	6,98	0,00	0,42	0,11	59,51	24,96	6,89	98,87	19dplg-acore5
6	7,17	0,00	0,40	0,07	59,55	24,90	6,88	98,97	19dplg-acore6
7	7,10	0,00	0,47	0,07	59,22	24,96	6,72	98,54	19dplg2-acore1
8	7,16	0,00	0,45	0,08	58,93	24,68	6,65	97,94	19dplg2-acore2
9	7,16	0,01	0,44	0,08	58,88	24,91	6,74	98,22	19dplg2-acore3
10	7,18	0,00	0,41	0,05	59,18	24,85	6,75	98,42	19dplg2-acore4
11	7,12	0,01	0,38	0,11	58,86	25,13	6,75	98,36	19dplg2-acore5
12	7,14	0,01	0,39	0,12	58,91	25,05	7,05	98,67	19dplg2-acore6
13	7,17	0,01	0,45	0,09	59,42	25,05	6,80	98,98	19dplg3-acore1
14	7,20	0,00	0,46	0,12	59,50	25,02	6,75	99,05	19dplg3-acore2
15	7,36	0,00	0,42	0,10	59,66	24,90	6,84	99,28	19dplg3-acore3
16	7,18	0,01	0,45	0,13	59,54	24,87	6,92	99,09	19dplg3-acore4
17	7,16	0,01	0,37	0,08	59,10	24,95	6,88	98,54	19dplg4-ac1
18	7,18	0,01	0,44	0,10	59,44	25,15	6,96	99,28	19dplg4-ac2
19	7,27	0,00	0,44	0,10	59,76	25,05	6,83	99,45	19dplg4-ac3
20	7,24	0,01	0,39	0,12	59,86	24,90	6,93	99,45	19dplg4-ac4
21	7,14	0,01	0,44	0,13	59,33	25,03	7,01	99,07	19dplg4-ac5
22	7,11	0,00	0,55	0,09	59,72	24,99	6,77	99,23	19dplg-a1c1
23	7,25	0,00	0,51	0,09	60,02	24,80	6,82	99,49	19dplg-a1c2
24	7,06	0,00	0,50	0,11	60,39	24,85	6,71	99,61	19dplg-b1c3
25	7,16	0,00	0,54	0,10	59,67	24,91	6,85	99,23	19dplg-b1c4
26	7,13	0,00	0,51	0,13	59,78	25,01	6,95	99,51	19dplg-b1c5
27	7,11	0,01	0,50	0,14	59,15	25,16	6,95	99,01	19dplg-b1c6
28	7,14	0,00	0,51	0,11	59,38	25,00	6,85	98,99	19dplg-b2c1
29	6,99	0,01	0,48	0,09	59,34	24,86	6,82	98,59	19dplg-b2c2
30	7,15	0,00	0,50	0,09	59,48	25,07	6,82	99,11	19dplg-b2c3
31	7,24	0,01	0,44	0,09	59,11	25,06	6,88	98,84	19dplg-b2c4
32	6,99	0,02	0,44	0,19	59,46	25,25	7,01	99,37	19dplg-b2c5
33	7,24	0,00	0,52	0,06	59,75	24,76	6,72	99,05	19dplg-c1copx1
34	7,31	0,01	0,55	0,09	59,31	24,88	6,58	98,72	19dplg-c1copx2
35	7,16	0,00	0,49	0,10	59,25	24,92	6,75	98,66	19dplg-c1copx3
36	7,20	0,00	0,50	0,13	58,89	25,00	6,89	98,60	19dplg-c1copx4
37	7,08	0,00	0,51	0,19	59,01	25,28	6,90	98,98	19dplg-c1copx5
38	6,90	0,02	0,42	0,40	58,84	25,53	7,28	99,39	19dplg-c1copx6
39	8,02	0,00	0,53	0,05	61,39	23,60	5,10	98,68	5219plg-f-cpore1
40	7,99	0,00	0,43	0,00	61,12	23,73	5,17	98,43	5219plg-f-cpore2
41	8,08	0,00	0,45	0,04	61,64	23,63	5,12	98,96	5219plg-f-cpore3
42	8,03	0,00	0,45	0,01	61,85	23,60	5,23	99,17	5219plg-f-cpore4
43	8,14	0,00	0,38	0,04	61,65	23,90	5,33	99,44	5219plg-f-cpore5
44	7,97	0,00	0,60	0,03	61,59	23,80	5,29	99,26	5219plg-f2-cpore1
45	7,96	0,00	0,69	0,05	62,04	23,72	5,27	99,72	5219plg-f2-cpore2
46	8,03	0,00	0,72	0,08	61,64	23,68	5,27	99,41	5219plg-f2-cpore3
47	7,96	0,01	0,65	0,10	61,63	23,75	5,26	99,36	5219plg-f2-cpore4
48	6,63	0,87	0,53	2,35	57,40	23,49	4,84	96,11	5219plg-f2-cpore5
49	8,05	0,00	0,50	0,03	61,62	23,58	5,18	98,96	5219plg-f1-cgrt1
50	8,15	0,00	0,51	0,04	61,14	23,43	5,02	98,30	5219plg-f1-cgrt2
51	8,14	0,00	0,47	0,02	60,25	23,75	4,96	97,59	5219plg-f1-cgrt3
52	8,06	0,00	0,46	0,04	61,03	23,83	5,12	98,54	5219plg-f1-cgrt4
53	8,04	0,01	0,30	0,05	61,30	23,83	5,28	98,82	5219plg-f1-cgrt5
54	8,80	0,01	0,79	0,12	62,09	23,41	3,22	98,43	5219plg-f1-cgrt6
55	0,00	0,01	0,01	0,11	96,65	0,04	0,00	96,82	5219plg-f1-cgrt7
56	0,00	0,00	0,02	0,04	96,27	0,03	0,00	96,36	5219plg-f1-qz1
57	0,02	0,00	0,01	0,05	97,48	0,02	0,01	97,59	5219plg-f1-qz2
58	7,95	0,01	0,59	0,02	61,38	23,67	5,04	98,65	5219plg-h1-c1
59	8,07	0,00	0,67	0,02	60,36	23,51	5,08	97,71	5219plg-h1-c2
60	8,05	0,00	0,58	0,06	61,31	23,64	5,15	98,79	5219plg-h1-c3
61	8,00	0,00	0,53	0,05	61,11	23,79	5,30	98,77	5219plg-h1-c4
62	0,00	0,00	0,03	0,04	97,86	0,05	0,02	97,99	5219plg-h1-qz
63	7,40	0,00	0,54	0,11	60,26	24,51	6,36	99,18	227plg-i1-core1
64	7,18	0,13	0,56	0,62	59,06	24,47	6,28	98,30	227plg-i1-core2
65	7,51	0,00	0,47	0,11	60,00	24,61	6,43	99,13	227plg-i1-core3

66	7,50	0,00	0,55	0,14	59,29	24,65	6,41	98,54	227plg-i1-core4
67	7,39	0,01	0,53	0,16	60,15	24,67	6,39	99,30	227plg-i1-core5
68	7,41	0,01	0,50	0,26	59,58	24,75	6,57	99,07	227plg-i1-core6
69	7,27	0,02	0,51	0,39	59,73	24,93	6,68	99,52	227plg-i1-core7
70	7,38	0,00	0,52	0,13	60,14	24,60	6,33	99,09	227plg-i2-core1
71	7,31	0,00	0,46	0,14	60,49	24,61	6,34	99,33	227plg-i2-core2
72	7,26	0,05	0,50	0,17	60,14	24,60	6,49	99,21	227plg-i2-core3
73	7,31	0,00	0,53	0,25	60,16	24,72	6,45	99,42	227plg-i2-core4
74	7,30	0,00	0,48	0,39	58,48	24,77	6,43	97,86	227plg-i2-core5
75	7,21	1,25	0,27	1,83	59,21	23,75	5,76	99,27	5212plg-l1-core1
76	7,41	0,00	0,40	0,03	60,06	24,78	6,34	99,02	5212plg-l1-core2
77	7,32	0,00	0,42	0,06	60,33	24,62	6,39	99,15	5212plg-l1-core3
78	7,30	0,00	0,47	0,09	60,38	24,86	6,45	99,55	5212plg-l1-core4
79	6,53	0,00	1,81	0,21	59,48	24,92	6,73	99,67	5212plg-l1-core5
80	7,29	0,01	0,39	0,02	59,40	24,62	6,43	98,16	5212plg-l2-core1
81	7,45	0,00	0,39	0,06	59,91	24,74	6,47	99,02	5212plg-l2-core2
82	7,43	0,00	0,39	0,05	59,25	24,78	6,43	98,32	5212plg-l2-core3
83	7,29	0,00	0,42	0,03	59,33	24,81	6,42	98,29	5212plg-l2-core4
84	7,42	0,00	0,36	0,04	59,07	24,80	6,44	98,13	5212plg-l2-core5
85	6,74	1,05	0,36	1,71	56,96	24,09	6,09	97,00	5212plg-l2-core6
86	7,42	0,00	0,37	0,04	60,06	24,86	6,41	99,16	5212plg-l3-core1
87	7,54	0,00	0,33	0,05	59,92	24,67	6,38	98,88	5212plg-l3-core2
88	7,49	0,00	0,37	0,04	60,11	24,72	6,46	99,18	5212plg-l3-core3
89	7,53	0,01	0,32	0,03	60,23	24,86	6,33	99,30	5212plg-l3-core4
90	7,41	0,00	0,38	0,03	60,17	24,93	6,44	99,36	5212plg-l3-core5
91	7,45	0,00	0,40	0,12	60,36	24,87	6,51	99,70	5212plg-l3-core6
92	7,34	0,02	0,41	0,24	59,71	25,19	6,68	99,58	5212plg-l3-core7
93	8,07	0,00	0,45	0,04	61,04	24,01	5,53	99,15	5186feld-p1-c1
94	7,97	0,01	0,46	0,05	61,33	23,85	5,37	99,04	5186feld-p1-c2
95	8,11	0,00	0,42	0,04	60,98	23,76	5,37	98,67	5186feld-p1-c3
96	8,11	0,01	0,19	0,02	61,42	24,09	5,51	99,34	5186feld-p1-c4
97	7,97	0,11	0,28	0,22	61,01	23,75	5,44	98,79	5186feld-p1-c5
98	8,05	0,00	0,35	0,04	61,35	24,03	5,68	99,50	5186feld-p1-c6
99	7,85	0,00	0,43	0,06	61,77	23,85	5,56	99,51	5186feld-p1-c7
100	7,93	0,01	0,44	0,05	61,03	24,06	5,56	99,08	5186feld-p2-c1
101	7,94	0,00	0,40	0,04	61,69	24,03	5,52	99,61	5186feld-p2-c2
102	8,01	0,01	0,43	0,06	60,41	23,92	5,46	98,30	5186feld-p2-c3
103	8,11	0,00	0,41	0,05	60,99	23,83	5,48	98,86	5186feld-p2-c4
104	8,03	0,00	0,32	0,03	60,95	23,88	5,60	98,81	5186feld-p2-c5
105	8,45	0,03	0,17	0,19	62,38	23,45	4,97	99,64	5042plg-q1-c1
106	8,30	0,00	0,19	0,07	62,61	23,66	5,07	99,89	5042plg-q1-c2
107	8,37	0,00	0,20	0,03	62,24	23,70	5,14	99,67	5042plg-q1-c3
108	8,76	0,03	0,58	0,21	62,32	23,41	3,15	98,45	5042plg-q1-c4
109	9,06	0,04	0,09	0,25	63,66	22,38	3,88	99,36	5042plg-q1-c5
110	7,95	0,00	0,67	0,04	61,69	23,53	5,15	99,02	5201plg-s1-c1
111	8,02	0,00	0,65	0,05	61,78	23,55	5,24	99,28	5201plg-s1-c2
112	7,74	0,02	0,46	0,04	61,04	23,80	5,72	98,81	5201plg-s1-c3
147	6,84	0,00	2,82	0,04	60,68	23,47	5,14	98,99	5201plg-s1-c4
148	7,95	0,00	0,58	0,05	61,14	23,52	5,21	98,45	5201plg-s2-c1
149	8,01	0,00	0,52	0,02	61,09	23,62	5,19	98,46	5201plg-s2-c2
150	8,04	0,01	0,53	0,05	61,18	23,58	5,21	98,59	5201plg-s2-c3
151	7,90	0,00	0,55	0,04	60,76	23,83	5,38	98,46	5201plg-s3-c1
152	7,89	0,00	0,57	0,03	60,75	23,98	5,62	98,82	5201plg-s3-c2
153	6,52	1,14	0,74	3,46	54,96	23,85	4,60	95,27	5201plg-s3-c3
154	7,96	0,00	0,72	0,01	61,67	23,54	5,31	99,21	5201plg-s3-c4
155	8,17	0,00	0,55	0,04	61,85	23,59	5,25	99,45	5201plg-s3-c5
156	7,82	0,00	0,65	0,04	61,97	23,84	5,51	99,83	5201plg-s3-c6
157	7,80	0,01	0,60	0,04	61,47	23,56	5,43	98,90	5201plg-s4-c1
158	7,63	0,01	0,96	0,03	60,91	23,84	5,73	99,12	5201plg-s4-c2
159	7,80	0,01	0,61	0,04	61,34	23,61	5,48	98,88	5201plg-s4-c3
160	8,04	0,00	0,58	0,04	61,37	23,64	5,26	98,93	5201plg-s4-c4
161	7,95	0,00	0,47	0,05	61,70	23,95	5,62	99,74	5201plg-s4-c5
162	7,89	0,00	0,68	0,05	62,02	23,60	5,29	99,52	5201plg-t5-c1
163	7,94	0,00	0,75	0,06	62,35	23,55	5,36	100,00	5201plg-t5-c2
164	8,00	0,00	0,63	0,03	62,20	23,72	5,35	99,93	5201plg-t5-c3
165	7,98	0,00	0,56	0,03	61,91	23,84	5,53	99,85	5201plg-t5-c4

APPENDIX XVIII

MICROPROBE ANALYSES OF K-FELDSPAR

(Acc. Voltage : 15 Kv, Probe Dia : 5, Beam Current: 1.959E-08)

Standard Data for K-feldspar

Element	Standard name	Wt.(%)	ZAF Fac.	Z	A	F
1 Na2O	Albite	11.4300	5.4858	10.7252	0.5094	1.0041
2 MgO	Diopside	17.9400	4.7341	7.8691	0.5985	1.0051
3 K2O	Orthoclase	16.9100	1.0758	1.2033	0.8940	1.0001
4 FeO	Fe2O3m	89.9830	0.2140	0.2170	0.9864	1.0000
5 SiO2	Orthoclase	65.0300	3.2797	4.4186	0.7415	1.0011
6 Al2O3	Orthoclase	16.9800	4.3209	5.8692	0.7244	1.0163
7 CaO	Diopside	25.1800	0.8662	0.9351	0.9261	1.0002

#	Na2O	MgO	K2O	FeO	SiO2	Al2O3	CaO	Total	Comment
1	0.718	0.000	16.414	0.024	62.923	18.460	0.020	98.559	5186feld-p3-c1
2	0.585	0.006	16.580	0.059	63.045	18.466	0.033	98.774	5186feld-p3-c2
3	0.680	0.007	16.591	0.075	63.441	18.496	0.003	99.293	5186feld-p3-c3
4	0.411	0.320	16.524	0.797	62.676	18.329	0.000	99.057	5186feld-p3-c4
5	0.677	0.000	16.589	0.012	63.524	18.420	0.043	99.265	5042k-feld-q1-c1
6	0.681	0.001	16.557	0.004	60.909	18.447	0.006	96.605	5042k-feld-q1-c2
7	0.508	0.000	16.861	0.068	63.635	18.507	0.009	99.588	5042k-feld-q1-c3
8	0.629	0.006	16.759	0.026	63.254	18.339	0.018	99.031	5042k-feld-q1-c4
9	0.746	0.006	16.338	0.042	63.363	18.461	0.027	98.983	5042k-feld-q1-c5
10	0.582	0.007	16.787	0.007	62.951	18.364	0.030	98.728	5042k-feld-q1-c6
11	0.576	0.007	16.779	0.016	63.042	18.392	0.042	98.854	5042k-feld-q1-c7
12	0.868	0.008	16.367	0.005	63.361	18.327	0.000	98.936	5042k-feld-q1-c8
13	0.814	0.000	16.428	0.002	63.970	18.522	0.036	99.772	5042k-feld-q1-c9
14	1.241	0.000	15.908	0.019	63.894	18.495	0.014	99.571	5042k-feld-q1-c10
15	0.913	0.000	16.086	0.006	63.411	18.330	0.027	98.773	5042k-feld-q1-c11
16	0.723	0.000	16.742	0.057	63.227	18.338	0.030	99.117	5042k-feld-q1-c12

Oxides are in wt %

APPENDIX XIX

MICROPROBE ANALYSES OF ORTHOPYROXENE

(Acc. Voltage : 15 Kv, Probe Dia : 5, Beam Current: 1.959E-08)

Standard Data for orthopyroxene

Element	Standard name	Wt.(%)	ZAF Fac.	Z	A	F
1 Na2O	Albite	11.4300	5.4858	10.7252	0.5094	1.0041
2 MgO	Diopside	17.9400	4.7341	7.8691	0.5985	1.0051
3 TiO2	tio2	100.0000	0.5904	0.6060	0.9742	1.0000
4 K2O	Orthoclase	16.9100	1.0758	1.2033	0.8940	1.0001
5 FeO	Fe2O3m	89.9830	0.2140	0.2170	0.9864	1.0000
6 SiO2	Diopside	55.1900	3.2336	4.4029	0.7338	1.0009
7 Al2O3	Orthoclase	16.9800	4.3209	5.8692	0.7244	1.0163
8 Cr2O3	chromite	45.6500	0.3562	0.3581	0.9776	1.0174
9 CaO	Diopside	25.1800	0.8662	0.9351	0.9261	1.0002
10 MnO	spessartine	40.5000	0.2676	0.2729	0.9805	1.0000

#	Na2O	MgO	TiO2	K2O	FeO	SiO2	Al2O3	Cr2O3	CaO	MnO	Total	Comment
1	0,05	22,76	0,05	0,10	20,69	49,88	0,87	0,11	0,53	0,45	95,48	19dopx-b2c-5
2	0,00	24,19	0,04	0,04	20,97	53,11	0,75	0,02	0,47	0,44	100,03	19dopx-c1core1
3	0,00	24,17	0,09	0,00	21,16	53,29	0,67	0,07	0,48	0,44	100,37	19dopx-c1core2
4	0,00	24,07	0,05	0,02	21,06	53,36	0,76	0,06	0,48	0,45	100,32	19dopx-c1core3
5	0,01	24,19	0,05	0,01	20,92	53,29	0,79	0,06	0,45	0,42	100,18	19dopx-c1core4
6	0,01	24,04	0,08	0,03	21,20	53,40	0,67	0,07	0,44	0,47	100,39	19dopx-c2c1bte
7	0,01	23,96	0,05	0,03	21,26	53,59	0,68	0,07	0,45	0,40	100,50	19dopx-c2c1bte
8	0,00	23,78	0,05	0,03	21,63	53,02	0,59	0,01	0,42	0,46	100,00	19dopx-c2c1bte
9	0,03	24,23	0,02	0,02	21,33	53,34	0,52	0,07	0,41	0,42	100,39	19dopx-c2c1bte5
10	0,02	23,99	0,03	0,01	21,30	53,31	0,55	0,06	0,47	0,42	100,14	19dopx-c3c1bte1
11	0,03	24,07	0,05	0,03	21,30	52,90	0,59	0,05	0,44	0,49	99,94	19dopx-c3c1bte2
12	0,00	24,04	0,02	0,01	21,31	53,05	0,54	0,03	0,44	0,43	99,87	19dopx-c3c1bte3
13	0,01	23,92	0,03	0,03	21,40	53,04	0,53	0,05	0,33	0,49	99,84	19dopx-c3c1bte4
14	0,00	24,13	0,06	0,03	21,09	53,22	0,65	0,06	0,45	0,45	100,14	19dopx-c3c1bte5
15	0,00	24,12	0,05	0,03	21,02	53,30	0,71	0,07	0,50	0,44	100,24	19dopx-c4cbte1
16	0,03	24,04	0,00	0,01	21,26	53,34	0,66	0,06	0,49	0,46	100,33	19dopx-c4cbte2
17	0,02	24,28	0,07	0,01	21,44	53,28	0,65	0,02	0,47	0,47	100,69	19dopx-c4cbte3
18	0,01	24,03	0,06	0,04	21,49	53,09	0,65	0,02	0,50	0,43	100,35	19dopx-c4cbte4
19	0,02	23,72	0,09	0,07	21,76	53,10	0,58	0,04	0,44	0,45	100,26	19dopx-c4cbte5
20	0,00	24,43	0,03	0,02	21,12	53,40	0,75	0,08	0,50	0,46	100,80	19dopx-c4cbte6
21	0,00	24,45	0,08	0,03	20,83	53,52	0,64	0,09	0,43	0,42	100,48	19dopx-c5cplg1
22	0,02	24,07	0,04	0,02	21,17	53,12	0,77	0,06	0,49	0,43	100,19	19dopx-c5cplg2
23	0,00	24,09	0,04	0,03	21,28	53,28	0,77	0,06	0,49	0,39	100,43	19dopx-c5cplg3
24	0,03	24,03	0,05	0,01	20,98	53,32	0,72	0,08	0,46	0,46	100,13	19dopx-c5cplg4
25	0,01	24,21	0,00	0,01	21,09	53,20	0,74	0,06	0,43	0,44	100,19	19dopx-c5cplg5
26	0,02	24,19	0,02	0,02	20,82	53,26	0,64	0,06	0,43	0,45	99,91	19dopx-c5cplg6
27	0,00	24,33	0,03	0,02	21,08	53,16	0,64	0,07	0,47	0,42	100,21	19dopx-c5cplg7
28	0,00	24,42	0,01	0,02	20,96	52,96	0,57	0,07	0,45	0,44	99,90	19dopx-c6cqz1
29	0,02	24,43	0,00	0,03	20,90	53,25	0,54	0,04	0,37	0,44	100,01	19dopx-c6cqz2
30	0,00	24,26	0,01	0,02	21,23	52,85	0,63	0,08	0,50	0,48	100,06	19dopx-c6cqz3
31	0,03	24,21	0,04	0,03	21,01	52,85	0,65	0,06	0,48	0,48	99,84	19dopx-c6cqz4
32	0,01	23,89	0,01	0,02	21,16	53,08	0,59	0,05	0,49	0,43	99,72	19dopx-c6cqz5
33	0,03	23,95	0,03	0,02	20,93	53,31	0,56	0,05	0,48	0,44	99,79	19dopx-c6cqz6
34	0,02	18,52	0,08	0,02	27,26	48,54	5,15	0,12	0,06	0,36	100,12	19dopx-c6cqz7
35	0,00	18,48	0,04	0,01	27,09	48,76	5,12	0,10	0,07	0,36	100,02	5219opx-e1
36	0,02	18,47	0,09	0,02	27,19	48,57	5,08	0,09	0,08	0,37	99,97	5219opx-e2
37	0,00	18,64	0,10	0,01	27,12	48,33	5,19	0,11	0,08	0,38	99,96	5219opx-e-c3
38	0,02	18,42	0,07	0,03	26,96	48,73	5,24	0,09	0,04	0,37	99,97	5219opx-e-c4
39	0,01	18,54	0,04	0,01	26,82	48,57	5,10	0,05	0,09	0,39	99,62	5219opx-e-c5
40	0,01	18,63	0,08	0,01	26,63	48,74	5,09	0,08	0,11	0,32	99,70	5219opx-e-c6
41	0,00	18,82	0,09	0,00	26,42	48,71	5,18	0,05	0,05	0,30	99,63	5219opx-h1-c1
42	0,00	18,50	0,06	0,04	26,64	46,70	4,83	0,09	0,10	0,33	97,27	5219opx-h1-c2
43	0,00	18,73	0,04	0,02	27,59	50,54	0,56	0,01	0,64	0,80	98,92	5219opx-h1-c4
44	0,00	18,83	0,04	0,03	27,67	51,45	0,60	0,02	0,57	0,78	100,00	227opx-i1-core1
45	0,02	18,92	0,04	0,04	27,35	51,29	0,57	0,00	0,55	0,82	99,59	227opx-i1-core2
46	0,03	18,81	0,05	0,03	27,48	51,46	0,57	0,05	0,56	0,82	99,84	227opx-i1-core3
47	0,02	18,83	0,05	0,04	27,71	51,36	0,52	0,00	0,56	0,84	99,93	227opx-i1-core4
48	0,00	18,70	0,00	0,01	27,99	51,39	0,51	0,01	0,55	0,84	100,01	227opx-i1-core5
49	0,01	18,62	0,02	0,04	27,46	50,75	0,96	0,00	0,51	0,80	99,16	227opx-i2-core1
50	0,00	18,94	0,02	0,02	27,54	51,34	0,51	0,00	0,54	0,82	99,73	227opx-i2-core2
51	0,02	19,19	0,03	0,03	27,52	51,27	0,51	0,00	0,57	0,78	99,92	227opx-i2-core3
52	0,03	18,82	0,05	0,02	27,52	50,89	0,59	0,01	0,61	0,83	99,38	227opx-i2-core4
53	0,00	19,03	0,03	0,02	27,80	51,51	0,56	0,00	0,63	0,84	100,42	227opx-i3-core1
54	0,00	18,79	0,05	0,02	27,60	50,51	0,63	0,00	0,64	0,78	99,04	227opx-i3-core2
55	0,01	19,04	0,05	0,01	27,83	49,65	0,60	0,01	0,56	0,88	98,62	227opx-i3-core3
56	0,00	18,95	0,05	0,02	27,56	51,33	0,55	0,00	0,63	0,81	99,89	227opx-i3-core4
57	0,01	18,98	0,07	0,01	27,33	51,19	0,65	0,00	0,65	0,80	99,68	227opx-i3-core5
58	0,01	18,99	0,08	0,01	27,76	50,89	0,59	0,00	0,65	0,79	99,78	227px-j1-core1
59	0,02	18,89	0,07	0,01	27,55	50,97	0,60	0,01	0,62	0,77	99,51	227px-j1-core2
60	0,00	18,71	0,03	0,02	27,51	50,67	0,67	0,01	0,60	0,79	99,00	227px-j1-core3
61	0,02	18,71	0,05	0,02	27,60	51,09	0,55	0,00	0,57	0,79	99,39	227px-j1-core4
62	0,01	19,06	0,06	0,03	27,83	51,26	0,70	0,00	0,62	0,79	100,35	227cpx-j2-cplg4
63	0,01	18,85	0,04	0,04	27,84	50,82	0,80	0,00	0,64	0,83	99,87	227cpx-j3-cplg1

64	0,01	19,22	0,05	0,03	27,80	51,60	0,58	0,00	0,60	0,79	100,67	227cpx-j3-cplg2
65	0,02	19,09	0,04	0,01	27,83	51,36	0,59	0,04	0,56	0,73	100,25	227cpx-j3-cplg3
66	0,02	18,94	0,02	0,02	27,87	51,08	0,55	0,00	0,53	0,83	99,86	227cpx-j3-cplg4
67	0,00	19,05	0,01	0,02	27,62	50,84	0,58	0,01	0,58	0,83	99,54	227cpx-j4-copx5
68	0,03	19,10	0,10	0,00	27,93	51,20	0,56	0,01	0,60	0,82	100,34	2270px-j4-ccpx1
69	0,02	18,98	0,04	0,01	27,65	50,82	0,52	0,00	0,55	0,83	99,42	2270px-j4-ccpx2
70	0,01	19,32	0,01	0,02	27,42	51,40	0,49	0,00	0,48	0,81	99,95	2270px-j4-ccpx3
71	0,01	18,02	0,05	0,02	27,36	48,32	5,09	0,03	0,05	0,53	99,48	2270px-j4-ccpx4
72	0,01	18,23	0,03	0,00	27,41	48,57	4,80	0,12	0,07	0,54	99,77	2270px-l1-core1
73	0,03	18,13	0,05	0,01	27,26	48,98	4,73	0,07	0,09	0,54	99,88	2270px-l1-core2
74	0,00	18,31	0,03	0,03	27,39	49,40	4,55	0,04	0,04	0,55	100,34	2270px-l1-core3
75	0,01	17,69	0,04	0,02	27,49	48,32	5,05	0,07	0,08	0,57	99,33	2270px-l1-core4
76	0,01	18,19	0,07	0,03	27,43	48,59	4,96	0,05	0,07	0,55	99,94	2270px-l2-core1
77	0,00	18,11	0,07	0,01	27,66	48,52	5,07	0,05	0,08	0,56	100,12	2270px-l2-core2
78	0,00	17,79	0,11	0,01	27,70	48,40	5,18	0,05	0,07	0,53	99,85	2270px-l2-core3
79	0,00	17,97	0,07	0,04	27,85	48,30	5,22	0,06	0,07	0,54	100,13	2270px-l3-core1
80	0,01	17,82	0,10	0,02	27,54	48,34	5,11	0,04	0,11	0,54	99,64	2270px-l3-core2
81	0,01	17,98	0,07	0,04	27,61	48,53	5,10	0,08	0,08	0,55	100,04	2270px-l3-core3
82	0,01	18,01	0,06	0,01	27,86	48,49	5,08	0,02	0,07	0,56	100,18	2270px-l3-core4
83	0,01	17,83	0,05	0,02	27,34	48,73	4,96	0,08	0,09	0,57	99,68	2270px-l3-core5
84	0,01	18,84	0,04	0,02	27,73	50,86	2,12	0,00	0,22	0,66	100,49	2270px-l3-core6
85	0,01	18,95	0,06	0,00	27,72	50,69	2,15	0,02	0,20	0,67	100,47	5186ox-1
86	0,05	18,86	0,03	0,02	27,82	50,46	2,16	0,01	0,24	0,65	100,29	5186ox-c2
87	0,01	18,97	0,04	0,01	27,85	50,33	2,15	0,04	0,21	0,71	100,33	5186ox-c3
88	0,04	18,92	0,03	0,02	27,85	50,62	2,06	0,00	0,21	0,76	100,48	5186ox-c4
89	0,00	19,00	0,00	0,03	27,91	50,74	2,05	0,00	0,16	0,68	100,58	5186ox-c5
90	0,01	18,82	0,04	0,02	28,11	50,58	2,11	0,03	0,23	0,70	100,66	5186ox-c6
91	0,00	18,84	0,02	0,02	28,15	50,43	2,11	0,02	0,17	0,72	100,48	5186ox-o2-c1
92	0,00	18,63	0,00	0,01	27,87	50,75	1,97	0,01	0,17	0,70	100,11	5186ox-o2-c2
93	0,01	19,13	0,03	0,01	27,93	50,77	1,87	0,01	0,20	0,74	100,68	5186ox-o2-c3
94	0,00	18,99	0,07	0,01	27,60	50,92	1,79	0,02	0,21	0,76	100,36	5186ox-o2-c4
95	0,01	18,89	0,02	0,01	27,94	50,46	1,76	0,00	0,14	0,74	99,98	5186ox-o2-c5
96	0,00	18,88	0,03	0,02	27,75	51,14	2,14	0,00	0,26	0,67	100,88	5186ox-o2-c6
97	0,00	18,77	0,06	0,02	27,71	50,42	2,07	0,04	0,23	0,65	99,98	5186ox-o3-c1
98	0,02	19,07	0,04	0,04	27,54	50,62	2,10	0,01	0,21	0,66	100,30	5186ox-o3-c2
99	0,00	19,03	0,03	0,02	27,47	50,58	2,13	0,02	0,21	0,66	100,15	5186ox-o3-c3
100	0,02	18,87	0,04	0,04	27,71	50,32	2,02	0,01	0,21	0,65	99,90	5186ox-o3-c4
101	0,01	18,74	0,01	0,01	27,82	50,49	1,98	0,01	0,19	0,74	99,98	5186ox-o3-c5
102	0,01	14,00	0,06	0,01	33,79	48,81	1,97	0,00	0,17	1,24	100,05	5186ox-o3-c6
103	0,00	14,10	0,01	0,03	33,59	48,68	1,83	0,00	0,16	1,31	99,71	5201ox-t1-c1
104	0,00	14,06	0,05	0,00	33,68	48,63	1,90	0,01	0,17	1,30	99,80	5201ox-t1-c2
105	0,00	14,00	0,09	0,00	33,61	48,97	1,87	0,00	0,15	1,27	99,96	5201ox-t1-c3
106	0,00	14,10	0,06	0,00	33,50	49,17	1,91	0,00	0,15	1,26	100,15	5201ox-t1-c4
107	0,00	14,24	0,08	0,01	33,59	49,18	2,02	0,00	0,14	1,29	100.54	5201ox-t1-c5
108	0,00	14,07	0,05	0,01	33,53	48,80	2,05	0,00	0,15	1,21	99,85	5201ox-t1-c6
109	0,00	14,12	0,06	0,05	33,69	49,09	2,07	0,00	0,15	1,28	100,51	5201ox-t2-c1
110	0,02	14,14	0,07	0,03	33,54	49,07	1,91	0,00	0,16	1,28	100,21	5201ox-t2-c2
111	0,00	14,14	0,06	0,01	33,47	49,24	1,73	0,03	0,16	1,31	100,15	5201ox-t2-c3
112	0,03	13,84	0,07	0,00	33,52	48,99	2,12	0,00	0,17	1,27	100,00	5201ox-t2-c4
113	0,00	14,02	0,06	0,03	33,58	49,52	2,19	0,00	0,18	1,30	100,88	5201ox-t3-c1
114	0,00	13,78	0,07	0,03	33,60	48,86	1,90	0,00	0,15	1,32	99,70	5201ox-t3-c2
115	0,00	13,82	0,05	0,01	33,64	48,95	2,09	0,00	0,14	1,29	99,98	5201ox-t3-c3
116	0,00	14,02	0,01	0,03	33,65	49,11	1,84	0,00	0,14	1,30	100,08	5201ox-t3-c4
117	0,00	13,96	0,07	0,03	33,59	49,35	1,95	0,00	0,14	1,27	100,35	5201ox-t3-c5
118	0,00	13,99	0,07	0,02	33,39	49,05	1,88	0,01	0,14	1,25	99,79	5201ox-t3-c6
119	0,03	14,11	0,06	0,01	33,47	48,60	1,97	0,00	0,13	1,31	99,70	5201ox-t3-c7

Oxides are in wt %

APPENDIX XX

MICROPROBE ANALYSES OF CLINOPYROXENE

(Acc. Voltage : 15 Kv, Probe Dia : 5, Beam Current: 1.959E-08)

Standard Data for clinopyroxene

Element	Standard name	Wt.(%)	ZAF Fac.	Z	A	F
1 Na2O	Albite	11.4300	5.4858	10.7252	0.5094	1.0041
2 MgO	Diopside	17.9400	4.7341	7.8691	0.5985	1.0051
3 TiO2	tio2	100.0000	0.5904	0.6060	0.9742	1.0000
4 K2O	Orthoclase	16.9100	1.0758	1.2033	0.8940	1.0001
5 FeO	Fe2O3m	89.9830	0.2140	0.2170	0.9864	1.0000
6 SiO2	Diopside	55.1900	3.2336	4.4029	0.7338	1.0009
7 Al2O3	Orthoclase	16.9800	4.3209	5.8692	0.7244	1.0163
8 Cr2O3	chromite	45.6500	0.3562	0.3581	0.9776	1.0174
9 CaO	Diopside	25.1800	0.8662	0.9351	0.9261	1.0002
10 MnO	spessartine	40.5000	0.2676	0.2729	0.9805	1.0000

#	Na2O	MgO	TiO2	K2O	FeO	SiO2	Al2O3	Cr2O3	CaO	MnO	Total	Comment
1	0,45	14,56	0,08	0,01	7,15	51,68	1,30	0,16	22,38	0,17	97,92	19dcpx-a1
2	0,47	14,63	0,16	0,03	7,52	51,71	1,48	0,22	22,24	0,18	98,63	19dcpx-a2
3	0,42	14,78	0,08	0,02	6,93	52,24	1,13	0,21	22,79	0,16	98,75	19dcpx-a3
4	0,48	14,77	0,09	0,03	7,79	51,93	1,38	0,21	21,96	0,20	98,82	19dcpx-a4core
5	0,51	14,50	0,13	0,02	7,32	52,14	1,40	0,17	22,36	0,19	98,74	19dcpx-a4core
6	0,47	14,71	0,12	0,00	7,29	52,44	1,45	0,23	22,61	0,17	99,49	19dcpx-a4core2
7	0,46	14,85	0,14	0,02	7,03	51,99	1,26	0,26	22,42	0,17	98,59	19dcpx-a4core3
8	0,51	14,74	0,09	0,01	7,53	52,03	1,40	0,19	22,26	0,19	98,95	19dcpx-a4core4
9	0,45	14,88	0,12	0,01	7,45	52,29	1,36	0,18	22,23	0,19	99,16	19dcpx-b4c-1
10	0,51	14,74	0,06	0,01	7,36	52,30	1,38	0,19	22,24	0,19	98,97	19dcpx-b1c-2
11	0,44	15,04	0,11	0,05	7,77	51,00	1,35	0,19	22,13	0,18	98,25	19dcpx-b1c-3
12	0,52	14,65	0,13	0,02	7,48	52,19	1,48	0,22	21,88	0,15	98,73	19dcpx-b1c-4
13	0,48	14,68	0,16	0,02	7,41	52,09	1,44	0,19	21,95	0,20	98,61	19dcpx-b2c-1
14	0,50	14,88	0,11	0,03	7,52	52,33	1,39	0,25	22,36	0,17	99,53	19dcpx-b2c-2
15	0,45	14,80	0,11	0,04	7,24	52,41	1,32	0,23	22,43	0,18	99,21	19dcpx-b2c-3
16	0,43	13,06	0,14	0,01	10,47	51,51	1,34	0,02	21,70	0,30	98,97	227cpx-j3-cplg5
17	0,44	12,94	0,19	0,00	10,45	51,43	1,40	0,00	21,54	0,29	98,68	227cpx-j4-copx1
18	0,45	13,19	0,11	0,00	10,56	51,64	1,36	0,01	21,64	0,32	99,29	227cpx-j4-copx2
19	0,34	13,50	0,02	0,02	10,04	51,47	0,98	0,03	22,09	0,34	98,84	227cpx-j4-copx3
20	0,34	13,48	0,10	0,02	10,03	51,65	1,14	0,00	22,23	0,31	99,29	227cpx-j4-copx4
21	0,44	12,93	0,13	0,04	10,53	51,29	1,49	0,02	21,30	0,30	98,47	227px-j1-core5
22	0,46	12,95	0,12	0,02	10,53	51,34	1,40	0,00	21,67	0,29	98,79	227cpx-j1-core1
23	0,50	13,13	0,11	0,02	10,61	51,37	1,40	0,02	21,71	0,33	99,20	227cpx-j1-core2
24	0,48	12,90	0,12	0,02	10,54	51,22	1,33	0,00	21,52	0,30	98,42	227cpx-j1-core3
25	0,52	12,87	0,15	0,02	10,66	50,72	1,51	0,03	21,44	0,28	98,20	227cpx-j1-core4
26	0,52	12,89	0,11	0,01	10,51	51,04	1,48	0,08	21,49	0,32	98,44	227cpx-j2-cplg1
26	0,49	12,85	0,16	0,02	10,55	51,16	1,41	0,03	21,79	0,32	98,76	227cpx-j2-cplg2
27	0,45	13,07	0,09	0,06	10,31	51,79	1,19	0,03	22,17	0,30	99,46	227cpx-j2-cplg3

Oxides are in wt %

APPENDIX XXI

MICROPROBE ANALYSES OF BIOTITE

(Acc. Voltage : 15 Kv, Probe Dia : 5, Beam Current: 1.959E-08)

Standard Data for biotite

Element	Standard name	Wt.(%)	ZAF Fac.	Z	A	F
1 Na2O	Albite	11.4300	5.4858	10.7252	0.5094	1.0041
2 F	CaF2	48.6700	5.4186	22.0589	0.2456	1.0000
3 Cl	vanadinite	2.6530	1.5715	2.6458	0.5937	1.0004
4 K2O	Orthoclase	16.9100	1.0758	1.2033	0.8940	1.0001
5 FeO	Fe2O3m	89.9830	0.2140	0.2170	0.9864	1.0000
6 SiO2	Diopside	55.1900	3.2336	4.4029	0.7338	1.0009
7 MgO	Diopside	17.9400	4.7341	7.8691	0.5985	1.0051
8 TiO2	tio2	100.0000	0.5904	0.6060	0.9742	1.0000
9 CaO	Diopside	25.1800	0.8662	0.9351	0.9261	1.0002
10 MnO	spessartine	40.5000	0.2676	0.2729	0.9805	1.0000
11 Al2O3	Orthoclase	16.9800	4.3209	5.8692	0.7244	1.0163
12 Cr2O3	chromite	45.6500	0.3562	0.3581	0.9776	1.0174

	Na2O	F	Cl	K2O	FeO	SiO2	MgO	TiO2	CaO	MnO	Al2O3	Cr2O3	Total	
#	(wt%)	(wt%)	(wt%)	(wt%)	(wt%)	(wt%)	(wt%)	(wt%)	(wt%)	(wt%)	(wt%)	(wt%)	(wt%)	Comment
1	0,07	0,20	0,04	7,90	13,75	37,15	16,99	3,09	0,07	0,10	12,56	0,60	92,50	19dbte-b1
2	0,12	0,39	0,00	10,50	12,56	37,47	15,94	4,33	0,00	0,06	14,01	0,52	95,89	19dbte-c1copx1
3	0,12	0,44	0,00	10,37	12,56	36,88	15,74	4,31	0,01	0,01	13,82	0,51	94,76	19dbte-c1copx2
4	0,09	0,33	0,00	10,42	12,59	36,98	16,38	4,20	0,02	0,02	14,07	0,55	95,64	19dbte-c1copx3
5	0,10	0,33	0,00	10,46	12,35	36,58	16,14	4,30	0,01	0,06	13,68	0,52	94,53	19dbte-c1copx4
6	0,11	0,29	0,00	10,38	12,83	37,23	15,83	4,37	0,02	0,04	14,10	0,46	95,64	19dbte-c1
7	0,11	0,29	0,00	10,52	12,90	37,32	16,12	4,43	0,03	0,03	14,09	0,49	96,32	19dbte-c2
8	0,13	0,29	0,00	10,44	12,49	37,16	16,18	4,38	0,00	0,01	14,05	0,48	95,60	19dbte-c3
9	0,10	0,38	0,00	10,59	12,73	37,11	15,97	4,42	0,00	0,04	14,10	0,53	95,97	19dbte-c4
10	0,08	0,28	0,00	10,42	12,66	36,45	15,69	4,37	0,01	0,00	13,95	0,45	94,35	19dbte-c5
11	0,12	0,29	0,00	10,24	12,63	37,29	15,94	4,29	0,03	0,04	14,08	0,48	95,45	19dbte-c6
12	0,11	0,28	0,00	10,58	12,75	37,11	15,85	4,35	0,00	0,01	14,04	0,55	95,64	19dbte-c7
13	0,07	0,23	0,00	10,47	12,85	37,27	16,17	4,07	0,00	0,06	14,27	0,50	95,94	19dbte-c8
14	0,09	0,30	0,00	10,43	12,80	37,50	15,96	4,21	0,02	0,04	14,00	0,55	95,89	19dbte-c9
15	0,09	0,32	0,00	10,36	12,45	37,10	15,69	4,41	0,03	0,01	14,13	0,54	95,12	19dbte-c10
16	0,09	0,42	0,00	10,40	12,61	37,26	16,21	4,51	0,02	0,01	14,42	0,52	96,46	19dbte-c11
17	0,10	0,57	0,01	10,12	16,35	35,31	11,76	5,72	0,00	0,06	15,82	0,17	95,98	5219bte-e1
18	0,10	0,54	0,00	10,46	16,25	35,79	11,91	5,99	0,02	0,03	15,72	0,16	96,97	5219bte-e2
19	0,15	0,71	0,01	10,33	15,49	35,82	12,42	5,46	0,03	0,05	15,64	0,19	96,30	5219bte-e3
20	0,15	0,55	0,01	10,16	15,47	35,54	12,42	5,79	0,03	0,04	15,87	0,18	96,20	5219bte-e4inclopx1
21	0,03	0,66	0,01	9,89	16,76	35,06	12,36	5,67	0,01	0,06	15,60	0,25	96,35	5219bte-e4inclopx2
22	0,10	0,46	0,00	10,31	15,90	35,63	12,11	5,75	0,01	0,04	16,05	0,18	96,54	5219bte-e4
23	0,11	0,57	0,00	10,48	16,27	35,60	12,11	5,82	0,00	0,04	15,70	0,22	96,91	5219bte-e5
24	0,06	0,56	0,01	10,02	16,59	35,47	12,23	5,60	0,01	0,03	15,58	0,15	96,32	5219bte-e6
25	0,03	0,66	0,00	10,51	16,27	35,51	12,38	5,60	0,00	0,05	15,84	0,20	97,06	5219bte-f1
26	0,05	0,56	0,01	10,47	16,26	35,58	12,18	5,80	0,04	0,01	15,68	0,23	96,86	5219bte-f2
27	0,08	0,55	0,01	9,62	16,21	35,82	11,98	5,50	0,08	0,05	16,18	0,17	96,22	5219bte-f3
28	0,06	0,55	0,00	10,20	15,82	35,34	12,01	5,82	0,00	0,02	15,76	0,21	95,78	5219bte-f4
29	0,04	0,60	0,00	10,50	15,79	35,87	11,98	6,04	0,01	0,03	15,76	0,21	96,83	5219bte-f5
30	0,04	0,51	0,00	10,45	15,97	35,63	11,75	6,33	0,01	0,01	15,91	0,20	96,82	5219bte-f6
31	0,09	0,65	0,00	10,32	16,01	35,44	12,10	5,88	0,00	0,01	15,59	0,16	96,23	5219bte-f7
32	0,07	0,53	0,00	10,21	15,76	35,43	11,56	6,02	0,01	0,03	15,68	0,20	95,50	5219bte-f8
33	0,04	0,28	0,01	10,36	17,53	36,42	12,76	4,52	0,01	0,09	14,24	0,07	96,32	227bte-i2
34	0,03	0,25	0,00	10,31	17,96	36,47	12,40	4,76	0,00	0,07	14,18	0,09	96,52	227bte-i3
35	0,41	0,00	0,01	0,00	10,22	51,49	13,04	0,12	22,29	0,27	1,14	0,05	99,03	227bte-i4
36	0,07	0,38	0,00	10,34	17,38	36,23	12,97	4,45	0,03	0,04	14,24	0,06	96,18	227bte-i5
37	0,04	0,33	0,00	10,13	17,56	36,22	11,94	5,52	0,04	0,11	14,41	0,08	96,37	227bte-i6
38	0,04	0,29	0,00	10,39	17,69	35,92	12,46	4,69	0,02	0,07	13,99	0,11	95,67	227bte-i7
39	0,37	0,01	0,00	0,02	9,48	52,22	13,56	0,05	22,39	0,29	0,81	0,02	99,22	227bte-i8incopx
40	0,04	0,32	0,00	10,51	17,50	36,20	12,44	4,73	0,01	0,10	14,07	0,04	95,96	227bte-i8
41	0,11	0,46	0,00	10,37	16,11	35,63	11,88	6,23	0,01	0,05	15,94	0,17	96,96	5212bte-l1-core1
42	0,14	0,52	0,01	9,14	16,70	35,23	12,66	5,15	0,05	0,09	15,68	0,13	95,51	5212bte-l1-core2
43	0,12	0,49	0,00	10,39	15,77	36,37	12,23	5,88	0,00	0,08	16,25	0,12	97,69	5212bte-l1-core3
44	0,04	0,28	0,01	9,45	20,46	34,44	9,53	5,56	0,12	0,15	15,15	0,12	95,32	5212bte-l1-core4
45	0,10	0,54	0,00	10,42	16,34	35,77	11,71	5,87	0,02	0,06	15,65	0,12	96,60	5212bte-l2-copx1
46	0,13	0,57	0,01	10,34	16,42	35,52	11,69	5,97	0,01	0,03	15,77	0,12	96,58	5212bte-l2-copx2
47	0,14	0,49	0,01	10,28	16,50	35,59	11,64	5,92	0,00	0,06	15,69	0,10	96,42	5212bte-l2-copx3
48	0,10	0,50	0,01	10,22	16,34	35,72	11,40	5,98	0,01	0,08	16,03	0,09	96,47	5212bte-l2-copx4
49	0,14	0,56	0,01	10,32	16,38	35,60	11,52	5,89	0,02	0,08	15,72	0,13	96,36	5212bte-l3-
50	0,12	0,44	0,01	9,75	18,09	34,75	10,51	5,86	0,00	0,10	15,15	0,15	94,91	5212bte-l3-
51	0,06	0,60	0,03	9,60	20,16	35,91	8,68	4,79	0,10	0,04	16,16	0,02	96,15	5201bte-t1-c1
52	0,11	0,45	0,01	10,16	16,67	37,22	13,64	3,70	0,00	0,21	14,40	0,06	96,64	5042bte-r1-c1
53	0,09	0,54	0,01	10,20	16,86	37,00	13,59	3,59	0,00	0,20	14,18	0,06	96,31	5042bte-r1-c2
54	0,11	0,48	0,01	10,28	16,89	37,28	13,37	3,57	0,03	0,15	14,26	0,04	96,47	5042bte-r1-c3
55	0,13	0,62	0,01	10,06	16,86	37,03	13,55	3,41	0,03	0,21	14,17	0,04	96,12	5042bte-r1-c4
56	0,07	0,47	0,01	9,62	17,31	36,11	13,43	3,75	0,04	0,36	14,16	0,05	95,39	5042bte-r2-c1
57	0,10	0,57	0,01	10,16	16,85	36,97	13,56	3,96	0,03	0,25	13,90	0,09	96,46	5042bte-r2-c2
58	0,06	0,39	0,01	9,12	17,78	35,80	13,17	3,51	0,02	0,34	14,39	0,12	94,68	5042bte-r2-c3
59	0,09	0,40	0,01	8,52	18,57	35,45	13,73	3,24	0,04	0,31	14,88	0,06	95,31	5042bte-r2-c4
60	0,08	0,50	0,01	10,20	16,62	36,72	13,70	3,82	0,01	0,20	13,83	0,05	95,74	5042bte-r2-c5
61	0,10	0,55	0,01	10,13	16,48	36,95	13,96	3,89	0,03	0,18	13,87	0,10	96,25	5042bte-r2-c6
62	0,08	0,64	0,01	10,11	16,70	36,96	13,94	3,83	0,00	0,19	13,94	0,08	96,47	5042bte-r2-c7
63	0,06	0,47	0,01	10,17	17,11	36,54	13,28	3,62	0,00	0,22	14,17	0,07	95,72	5042bte-r2-c8

64	0,12	0,51	0,01	10,27	16,62	36,56	14,08	3,80	0,01	0,24	13,91	0,09	96,21	5042bte-r2-c9
65	0,10	0,55	0,01	10,23	16,49	37,20	13,78	3,68	0,00	0,26	14,03	0,10	96,42	5042bte-r2-c10
66	0,10	0,53	0,01	9,60	17,12	36,37	13,72	3,91	0,05	0,40	14,27	0,12	96,19	5042bte-r3-c1
67	0,09	0,44	0,01	9,94	16,78	36,82	13,56	3,83	0,01	0,22	14,02	0,11	95,82	5042bte-r3-c2
68	0,08	0,50	0,01	10,05	16,55	37,07	13,54	3,99	0,02	0,21	14,35	0,11	96,48	5042bte-r3-c3
69	0,09	0,53	0,00	10,08	16,49	36,93	13,69	3,91	0,01	0,22	13,98	0,04	95,95	5042bte-r3-c4
70	0,10	0,48	0,01	9,78	18,48	36,37	12,47	3,76	0,00	0,29	14,45	0,08	96,25	5042bte-r4
71	0,12	0,54	0,01	10,12	16,63	37,03	13,75	3,77	0,03	0,22	14,34	0,10	96,65	5042bte-r5
72	0,10	0,44	0,01	9,94	16,55	36,54	13,41	3,76	0,10	0,22	13,88	0,08	95,01	5042bte-r6
73	0,12	0,59	0,01	10,39	16,33	37,39	13,59	3,77	0,02	0,21	14,56	0,09	97,07	5042bte-r7
74	0,09	0,56	0,01	10,30	16,97	36,81	13,74	4,06	0,02	0,25	13,93	0,09	96,83	5042bte-r8
75	0,07	0,42	0,02	10,20	16,96	36,56	13,53	2,94	0,02	0,11	15,96	0,13	96,91	5186bte-n1-c1
76	0,07	0,46	0,02	10,56	17,00	36,47	13,66	2,87	0,01	0,05	15,89	0,10	97,16	5186bte-n1-c2
77	0,06	0,41	0,02	10,41	17,10	36,09	13,42	3,05	0,01	0,07	15,85	0,08	96,56	5186bte-n1-c3
78	0,10	0,34	0,02	10,47	17,08	36,41	13,39	2,99	0,00	0,07	15,75	0,09	96,69	5186bte-n1-c4
79	0,06	0,44	0,02	10,32	17,05	36,21	13,55	3,00	0,00	0,06	15,75	0,13	96,59	5186bte-n1-c5
80	0,07	0,35	0,02	10,43	16,96	36,36	13,37	2,98	0,00	0,08	15,72	0,10	96,43	5186bte-n1-c6
81	0,10	0,32	0,02	10,50	16,83	36,46	13,80	2.86	0,00	0,09	15,56	0,09	96,62	5186bte-n2-c1
82	0,08	0,32	0,03	10,45	16,71	36,29	13,66	2,79	0,00	0,09	15,87	0,07	96,36	5186bte-n2-c2
83	0,09	0,29	0,03	10,37	16,40	36,40	13,98	2,72	0,00	0,10	15,93	0,07	96,38	5186bte-n2-c3
84	0,08	0,29	0,03	10,32	15,85	36,28	14,18	2,71	0,00	0,07	16,06	0,05	95,92	5186bte-n2-c4
85	0,08	0,31	0,02	10,30	13,86	36,76	15,13	2,81	0,02	0,07	16,05	0,02	95,41	5186bte-n2-copx1
86	0,04	0,37	0,03	10,31	14,45	36,55	14,97	2,73	0,02	0,06	16,04	0,04	95,61	5186bte-n2-copx2
87	0,08	0,31	0,03	10,30	17,52	35,96	12,78	3,26	0,00	0,08	15,73	0,11	96,16	5186bte-n3
88	0,07	0,35	0,02	10,64	17,17	35,87	13,12	3,33	0,01	0,08	15,83	0,11	96,58	5186bte-n4
89	0,07	0,43	0,02	10,34	17,27	36,01	12,86	3,45	0,00	0,08	16,09	0,12	96,72	5186bte-n5
90	0,06	0,34	0,02	10,55	17,20	36,03	13,16	3,21	0,00	0,10	15,84	0,06	96,56	5186bte-n6
91	0,14	0,32	0,05	10,33	16,62	35,78	13,52	2,83	0,02	0,08	15,60	0,09	95,37	5186bte-n7

APPENDIX XXII

A COMPARAISON OF ANALYTICAL RESULTS FROM THE MRNQ AND UQAC FOR AN INTERNAL STANDARD (EQ256) AND A MELT-DEPLETED METAGREYWACKE (1133)

Samples counted for 60 minutes at MRNQ

Samples counted for 2 hours at UQAC

Analytical method	XRF	XRF	INAA	INAA
Laboratory	**UQAC**	**MRNQ**	**UQAC**	**MRNQ**
Sample	EQ256	EQ256	1133	1133
SiO_2 (Wt%)	61,51	61,30		
TiO_2	0,67	0,69		
Al_2O_3	17,49	17,40		
Fe_2O_{3t}	6,88	6,74		
MnO	0,09	0,09		
MgO	3,31	3,23		
CaO	1,44	1,42		
Na_2O	3,34	3,19	3,11	2,98
K_2O	3,88	3,93		
P_2O_5	0,09	0,09		
LOI	1,65	1,82		
Total	100	99,9		
Cr (ppm)			320	276
Ni				
Co			27	0,6
Sc			20,59	18,4
V	128	129		
Cu				
Pb				
Zn				
Rb	187	190	114	105
Cs				
Ba				
Sr	267	268		
Ga	25	26		
Ta			0,43	0,50
Nb	17	16		
Hf			3,78	3,60
Zr	143	140		
Y	16	13		
Th			10,72	7,60
U			2,26	1,50
La			31,60	29
Ce			65	50
Nd			23,90	20
Sm			4,64	4,30
Eu			1,51	1,30
Tb			0,56	0,20
Yb			1,61	1,50
Lu			0,24	0,200

REFERENCES

Allibone, A.H. & Norris, R.J. 1992. Segregation of leucogranite microplutons during syn-anatectic deformation: an example from the Taylor Valley, Antartica. Journal of Metamorphic Geology, **10,** 589-600.

Arculus, R. J. & Ruff, L., 1990. Genesis of continental crust: evidence from island arcs, granulites and exospheric processes. In: *Granulites and Crustal Evolution* (eds. Vielzeuf, D. & Vidal, Ph.), pp. 7-23. Kluwer Academic Publishers, Dordrecht

Arth, J. G., 1876. Behavior of trace elements during magmatic processes—a summary of theoretical models and their applications. *Journal of Research* of the US.Geological Survey, **4**, 41–47.

Ashworth, J.R., 1985. Introduction to migmatites. In: Migmatites (ed. Ashworth, J.R.), Blackie, 1-35, Glasgow.

Ayres, M. & Harris, N., 1997. REE fractionation and Nd-isotope disequilibrium during crustal anatexis: Constraints from Himalayan leucogranites. *Chemical Geology,* **139**, 249–269

Bailey, D.K. & Macdonald, R., 1975. Fluorine and chlorine in peralkaline liquids and the need for magma generation in an open system. *Mineralogical Magazine*, **40**, 405–414.

Barbey, P. & Cuney, M., 1982. Rb, Sr, Ba, U and Th geochemistry of the Lapland granulites. *Contributions to Mineralogy and Petrology,* **81**, 304-316.

Barbey, P., Bertrand, J.-M., Angoua, S. & Dautel, D., 1989. Petrology and U/Pb geochronology of the Telohat migmatites, Aleksod, Central Hoggar, Algeria. *Contributions to Mineralogy and Petrology,* **101**, 207-219.

Barbey, P., Brouand, M., Le Fort, P. & Pêcher, A., 1996. Granite-migmatite genetic link: example of the Manaslu Granite and Tibetan slab migmatites in central Nepal. *Lithos,* **38**, 63-79.

Bea, F., 1991. Geochemical modelling of low melt-fraction anatexis in a peraluminous system: the Peña Negra Complex (central Spain). *Geochimica et Cosmochimica Acta,* **55**, 1859-1874.

Bea, F., 1996. Controls on the trace element composition of crustal melts: Royal Society of Edinburgh Transactions. *Earth Sciences*, **87**, p. 133–141.

Bea, F., Pereira, M. D. & Stroh, A., 1994. Mineral/leucosome trace-element partitioning in a peraluminous migmatite (a laser ablation- ICP-MS study). *Chemical Geology,* **117**, 291-312.

Beaumont, C., Jamieson, R.A., Nguyen, M.H. & Medvedev, S., 2004. Crustal channel flows: 1. Numerical models with applications to the tectonics of the Himalayan-Tibetan orogen. *Journal of Geophysical Research,* **109**, B06406, doi:10.1029/2003JB002809

Bédard, L. P & Barnes, S. J., 1990. Instrumental neutron activation analysis by collecting only one spectrum: results for international geochemical reference samples. *Geostandards Newsletter,* **14**, 479-484.

Bédard, L. P & Barnes, S. J., 2002. Comparison of N-type semi-planar and coaxial INAA detectors for 33 geochemical reference samples. Journal of Radioanalytical and Nuclear Chemistry, **254**: 485-497.

Blumenfeld, P. & Bouchez, J. L., 1988. Shear Criteria in granite and migmatite deformed in the magmatic and solid states. *Journal of Structural Geology,* **10**, 361-372.

Bowen. N. L. 1928. *The Evolution of the Igneous Rocks*. Princeton University Press reprinted by Dover Publications (1956). 332pp

Brown, G. C. & Fyfe W. S., 1970. The production of granitic melts during ultrametamorphism. *Contributions to Mineralogy and Petrology,* **28**, 310-318.

Brown, M. & Solar, G., 1999. The mechanism of ascent and emplacement of granite magma during transpression: a syntectonic granite paradigm. *Tectonophysics,* **312**, 1-33.

Brown, M. A., Brown, M., Carlson, W. D. & Denison, C., 1999. Topology of syntectonic melt flow networks in the deep crust: inferences from three dimensional images of leucosome geometry in migmatites. *American Mineralogist,* **84**, 1793-1818.

Brown, M., Averkin, Y. A., McLellan, E. & Sawyer, E. W., 1995. Melt segregation in migmatites. *Journal of Geophysical Research,* **100**, 15, 655-679.

Brown, M., 1995. Late-Precambrian geodynamic evolution of the Armorican segment of the Cadomian Belt (France): distortion of the active continental margin during south-west directed convergence and subduction of a bathymetric high. *Géologie de France,* **3**, 3-22.

Brown, M., 1979. The petrogenesis of the St-Malo migmatite belt, Armorican Massif, France, with particular reference to the diatexites. *Neues Jahrbuch fur Mineralogie, Abhandlungen,* **135**, 48-74.

Bryan, W.B., Finger, L.W., Chayes, F.,1969. Estimating proportions in petrographic mixing equations by least-squares approximation. *Science,* **163**, 926-927.

Burg, J.P., Vanderhaeghe, O., 1993. Structures and way-up criteria in migmatites, with application to the Velay dome (French Massif central). *Journal of Structural Geology,* **15**, 1293–1301.

Cadéron, S., Goulet, N. & Lamothe, D., 1999. Étude de la partie centre-est de la Province du Superiéur (sous-provinces de La Grande/Opinaca/Ashuanipi): traits structuraux communs et évolution métamorphique, Québec. In: *Project de cartographie du Grand-Nord. Premier Atelier Annuel (avril 7-8, 1999), Géologie Québec, Rapport* **1**, pp. 83-104.

Calvert, A. J. & Ludden, J. N., 1999. Archean continental assembly in the southeastern Superior Province of Canada. *Tectonics,* **18**, 412-429.

Card, K. D. & Ciesielski, A., 1986. DNAG #1. Subdivisions of the Superior Province of the Canadian Shield. *Geoscience Canada*, **13**, 5-13.

Castro A. Corretgé L. G., El-Biad M.; El-Hmidi H.; Fernandez C. & Patino Douce A.E. 2000. Experimental constraints on Hercynian anatexis in the Iberian Massif, Spain. *Journal of Petrology,* **41**, 1471-1488.

Castro, A., 2004. The source of granites: inferences from the Lewisian complex. *Scottish Journal of Geology*, **40**, (1), 49-65.

Castro, A., Garcia-Moreno, O., El-Hmidi, H. & Corretge, L. G., 2002. Dissolution of mafic microgranular enclaves by decompression melting in water-saturated granitic magma. *Journal of Conference Abstracts*, **7**, 23.

Chevé, S. R. & Brouillette, P., 1991. Radiogenic age constraints on the geological evolution of the northeastern Ashuanipi Complex, Superior Province, New Quebec. *Geological Association of Canada-Mineralogical Association of Canada Abstracts,* **16**, A-23.

Chevé, S. R. & Brouillette, P., 1992. Reconnaissance géologique et métallogénique au NO de Schefferville: région des lacs Weeks (1/2E) et Pailleraut (1/2O) (Territoire du Nouveau-Québec). *Ministère des Ressources Naturelles du Québec,* MB**92-12**, 215 pp.

Chevé, S. R. & Brouillette, P., 1995. Géologie et métallogénie de la partie nord-est de la sous-province d' Ashuanipi (Nouveau-Quebéc). *Ministère des Ressources naturelles du Québec,* MM **95-01**. 7 pp.

Christensen, N.I. & Mooney W.D., 1995. Seismic velocity structure and composition of the continental crust: A global view. *Journal of Geophysical Research,* **100**, 9761-9788.

Clemens, J. D. & Vielzeuf, D., 1987. Constraints on melting and magma production in the crust. *Earth and Planetary Sciences Letters,* **86**, 287-306.

Clemens, J. D. & Watkins, J. M., 2001. The fluid regime of high-temperature metamorphism during granitoid magma genesis. *Contributions to Mineralogy and Petrology,* **140**, 600-606.

Clemens, J. D., 1990. The granulite - granite connexion. In: *Granulites and Crustal Evolution* (eds. Vielzeuf, D. & Vidal, Ph.), pp. 25-36. Kluwer Academic Publishing, Dordrecht.

Clemens, J.D. & Mawer, C.K., 1992. Granitic magma transport by fracture propagation. *Tectonophysics* **204**, 339-360.

Collins, W. J. & Sawyer, E.W., 1996. Pervasive granitoid magma transfer through the lower-middle crust during non-coaxial compressional deformation. *Journal of Metamorphic geology*, **14**, 565-579.

Condie, K.C., 1978. Geochemistry of Proterozoic granitic plutons from New Mexico, U.S.A. *Chemical Geology*, **21**, 131–149.

David, J. & Parent, M., 1997. Géochronologie U-Pb du Projet Moyen Nord: Ministère des Ressources naturelles, Québec, CM59903, 88p.

Davies, W. J., Machado, N., Garièpy, C., Sawyer, E. W. & Benn, K., 1995. U-Pb geochronology of the Opatica tonalite-gneiss belt and its relationship to the Abitibi greenstone belt, Superior Province, Quebec. *Canadian Journal of Earth Science,* **32**, 113-127.

Davis, D. W., Pezzutto, F. & Ojakangas, R. W., 1990. The age and provenance of metasedimentary rocks in the Quetico subprovince, Ontario, from single zircon

analyses: implications for Archaean sedimentation and tectonics in the Superior Province. *Earth and Planetary Science Letters,* **99**, 195-205.

Dodge, F.C.W., and Mays, R.E., 1972. Rare-earth element fractionation in accessory minerals, Central Sierra Nevada Batholith. *USGS PP*, **800D**, D165-D168.

Dougan, T. W., 1981. Melting reactions and trace elements relationships in selected specimens of migmatitic metapelites from New Hampshire and Maine. *Contributions to Mineralogy and Petrology*, **78**, 337-344.

Drummond, B. J., 1988. A review of the crust / upper mantle structure in the Precambrian areas of Australia and implications for Precambrian crustal evolution: *Precambrian Research*, **40**, 101–116.

Doyon, J., 2004. Étude géochimique des sous-provinces métasédimentaires archéennes de la province du Supérieur. Mémoire de maitrise.

Eade, K. E., 1966. Fort George River and Kaniapiskau River (west half) map-areas, New Quebec. *Geological Survey of Canada, Memoir* **339**, 84 pp.

Ellis, D. J. & Thompson, A. B., 1986. Subsolidus and partial melting reactions in the quartz-excess $CaO+MgO+Al_2O_3-H_2O$ system under water-excess and water-deficient

conditions to 10 kb: some implications for the origin of peraluminous melts from mafic rocks. *Journal of Petrology,* **27**, 91-212.

Ellis, S., Beaumont, C., Jamieson, R.A. & Quinlan, G.,1998. Continental collision including a weak zone: The vise model and its application to the Newfoundland Appalachians. *Canadian Journal of Earth Sciences*, **5**, 1323-1346

Fahrig, W. F., 1967. Shabogamo Lake map-area, Newfoundland-Labrador and Quebec 23G and E (east half). *Geological Survey of Canada, Memoir,* **354**, 23 pp.

Finger, F. & Clemens, J. D., 1995, Migmatization and "secondary" granitic magmas: effects of emplacement and crystallization of "primary" granitoids in southern Bohemia, Austria. *Contributions to Mineralogy and Petrology,* **120**, 311-326.

Fralick, P. & Davis, D., 1999. The Seine-Coutchiching problem revisited: sedimentology, geochronology and geochemistry of sedimentary units in the Rainy Lake and Souix Lookout areas. *Lithoprobe Western Superior Transect, 5th. Annual Workshop, Lithoprobe Report* **70**, pp. 66-75.

Fyfe, W. S., 1973. The granulite facies, partial melting and the Archaean crust. *Philosophical Transactions of the Royal Society of London, Series A,* **273**, 457-461.

Gardien, V., Thompson, A. B., Grujic, D. & Ulmer, P., 1995. Experimental melting of biotite + plagioclase + quartz + muscovite assemblages and implications for crustal melting. *Journal of Geophysical Research,* **100**, 15581-15591.

Goutier, J., Dion, C. & Ouellet, M.-C., (2001). Géologie de la région de la colline Bezier (32G/12) et du lac de la Montagne du Pin (32G/13). *Minisitère des Ressource naturelles du Québec,* RG **2001-13**.

Goutier, J., Dion, C., Ouellet, M.-C., Davis, D. W., David, J. & Parent, M., 2002. Géologie de la région du Lac Guyer (33G/05, 33/G06 et 33G/11). *Ministère des Ressources Naturelles du Québec,* RG **2001-15**.

Grant, J. A., 2004. Liquid compositions from low-pressure experimental melting of pelitic rock from Morton Pass, Wyoming, USA. *Journal of Metamorphic Geology,* **22**:2, 65-78

Greenfield, J. E., Clarke G. L., Bland M. & Clarke D. J., 1996. *In situ* migmatite and hybrid diatexite at Mt. Stafford, central Australia. *Journal of Metamorphic Geology,* **14**, 413-426.

Guernina, S. & Sawyer, E. W., 2003. Large-scale melt-depletion in granulite terranes: an example from the Archean Ashuanipi Subprovince of Québec. *Journal of Metamorphic Geology*, **21**, 181–201.

Hansen E. & Stuk M., 1993. Orthopyroxene-bearing, mafic migmatites at Cone Peak, California: evidence for the formation of migmatitic granulites by anatexis in an open system. *Journal of Metamorphic Geology,* **11**, 291-307.

Hansen E., and Stuk, M., 1993. Orthopyroxene-bearing, mafic migmatites at ConePeak, California; evidence for the formation of migmatitic granulites by anatexis in an open system. *Journal of Metamorphic Geology*, **11**, 291–307.

Hanson G, N., & Langmuir, C. H., 1978. Modelling of major elements in mantle-melt systems using trace element approaches. *Geochemica et Cosmochemica Acta* **42**, 725-741.

Harris, N. B. & Inger, S., 1992. Trace element modelling of pelite-derived granites. *Contributions to Mineralogy and Petrology,* **110**, 46-56.

Harrison T.M. & Watson E.B., 1983. Kinetics of zircon dissolution and zirconium diffusion in granitic melts of variable water content. *Contributions to Mineralogy and Petrology.* **84**, 67-72.

Harrison T.M. & Watson E.B., 1984. The behavior of apatite during crustal anatexis: Equilibrium and kinetic considerations. *Geochimica. Cosmochimica. Acta*, **48**, 1467-1477.

Harte, B., Pattison, D.R.M. & Linklater, C. (1991) Field relations and petrography of partially melted pelitic and semipelitic rocks. In: Voll, G., Topel, J., Pattison, D.R.M. and Seifert, F. (eds.) *Equilibrium and kinetics in contact metamorphism: The Ballachulish Igneous Complex and its thermal aureole.* Springer Verlag: Heidelberg, 181-209.

Hartel T H D and Pattison D R M 1996 Genesis of the Kapuskasing (Ontario) migmatitic mafic granulites by dehydration melting of amphibole: The importance of quartz to reaction progress. *Journal of. metamorphic Geology*, **14**,591–611

Heier, K.S., 1960. Petrology and geochemistry of high-grade metamorphic and igneous rocks on Langøy, northern Norway Norges. Geological Unders Bulletin **207**

Holness, M. & Watt, G. R., 2002. The aureole of the Traigh Bhàn na Sgùrra sill, Isle of Mull: reaction driven microcracking during pyrometamorphism. *Journal of Petrology,* **43**, 511-534.

Hoskin, P.W.O., Kinny, P.D., Wyborn, D & Chappell, B.W., 2000. Identifying accessory mineral saturation during differentiatiom in granitoid magmas: an integrated approach. Journal of Petrology, **41**, 1365-1396.

Huerta, A.D., Royden, L.H., and Hodges K.V., 1996. The interdependence of deformational and thermal processes in mountain belts. *Science*, **273**, 637-639.

Hunter, R. H., 1987. Textural equilibrium in layered igneous rocks. In: *Origin of Igneous layering,* (ed. Parsons, I), pp. 473-503, Reidel, Dordrecht.

Hutton, J., 1794. Dissertation on the philosophy of light, heat, and fire. *Edinburgh*

Hynes, A., 1999. Seismic reflections and the gravity field: implications of the deep structure of the Uchi, English River and Winnipeg River Subprovinces. *Lithoprobe Western Superior Transect, 5th. Annual Workshop, Lithoprobe Report* **70**, pp. 80-89.

Icenhower, J. & London, D., 1995. An experimental study of element partitioning among biotite, muscovite and coexisting peraluminous silicic melt at 200 Mpa (H_2O). *American Mineralogist,* **80**, 1229-1251.

Icenhower, J. & London, D., 1996. Experimental partitioning of Rb, Cs, Sr and Ba between alkali feldspar and peraluminous melt. *American Mineralogist,* **81**, 719-734.

James, D. T., 1997. Geology of the Archean Ashuanipi Complex, Western Labrador. *Newfoundland Department of Mines and Energy; Report* **97-2**, 27p.

Jamieson, R.A., Beaumont, C., Medvedev, S. & Nguyen, M.H., 2004. Crustal channel flows: 2. Numerical models with implications for metamorphism in the Himalayan-Tibetan orogen. *Journal of Geophysical Research* **109**, B06406.

Kosinowski, M.H.F., 1982. MSONRM, a fortran program for the improved version of mesonormative calculation computers and geosciences, **8,** #1, pp111-20.

Kretz, R., 1983. Symbols for rock forming minerals. *American Mineralogist,* **68**, 277-279.

Kriegsman, L.M., 2001. Partial melting, partial melt extraction and partial back reaction in anatectic migmatites. *Lithos*, **56**, 75-96.

Lambert, I. B. & Heier, K. S., 1968. Geochemical investigations of deep-seated rocks in the Australian Shield. *Lithos,* **1**, 30-53.

Lamothe, D., Leclair, A.D. & Choinière, J., 1998. Cadre tectonique des sous provinces d'Ashuanipi, d'Opinaca et d'Opatica, Province du Supérieur, Moyen-Nord québécois. *Geological Association of Canada-Mineralogical Association of Canada Abstracts,* **23**, A-101.

Lamothe, D., Leclair, A.D. & Choinière, J., 1998. Géologie de la région du Lac Vallard (SNRC 23C) : Ministère des Ressources naturelles, Québec, RG 99-14, 40p.

Lamothe, D., Thériault, R & Leclair, A., 2000. Géologie de la région du Lac Nitchequon (SNRC 23E) : Ministère des Ressources naturelles, Québec, RG 98-13, 29p.

Lapointe, B., 1996. Un exemple de mineralisation aurifère en milieu profond: l'indice d'or du Lac Lillois dans le complexe d'Ashuanipi, province du Supérieur, Nouveau-Québec. Unpublished Ph.D. thesis, Université du Québec à Chicoutimi.

Le Breton, N., & Thompson A. B., 1988. Fluid-absent (dehydration) melting of biotite in metapelites in the early stages of crustal anatexis. *Contributions to Mineralogy and Petrology,* **99**, 226-237.

Leclair, A., Lamothe, D., Choinière, J. & Parent, M., 1998b. Géologie de la région du Lac Bermen (SNRC 23F). *Ministère des Ressources Naturelles du Québec,* Rapport **97-11**, 40 p.

Leclair, A.D., Lamothe, D. & Parent, M., 1998a Événements magmatiques et tectono-métamorphiques dans le sud-est de la Province du Supérieur, Canada. *Geological Association of Canada-Mineralogical Association of Canada Association Abstracts,* **23**, A-106.

Ledru, P., Faure, M., Bouchot, V., 2001. Le Massif central, témoin de la chaîne varisque ouest-européenne. *Géologues*, **130**, 30-46.

Lemaitre, R. W., (ed.), 1989. A classification of igneous rocks and glossary of terms, Blackwell, Oxford, 193pp.

Marchildon, N. & Brown, M., 2002. Grain-scale melt distribution in two contact aureole rocks: implications for controls on melt localization and deformation. *Journal of Metamorphic Geology*, **20**, 381-396.

McCarthy T. S., & Kable E. J. D., 1978. On the behaviour of rare-earth elements during partial melting of granitic rock. *Chemical Geology*, **22**, 21-29.

McCarthy. T. C. & Grove, D. I., 1979. The blue Tier batholith, Northeastern Tasmania. *Ibid*, **71**, 193-209.

McCarthy. T. C. & Patiño Douce, A. E., 1998. Empirical calibration of the silica - Catschermak's-anorthite (Scan) geobarometer. *Journal of Metamorphic Geology,* **16**, 675-686.

Menhert, K. R., 1968. Migmatites and the origin of granitic rocks. *Elsevier Publications*. Co., Amsterdam - Oxford - New York.

Miller, C. F. & Mittlefehldt, D. W., 1982. Depletion of light rare-earth elements in felsic magmas. *Geology,* **10**, 129-133.

Miller, C.F., Hanchar, J.M., Wooden, J.L., Bennett, V.C., Harrison, T.M., Wark, D.A., & Foster, D.A., 1992. Source region of a granite batholith: Evidence from lower crustal xenoliths and inherited accessory minerals. *Transactions of the Royal Society of Edinburgh, Earth Sciences*, **83**, 49-62.

Milord, I. & Sawyer, E. W., 2003. Schlieren formation in diatexite migmatite: examples from the St Malo migmatite terrane, France. *Journal of Metamorphic Geology,* **21** (4), 347-362.

Milord, I., Sawyer, E. W. & Brown, M., 2001. Formation of diatexite migmatite and granite magma during anatexis of semi-pelitic metasedimentary rocks: an example from St.Malo, France. *Journal of Petrology,* **42**, 487-505.

Montel J. M. & Vielzeuf, D., 1997. Partial melting of metagreywackes. Part II: compositions of minerals and melts. *Contributions to Mineralogy and Petrology,* **128**, 176-196.

Moukhsil, A., Legault, M., Boily, M., Doyon, J., Sawyer, E. W. & Davis, W. D., 2003. Synthèse géologique et métallogénique de la ceinture de roches vertes de la moyenne et de la Basse-Eastmain, Baie James, Québec. *Ministère des Ressources Naturelles du Québec*. ET **2002-06**, 55 pp.

Moukhsil, A., Voicu, G., Dion, C., David, J., Davis, D. W. & Parent, M., 2001. Géologie de la région de la Basse-Eastmain centrale (33C/03, 33C/04, 33C/05 et 33C/06). *Ministère des Ressources Naturelles du Québec*. RG **2002-08**. 52 pp.

Nabelek, P.I. and Bartlett, C., 2000. Fertility of metapelites and metagraywackes during leucogranite generation: An example from the Black Hills, USA. *Transactions of the Royal Society of Edinburgh*, **91**, 1-14.

Nabelek, P.I.& Glascock, M.D., 1995. Rare earth element-depleted leucogranites Black Hills, South Dakota: A consequence of disequilibrium melting of monazite-bearing schists. *Journal of Petrology,* **36**, 1055-1071.

Nédélec, A., Minyem, D. & Barbey, P., 1993. High-P-high-T anatexis of Archaean tonalitic grey gneiss: the Eseka migmatites, Cameroon. *Precambrian Research,* **62**, 191-205.

Nyman, M. W., Pattison, D.R.M. and Ghent, E.D., 1995. Melt extraction during formation of K-feldspar + sillimanite migmatites, west of Revelstoke, British Columbia. *Journal of Petrology*, **36**, 351-372

Olsen, S. N., Mass balance in migmatites, 1982. In: Migmatites, 1985. (ed. Ashworth, J.R.), Blackie, 145-178, Glasgow.

Olsen, S.N. and Grant, J.A., 1991. Isocon analysis of migmatization in the Front Range, Colorado, USA. *Journal of Metamorphic Geoogy,* **9**, 151-164.

Pan, Y., Fleet, M. E. & Heaman, L., 1998. Thermo-tectonic evolution of an Archaean accretionary complex: U-Pb geochronological constraints on granulites from the Quetico subprovince, Ontario, Canada. *Precambrian Research,* **92**, 117-128.

Parent, M., 1998. Géochronologie U-Pb du projet Moyen-Nord, Phase II. Ministère des Ressources Naturelles du Québec, GM59904, 61p.

Patiño Douce, A. E. & Beard, J. S., 1995. Dehydration-melting of biotite gneiss and quartz amphibolite from 3 to 15 kbar. *Journal of Petrology,* **36**, 707-738.

Patiño Douce, A. E. & Beard, J. S., 1996. Effects of P, $f(O_2)$ and Mg/Fe ratio on dehydration melting of model metagreywackes. *Journal of Petrology*, **37**, 999-1024.

Patiño Douce, A. E. & Harris, N., 1998. Experimental constraints on Himalayan anatexis. *Journal of Petrology*, **39**, 689-710.

Percival, J. A. & Sullivan, R. W. 1998. Age constraints on the evolution of the Quetico belt, Superior Province. In*: Radiogenic age and isotope studies: report 2* (ed. Mortensen, J. K.); *Geological Survey of Canada* Paper **88-2**, pp. 97-108.

Percival, J. A. Stern, R. A. & Rayner, N., 2003. Archaean adakites from the Ashuanipi complex, eastern Superior Province, Canada: geochemistry, geochronology and tectonic significance. *Contributions to Mineralogy and Petrology*, **145**, 265–280

Percival, J. A., 1989. A regional perspective of the Quetico metasedimentary belt, Superior Province, Canada. *Canadian Journal of Earth Sciences,* **26**, 677-693.

Percival, J. A., 1991a. Orthopyroxene-poikilitic tonalites of the Desliens igneous suite, Ashuanipi granulite complex. Labrador-Quebec, Canada. *Canadian Journal of Earth Sciences*, **28**, 743-753.

Percival, J. A., 1991b. Granulite-facies metamorphism and crustal magmatism in the Ashuanipi complex, Quebec-Labrador, Canada. *Journal of Petrology,* **32**, 1261-1297.

Percival, J. A., Mortensen, J. K., Stern, R. A., Card, K. & Begin, N. J., 1992. Giant granulite terranes of northeastern Superior Province: the Ashuanipi complex and Minto block. *Canadian Journal of Earth Sciences*, **29**, 2287-2308.

Percival. J. A., 1993. Géologie complexe d'Ashuanipi, région de Schefferville, Terre-Neuve-Québec. *Commission géologique du Canada*; Carte 1785A, échelle 1:125000.

Pickering, J. M. & Johnston, A.D., 1998. Fluid-absent melting behavior of a two-mica metapelites: experimental constraints on the origin of Black Hills Granite. *Journal of Petrology,* **39**, 1787-1804.

Pirie, J. & Mackasey, W. O., 1978. Preliminary examination of regional metamorphism in parts of Quetico metasedimentary belt, Superior Province, Ontario. In: *Metamorphism in the Canadian Shield* (eds, Fraser, J. A. & Heywood, W. W.), *Geological Survey of Canada*, Paper **78-10**, 37-48.

Platten, I. M., 1982. Partial melting of feldspathic quartzite around late Caledonian minor intrusions in Appin, Scotland. *Geological Magazine*,**119**, 413-419.

Platten, I. M., 1983. Partial melting of semipelite and the development of marginal breccias around a late Caledonian minor intrusion in the Grampian Highlands of Scotland. *Geological Magazine*; **120**, 37-49.

Poulsen, K. H., Borradaile, G. J. & Kehlenbeck, M. M., 1980. An inverted Archaean succession at Rainy Lake, Ontario. *Canadian Journal of Earth Sciences,* **17**, 1358-1369.

Powell, R. & Downes, J., 1990. Garnet porphyroblast-bearing leucosomes in metapelites: mechanisms phase diagrams, and an example from Broken Hill, Australia. In: Ashworth, J.R. & Brown, M. (eds) High temperature metamorphism and crustal anatexis. London: Unwin Hyman. pp. 105-123.

Powell, R., 1983. Processes in granulite facies metamorphism. In: Migmatites, melting and metamorphism. (eds Atherton. M. P., & Gribble C. D.). pp 127-139. Shiva. London.

Raith, M., Karmakar. S. & Brown, M., 1997. Ultrahigh-temperature metamorphism and multi stage decompressional evolution of sapphirine granulites from the Palni Hill Ranges, Southern India; *Journal of. Metamorphic Geology,***15,** 379–399

Ramsey, C. R. & Kamineni, D. C., 1977. Petrology and evolution of an Archaean metamorphic aureole in the Slave Craton, Canada. *Journal of Petrology,* **18**, 460-486.

Rudnick, R. L., & Taylor, S. R., 1987. The composition and petrogenesis of the lower crust: a xenolith study. *Journal of Geophysical Research*, **92**, 13981-14005.

Rapp, R.P., and Watson, E.B., 1986. Monazite solubility and dissolution kinetics: Implications for the Th and light rare-earth chemistry of felsic magmas. *Contributions to Mineralogy and Petrology*, **94**, 304–316

Read, H. H., 1957. The granite controversy. Thomas Murby and Co., London, **430pp**.

Robin, P-Y. F., 1979. Theory of metamorphic segregation and related processes. *Geochimica et Cosmochimica Acta,* **43**, 1587-1600.

Rosenberg, C.L., & Handy, M.R., 2005. Experimental deformation of partially-melted granite revisited: implications for the continental crust. *Journal of Metamorphic Geology,* **23**, 19-28.

Rubatto, D., Williams, I. S. & Buick, I. S., 2001. Zircon and monazite response to prograde metamorphism in the Reynolds Range, Central Australia. *Contributions to Mineralogy and Petrology*, **140**, 458-468.

Rudnick, R. L., & Taylor, S. R., 1987. The composition and petrogenesis of the lower crust: a xenolith study. *Journal of Geophysical Research,* **92**, 13981-14005.

Rushmer, T., 2001. Volume change during partial melting reactions: implications for melt extraction, melt geochemistry and crustal rheology. *Tectonophysics,* **342**, 389-405.

Rutter, E. H., 1997. The influence of deformation on the extraction of crustal melts: In: *Deformation-Enhanced Melt Segregation and Metamorphic Fluid Transport.* (ed. Holness, M.), pp. 82-110. *Mineralogical Society Series* **8**. London: Chapman and Hall.

Sawka, W, N., 1988. REE and trace element variations in accessory minerals and hornblende from the strongly zoned McMurry Meadows Pluton, California. *Trans. Royal Society of Edinburgh,* **79**,157

Sawyer, E. W. & Benn, K., 1994. Structure of the high-grade Opatica Belt and adjacent low-grade Abitibi Subprovince, Canada: An Archaean mountain front. *Journal of Structural Geology*, **15**, 1443-1458.

Sawyer, E. W. 2001. Melt segregation in the continental crust: distribution and movement of melt in anatectic rocks. *Journal of Metamorphic Geology,* **12**, 291-309.

Sawyer, E. W., 1983. The structural history of a part of Archaean Quetico Metasedimentary Belt, Superior, Province Canada. *Precambrian Research,* **22**, 271-294.

Sawyer, E. W., 1986. The influence of rock source type, chemical weathering and sorting on the geochemistry of clastic sediments from Quetico Metasedimentary Belt, Superior Province, Canada. *Chemical Geology,* **55**, 77-95.

Sawyer, E. W., 1987. The role of partial melting and fractional crystallization in determining discordant migmatite leucosome compositions. *Journal of Petrology,* **28**, 445-73.

Sawyer, E. W., 1994. Melt segregation in the continental crust. *Geology,* **22**, 1019-1022.

Sawyer, E. W., 1998. Formation and evolution of granite magmas during crustal reworking: the significance of diatexites. *Journal of Petrology*, **39**, 1147-1167.

Sawyer, E. W., 1999. Criteria for the recognition of partial melting. *Physics and Chemistry of the Earth (A),* **24**, 269-279.

Sawyer, E. W., 2000. Grain-scale and outcrop-scale distribution and movement of melt in a crystallizing granite. *Transactions of the Royal Society of Edinburgh: Earth Sciences,* **91**, 73-85.

Sawyer, E. W., Barnes, S. J., 1988. Temporal and compositional differences between subsolidus and anatectic migmatite leucosomes from the Quetico metasedimentary belt, Canada. *Journal of Metamorphic Geology*, **6**, 437-540.

Sawyer, E. W., Dombrowski, C. & Collins, W. J., 1999. Movement of melt during synchronous regional deformation and granulite-facies anatexis, an example from the Wuluma Hills, central Australia. In: *Understanding Granites; integrating New and*

Classical Techniques (eds. Castro, A., Fernández, C. & Vigneresse, J.-L.), pp. 221-237. *Geological Society of London Special Publication,* **158**, London.

Sevigny, J.H., 1993. Monazite controlled Sm/Nd fractionation in leucogranite: An ion microprobe study of garnet phenocrysts: *Geochimica et Cosmochimica Acta*, **57**, 4095–4102.

Shimura, T., Fraser, G. L. Tsuchiya, N., & Kagami, H., 1998. Genesis of the migmatites of Breidvagnipa, east Antartica. *Memoirs of the National Instutue of Polar Research Tokyo, Special Issue,* **53**, 109-136.

Simakin, A. & Talbot, C., 2001. Tectonic pumping of pervasive granitic melts. *Tectonophysics,* **332**, 387-402.

Slagstad, T., Jamieson, R.A. & Culshaw, N.G., 2005. Formation, crystallization, and migration of melt in the mid-orogenic crust: Muskoka domain migmatites, Grenville Province, Ontario. *Journal of Petrology*, **46**, 893-919.

Solar, G. S. & Brown, M., 2001. Petrogenesis of migmatites in Maine, USA: Possible Source of Peraluminous leucogranite in Plutons? *Journal of Petrology,* **42**, 789-823.

Spear F. S., Kohn, M. J.,& Cheney, J.T., 1999. P–T paths from anatectic pelites. *Contributions to Mineralogy and Petrology*, **134**, 17-32.

Stevens, G., & Clemens, J. D., 1993. Fluid-absent melting and the roles of fluids in the lithosphere: a slanted summary. *Chemical Geology,* **108**, 1-17.

Stevens, G., Clemens, J. D. & Droop, G. T. R., 1997. Melt production during granulite-facies anatexis: experimental data from "primitive" metasedimentary protoliths. *Contributions to Mineralogy and Petrology*, **128**, 352-370.

Stevenson, D. J., 1989. Spontaneous small-scale melt segregation in partial melts undergoing deformation. *Geophysical Research Letters,* **16**, 1067-1070.

Stevenson, D.J., 1986. Importance of variation in algal immigration and growth rates estimated by modeling benthic algal colonization. Pages 193–210 *in* L. V. Evans and K.D. Hoagland, editors. Algal biofouling. Elsevier Press, Amsterdam, The Netherlands.

Stevenson, I. M., 1964. Lac La Jannaye, Quebec and New-foundland. *Geological Survey of Canada,* Paper **64-8**. 5 pp.

Tait, R. E. & Harley, S. L., 1988. Local processes involved in the generation of migmatites within mafic granulites. *Transactions of the Royal Society of Edinburgh: Earth Sciences,* **79**, 209-222.

Tuttle, O.F. & Bowen, N.L., 1958. Origin of granite in the light of experimental studies in the system NaAlSi3O8-KAlSi3O8-SiO2-H2O. *The Geological Society of America Memoir **74**.*

Taylor, S. R. & McLennan S.M., 1985. The continental crust: Its composition and evolution, Blackwell, Oxford, 312pp.

Thériault, R. & Chevé, S., 2001. Géologie de la région du lac Hurault (SNRC 23L). *Ministère des Ressources Naturelles du Québec*, RG **2000-11**, 49p.

Thompson, A. B. & Algor. J. R., 1977. Model systems for anatexis of pelitic rocks. I Theory of melting reactions in the system $KAlO_2$-$NaAlO_2$- SiO_2-H_2O. *Contributions to Mineralogy and Petrology*, **63**, 247-269.

Thompson, A. B. & Tracy, R. J., 1979. Model systems for anatexis of pelitic rocks. II. Facies series melting and reaction in the system CaO-$KAlO_2$-$NaAlO_2$-Al_2O_3-SiO_2-H_2O. *Contributions to Mineralogy and Petrology*, **98**, 257-276.

Thompson, A. B., 1996. Fertility of crustal rocks during anatexis. *Transactions of the Royal Society of Edinburgh: Earth Sciences,* **87**, 1-10.

Tindle, A. G. & Pearce, J. A., 1981. Petrogenetic modelling of in situ fractional crystallization in the zones Loch Doon Pluton, Scotland. *Contributions to Mineralogy and Petrology,* **78**, 196-207.

Tindle, A.G., McGarvie, D.W. and Webb, P.C., 1988 The relative roles of hybridization and crystal fractionation in the evolution of the Cairnsmore of Carsphairn Intrusion, Southern Uplands of Scotland. *Journal of Geoogical Society of London*, **145**, 11-21.

van der Mollen, I. & Patterson M. S., 1979. Experimental deformation of partially-melted granite. *Contributions to Mineralogy and Petrology,* ***70***, 299-318.

Vanderhaeghe, O. & Teyssier C., 2001a. Crustal-scale rheological transitions during late-orogenic collapse. *Tectonophysics*, 335, 211-228.

Vanderhaeghe, O. 2001b. Melt segregation, pervasive melt migration and magma mobility: the structural record from pores to orogens. *Physics and Chemistry of the Earth*, **26**, 213-223.

Vernon, R. H. & Collins, W. J., 1988. Igneous microstructures in migmatites. *Geology*, **16,** 1126–1129.

Vielzeuf, D. & Holloway J. R., 1988. Experimental determination of the fluid-absent melting relations in the pelitic system: Consequences for crustal differentiation. *Contributions to Mineralogy and Petrology*, **98**, 257-276.

Vielzeuf, D. & Montel, J. M., 1994. Partial melting of metagreywackes. 1. Fluid-absent experiments and phase relationships. *Contributions to Mineralogy and Petrology,* **117**, 375-393.

Vielzeuf, D., Clemens, J. D., Pin, C. & Minet, E., 1990. Granite, granulites and crustal differentiation. In: *Granulites and Crustal Evolution* (eds. Vielzeuf, D. & Vidal, Ph.), pp. 59-85. Kluwer Academic Publishers, Dordrecht.

Vigneresse, J.-L., Barbey, P. & Cuney, M., 1996. Rheological transitions during partial melting and crystallization with application to felsic magma segregation and transfer. *Journal of Petrology*, **37**, 1579-1600.

Waters, D. J. & Whales, C. J., 1984. Dehydration melting and the granulite transition in metapelites from southern Namaqualand, S. Africa. *Contributions to Mineralogy and Petrology,* **88**, 269-275.

Waters, D. J., 1988. Partial melting and the formation of granulite facies assemblages in Namaqualand, South Africa. *Journal of Metamorphic Geology,* **6**, 387-404.

Waters, D. J., 2001. The significance of prograde and retrograde quartz-bearing intergrowth microstructures in partially-melted granulite-facies rocks. In: Kriegsman, L. (ed.) Prograde and retrograde processes in crustal melting. *Lithos*, 56, 97-110.

Watson E.B., 1976.Two-liquid partition coefficients: Experimental data and geochemical implications.*Contributions to Mineralogy and Petrology*, **56**, 119-134

Watson, E. B. & Harrison, T. M., 1983. Zircon saturation revisited and compositional effects in a variety of crustal magma types. *Earth and Planetary Science Letters*, **64**, 295-304.

Watt, G.R., and Harley, S.L., 1993, Accessory phase controls on the geochemistry of crustal melts and restites produced during water-undersaturate partial melting. *Contributions to Mineralogy and Petrology*, **114**, 550–556.

Weber, C., Barbey, P., & Martin, H., 1985. Trace element behaviour during migmatization. Evidence for a complex melt-residuum fluid interaction in the St. Malo migmatitic dome (France). *Contributions to Mineralogy and Petrology,* **90**, 52-62.

White, A. JR & Chappell, B. W., 1990. Per migma ad magma downunder. *Geological Journal,* **25**, 221-225.

White, R. W. & Powell, R., 2002. Melt loss and the preservation of granulite facies mineral assemblages. *Journal of Metamorphic Geology,* **20**, (7), 621-632.

White, R.W., Powell, R. & Holland T.J.B., 2001. Calculation of partial melting equilibria in the system CaO-Na2O-K2O-FeO-MgO-Al2O3-SiO2-H2O (CNKFMASH). *Journal of Metamorphic Geology,* **19**, 139-153.

Wickham, S. M., (1987). The segregation and emplacement of granitic magmas. *Journal of the Geological Society, London*, **144**, 281-297.

Willigers, B. J. A., Krogstad, E. J. & Wijbrans, J. R., 2001. Comparison of thermochronometers in a slowly cooled granulite terrain: Nagssugtoqidian Orogen, west Greenland. *Journal of Petrology*, **42**, 1729-1749.

Zaleski, E., van Breemen, O. & Peterson, V. L., 1999. Geological evolution of the Manitouwadge greenstone belt and Wawa-Quetico subprovince boundary, Superior Province, Ontario, constrained by U-Pb zircon dates of supracrustal and plutonic rocks. *Canadian Journal of Earth Science,* **36**, 945-966.